OXYGENATION AND RADIOSENSITIVITY CONSEQUENCES OF SOLID TUMOUR PERFUSION

by

Brennan Wadsworth

B.Sc., University of Waterloo, 2014

A THESIS SUBMITTED IN PARTIAL FULFILLMENT OF

THE REQUIREMENTS FOR THE DEGREE OF

DOCTOR OF PHILOSOPHY

in

THE FACULTY OF GRADUATE AND POSTDOCTORAL STUDIES

(Pathology and Laboratory Medicine)

THE UNIVERSITY OF BRITISH COLUMBIA

(Vancouver)

July 2020

The following individuals certify that they have read, and recommend to the Faculty of Graduate and Postdoctoral Studies for acceptance, the dissertation entitled:

Oxygenation and radiosensitivity consequences of solid tumour perfusion.

submitted by Brennan Wadsworth in partial fulfillment of the requirements for

the degree of Doctor of Philosophy

in Pathology and Laboratory Medicine

Examining Committee:

Dr. Kevin L Bennewith, Associate Professor, Pathology and Laboratory Medicine
Supervisor

Dr. François Bénard, Professor, Radiology
Supervisory Committee Member

Dr. Andrew Minchinton, Associate Professor, Pathology and Laboratory Medicine
University Examiner

Dr. Christina Haston, Professor, Medical Physics
University Examiner

Additional Supervisory Committee Members:

Dr. Calum MacAulay, Clinical Associate Professor, Pathology and Laboratory Medicine
Supervisory Committee Member

Dr. Pascal Bernatchez, Associate Professor, Pharmacology and Therapeutics
Supervisory Committee Member

Abstract

Solid tumours often develop regions that are poorly oxygenated (hypoxic). Hypoxic tumour cells are resistant to radiation and are associated with poor patient outcome. “Chronic hypoxia” develops where vascular density is insufficient, causing tumour cells beyond ~70-100 μm from blood vessels to receive little oxygen. “Transient hypoxia” occurs in solid tumours where fluctuating microregional perfusion exposes tumour cells to cycles of hypoxia and reoxygenation. The fundamental understanding of transient hypoxia *in vivo* is lacking, and there are no available strategies to eliminate transient hypoxia. This thesis hypothesizes that transiently hypoxic tumour cells are long-lived radiation resistant cells and that eliminating the development of transient hypoxia will improve tumour radiation response.

This thesis first investigated the rate of hypoxic cell turnover *in vivo*. Exogenous hypoxia reporters were used to label hypoxic tumour cells, while loss of labelled cells over time indicated loss of hypoxic cells. The perfusion-modifying drug pentoxifylline was used to control which hypoxic populations were labelled and therefore which populations were lost over time. We find that transiently hypoxic tumour cells survive longer than neighbouring chronically hypoxic cells, further justifying transient hypoxia as an important therapeutic target.

To better study tumour perfusion-modifying interventions, this thesis next validated 2-^{18}F-fluoroethanol as a novel reporter of solid tumour perfusion compatible with positron emission tomography. We found 2-^{18}F-fluoroethanol to effectively respond to established tumour perfusion-modifying interventions and applied 2-^{18}F-fluoroethanol to characterize novel interventions aiming to modify tumour perfusion and transient hypoxia.

This thesis then focused on the angiotensin II type 1 receptor blocker telmisartan. Telmisartan treatment reduced tumour collagen 1 content, increased and stabilized tumour perfusion, reduced the development of transient hypoxia, and improved tumour radiation response. This presents the target of telmisartan, cancer associated fibroblast activity and tumour collagen 1 content, as a potential microenvironmental cause of transient hypoxia.

Overall, this thesis provides insight into the basic biology of transient hypoxia *in vivo*, validates a novel non-invasive reporter of solid tumour perfusion, and identifies telmisartan as a clinically relevant treatment to stably reduce the development of transient hypoxia in solid tumours and improve radiation response.

Lay Summary

Solid tumours are often supplied with lower levels of oxygen than is normal for most of the body. This is actually a problem because poorly oxygenated (hypoxic) tumour cells are resistant to radiotherapy and chemotherapy and are more likely to spread throughout the body. Thus, hypoxia makes tumour cells more difficult to kill and more aggressive.

"Transient hypoxia" may occur in tumours due to changes in blood flow over time leading to changes in oxygen delivery to the tumour. Transient hypoxia has been difficult to study because there are no known specific causes of dynamic blood flow in tumours. This thesis provides important insight into the biology of transient hypoxia that will guide future research towards developing treatments against this source of therapy resistance. This thesis also finds that certain drugs usually used to treat high blood pressure are able to reduce transient hypoxia and improve tumour response to radiation.

Preface

Chapter 2 is adapted from a manuscript currently submitted for publication as: Brennan J Wadsworth, Che-Min Lee, Kevin L Bennewith. "The lifetime of transiently hypoxic tumour cells in solid tumour xenografts". I designed the experiments for this project with input from Kevin Bennewith. I collected and analyzed the data for *in vitro* experiments and all pimonidazole and EF5 experiments. Che-Min Lee assisted with collection of data for clonogenic assays. I interpreted the data and wrote the manuscript.

Chapter 3 is adapted from the following published manuscript: Brennan J Wadsworth, Jinhe Pan, Iulia Dude, Nadine Colpo, Momir Bosiljcic, Kuo-Shyan Lin, Francois Benard, and Kevin L Bennewith. (2017) 2-^{18}F-Fluoroethanol is a PET reporter of solid tumor perfusion. *J Nucl Med*. 58:815-820. I designed the experiments for this project with input from Kevin Bennewith and Francois Benard. I collected the data with assistance from the Benard group as follows: Jinhe Pan prepared the radiotracer for all experiments, Nadine Colpo operated the small animal imaging equipment, and Iulia Dude handled the radiotracer for radiography experiments. I analyzed the PET, immunofluorescence, and radiography data, interpreted the results, and wrote the manuscript.

Chapter 4 is adapted from a manuscript currently accepted for publication in *Cancer Letters* as: Brennan J Wadsworth, Rachel A Cederberg, Che-Min Lee, Natalie S Firmino, S Elizabeth Franks, Jinhe Pan, Nadine Colpo, Kuo-Shyan Lin, Francois Benard, Kevin L Bennewith. "Angiotensin II type 1 receptor blocker telmisartan inhibits the development of transient hypoxia and improves tumour response to radiation." The following attributions are regarding the data included in this thesis. I designed the experiments with input from Kevin Bennewith. Jinhe Pan prepared the 2-^{18}F-FEtOH radiotracer for PET experiments and Nadine Colpo operated the small animal imaging equipment. Rachel A Cederberg assisted in collection and analysis of data for *ex vivo* clonogenic assays. Che-Min Lee assisted in collection of data for *in vitro* clonogenic assays, monitoring of mice in radiation growth delay, and immunofluorescent microscopy detection of pimonidazole, CD31, and Hoechst 33342. Che-Min Lee created the summary figure. Animal facility staff conducted tumour measurements for radiation growth delay experiments. I collected the data for flow cytometry experiments, *in vitro* and *ex vivo* clonogenic assays,

immunofluorescent microscopy for the delayed telmisartan experiment, and immunofluorescent microscopy detection of collagen 1, α-smooth muscle actin, and Hoechst 33342 with $DiOC_7$. I analyzed all of the data and wrote the manuscript.

Chapters 1 and 5 are unpublished material written by me.

All animal experiments were performed in accordance with Canadian Council on Animal Care guidelines. Animal experiments were conducted under UBC research ethics certificates: A17-0231 “Promotion of metastasis by tumour hypoxia and immune cells” and A16-0128 “Preclinical evaluation of radiotracers for cancer imaging”.

Table of Contents

Abstract ... **iii**
Lay Summary ... **iv**
Preface ... **v**
Table of Contents ... **vii**
List of Figures ... **xi**
List of Abbreviations ... **xiii**
Acknowledgements ... **xvi**
Dedication ... **xviii**
Chapter 1: Introduction ... **1**
1.1 Solid tumour microenvironment ... 1
1.1.1 Perfusion physiology and solid tumours ... 2
1.1.1.1 Perfusion physiology ... 2
1.1.1.2 Structure and function of tumour vasculature ... 3
1.1.1.3 Methods for perfusion measurement and characterization ... 7
1.1.2 Cancer associated fibroblasts and tumour extracellular matrix ... 11
1.2 Patterns of tumour hypoxia ... 13
1.2.1 Chronic hypoxia ... 14
1.2.2 Transient hypoxia ... 15
1.3 Tumour cell turnover ... 20
1.4 Ionising radiation and oxygen ... 23
1.5 Detection & characterization of tumour hypoxia ... 28
1.5.1 Oxygen electrode probes ... 28
1.5.2 Radiation-based assays ... 29
1.5.3 2-Nitroimidazoles ... 32
1.5.4 HIF and endogenous hypoxia markers ... 36
1.6 Tumour perfusion modifying interventions ... 38
1.6.1 Short-term interventions and pentoxifylline ... 38
1.6.2 Angiotensin system inhibitors ... 43
1.7 Research objectives ... 44

1.7.1 Specific aims 45
1.7.2 Thesis overview 45
Chapter 2: The lifetime of transiently hypoxic cells in solid tumours. 47
2.1 Introduction 48
2.2 Materials and methods 51
2.2.1 Cells and mice 51
2.2.2 Chemicals 52
2.2.3 Flow cytometry and immunofluorescent microscopy 52
2.2.4 Statistical analysis 53
2.3 Results 53
2.3.1 Pimonidazole fluorescence *in vitro* 53
2.3.2 WiDr growth rate *in vitro* 56
2.3.3 Stabilization of hypoxic fraction *in vivo* 60
2.3.4 Pimonidazole and EF5 positive tumour area over time 62
2.3.5 Pentoxifylline reoxygenation of transient hypoxia 65
2.3.6 Rate of chronic and transient hypoxic cell loss 68
2.3.7 Radiation-induced vascular failure 69
2.3.8 Hypoxic cell survival following irradiation 71
2.4 Discussion 74
Chapter 3: 2-^{18}F-Fluoroethanol is a novel positron emission tomography reporter of solid tumour perfusion 79
3.1 Introduction 80
3.2 Materials and methods 81
3.2.1 2-^{18}F-Fluoroethanol synthesis 81
3.2.2 Gamma counting and liquid scintillation counting 82
3.2.3 Tumour models 82
3.2.4 Antibodies 82
3.2.5 *Ex vivo* radiography experiments 82
3.2.6 PET imaging experiments 83
3.3 Results 83
3.3.1 2-^{18}F-FEtOH uptake depicts regional perfusion differences 83

3.3.2 2-^{18}F-FEtOH uptake agrees with ^{14}C-iodoantipyrine 85
3.3.3 2-^{18}F-FEtOH provides distinction between 67NR and 4T1 tumours..... 89
3.3.4 Irreversible uptake rate of 2-^{18}F-FEtOH is dependent on perfusion..... 89
3.3.5 2-^{18}F-FEtOH uptake is modified by perfusion-modifying drugs..... 92
3.4 Discussion..... 97
Chapter 4: Angiotensin II type 1 receptor blocker telmisartan inhibits the development of transient hypoxia and improves response to radiation. 100
4.1 Introduction..... 101
4.2 Materials and methods..... 102
4.2.1 Cell lines and mice..... 102
4.2.2 Drugs..... 102
4.2.3 Flow cytometry and immunofluorescent microscopy..... 102
4.2.4 Mismatch of Hoechst 33342 and carbocyanine ($DiOC_7$) 103
4.2.5 Clonogenic assay and radiation growth delay experiments..... 104
4.2.6 PET imaging 104
4.2.7 Statistical analysis..... 104
4.3 Results..... 104
4.3.1 Telmisartan reduces Col1 in the tumour microenvironment 104
4.3.2 Telmisartan improves and stabilizes WiDr tumour perfusion 106
4.3.3 Telmisartan reduces the development of transient hypoxia..... 111
4.3.4 Telmisartan improves WiDr tumour radiation response..... 113
4.3.5 Improved radiation response from telmisartan treatment is dependent on altering the development of the tumour microenvironment..... 113
4.4 Discussion..... 117
Chapter 5: Conclusions and future directions 122
5.1 Summary and contributions to the research field from Chapter 2 122
5.2 Summary and contributions to the research field from Chapter 3 125
5.3 Summary and contributions to the research field from Chapter 4 128
5.4 Future directions 130
References.....136
Appendices.....164

Appendix A 164
A.1 Hagen-Poiseuille equation of laminar flow 164
A.2 Tumour kinetics equations and examples 164

List of Figures

Figure 1.1 Chronic and transient hypoxia 16
Figure 1.2 Theoretical survival curves for determining the hypoxic fraction 30
Figure 1.3 2-Nitroimidazole structure and reduction 33
Figure 2.1 Pimonidazole loss in *in vitro* tracks with cell divisions. 55
Figure 2.2 Cell viability over time with CDK4/6 inhibitors 57
Figure 2.3 Loss of pimonidazole *in vitro* can be inhibited by cytostatic agents. 58
Figure 2.4 Cells cycling between hypoxia and normoxia exhibit intermediate growth rates. 59
Figure 2.5 Hypoxic fraction stabilizes during tumour growth 61
Figure 2.6 2-Nitroimidazole positive tumour area over time 63
Figure 2.7 Pimonidazole and EF5 singly-labelled tumour area over time 64
Figure 2.8 Time course of hypoxic area lost 66
Figure 2.9 Perfusion limited hypoxia in WiDr tumours is reoxygenated by pentoxifylline 67
Figure 2.10 Radiation-induced vascular failure 70
Figure 2.11 Hypoxic cell response to direct and indirect effects of irradiation. 72
Figure 3.1 4T1 and 67NR hypoxia and vascularity 84
Figure 3.2 Comparison of 2-^{18}F-FEtOH *ex vivo* radiography with Hoechst 33342 86
Figure 3.3 Sample line profiles 87
Figure 3.4 Comparison of 2-^{18}F-FEtOH uptake with ^{14}C-IAP 88
Figure 3.5 2-^{18}F-FEtOH PET uptake distinguishes between 4T1 and 67NR tumours 90
Figure 3.6 Sample arterial input function 91
Figure 3.7 Patlak modeling of dynamic 2-^{18}F-FEtOH uptake 93
Figure 3.8 2-^{18}F-FEtOH uptake in response to perfusion modifying drugs 94
Figure 3.9 Sample 2-^{18}F-FEtOH images from dynamic PET 95
Figure 3.10 Response of 2-^{18}F-FEtOH uptake to hydralazine in dynamic PET 96
Figure 4.1 Consumption and growth effects of losartan and telmisartan. 105
Figure 4.2 Telmisartan treatment alters the tumour microenvironment. 107
Figure 4.3 Telmisartan increases and stabilizes WiDr tumour perfusion. 108
Figure 4.4 Pentoxifylline does not affect 2-^{18}F-FEtOH uptake in SiHa tumours 110
Figure 4.5 Telmisartan reduces WiDr tumour hypoxia. 112

Figure 4.6 Telmisartan and pentoxifylline do not modify radiation sensitivity *in vitro*..... 114
Figure 4.7 Telmisartan treatment reduces WiDr tumour cell survival following irradiation 115
Figure 4.8 Telmisartan treated WiDr tumours exhibit a significant radiation growth delay. 116
Figure 4.9 Delayed telmisartan treatment does not modify radiation response..... 118
Figure 4.10 Proposed mechanism for the effect of telmisartan on the WiDr tumour microenvironment 120
Figure 5.1 WiDr tumour 2-^{18}F-FEtOH uptake after pentoxifylline 126

List of Abbreviations

2-^{18}F-FEtOH	2-^{18}F-Fluoroethanol
αSMA	α Smooth muscle actin
ACE	Angiotensin converting enzyme
ACEi	Angiotensin converting enzyme inhibitor
AngII	Angiotensin II
ARB	Angiotensin II type 1 receptor blocker
AT1R	Angiotensin II type 1 receptor
AT2R	Angiotensin II type 2 receptor
ATP	Adenosine triphosphate
BER	Base excision repair
CAIX	Carbonic anhydrase IX
CAF	Cancer associated fibroblast
cAMP	Cyclic adenosine monophosphate
CDK	Cyclin-dependent kinase
Col1	Collagen 1
CT	Computed tomography
CTY	Cell Trace Yellow
DAPI	4,6-diamidino-2-phenylindole
DMSO	Dimethyl sulfoxide
DNA	Deoxy-ribonucleic acid
DSB	Double strand break
ECM	Extracellular matrix
EGFR	Epidermal growth factor receptor
ELISA	Enzyme-linked immunosorbent assay
FAP	Fibroblast activation protein
FAZA	Fluoroazomycinarabinofuranoside
FETA	Fluoroetanidazole
FETNIM	Fluoroerythronitroimidazole
FIH	Factor inhibiting HIF

FITC	Fluorescein Isothiocyanate
FGFR	Fibroblast growth factor receptor
FMISO	Fluoromisonidazole
FSP1	Fibroblast specific protein 1
GFP	Green fluorescent protein
GLUT1	Glucose transporter 1
HIF	Hypoxia inducible factor
HR	Homologous recombination
HRE	Hypoxia response element
IAP	Iodoantipyrine
IdUr	Iododeoxyuridine
IFP	Interstitial fluid pressure
IHC	Immuno-histochemistry
LDF	Laser doppler flowmetry
MasR	Mas receptor
MFI	Mean fluorescence intensity
mRNA	Messenger RNA
MSC	Mesenchymal stem cell
NER	Nucleotide excision repair
NHEJ	Non-homologous end joining
NOD/SCID	Non-obese diabetic/severe combined immunodeficient
NRG	NOD/Rag gamma
NSG	NOD/SCID gamma
OER	Oxygen enhancement ratio
PBS	Phosphate-buffered saline
PDGFR	Platelet-derived growth factor receptor
PET	Positron emission tomography
PHD	Prolyl hydroxylase
PI3K	Phosphoinositide 3-kinase
PKA	Protein kinase A
RAS	Renin angiotensin system

RNA	Ribonucleic acid
SD	Standard deviation
SEM	Standard error of the mean
SPECT	Single photon emission computed tomography
SSB	Single strand break
TME	Tumour microenvironment
VEGF	Vascular endothelial growth factor

Acknowledgements

I am thankful to have landed at BCCRC for my graduate studies. Coming with no expertise in cancer biology as an immature new graduate it took support from a wide network to get me to writing a thesis. I would like to thank my supervisor Dr. Kevin Bennewith for accepting me into his lab. Kevin's open door and enthusiasm for his trainees made it no challenge to have regular meetings with him to discuss my project and instead more of a challenge to manage to leave his office on time before the next person's time slot. From day one Kevin was interested and excited in my project despite the enormous amount of independence that he provided, and I am thankful for his ability to provide actionable input from each meeting regardless of the topic or any time crunch that he was under.

Thank you to Drs. Alistair Kyle, Jenn Baker, Andrew Minchinton, and the rest of the AIM lab. The AIM lab slide scanner and image processing programs easily saved me days upon days of my life in what was a microscopy heavy project. The AIM group was one of the few sources of local researchers interested in discussing radiation, DNA repair, hypoxia, and tumour perfusion, so thank you for the input and expertise.

Thank you to my committee members Dr. Francois Benard, Dr. Pascal Bernatchez, and Dr. Calum MacAulay for being interested in improving my project and providing input at both committee meetings and one-on-one meetings. Thank you to the BCCRC PET group, especially Drs. Jinhe Pan and Kuo-Shyan Lin for kindly producing the 2-^{18}F-FEtOH used in our imaging experiments. Thank you to Nadine Colpo for conducting the PET imaging and working tirelessly to make sure that the PET scanner was working on the days it was needed. Thank you to Gayle Paquette and all of the ARC staff for supporting our research with reliable efficiency.

Thank you to my high school science teacher Mr. Brent Campbell for providing me an early fascination with science. Your enthusiasm and commitment make a difference. Thank you to Dr. Russell Tupling and the SERCA group for providing me with the opportunity to volunteer and work in the skeletal muscle physiology labs. From the first day touring the labs at BMH I knew that I wanted to pursue research and my experience with the Tupling lab only confirmed that desire over time.

Thank you to all of the BCCRC 10th floor trainees (and others who would frequent the lunch area), in particular the Bennewith lab members. Your companionship for coffee runs, commiserating, and celebrating was a huge part of making it through graduate school. Also,

thank you for humouring Adam and I by joining the Buntsen Burners slow pitch softball team. An additional huge thank you to the Bennewith lab members for all of the assistance with my lab work over the years.

Thank you to my family, the Wadsworths and Buttons, for shaping me as a person and always being supportive of Emily and I pursuing our dreams so far from home. Finally, thank you to my wife Emily for your encouragement and everyday support.

Dedicated to my parents.

Chapter 1: Introduction

1.1 Solid tumour microenvironment

Cancer is traditionally described as a genetic disease. Mutations in individual cells lead to uncontrolled cell growth and thus define a problem that is intrinsic to tumour cells. However, tumour cells interact with and even depend upon their host. One of the most fundamental interactions between tumour cells and the host system is the development of a vascular network that provides tumour cells with oxygen and nutrients with which to maintain tumour growth. The balance of tumour growth with angiogenesis leads to biological phenomenon that impact disease progression across tumour sites and in tumours with distinct genetic signatures. This thesis investigates the connection between the solid tumour vasculature, its function and dysfunction, and tumour response to radiation therapy.

The solid tumour microenvironment describes both the non-cancerous cells found in tumours and the extracellular matrix housing the cells. Inflammatory signals and growth factors produced by tumour tissue recruit and activate local fibroblasts. Fibroblasts found within solid tumours are commonly described as cancer associated fibroblasts (CAFs) to recognize their increase in growth factor production and activity for extracellular matrix remodelling. Solid tumours commonly contain significant fibrosis, which is attributed to CAF activity. Tumour fibrosis will be discussed for its potential impact on the vascular microenvironment (Chapter 1.1.2). Inflammatory signals also recruit a wide range of immune cells. Aside from roles in anti-tumour immunity, or immune suppression, immune cells may also contribute to the processes of angiogenesis and fibrosis via production of cytokines and growth factors. Immune cell populations will not be a focus of this thesis as the majority of the work was conducted in mice deficient of adaptive immune cells. Instead, this thesis introduction will discuss relevant background in solid tumour perfusion (Chapter 1.1), oxygen within solid tumours (Chapter 1.2), the turnover of hypoxic tumour cells (Chapter 1.3), the relation between oxygen and radiation response (Chapter 1.4), and some specific methods and interventions relevant to the thesis work (Chapters 1.5 and 1.6).

1.1.1 Perfusion physiology and solid tumours

1.1.1.1 Perfusion physiology

The mammalian circulatory system is a set of physical structures including a pump (i.e. the heart) and vessels within which blood is transported. The total volume of blood flowing out of the left ventricle of the heart per unit time is termed the cardiac output, which is equal to the product of stroke volume (i.e. volume ejected by the left ventricle each contraction) and heart rate (i.e. contractions per unit time)[1]. Blood flow, referring to the volume of blood passing through a vessel per unit time, throughout the circulatory system is proportional to the pressure gradient between two points in the system and inversely proportional to the vascular resistance (Hagen-Poiseuille equation displayed in Appendix A.1)[2]. To deliver the proper cardiac output to each organ, the body must therefore regulate flow based on pressure gradients and vascular resistance.

Left ventricular contraction creates high blood pressure in the aorta, driving blood flow through the rest of the vascular tree. Vascular resistance creates friction to flow that progressively decreases the perfusion pressure as blood traverses the circulatory system[1,3]. Vascular resistance is therefore how the body regulates blood flow downstream of the large arteries. Vascular resistance is determined by vessel diameter, viscosity of the blood, vessel length, and extravascular mechanical forces acting on the vessel[1,2]. Blood viscosity and vessel length are largely not dynamic in healthy tissue; thus, these factors will not be discussed until later as causes of tumour vascular dysfunction (Chapter 1.1.1.2). Rather, the most potent modulator of vascular resistance and most dynamic of these variables in normal physiology is vessel diameter. Vessel diameter is determined by vessel structure, compliance (i.e. ability to expand in response to high pressure), and in turn by extravascular forces that limit compliance. In healthy vessels, diameter is dynamic in the case of elastic arteries that are highly compliant, and in arterioles that possess a layer of circumferential smooth muscle cells that respond to local and systemic signals to either dilate or constrict the arteriole. Arterioles are the small vessels carrying oxygenated blood from the heart that are just upstream of exchange capillaries. The constriction or dilation of arterioles therefore controls vascular resistance to regulate blood flow to exchange vessels. In most cases, the majority of the perfusion pressure provided by cardiac left ventricle contraction is lost at the stage of arterioles[1]. The drop in perfusion pressure is likely beneficial for safe flow in thin-walled capillaries and reduces blood velocity for more efficient

blood-to-tissue exchange in capillaries[4]. However, the loss in perfusion pressure leaves downstream flow from capillaries to the venous system reliant on small pressure gradients that are susceptible to pressure deregulation, as will be discussed in the next section (Chapter 1.1.1.2). In healthy vasculature, output flow from capillaries to venules and veins is supported by the very low vascular resistance in the venous system and, ultimately, by the negative pressure in the right ventricle during ventricular relaxation[1,3]. Overall, tissue perfusion is dependent on regulating vascular resistance to maintain a functional pressure gradient that both favours input flow to tissue capillaries and output flow to collecting venules.

Blood flow reaching an organ of interest is often described as 'organ perfusion'. Perfusion refers to the blood flow (vol per unit time) to a particular tissue per unit volume or mass of the organ or tissue in question. As a relative quantification, perfusion is commonly reported as the percent cardiac output per gram of tissue. Thus, a highly perfused tissue would be one with a greater percent cardiac output than its percentage of body mass, e.g. resting kidney. The term 'perfusion' will be used throughout this thesis in both the macroscopic sense described here for blood flow to a tissue relative to the mass of the tissue, as well as a granular sense as in to describe blood flow to microscopic regions of a solid tumour.

1.1.1.2 Structure and function of tumour vasculature

Newly formed tumours use the local host vasculature for nutrient supply, although this becomes inadequate for a tumour mass beyond approximately 1 mm in diameter. Thereafter, continuous tumour growth occurs with significant and continuous signaling for the construction of new blood vessels to feed the tumour[5]. Angiogenesis refers to recruitment and proliferation of local host endothelial cells to create branches from existing blood vessels in the direction of pro-angiogenic signals. Vasculogenesis is the process of recruiting bone-marrow derived endothelial progenitor cells to the tumour, where the recruited cells incorporate into the neo-vasculature. Angiogenesis is the better understood process of the two and currently accepted as the primary method of neo-vascularization in untreated tumours. However, the regrowth of tumours after irradiation, when proliferation of local endothelial cells may be inhibited, and the development of resistance to anti-angiogenic therapies suggest that alternatives to angiogenesis may be sufficient to produce vasculature for tumour growth[6–9]. Tumour vascularization achieves varying

degrees of success between and within tumours. This section will discuss patterns of dysfunction in solid tumour vascular networks.

Poor blood flow in solid tumours may be attributed to a combination of the dysfunctional structure of the vessels and complications from the surrounding microenvironment. Many of the fundamental observations of solid tumour vascular structure come from intra-vital imaging of solid tumours grown as subcutaneous implants between glass plates on the backs of mice or rats, or in the cheek pouch of hamsters. With this set-up, vessels may be observed repeatedly throughout tumour growth to observe the process of angiogenesis and describe the overall structure of the vascular network. Further, individual vessels may be characterized for size, direction of flow, erythrocyte flux, and dynamics of flow. Multiple reports across tumour models agree on some general observations. Firstly, new vessels sprout preferentially from venules, distinguished from arterioles and capillaries based on vessel diameter and direction of blood flow[10–13]. Sprouting vessels elongate towards tumour tissue and form hairpin loops by anastomosing with other venule sprouts. As this process continues over time patterns emerge in the final product. Few vessels within subcutaneous tumours are smaller than 10 μm in diameter and therefore do not fit the typical description of capillaries. Instead, tumours contain a network of vessels more similar to venules, supplied by a relatively small number of arterioles[4,10–12,14]. Secondly, tumours are commonly characterized by a vascular capsule that communicates with input arterioles and output venules. Vessels inside the tumour mass are described as tortuous with a low rate of branching, creating long vessels running radially towards the tumour centre[11,14]. The abundance of large diameter unbranching vessels as the main exchange vessels in tumours represents a failure in developing a hierarchical vascular network.

The lack of vascular hierarchy in solid tumours leads to pressure dysfunction in tissue exchange vessels as perfusion pressure cannot be optimally directed from input arterioles to tissue exchange vessels then to outflow venules. Studies employing micro-pressure measurement apparatus operated by a micromanipulator have assayed intravascular pressure of individual vessels in normal and tumour tissue. The first observation of note is that the intra-vascular pressure of arterioles supplying tumour tissue is similar to that of normal tissue, approximately 20-40 mmHg and increasing with arteriole diameter[2,12,15–17]. However, pressure of venule-sized vessels in tumours is either similar or reduced compared to normal tissue[2,12,15–17]. As venule-sized vessels are the dominant vessels within tumours[4,10–12,14], this represents a poor pressure

gradient for flow out of the tumour into the venous system. With the pressure deregulation of solid tumours in mind, it is unsurprising that independent intra-vital imaging studies reliably report hemostasis and flow reversal within individual tumour blood vessels without any acute changes in vessel diameter[4,10–12]. Many researchers also observe 'vascular shunting' wherein flow to exchange vessels is bypassed due to the lack of hierarchical structure and poor perfusion gradients[4,10–12,18]. Thus, blood flow in tumours may be dysfunctional based on poorly regulated perfusion pressures resultant from a poor vascular structure, as opposed to the widely discussed dependence of tumour perfusion stasis on vascular collapse. Overall, the tumour angiogenic process produces vascular networks that are dominated by large venule-like vessels with poor or no hierarchy, resulting in poor perfusion gradients and abnormalities in blood flow.

Shortfalls of the angiogenic process in tumours can be further assessed at the level of the vascular wall. A fully formed capillary should have a smooth luminal surface with low permeability to support laminar flow, a complete basement membrane, and potentially pericyte coverage to provide structural and growth factor support for endothelium. However, the constant production of angiogenic signals in solid tumours limits the ability of endothelium to initiate the resolution stage of angiogenesis[19]. Production of the angiogenic factor vascular endothelial growth factor A (VEGFA) is indeed significantly upregulated in many tumours. Tissue from breast, colorectal, and prostate cancer patient tumours has been found to contain between 5-10 times greater concentration of VEGFA than control healthy tissue[5]. Meta-analysis of clinical data concluded that the angiogenic signalling from tumours is significant enough to increase plasma and urine concentrations of VEGFA by 2-5 fold in most patients, despite many solid tumours being a very small percentage of body mass relative to the main basal producer of VEGFA, skeletal muscle[5]. Without resolution of the angiogenic signaling, pericytes are either absent or abnormal in tumours[20,21] and vessel basement membrane is often too sparse or excessive[21,22]. Tumour vessels have been observed to possess fenestrations in diameter up to 500 nm and gaps between endothelial cells of up to 5000 nm in diameter, although permeability and vessel wall morphology may vary between tumours[23]. Tumour vessel permeability may reflect incomplete angiogenesis, suggested by electron microscopic observation of various abnormal endothelium protrusions into the vessel lumen, which likely contribute resistance to blood flow[21,23,24]. Alternatively, permeability may reflect individual endothelial cells initiating a new angiogenic response; exposure of endothelial cells *in vivo* to VEGFA induces permeability to 70 kDa ficoll

in capillaries and venules[25] (unsurprisingly, a lesser used name of VEGFA is 'vascular permeability factor'). In either scenario, the ongoing angiogenesis in solid tumours appears to produce vascular permeability. However, in modelling reports, vascular permeability alone is not predicted to directly modify blood flow. A greater predictor of blood flow is vessel compliance (i.e. ability to increase radius in response to an increased input perfusion pressure). Vessel compliance in turn is dependent on the local physical forces placed upon the vessel wall. Interstitial fluid pressure (IFP) is one of the sources of external compression on tumour vessels. Solid tumours are widely characterized to exhibit high IFP, which is attributed to a combination of the vascular permeability allowing for fluid and solute leakage to the interstitial space[26–30], and an absence of functional lymphatics to drain the interstitial fluid[26,31,32]. Alleviating IFP is associated with improved blood flow during the vascular normalization response of solid tumours treated with anti-angiogenic therapy[26–29]. Overall, vascular permeability in solid tumours is a common structural error that is most likely due to endothelial cell response to the high and continuous angiogenic signalling. Vascular permeability may indirectly increase vascular resistance by increasing IFP and limiting vessel compliance.

Dysfunction in the tumour vasculature may also arise from within the vessels. Resistance to flow is proportional to the viscosity of the fluid being transported. Local hematocrit is a major determinant of blood viscosity[33]. To circulate erythrocytes in small capillaries, the healthy circulatory system takes advantage of erythrocyte deformability and the Fahraeus-Lindqvist effect. The Fahraeus-Lindqvist effect is the observation that the apparent viscosity of blood tends to decrease as vessel diameter decreases, beginning below a diameter of 300 μm and reaching a minimum at the typical diameter of erythrocytes between 6-8 μm[33,34]. This phenomenon occurs as erythrocytes concentrate at the centre of the vessel with a lubricating layer of fluid between the erythrocytes and the vessel wall. This is most striking in capillaries of diameter below 10 μm where erythrocytes tend to flow single-file, easily observable in glass capillaries[33]. In order to achieve the Fahraeus-Lindqvist reduction in viscosity, erythrocytes must maintain their deformability. Mammalian erythrocytes are unique cells with no nucleus or mitochondria, and a biconcave cell membrane shape that allows them to bend or stretch in order to flow within small capillaries[33]. This deformability of erythrocytes depends on the integrity of the cytoskeleton that gives the cells their unique shape and on regulating ATP levels in order to operate plasma membrane ion pumps that maintain cell volume homeostasis[35]. Stiffening of erythrocytes by *ex*

vivo exposure to either glutaraldehyde or hyperglycemia significantly increases measures of viscosity in glass capillaries and measures of apparent viscosity via perfusion through isolated tumour tissue[36]. In turn, treatment with the phosphodiesterase inhibitor pentoxifylline increases erythrocyte deformability and decreases blood viscosity, attributed to an increase in cellular cAMP signaling[37–39].

Solid tumours pose a problem to almost each facet of regulating local blood viscosity. Firstly, apparent viscosity of blood increases with decreased flow rate[40], and as noted above blood flow is at high risk of hemostasis and slow flow in solid tumours due to small pressure gradients and high resistance[4,10–12,14]. Secondly, the over-abundance of venule-like vessels and lack of small capillaries reduces the benefits of the Fahraeus-Lindqvist effect in tumours. Finally, the permeability of tumour vessels allows for plasma leakage that increases the local hematocrit[26–30]. It is therefore no surprise that for a given perfusion pressure with blood of known erythrocyte concentration, that the apparent blood viscosity is 50% greater when perfused through isolated solid tumours than for healthy skeletal muscle[40].

Overall, solid tumours commonly develop a dysfunctional vascular network that results in poor tissue perfusion with abnormalities in blood flow[4,10–12,18]. This vascular dysfunction is due in part to a lack in vascular hierarchy that creates poor perfusion gradients[2,12,15–17] and allows for vascular shunting[4,10–12,18]. Tumour vascular dysfunction is further a result of the high vascular resistance in solid tumours, which is brought about by a combination of the following: (1) long tortuous vessels due to the low rate of vascular branching[11,14], (2) the lack of resolution in the angiogenic process leading to high vascular permeability, increased IFP, and ultimately poor vascular compliance[26–30], and (3) high blood viscosity[36,40].

1.1.1.3 Methods for perfusion measurement and characterization

There are three variables of interest for characterizing solid tumour perfusion as concerns this thesis work: (1) bulk tumour perfusion or estimates of percent cardiac output, (2) density of perfused blood vessels or perfusion distribution, and (3) stability of microregional perfusion.

The ideal method for quantification of percent cardiac output delivered to an organ would be the input of a known quantity of a substance into the left ventricle that would be delivered to capillary beds throughout the body. The ideal substance would be completely extracted from the blood on the first pass through any tissue capillary bed and not rapidly diffuse to other tissues.

The ideal substance would also be detectable by methods of sufficient resolution to distinguish organs of interest. The substance that currently best fits these descriptions, for terminal endpoints in pre-clinical study, are radioactive plastic microspheres. Microspheres employed for perfusion assays are selected to be a diameter sufficiently small to reach capillaries but oversized to traverse the capillary and therefore become trapped. Microspheres used for this purpose are often greater than 10 μm in diameter[41–44]. Upon harvest, the radioactivity of a given organ divided by the known amount of total radioactivity injected to the left ventricle will indicate the percent cardiac output delivered to each organ[41,44]. This strategy of injecting a known amount of a substance into the circulation and detection after distribution is central to quantification of tissue perfusion.

There is of course a desire for non-terminal and clinically applicable measures of tissue perfusion. An alternative to microspheres is the use of small molecules. Molecules applied for perfusion reporting are often non-polar, structurally stable, not metabolized preferentially by any organs, and are either positron emitters for compatibility with positron emission tomography (PET), gamma emitters for compatibility with single photon emission tomography (SPECT), or otherwise radioactive. Examples include: ^{15}O-H_2O (^{15}O is PET compatible, half-life: 2 minutes)[42,45,46], ^{15}O-butanol[47], ^{13}N-NH_3[48] (^{13}N is PET compatible, half-life: 10 minutes), rubidium-chloride (^{82}Rb is PET compatible, half-life: 1.25 minutes)[49,50], thallium-201 (^{201}Tl is SPECT compatible, half-life: 73.1 hours)[51], technetium-99m sestamibi (^{99m}Tc is SPECT compatible, half-life: 6 hours)[51], and ^{14}C-iodoantipyrine (^{14}C-IAP; ^{14}C is neither PET or SPECT compatible, half-life: >5000 years)[43]. Compatibility with non-invasive imaging provides the ability to conduct non-terminal measures, including repeated measures on the same individual before and after perfusion modifying interventions and the possibility for clinical translation[42,45,46,52]. However, data from small molecule perfusion reporters must be interpreted with limitations relative to microspheres. Small molecule extraction from the blood may be incomplete[53], allowing for a second pass exposure to the radiotracer that could exaggerate differences between organs if conducting a cross-sectional measurement. Thus, uptake of small molecule perfusion reporters following intravenous injection provides estimates of percent cardiac output that are useful for indicating response to perfusion modifying interventions, but, contain error in measurement of absolute percent cardiac output in $mL*g^{-1}*min^{-1}$ [53,54]. For absolute measurement, the rate of radiotracer uptake can be corrected for the amount of

radiotracer being delivered in the arterial system by measurement of the arterial input function through repeated arterial sampling or image-based methods[55,56]. Overall, validated small molecule perfusion reporters provide a means to compare perfusion and investigate the ability of various interventions to increase or decrease organ perfusion.

To this end, multiple of the above reporters have been validated for reporting tumour perfusion and response to interventions modifying tumour perfusion[43,50,52,57–59]. However, no ^{18}F-based perfusion reporters have been validated to report solid tumour perfusion. ^{18}F provides benefits relative to other positron emitting radioisotopes including: (1) smallest positron range, and therefore greatest resolution, of all positron emitting radioisotopes used in PET[60], and (2) a half-life of ~110 minutes, which is orders of magnitude larger than the half-life of other radioisotopes used in PET-based perfusion reporters. The extended half-life of ^{18}F allows for delayed imaging and the possibility for *ex vivo* radiography, which allows for greater comparison with immunofluorescent microscopy to relate PET data with microscopic tumour biology. This thesis validates a novel ^{18}F-based reporter of solid tumour perfusion for use with PET, 2-^{18}F-fluoroethanol (2-^{18}F-FEtOH; Chapter 3)[52], and therefore the technology of PET will be briefly described and contrasted with SPECT in the following paragraphs.

SPECT and PET are two non-invasive imaging technologies widely used to quantify tissue perfusion, particularly for the identification of cerebral and cardiac ischemia[53,54]. Both technologies employ a large number of high energy photon detectors to quantify radioactivity emitted by intravenously injected radiotracers and then determine the origin of the emitted radioactivity in 3-dimensional (3D) space in order to create a 3D image of radiotracer distribution. PET determines the location of radioactivity emission based upon the nature of positrons. Positrons emitted from radioactive isotopes travel a short distance (~0.5-4 mm on average depending on isotope[60]) before colliding with an electron. Positrons are the anti-matter counterpart of electrons, thus upon collision the particles are destroyed and converted into energy, in the form of a pair of anti-parallel gamma rays that may be detected by the PET machine. Images are reconstructed based on identifying coincident anti-parallel gamma ray pairs, which allows for accurate determination of the location of positron annihilation[51].

SPECT scanners detect high energy photons from photon-emitting radioisotopes. This means there are no gamma ray pairs to determine the origin of emission. Instead, SPECT scanners contain collimators that restrict photon access to the detectors within a small angular

range so that the direction a photon travelled to reach the detector is known. The use of collimators reduces the sensitivity (i.e. percent of emitted radioactivity that is actually detected) of SPECT relative to PET, and the ability to detect gamma ray pairs in PET allows for greater spatial resolution than SPECT[51]. Further, positron emitting radioisotopes include elements that are found in biological molecules (e.g. oxygen and fluorine), allowing for the incorporation of positron-emitting isotopes into biological molecules. This allows for radiotracers that are minimally modified biological molecules, while there are no such radioisotopes fit for use with SPECT. However, SPECT machines are significantly cheaper to acquire and operate, are more plentiful in Canada compared with PET, and the radioisotopes are more readily accessible[61]. Overall, the advantages of SPECT are largely logistical, and PET is considered the superior technology for non-invasive quantification of bulk tissue perfusion. Previous data clearly demonstrate that PET perfusion reporters are fit for quantifying perfusion in tissue sub-regions and for quantifying the response of tissue perfusion to perfusion-modifying interventions[43,50,52–54,57–59]. Therefore, this thesis employed PET for quantification of bulk tumour perfusion (Chapters 3 & 4).

Beyond bulk tumour perfusion, it is of interest to understand the spatial and temporal differences in tumour perfusion. A major consideration for these measures is spatial resolution. The resolution of PET is on the order of 1 mm for rat and mouse sized 'micro-PET' machines or 2-3 mm for clinical PET machines[62], compared to the 1-2 μm resolution achievable with widely available immunofluorescent microscopy. The ability to characterize individual blood vessels in microscopy provides information that can be more directly connected with the biology of tumour hypoxia. For this reason, it is preferable to use fluorescent reporters injected intravenously and detected via microscopy. Fluorescent reporter options include Hoechst 33342[63–65], $DiOC_7$ carbocyanine[50,64,66–69], lectin proteins[70], or fluorescent nanoparticles[23]. These reporters label endothelial cells and neighbouring extravascular cells of functionally perfused blood vessels. Fluorescent reporters may be imaged in combination with immunofluorescent identification of CD31+ vascular endothelium to quantify function of individual blood vessels. It is therefore possible to determine the fraction of perfused blood vessels, density of perfused blood vessels, and response of these measures to perfusion-modifying interventions. Characterization of Hoechst 33342 and $DiOC_7$ in particular has demonstrated that fluorescence is proportional to vessel blood flow[63–66,71]. Therefore, by administering Hoechst 33342 followed by $DiOC_7$ at a

later time point, the change in blood flow for an individual blood vessel may be quantified in relative terms based on any change in fluorescence intensity[63–66,71]. However, unlike radioactive reporters, it is not possible to input a known amount of 'fluorescence' and report the fraction of reporter delivered to a particular tumour region. Thus, fluorescent reporters are not suitable for quantification of percent cardiac output delivered to a tumour or tumour sub-region. Overall, fluorescent perfusion reporters do not relay information on bulk tumour perfusion but allow for investigating microregional perfusion with individual-vessel resolution not possible with PET based reporters. In order to fully understand the response of a tumour to a perfusion modifying strategy, it is advantageous to quantify both measures of bulk tumour perfusion and measures of microregional function, as is conducted in Chapters 3 and 4 of this thesis.

1.1.2 Cancer associated fibroblasts and tumour extracellular matrix

Beyond the vasculature and the tumour cells themselves, solid tumours also contain varying amounts of fibroblasts. Fibroblasts found in tumours are more active than those found in healthy tissue; they are proliferative, exhibit increased production of growth factors and cytokines, actively produce collagen, and remodel the extracellular matrix[72]. These activated fibroblasts found in tumours are broadly termed cancer associated fibroblasts (CAFs) to distinguish them from the quiescent normal fibroblasts[72,73]. CAFs themselves are a heterogeneous population of cells that have inspired controversy in the field of cancer research. The controversy is largely due to a lack of unique and reliable cellular markers for CAFs or CAF sub-populations, as well as observations that many cell types appear able to acquire CAF-like activity. It is therefore worth discussing the current state of the literature regarding CAF phenotypes based on the most common markers and the most likely origins of CAFs.

Fibroblast specific protein 1 (FSP1) expression is observed in both quiescent normal fibroblasts and bone marrow-derived mesenchymal stem cells (MSCs)[74]. Both normal fibroblasts and MSCs may be activated by co-culture with tumour cells, culture with conditioned media from tumour cells, or treatment with transforming growth factor β (TGFβ)[75,76]. Activation is indicated by increased mRNA expression of FSP1, among many other genes. FSP1 has been employed to identify CAFs[77], however, many reports suggest that activated fibroblasts in solid tumours are negative for FSP1 protein expression. Loss of FSP1 despite increased gene expression is attributed to secretion of FSP1 upon activation[78,79]. Data from FSP1 knockout mice

or implanting tumours mixed with a population of FSP1+ CAFs indicate a strong supportive role of FSP1+ cells for tumour growth, promoting angiogenesis, extracellular matrix remodeling, and promoting metastasis[78–80]. These observations support that FSP1+ cells are recruited to tumour tissue and become activated 'CAFs' that support tumour growth. Overall, FSP1 is upregulated upon fibroblast activation, but, FSP1 protein expression is a more reliable marker of quiescent fibroblasts than for CAFs.

A recent 2020 community consensus publication recommends that CAFs be identified by staining for one of two markers: fibroblast activation protein (FAP) or α-smooth muscle actin (αSMA)[73]. Multiple observations suggest a multi-step model of CAF activation wherein FAP+ cells may be further activated to express αSMA. Firstly, αSMA+ cells can be observed as a clear sub-population of FAP+ cells in clinical samples and pre-clinical tumour models[81–83]. FAP expression may be induced in normal fibroblasts or MSCs by tumour cell conditioned media or co-culture with tumour cells, while αSMA induction is more specific to treatment with TGFβ[75,76,84]. Expression of αSMA is further suggested to be, in part, dependent on autocrine signaling of already activated CAFs. Specifically, CAFs isolated from tumours and cultured *ex vivo* secrete TGFβ, activate extracellular TGFβ, and gain αSMA expression[85,86]. This self-activation may be inhibited by treatment with losartan, an angiotensin II type 1 receptor blocker (ARB) demonstrated to reduce CAF ability to activate extracellular TGFβ as well as reduce CAF TGFβ production[85,86]. ARB drugs have been further demonstrated to reduce αSMA+ CAFs *in vivo* in over a dozen human and murine tumours[85–90]. These data suggest that CAFs must be activated in order to produce, cleave, and respond to TGFβ, which is required for αSMA induction.

Targeted depletion of CAF populations further supports the model of multi-step CAF activation. Mice genetically modified to express viral thymidine kinase in cells that express αSMA (αSMA-tk mice) allow for specific depletion of αSMA+ cells upon treatment with ganciclovir, which is converted by thymidine kinase to a cytotoxic product. Depletion of αSMA+ cells in tumours significantly depletes the αSMA+ CAF population, but, does not decrease the FAP+ population[91]. Conversely, pharmacological inhibition of FAP or pro-drugs targeted to FAP+ cells induce apoptosis in αSMA+ cells and reduce the αSMA+ population in tumours[92,93]. Overall, these data suggest that αSMA+ cells are an activated sub-population of CAFs.

αSMA+ CAFs are associated with high production of Col1 in inflammatory injuries and in solid tumours[72]. Accordingly, treating CAFs with TGFβ not only induces αSMA expression, but also increases Col1 production[75,76,84–86,94,95]. Depletion of αSMA+ CAFs by ganciclovir in αSMA-tk mice[91], by ARB treatment[85–90], or treatment with inhibitors against other CAF-activating receptors including platelet derived growth factor receptor (PDGFR)[94,95], fibroblast growth factor receptor (FGFR)[94,95], or CXCR4[96] all significantly reduce collagen 1 (Col1) content in solid tumours. These data support that αSMA in particular is a marker for Col1-producing CAFs.

The tumour extracellular matrix constitutes large masses of protein in the extracellular space. A dense extracellular matrix in tumours builds mechanical pressure within the tumour as proliferative tumour cells push against a network of collagen[85,86,97]. These compressive forces are understood to inhibit local vessel perfusion by reducing vessel compliance and increasing vascular resistance[2,85–89,97,98]. Accordingly, collagen abundance is shown to negatively correlate with net tumour perfusion, and regions within individual tumours with increased collagen abundance exhibit fewer perfused blood vessels[98]. Inhibiting the deposition of collagen has been shown to improve drug delivery, suggestive of improved perfusion, in both murine and human tumours in pre-clinical study[85,86,88–90].

Overall, the abundance of αSMA positive cells is strongly linked with the production of collagen in solid tumours. The abundance of collagen is well demonstrated to modify net tumour perfusion and microregional perfusion. Desmoplasia (pathology descriptor of tumour fibrosis), a high stroma-to-tumour ratio in pathology, and the abundance of αSMA+ cells all independently predict poor patient outcome[99–102], and pre-clinical data support that collagen limits delivery of chemotherapeutics. Thus, αSMA positive cells and collagen deposition are targets of interest to modify tumour perfusion and tumour response to therapy. Chapter 4 will target this pathway with the aim of improving tumour perfusion and reducing tumour hypoxia.

1.2 Patterns of tumour hypoxia

Solid tumours often develop regions with low oxygen content (i.e. hypoxia). Hypoxia is well characterized to directly provide tumour cells with resistance to radiation (the mechanism behind this will be detailed in Chapter 1.4)[103–105], and is associated with poor patient outcome[106,107]. Direct measurement of oxygen content in clinical and pre-clinical solid tumours

with oxygen electrode probes inserted directly into the tumour mass demonstrates that tumours are commonly very poorly oxygenated[107]. The dysfunctional vascular network in solid tumours contributes to the development of tumour regions with poor oxygen content (i.e. hypoxia). However, tumours are variable in terms of their vascular function. It is therefore worth noting that tumours are also variable in their hypoxic phenotypes, including pre-clinical tumour models and clinical tumours that do not develop an appreciable level of hypoxia or necrosis[52,108]. Thus, the following discussion of tumour hypoxia should be considered to describe phenomena that are pervasive, although not universal.

Hypoxia manifests in solid tumours in particular spatial and temporal patterns. Currently, two patterns of hypoxia are widely accepted to exist, chronic hypoxia and transient hypoxia. This section will discuss the evidence that describes the current understanding for both chronic hypoxia and transient hypoxia.

1.2.1 Chronic hypoxia

A critical observation in the balance of tumour growth with oxygen supply was made in a 1955 publication studying clinical bronchus carcinoma. The structure of these tumours was known to be that the carcinoma cells would proliferate to produce layers of tumour cells, but that the vascular supply was restricted to the adjacent stroma. In this system it was observed that layers of tumour cells reliably did not grow beyond ~150 μm in width, beyond which existed regions of necrosis[109]. This limit of growth was attributed to the limit of oxygen diffusion from the vasculature, calculations of which aligned more strongly with the onset of necrosis than calculations of glucose diffusion limits[109]. Later, the oxygen diffusion equation was solved for modeling diffusion of oxygen radially outwards from a central blood vessel supplying a surrounding cylinder of tumour cells[110]. This structure of a single blood vessel supplying a cylinder of tumour cells is referred to as a ‘tumour cord’. Tumour cord structures have since been identified extensively in clinical and preclinical tumours. In clinical and pre-clinical samples, maximum tumour cord radius is reported to range from 40-200 μm[109–113]. Thus, tumours develop common substructures of tumour cells dependent on local blood vessels and tumour-characteristic distances for the onset of necrosis.

If necrosis occurs at distances from blood vessels where anoxia is reached, then the maximum tumour cord width would be dependent on vascular oxygen content, tumour cell

density, and tumour cell oxygen consumption rate. Oxygen consumption rates of tumour tissue have been measured by growing tumours in mice, harvesting the tumour, and cutting ~2 mm sided 'tumour cubes'[114]. The maximum oxygen diffusion distance into the tumour cube can then be determined in culture and the cellular oxygen consumption rate determined mathematically. Thus, the oxygen consumption rate can be determined accounting for cellular density that was present *in vivo*. The interesting observation from these studies is that the rate of oxygen consumption between central and peripheral tumour regions is similar, despite regional differences in the amount of hypoxia that would be present *in vivo*[113,114]. The tumour-cube data imply that the occurrence of hypoxia must be dependent on oxygen supply and not intra-tumoural differences in oxygen consumption. The dependence of tumour cord maximum width on oxygen supply is further confirmed via gassing mice with either low (10% O_2) or high (100% O_2) gas for 68 hours. In one study employing this strategy, mean tumour cord radius decreased in mice subject to low O_2, and increased in mice subject to high O_2 gas[112]. Overall, a similar oxygen consumption rate across a tumour cell population within a tumour means that hypoxia, and necrosis, will occur at a predictable distance from a functionally perfused blood vessel based on vessel oxygen content. Thus, hypoxia will occur beyond the oxygen diffusion distance in regions where vascular density is sufficiently low. The onset of hypoxia will be tumour-specific, but often hypoxia is observed in tumour cells that exist beyond ~70-100 μm from the nearest perfused blood vessel[106,114,115]. This pattern of hypoxic cells at a distance from functional blood vessels is termed 'chronic hypoxia' or 'diffusion-limited hypoxia' (Figure 1.1).

1.2.2 Transient hypoxia

The oxygen content of a vessel will clearly modify the diffusion distance of oxygen, in turn modifying the distance from a perfused blood vessel at which hypoxia will occur. This is perhaps most obvious in the scenario of unstable microregional perfusion. As described in Chapter 1.1.1., microregional tumour perfusion may be dysfunctional for a number of reasons. The following paragraphs will further discuss the observations of unstable tumour perfusion and then describe their implications for hypoxia.

Researchers have observed fluctuations in erythrocyte flux in both model and clinical tumours. One method of detecting erythrocyte flux is laser doppler flowmetry (LDF), which is essentially a motion detection system that can sense flow of erythrocytes. By setting a number of

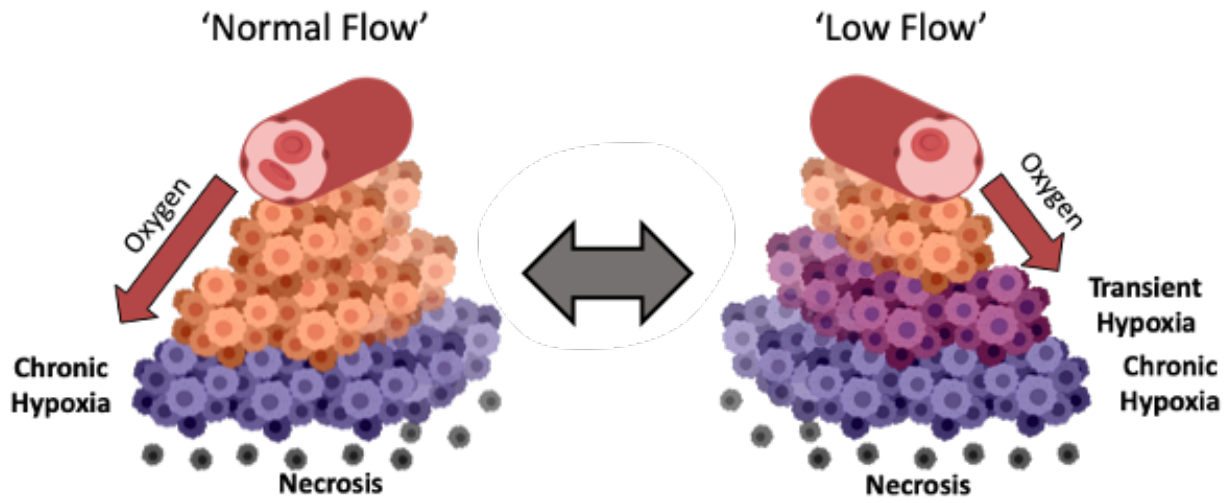

Figure 1.1 Chronic and transient hypoxia

Chronically hypoxic tumour cells reside beyond the oxygen diffusion limit of functional blood vessels, typically beyond ~70-100 μm from perfused blood vessels. Fluctuations in microregional perfusion may cause periods of low or poor blood flow, which may expose additional cell layers to hypoxia. These transiently hypoxic tumour cells may be reoxygenated if blood flow returns. Beyond ~150 μm from perfused blood vessels, oxygen and nutrients are so limiting that tumour cells may no longer survive and undergo necrosis. Figure created with BioRender.com.

LDF probes in different locations of a tumour, studies have made multiple important observations. Firstly, total erythrocyte flux summed across all LDF probes of a single tumour generally remains stable over time[116]. This indicates that bulk tumour perfusion is largely stable over time for solid tumours. However, across murine tumours, rat tumours, human tumour xenografts, and human clinical tumours, in almost all cases a sub-set of LDF probes report significant fluctuations in erythrocyte flux. The specifics of the fluctuations vary (i.e. magnitude and frequency), however, significant fluctuations that were maintained for 10-40 minutes before reversal were observed across species[116–119]. These two observations are evidence that unstable regional perfusion is a common feature of solid tumours, that perfusion may be stable in some tumour regions and not others, and that regional perfusion instability is not likely due to changes in bulk tumour perfusion.

Unclear from the LDF experiments is how fluctuations occur at the level of a tumour cord. Since this has implications for the development of hypoxia, microregional perfusion fluctuations have been assayed for individual tumour blood vessels by administering the fluorescent perfusion dyes Hoechst 33342 and $DiOC_7$ intravenously between 0-60 minutes apart[50,63,65,67,68,71]. Depending on the tumour, between 0 and 30% of vessels may be identified as experiencing a significant mismatch between the perfusion dyes, i.e. a perfusion fluctuation[50,63,67,71]. Durand et al employed this strategy and observed that the fraction of vessels experiencing a fluctuation increased as the separation time between dyes increased up to 10 minutes. The fraction of vessels experiencing a fluctuation was similar with 10 minutes through 60 minutes of separation between perfusion dyes[71]. These data suggest that a significant portion of the microregional perfusion fluctuations take at least 10 minutes to be realised and that quantification of longer cycles in this assay may be masked by reversal of the more rapid cycles. Overall, the data from fluorescent perfusion dye mismatch provide confirmation that significant fluctuations in LDF data can be recapitulated in the function of individual blood vessels and within similar time frames.

The observation that individual blood vessels may experience significant fluctuations in function provides the possibility that hypoxia may occur during periods of poor blood flow. Intravital microscopy provides a means to combine observation of the physical vascular network and time course quantification of erythrocyte flux with matched perivascular oxygen electrode probe measures. In these studies, fluctuations in erythrocyte flux are reflected by a positively

correlated change in perivascular oxygen content in most, but intriguingly not all blood vessels[119,120]. The positive correlation between erythrocyte flux and oxygen content supports that the degree of change in erythrocyte flux will contribute to deciding if hypoxia occurs due to a drop in blood flow. The observation that not all perivascular oxygen readings reflect changes in erythrocyte flux support that at least a second variable is at play. A potential explanation for vessels whose perivascular oxygen content does not acutely respond to fluctuations in erythrocyte flux is compensatory oxygen supply from nearby blood vessels. Oxygen electrode probes employed for these studies are cited to possess a spatial resolution of ~50 μm, and therefore in tumour regions of high vascular density the oxygen readings may be affected by multiple vessels. In agreement with this explanation, intra-vital imaging experiments report that the response of oxygen readings to erythrocyte flux is inversely linear with local vascular density[119]. That is, the perivascular oxygen content is more sensitive to vascular erythrocyte flux in tumour regions with lower vascular density. The interesting implication of the above studies is that tumour regions most sensitive to fluctuations in local perfusion are the same regions that are most likely to exhibit chronic hypoxia, due to low vascular density. Thus, tumour cords that contain chronic hypoxia due to limited oxygen diffusion may also contain cell layers subject to intermittent hypoxia during periods of low erythrocyte flux.

To review, intravital imaging studies reveal that fluctuations in erythrocyte flux induce significant fluctuations in oxygen delivery and subject additional tumour tissue to hypoxia. Further, these studies reveal that oxygenation in tumour regions with poor vascular density will be most sensitive to fluctuations in erythrocyte flux. Finally, these studies display explicitly that the fluctuations in erythrocyte flux do induce *reversible* fluctuations in oxygenation. These observations are further validated in studies employing only oxygen electrode probes, where fluctuations within the 10-60 min length observed in LDF and Hoechst 33342-$DiOC_7$ experiments may be observed across model tumours, spontaneous canine tumours, and human clinical tumours[118,119,121–125]. These data strongly support the existence of a population of tumour cells that are subject to reversible hypoxia. This pattern of hypoxia is referred to by a variety of names in the literature, such as “acute hypoxia”, “cycling hypoxia”, and “transient hypoxia”. In this thesis it will be referred to as “transient hypoxia” (Figure 1.1).

LDF data and fluorescent dye mismatch suggests that microregional perfusion fluctuates commonly in tumours, although to different degrees between tumours. Fluctuations in

erythrocyte flux correlate with significant fluctuations in local oxygenation for tumour regions with low vascular density, and this creates transient hypoxia. However, low vascular density also causes chronic hypoxia because in regions of low vascular density it is more likely that tumour cords will contain tumour cells beyond the oxygen diffusion limit. Since a defining feature of transient hypoxia is being non-hypoxic during periods of 'normal flow', it is hypothesized that transiently hypoxic tumour cells will reside more proximal to blood vessels than chronically hypoxic cells. If this model were true, then it should be possible to observe some hypoxic phenotype constant in cells at greater distances from blood vessels and variable over time in cells more proximal to blood vessels.

To provide evidence for transient hypoxia and in turn demonstrate the significance of transient hypoxia, researchers have made clever usage of Hoechst 33342. Hoechst 33342 diffuses outwards from perfused blood vessels, labelling cells with fluorescent intensity inversely correlated with distance from the blood vessel. Thus, fluorescence activated cell sorting may be applied to sort cells based on distance from perfused vessels. Two experimental designs in KHT murine sarcoma and SCCVII murine squamous cell carcinoma have yielded important observations. Firstly, if Hoechst 33342 is intravenously injected immediately prior to irradiation, then tumour cell survival from irradiation is inversely correlated with Hoechst 33342 fluorescence[64,65,69]. This indicates that tumour cells further away from blood vessels that are functional at the time of irradiation are most likely to be radiation resistant and hypoxic. Secondly, if Hoechst 33342 is intravenously injected 20 or 30 minutes prior to irradiation, then both Hoechst-bright and Hoechst-dim cell populations exhibit survival similar to the Hoechst-dim population from the first experiment[64,65,69]. These experiments provide two pieces of information: (1) that the oxygenation status of the Hoechst-bright cells must have decreased, and (2) that well-oxygenated cells are not contributing significantly to tumour cell survival at the radiation doses employed, otherwise the Hoechst 33342 bright cells should always exhibit reduced survival. That the survival of the Hoechst dim cells remains similar implies that the major population of the Hoechst dim cells are chronically hypoxic cells. These observations indicate that perfusion status is only predictive of radiation response at the time of irradiation, strongly supporting a link between microregional perfusion status and radiation response and supporting that periods of poor perfusion may expose tumour cells to hypoxia sufficient to

provide cells with resistance to radiation. These data also support the model that transient hypoxia occurs more proximal to blood vessels than chronic hypoxia (Figure 1.1).

Collectively, these observations describe the model of hypoxic tumour cords; well oxygenated tumour cells most proximal to blood vessels, transiently hypoxic cells at intermediate distances from blood vessels, and chronically hypoxic cells at greater distances on the border with necrosis (Figure 1.1).

1.3 Tumour cell turnover

Identification of the fraction of tumour cells in a solid tumour that are proliferative yields values between 20-50% for most tumours[67,68,126,127]. Multiple methods for determining the *in vivo* cell cycle time have been published, although data suggest it is similar to *in vitro* cell cycle time for many cell lines[128,129]. With both the growth fraction and cell cycle time known, one could hypothesize that a tumour will double in size in a matter of time equal to the cell cycle time divided by the growth fraction (sample tumour kinetics calculations in Appendix A.2). This value represents the ideal potential doubling time (T_{pot}) of the tumour. However, measuring model tumours by imaging or calipers indicates that tumours often do not double in the time predicted by T_{pot}. If the true doubling time (T_D) does not match T_{pot}, the difference is attributed to cell loss. The cell loss factor (calculation in Appendix A.2) represents the relation between T_D and T_{pot}; a cell loss factor of zero indicates growth fitting T_{pot} with no cells lost, a cell loss factor of 1.0 indicates loss of one cell per cell division and no tumour growth[130]. Tumours exhibit a range of cell loss factors, although many are greater than 0.5, indicating inefficient tumour growth with significant cell loss[128–130]. Tumour cells may be lost from the tumour due to necrosis, apoptosis, immune cell killing, or metastasis. Metastasis is usually disregarded as a minor contribution to cell loss, and apoptosis disregarded as tumour cells are generally resistant to apoptosis. The significant increase in growth rate of murine tumours implanted in immunodeficient mice instead of their syngeneic host indicates that immune cell killing is a significant source of cell loss[131]. However, immune cell killing may be ignored if studying human tumour xenografts in immunodeficient mice. Therefore, in human tumour xenografts tumour cell loss to necrosis is regarded as the major source of cell loss.

Necrosis is often observed beyond approximately 150 μm from perfused blood vessels in solid tumours, where nutrients become too limiting for tumour cell survival[109–113]. The tumour

cord model depicts chronically hypoxic tumour cells existing at the border between viable cells and necrosis. Thus, tumour cell turnover is in essence reflecting the turnover of hypoxic tumour cells. Three distinct methods have provided evidence that tumour cells typically 'flow' radially outwards from perfused blood vessels based on cell proliferation, i.e. as a normoxic tumour cell divides one of the daughter cells is pushed outwards, pushing a 'downstream' cell into a region of chronic hypoxia, and in turn a chronically hypoxic cell into a region of necrosis.

The first example of this tumour cell flow comes from injecting tumour-bearing mice with a single bolus dose of a uridine analogue to label cells that are actively proliferating. Many reports agree that tumour cells more proximal to blood vessels are more likely to be proliferating, and this is reflected in uridine analogue labelling[111,127]. However, over time uridine labelled cells are observed to occupy tumour cell layers at greater distances from blood vessels. As the uridine analogues are incorporated into the DNA of labelled cells, it is unlikely that the label is released and transferred to more distant cell layers. Instead, it is concluded that daughter cells of the initially proliferating tumour cells come to occupy more distant cell layers.

A second observation of outward flow of tumour cells comes from hypoxia-induced luciferase. Harada et al[132] produced tumours cells that would constitutively express luciferase after cleavage of an inhibitory gene sequence, dependent upon hypoxia-induced Cre expression. Cre expression is induced by hypoxia via inclusion of hypoxia response elements in the gene promoter, which are targeted by the hypoxia inducible factor (HIF) transcription factor in hypoxic cells. Temporal specificity was provided by the ER^{T2} technique, wherein Cre-ER^{T2} is only active in the presence of tamoxifen. Thus, treatment of mice bearing these tumours with tamoxifen induces constitutive expression of luciferase in tumour cells hypoxic at that point in time. Luciferase labelled cells were compared against staining for HIF1α, a HIF subunit only detected in hypoxia, and pimonidazole, an exogenous hypoxia reporter administered 2 hours prior to harvest. Twenty-four hours after tamoxifen treatment, tumour cord structures were observed with cells layered outwards from perfused blood vessels as follows: triple-negative non-hypoxic cells, cells positive for both luciferase and HIF1α, cells positive for only pimonidazole, and regions of necrosis. Forty-eight hours after tamoxifen, the distance from perfused blood vessels to either HIF1α or pimonidazole positive cells did not change as these report hypoxia at the time of harvest. However, the average distance from perfused blood vessels to luciferase positive cells increased to a value similar to the pimonidazole-positive cells.

Seventy-two hours after tamoxifen, luciferase positive cells were on average further from perfused blood vessels than both HIF1α and pimonidazole positive cells. Further, the total number of luciferase cells decreased each day after the initial 24-hour observation point, suggesting cell loss. These data show that hypoxic tumour cells 'flow' outwards from blood vessels and into regions of necrosis. Importantly, if tumours were irradiated 48 hours after tamoxifen (when luciferase positive cells were in pimonidazole positive regions), then the loss of luciferase positive cells was inhibited. This data supports that the flow of hypoxic tumour cells is due to proliferation of well-oxygenated tumour cells, which was inhibited following irradiation.

Finally, Van Der Kogel's research group published a report on the turnover of hypoxic tumour cell populations by administering pimonidazole 2, 24, 48, 72, 96, or 120 hours prior to CCI-103F (another exogenous hypoxia reporter), and CCI-103F always 2.5 hours prior to harvest[129]. CCI-103F and pimonidazole were shown to exhibit good agreement when administered only 2 hours apart. With this strategy the change in the fraction of positive cells over time was interpreted as turnover of hypoxic tumour cells, e.g. if the amount of tumour area labelled by pimonidazole is 50% of the area labelled by CCI-103F then 50% of the hypoxic fraction was lost in the separation time. Similar to Harada et al[132], with increased separation between the 2-nitroimidazoles the total tumour area positive for pimonidazole decreased and pimonidazole came to exclusively label cells bordering regions of necrosis. Reported hypoxic cell half-lives ranged from only 17 hours in the rapidly proliferating C38 murine colon carcinoma, to still only 49 hours in the SCCNij3 human laryngeal carcinoma. To date, this is the only publication explicitly reporting a value for the expected rate of turnover for specifically hypoxic tumour cells. A limitation of this study is a lack of consideration for other potential sources of 2-nitroimidazole loss, which will be considered in Chapter 2 when this thesis investigates hypoxic cell turnover. This study, along with the study by Harada et al, indicates that a significant number of hypoxic cells are likely to turnover within 48 hours after labelling.

Taken together, these three experimental approaches display the connection between tumour cell proliferation and passive movement of tumour cells radially outwards from perfused blood vessels. These studies indicate that turnover of hypoxic tumour cells is continuous and that the half-life of hypoxic cells may be within two to three days. Further, these data support that hypoxic cell turnover is due to flow of cells into regions of necrosis. However, these studies do not consider distinguishing between chronic and transient hypoxia, and to date the relative

lifetime of each hypoxic population is unknown. Addressing this gap in knowledge will be the focus of the research in Chapter 2.

1.4 Ionising radiation and oxygen

Perhaps the most well-known effect of tumour hypoxia is that it provides tumour cells with resistance to radiation. The presence of hypoxia predicts for poor tumour response and worse patient outcome, indicating that hypoxic tumour cell radiation resistance is clinically significant[106,133,134]. This thesis is interested in addressing tumour hypoxia in order to improve tumour radiation response. This section will briefly introduce radiation, radiotherapy, discuss how radiation is toxic to cells, and discuss the importance of oxygen for radiation cytotoxicity. For discussing radiotherapy, this section will focus on external beam radiation and not brachytherapy (implanting a radioactive source into the tumour).

Radiation is any emitted or transmitted energy in the form of particles or photons. The biological response of cells to irradiation may differ between particle and photon radiation. This thesis will be focused on photon radiation as this is currently much more widely used for radiotherapy. Ionising radiation is radiation that possesses sufficient energy to liberate an electron from an atom and thus break covalent bonds. This threshold in energy is achieved by x-rays and gamma-rays, while ultraviolet radiation is the highest energy form of non-ionising electromagnetic radiation. It may be noted that the standard energy level of radiation produced by experimental x-ray machines is 250 keV (kiloelectron volts), while clinical linear accelerators may produce radiation with energy levels in excess of 1 MeV. Thus, radiation for radiotherapy generally refers to high-energy x-rays.

Radiation dosing is measured in “gray” (Gy). One gray is defined as the absorption of one joule per kilogram of matter. For scale, the annual background radiation exposure for a person living in Vancouver, Canada is equivalent to 1.3 mGy, mild symptoms of radiation sickness may arise from exposure to as low as ~300-500 mGy if received within a short period of time (order of minutes), a single-exposure dose of 4 Gy is often lethal if a large portion of the body is exposed, and an entire clinical course of radiotherapy is often in excess of 50 Gy[135,136]. Clearly, radiotherapy protocols must minimize normal tissue exposure in order to limit side effects. The most obvious method to protect normal tissue is to target the radiation to the tumour site with most of the body shielded. However, normal tissue at the margins of the tumour is often

intentionally included within the radiation field in order to ensure killing of microscopic disease outside of the obvious tumour mass. Further, some normal tissue may be difficult or impossible to shield due to the location of a tumour, e.g. for a centrally located lung tumour the radiation must travel through and expose the skin, skeletal muscle, and some normal lung. Due to the inevitable exposure of normal tissue, traditional radiotherapy reduces the acuteness of radiation by spreading out a patient's total clinical dose (~50-70 Gy) into "fractions". Fractionated radiotherapy typically consists of 2 Gy per day five days per week. Dose fractionation is conducted based upon understanding that normal cells are more capable of repairing damage induced by radiation than tumour cells, thus the time in between doses may allow normal cells to recover while still killing tumour cells[130]. However, improvements in imaging and engineering of radiation-delivering devices are progressively allowing for reduced normal tissue exposure, motivating many to test "hypo-fractionated" radiotherapy protocols with increased dose per fraction and fewer total fractions required. Overall, tissue response to radiation depends on the magnitude of radiation dose received and the time frame within which the radiation dose is delivered.

As mentioned above, ionising radiation has the potential to liberate electrons from atoms and therefore break covalent bonds. Radiation may disrupt the structure of a variety of biological macromolecules, however, radiation cytotoxicity is dependent on damaging cellular DNA. A fundamental observation in support of this fact was performed by precise irradiation of hamster fibroblasts with alpha particles emitted from a microneedle; T.R. Munro found that high doses of irradiation to the cell cytoplasm had no effect on cell proliferation, but, that substantially smaller doses of irradiation targeting the cell nucleus were lethal[137]. This observation made clear that chemical changes induced by radiation outside of the nucleus are not lethal and justifies focusing on radiation-induced damage to nuclear material, of which DNA is the major concern.

Radiation may damage DNA by directly liberating electrons in DNA molecules, producing a DNA radical (i.e. molecule with an unpaired electron) that may resolve by breaking chemical bonds[138]. If radiation ionizes a molecule in the phosphate-sugar backbone of DNA, it has the potential to cause a break in the strand of DNA. Radiation as low in energy as 1-5 keV has potential to induce DNA strand breaks[139,140], thus it is clearly possible for experimental and clinical x-rays in excess of 100 keV to directly induce DNA strand breaks. Alternatively, radiation may deposit energy in molecules near to DNA. As 70-80% of cell composition is

water, it is useful to consider the case of radiation-induced ionisation of water molecules nearby a DNA molecule[130]. Ionisation of water molecules may induce DNA strand breaks in two ways: (1) the released electron from the ionisation event ($H_2O \rightarrow H_2O^+ + e^-$) is a form of radiation itself, commonly of 10 keV in energy, that may produce DNA strand breaks[139,140], and (2) the resulting hydroxy radical ($H_2O^+ + H_2O \rightarrow H_3O^+ + HO^-$) may cause DNA strand breaks by extracting an electron from the DNA backbone, leaving behind a DNA radical that may resolve as a strand break[130,138–140]. Overall, radiation may cause ionisation of DNA into a DNA radical, either directly or indirectly, leading to DNA strand breaks.

Upon ionisation into a radical, the fate of a DNA molecule depends upon the chemical milieu. As mentioned just previously, left alone a DNA radical may resolve as a strand break[138]. DNA radicals may also be resolved through redox reaction with intranuclear thiols such as glutathione to restore the stable DNA molecule[105,138,141]. This observation is supported by experiments that treated cells with buthionine sulfoximine to deplete cellular glutathione prior to irradiation and found increased DNA damage after harvesting cells within 20 seconds of irradiation[105]. Alternatively, molecular oxygen (O_2) is highly reactive with radicals and can react with radicals in DNA ribose groups to form an organic peroxide, which leads to release of phosphodiester bonds and causes DNA strand breakage[130,138]. This role of O_2 comes from a number of experiments that demonstrate: (1) the presence of O_2 at the time of irradiation significantly increases the number of induced DNA strand breaks and reduces cell survival[103–105,142–148], and (2) that addition of O_2 to previously anoxic cells within ~50-100 μs after irradiation produces similar cell kill and DNA damage as when O_2 is present during irradiation[104]. The latter experiment is interpreted to exclude the possibility that O_2 sensitizes cells to irradiation by contributing to production of DNA radicals. Instead, these experiments indicate that O_2 reacts with DNA radicals produced by radiation in order produce stable DNA strand breaks. Herein lies the ‘oxygen fixation hypothesis’ where the presence of oxygen at the time of irradiation fixes (i.e. makes permanent) radiation-induced damage in the form of stable DNA strand breaks[130]. Of course, hypoxic tumour cells possess less oxygen and therefore fewer DNA breaks are induced by radiation. This is the accepted mechanism for why hypoxic tumour cells are resistant to radiation therapy across tumour sites.

Implied in the discussion of the oxygen fixation hypothesis above is that DNA strand breaks directly lead to cell death. In a simplified sense this is true, as the probability of cell

survival is inversely proportional to the number of DNA strand breakages observed following irradiation[149–151]. However, cells contain machinery to repair DNA breaks, which makes some DNA damage more harmful than others. Single strand breaks (SSB) refer to a breakage in one of the two DNA backbone chains. SSBs may be repaired by processes of base excision repair (BER) or nucleotide excision repair (NER). SSB repair involves, briefly, excision of nucleotides on the damaged strand of DNA in the vicinity of the lesion, followed by fresh polymerization based on the in-tact template strand, and then ligation[130]. Error in repair of isolated SSBs may result in mutation, but error is unlikely to significantly disrupt cell function as the DNA molecule will remain in-tact. Further, the number of SSBs induced by radiation is reported to be on the order of thousands per Gy per cell and therefore the induction of SSBs does not match the modest cytotoxicity of low radiation doses[130,152]. Overall, SSBs are abundant DNA lesions induced by radiation, but in isolation are not toxic.

If two or more SSB occur on opposing DNA strands in relative proximity, then the DNA molecule may break into two pieces. This describes a double strand break (DSB). DSBs may be repaired by two mechanisms, homologous recombination (HR) and non-homologous end joining (NHEJ). A cell in the G2 cell cycle phase may employ HR, which entails use of a sister chromatid as a template to reconstruct and ligate the broken strands. In cells lacking sister chromatids, the only option remaining is attempting to rejoin the ends of two broken pieces of DNA via NHEJ. Experimentally based estimates for the induction of DSBs by radiation range from 20-60 DSBs per Gy per cell[130,152–155]. The majority of the initial DSBs produced by irradiation are rejoined within 1 hour of irradiation via NHEJ, leaving ~20% that are repaired slowly by either NHEJ or HR[156,157]. Notably, unlike SSB repair, error in DSB repair may result in chromosome abnormalities if DNA fragments are ligated to incorrect partners or not ligated at all (e.g. large deletions or dicentric chromosomes)[130,158]. DSBs may therefore result in significant disruption to cellular function.

In normal cells, the DNA damage response pathway will ultimately signal for apoptosis if DNA cannot be adequately repaired. Tumour cells commonly exhibit mutations in DNA repair and apoptosis pathways, which allows tumour cells to progress through the cell cycle despite the presence of unrepaired DNA damage or chromosome abnormalities. However, chromosome abnormalities may cause significant loss of genetic material in daughter cells upon mitosis, leading to cell death. This form of cell death is often termed “replicative cell death” or “mitotic

cell death" and is the dominant form of cell death induced by radiation for tumour cells. Cornforth and Bedford[158] quantified radiation-induced chromosomal aberrations in human fibroblasts and reported a number of significant findings. First, the average number of chromosome abnormalities increased from ~1.0 per cell following 4 Gy radiation to ~5.5 per cell following 12 Gy, and the abundance of chromosome abnormalities was significantly greater in fibroblasts with reduced capacity for DSB repair. Together these observations indicate that chromosome aberrations are a result of erroneous or incomplete repair of DSBs induced by radiation. Second, the average number of chromosome aberrations per cell inversely correlates nearly one-to-one with the natural logarithm of cell survival, as would be expected from a random distribution of lethal chromosome aberrations. Finally, the fraction of cells *without* chromosome aberrations correlates strongly with the fraction of cells that survive radiation. Together, these observations strongly suggest that chromosome aberrations are the lethal lesion induced by radiation as a result of erroneous or incomplete DSB repair.

To review, radiation may produce DNA radicals either directly or indirectly, the presence of O_2 significantly increases the likelihood that DNA radicals resolve as DNA SSBs, multiple SSBs in proximity of one another may produce DSBs, which if inefficiently repaired may induce apoptosis in normal cells or lead to lethal chromosome abnormalities. Importantly, oxygen is the main factor within this process that will vary strongly within a given tumour. The oxygen dependence of tumour cell radiation response may be assessed by simply irradiating tumour cells *in vitro* and quantifying cell survival or the induction of DSBs. The extreme scenario, comparing anoxic cells gassed with N_2 against aerobic cells (atmospheric 21% O_2), yields the observation that across a wide range of radiation doses anoxic cells require ~2.5-3 times the radiation dose to induce similar cell kill as for aerobic cells[134,159,160]. This factor of 2.5-3 is referred to as the oxygen enhancement ratio (OER). By repeating *in vitro* experiments with varying O_2 concentrations, multiple studies observe the O_2 concentration that induces half-maximal radiosensitization is approximately 0.5% O_2 (~3.8 mmHg)[143,159,160]. Little change in radiation sensitivity is observed by increasing O_2 concentrations above 2% (~15 mmHg)[143,159,160]. Thus, to optimize radiation response the population of tumour cells below 0.5% O_2 should be minimized, and ideally the population of tumour cells above 2% O_2 should be maximized.

Alternatives to increasing oxygen content at the time of irradiation include novel strategies for radiation itself. Photon radiation is an example of low linear energy transfer (LET)

radiation, a measure of the amount of energy deposited by radiation per unit distance travelled. In other words, photon radiation deposits energy relatively sparsely, which limits the probability of SSBs occurring in close enough proximity to produce DSBs. Conversely, particle radiation – whether proton or heavy ion – deposits energy more densely, i.e. with high LET. Pre-clinical data display clearly that with increasing LET there is a reduced OER[161]. Hypotheses to explain the reduced OER observed with increasing LET radiation are varied[161]. These range from a simple suggestion that oxygen is no longer required if the LET radiation is able to induce sufficiently dense DNA breaks to cause cytotoxicity, to suggesting that high LET radiation actually generates oxygen along the tracks of radiation particles via radiolysis of water[162]. Regardless, proton and carbon ion radiation therapy are being applied for clinical care in some parts of the world and may provide a solution to hypoxia-induced radiation resistance.

1.5 Detection & characterization of tumour hypoxia

Hypoxia in solid tumours is largely quantified by one of four methods: direct measurement of oxygen content using oxygen electrode probes, inference of hypoxia based on the presence of tumour cells resistant to radiation, labelling of cells by exogenous markers of hypoxia, or detection of cells expressing proteins induced by hypoxia.

1.5.1 Oxygen electrode probes

The gold standard for quantifying oxygen content in solid tumours is with an oxygen electrode probe. An oxygen electrode probe is the only method capable of reporting a particular local oxygen content in mmHg, allowing for tumour oxygenation to be directly correlated with tumour biology or patient outcome. Oxygen electrode probes have been widely applied to quantify oxygenation in clinical tumours, particularly in tumour sites where measurements can be made relatively non-invasively such as head and neck cancers, prostate cancer, or cervical cancer. By taking numerous readings across multiple tumour regions it is possible to make generalizations of the oxygen content in the tumour and correlate these measures with outcome. A drawback of oxygen electrode probes is the requirement to define a threshold for hypoxia with which to divide a patient population and compare survival curves. This has produced variability in the published reports of oxygen readings from clinical tumours with no consensus definition for a ‘hypoxic’ tumour. Although, hypoxic tumours are most commonly defined as exhibiting a

median oxygen reading being below 5-10 mmHg pO_2. Regardless, the direct quantification of oxygen content with electrode probes has yielded valuable data on tumour oxygenation and correlating oxygen content with patient outcome. Firstly, oxygen electrode probe readings have made it clear that oxygenation is significantly lower in solid tumours relative to most normal tissue[13,107,163,164]. Oxygen electrode probe readings demonstrate that poorly oxygenated tumours are associated with worse patient outcome than better oxygenated tumours across tumour sites whether patients receive chemotherapy, radiotherapy, or even curative-intent surgery[13,106,133,164–166]. Overall, oxygen electrode probes have provided the most direct quantification of tumour tissue oxygenation and the clearest evidence that poor oxygenation predicts poor patient outcome.

1.5.2 Radiation-based assays

Two significant limitations of using oxygen electrode probes for pre-clinical study include the lack of single cell resolution and the potential of unknowingly quantifying oxygen within regions of necrosis, which may underestimate the oxygenation of viable tumour cells. To address these concerns researchers traditionally applied the knowledge that hypoxic tumour cells are significantly resistant to ionising radiation[103,130,167]. Numerous radiation-based survival assays may be applied, typically comparing the survival of untreated tumours to paired tumours that are made completely hypoxic (e.g. clamping off the blood supply to the tumour during irradiation for tumour control assays or asphyxiating the host animal prior to irradiation and harvest of the tumour cells for *ex vivo* survival assay)[167,168]. In a paired *ex vivo* survival assay, a series of untreated and hypoxic tumours are irradiated with different radiation doses. The survival of the tumour cells from the untreated mice is demonstrated to produce a biphasic curve. With low doses of irradiation there is a steep slope in survival reflecting the high sensitivity of the well-oxygenated tumour cells. With higher radiation doses (≥ ~10 Gy) the slope of tumour cell survival slows, reflecting the radiation resistance of hypoxic tumour cells. The hypoxic phase of the survival curve for tumour cells from untreated mice is demonstrated to be parallel to the survival curve produced from tumour cells of asphyxiated mice. The ratio of tumour cell survival in cells from the untreated mice over the cells from the hypoxic mice gives the fraction of cells that were hypoxic in the untreated tumours (Figure 1.2)[167]. In summary, radiation-based

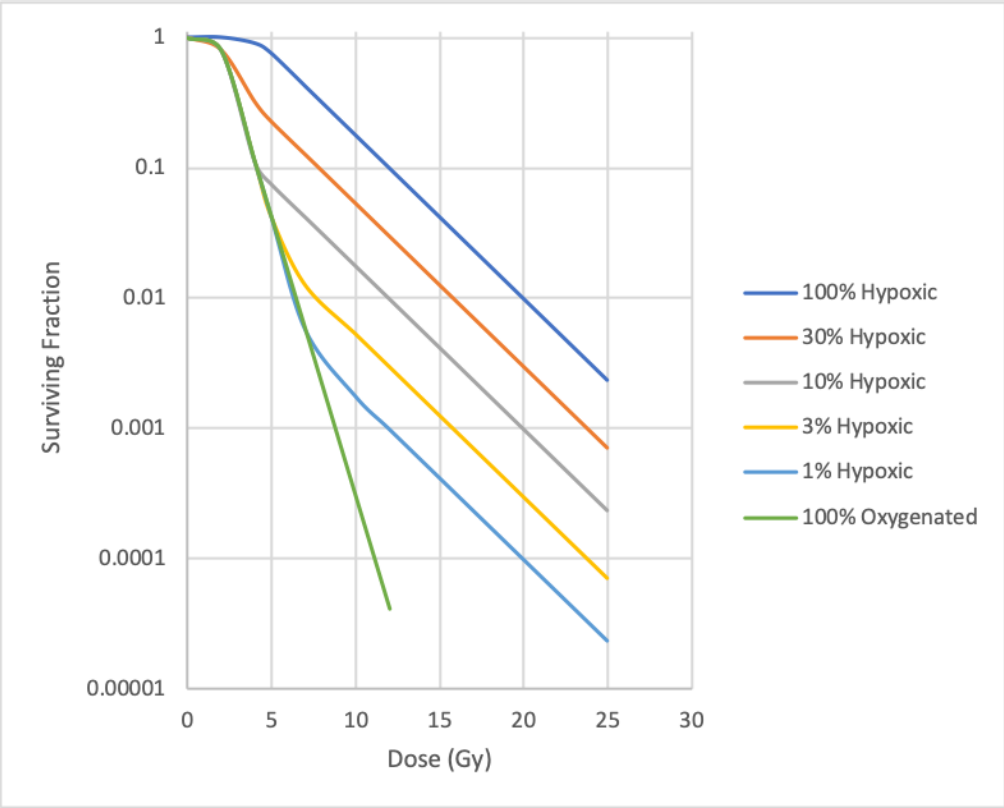

Figure 1.2 Theoretical survival curves for determining the hypoxic fraction

Theoretical survival curves for tumour cells derived from tumours with varying populations of radiobiological hypoxia. Survival is plotted on a logarithmic scale. With increasing dose, the survival curves become parallel to that of a tumour made to be 100% hypoxic. The hypoxic fraction of a tumour is determined by comparison of survival against the 100% hypoxic curve. For example, consider the surviving fraction plotted for a radiation dose of 20 Gy: 0.01 for the 100% hypoxic tumour, 0.001 for a tumour that is 10% hypoxic, and 0.0001 for a tumour that is 1% hypoxic. Figure adapted from Van Putten LM and Kallman RF. *JNCI*. 40(3):441-451.

assays determine the hypoxic fraction characteristic of a particular tumour line by comparison of untreated tumours with a paired set of tumours made to be hypoxic.

The assumptions of radiation based assays include (1) that cells in tumours made to be hypoxic will respond to radiation similarly to those that are naturally hypoxic, (2) that nothing else in the tumour is altering radiation response other than tumour cell oxygenation, and (3) that the untreated tumours contain only two populations, a well-oxygenated sensitive population and a hypoxic resistant population. Setting aside the first assumption, the second assumption is a concern for tumour control assays, where tumours are not harvested following irradiation and the hypoxic fraction is inferred based upon the dose required to cure 50% of the tumours. It is now well demonstrated that large single doses of radiation above ~8 Gy induce apoptosis of tumour endothelial cells, resulting in the killing of large populations of tumour cells regardless of oxygenation at the time of irradiation[169,170]. Tumour control assays often rely upon high doses in excess of 30 Gy[168]. Thus, the hypoxic fraction estimate from tumour control assays will carry a significant error in determining the fraction of cells that were hypoxic at the time of irradiation.

Regarding the third assumption, it can be shown *in vitro* that tumour cell sensitivity to radiation decreases incrementally below approximately 15 mmHg pO_2 (~2% O_2), reaching 50% of the sensitivity of matched well-oxygenated cells at approximately 3.8 mmHg pO_2 (0.5% O_2), and reaching minimal sensitivity in anoxia[130]. Thus, radiation resistance versus oxygenation is continuous, not a step function. Oxygen electrode readings clearly indicate that tumours should be expected to contain regions of both severe (< 5 mmHg) and intermediate (5-15 mmHg pO_2) levels of hypoxia[13,171]. However, it is likely that radiation-based assays of the 'hypoxic fraction' are specific to the severely hypoxic population. Firstly, the 'hypoxic fraction' calculated from the radiation assays correlates more strongly with the fraction of oxygen electrode readings below 5 mmHg pO_2 (~0.65% O_2) than with the fraction of oxygen readings below 10 mmHg pO_2 (~1.3% O_2)[172,173]. Secondly, intermediately hypoxic tumour cells are predicted in modelling studies to contribute to tumour cell survival following modest radiation doses and to not modify survival following relatively high (≥ ~10 Gy) doses[174]. Further, it is likely that the paired hypoxic tumours (e.g. asphyxiated mice) contain exclusively severely hypoxic cells and therefore survival ratios will calculate the content of severely hypoxic cells[174]. Thus, it is likely that radiation-based determinations of the 'hypoxic fraction' reflect tumour cells that are very hypoxic, likely below or well below 5 mmHg pO_2 (~0.65% O_2). Publications today more

commonly describe the results of radiation-based assays as estimations of the 'radiobiological hypoxic fraction'.

1.5.3 2-Nitroimidazoles

Radiation-based assays provide an estimate of the whole tumour hypoxic fraction characteristic for the studied tumours, but these assays are restricted in that hypoxic cells may not be identified without the significant intervention of irradiation and these assays cannot be applied to clinical tumours. Exogenous reporters of hypoxia that label tumour cells based on oxygenation address these issues by allowing for antibody-based detection of labelled hypoxic cells. The most widely used exogenous hypoxia reporters are 2-nitroimidazole compounds. When 2-nitroimidazoles are taken up into cells they may be reduced to a nitro radical by various nitroreductase enzymes in the cell. Molecular oxygen is highly reactive to radicals, thus in the presence of oxygen the 2-nitroimidazole radical may be rapidly oxidized back to the neutral parent compound. In the absence of oxygen, the 2-nitroimidazole radical may undergo further reduction to a hydroxylamine, which may covalently bind to protein thiols in the cell[175,176] (Figure 1.3). Binding of the reduced hydroxylamine to protein traps the 2-nitroimidazole inside of the cell, effectively labelling the cell. Therefore, the degree of 2-nitroimidazole labelling is dependent upon the following: (1) cell viability as functional nitroreductase enzymes and reducing equivalents are required for the reaction, (2) degree of hypoxia as the production of the 2-nitroimidazole radical is rapidly reversible in the presence of oxygen, and (3) concentration of 2-nitroimidazole and duration of cell exposure to 2-nitroimidazole in hypoxia. The latter point refers to the mechanism of cell labelling as an accumulation of 2-nitroimidazole adducts to thiols, which may increase with time and 2-nitroimidazole concentration. Numerous 2-nitroimidazoles have been developed and validated based on this principle of oxygen-sensitive cell labelling. This thesis work includes the use of the 2-nitroimidazoles pimonidazole and EF5 (Figure 1.3).

The most common readout of 2-nitroimidazole labelling for pre-clinical study is fluorescence intensity in flow cytometry or microscopy. Antibody detection of 2-nitroimidazoles and fluorescence-based readouts of 2-nitroimidazole cell labelling appear reasonable based upon *in vitro* experiments observing excellent correlation between radioactivity and fluorescence intensity of cells labelled with radioactive EF5[177,178]. However, in either flow cytometry or

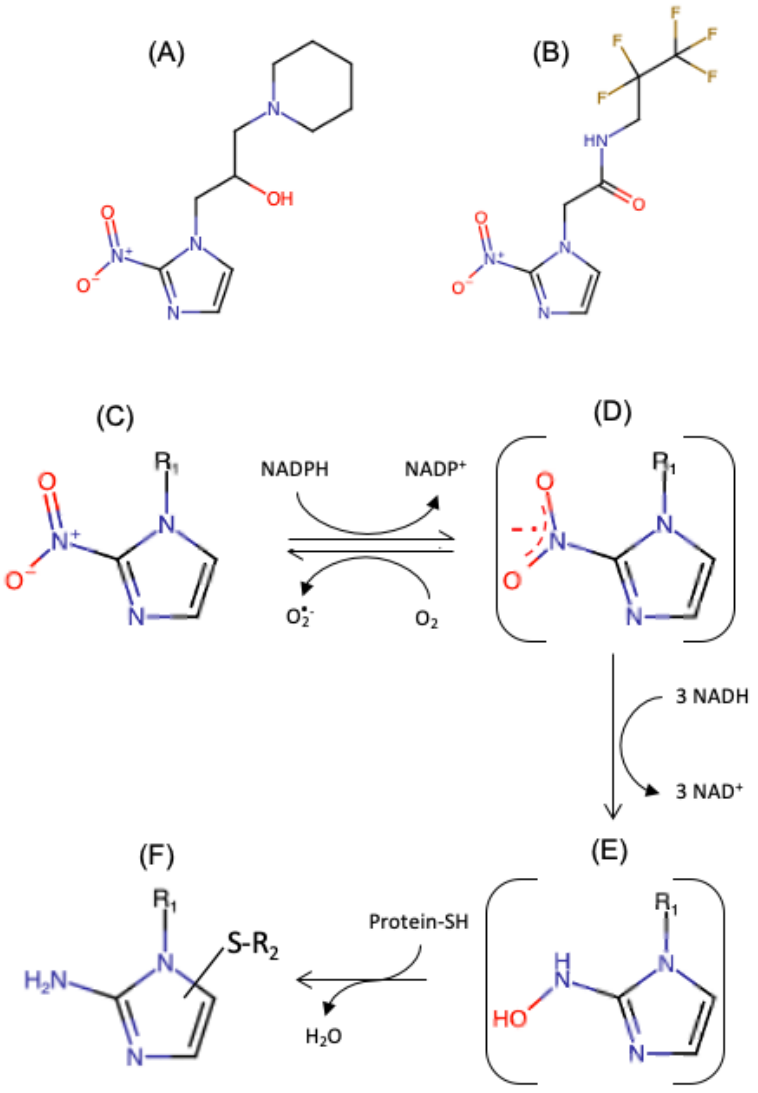

Figure 1.3 2-Nitroimidazole structure and reduction

(A) Pimonidazole, (B) EF5. Mechanism of 2-nitroimidazole labelling is displayed. (C) 2-Nitroimidazole base structure, R = side group. (D) Nitro-radical anion intermediate. The conversion of (C) to (D) is reversible in the presence of oxygen. (E) Hydroxylamine intermediate. (F) 2-Nitroimidazole adduct bound to intracellular protein thiols (S-R_2).

immunofluorescent microscopy analysis, it is standard to set a threshold and binarize the tumour cell population as either 2-nitroimidazole positive or negative, and in turn hypoxic or non-hypoxic. It is therefore important to consider at which oxygen tension 2-nitroimidazole labelling will result in significantly greater fluorescence intensity compared with background. Binding curves for 2-nitroimidazoles have been produced *in vitro* and through a variety of methods *in vivo*. EF5 fluorescence assessed by flow cytometry from multiple cell lines cultured with EF5 *in vitro* found that fluorescence intensity increased incrementally as oxygen decreased from 5% O_2 to 0.5% O_2. Above 5% O_2 little change in 2-nitroimidazole labelling is observed, and below 0.5% O_2 the rate of change in fluorescence intensity decreased[177,178]. In murine tumours, mean tumour EF5 fluorescence intensity in microscopy was non-linear when plotted as a function of mean tumour oxygenation determined prior to sacrifice using electron paramagnetic resonance oximetry. In these experiments, the greatest increase in fluorescence intensity occurred in tumours with a mean oxygenation below 0.5% O_2[179]. In comparison with radiation-based assays in tumour xenografts, the fraction of EF5 positive tumour cells assessed from flow cytometry was shown to have a strong correlation with radiation-based estimates of the hypoxic fraction, indicating strong correlation with severe hypoxia. In one study EF5 exhibited a weak correlation with the fraction of oxygen electrode readings below 5mmHg, although the oxygen electrode readings were similarly only weakly correlated with radiation assays, suggesting bias in the electrode readings[179–181]. As for pimonidazole, *in vitro* pimonidazole labelling detected by ELISA found strong labelling in cells cultured in 0.5% O_2 or below compared with cells cultured in 5% O_2 or above[182]. Pimonidazole is reported to exhibit a similar labelling curve as misonidazole, an earlier generation 2-nitroimidazole, which was demonstrated to label tumour cells in spheroids where oxygen electrode readings dropped below 10 mmHg pO_2 (~1.3%)[183]. Finally, pimonidazole positive tumour area in IHC of orthotopically implanted murine mammary carcinomas strongly correlated with the oxygen electrode readings and estimations of the radiobiological hypoxic fraction of matched tumours[184,185]. In summary, EF5 and pimonidazole are well validated compounds that label viable cells below approximately 1% O_2 with fluorescence intensity increasing as oxygen content during exposure decreases. Reports for both pimonidazole and EF5 have observed the strongest increase in labelling for cells cultured at or below 0.5% O_2. Overall, the oxygenation threshold leading to identifying a tumour cell as

positive for EF5 or pimonidazole, and therefore identified as hypoxic, likely lies between 0.5-1% O_2.

Both pimonidazole and EF5 have shown strong ability to distinguish hypoxic from well-oxygenated tumour cells across multiple tumour models, as well as accurately identifying hypoxia in non-tumour tissues[127,176–178,182]. The published literature suggests that the oxygen dependency of pimonidazole and EF5 labelling is robust enough to accurately distinguish hypoxic and non-hypoxic cell populations *within* a tumour despite potential cell intrinsic differences such as nitroreductase enzyme expression. However, differences in relative fluorescence intensity across tumour xenografts does suggest caution in applying 2-nitroimidazoles as a means to compare absolute oxygen tensions *between* tumour types.

An additional benefit of exogenous hypoxia reporters is the potential for radiolabelling and non-invasive imaging of hypoxia using PET. The first 2-nitroimidazole tested for non-invasive detection of hypoxia in clinical tumours was fluorinated misonidazole (FMISO), a precursor to compounds including pimonidazole, in non-small cell lung cancer, head and neck cancer, and prostate cancer[186]. Fractional hypoxic volumes ranging from 0-95% indicated a strong dynamic range of the radiotracer, suggesting utility of non-invasive imaging to distinguish well-oxygenated from poorly-oxygenated tumours[186]. Optimization of PET hypoxia radiotracers is a balance between increasing diffusion into tumour tissue to increase uptake signal in hypoxic regions, against achieving rapid clearance of the tracer so as to reduce background. To achieve greater tissue distribution at the cost of clearance, the relatively lipophilic EF5 has been radiolabelled for PET imaging. Initial study with ^{18}F-EF5 in head and neck cancer observed that tumour regions of high ^{18}F-EF5 uptake corresponded to regions with low perfusion, indicated by low ^{15}O-H_2O uptake[187]. Follow-up studies in head and neck cancer patient concluded that ^{18}F-EF5 uptake was predictive of radiation response and patient outcome[188,189], supporting further use of ^{18}F-EF5 in head and neck sites, with pre-clinical studies suggesting utility in additional sites such as prostate and lung cancers[190,191]. Other 2-nitroimidazoles have been developed that are more hydrophilic than ^{18}F-EF5 and FMISO with the goal of optimizing clearance to improve the signal over background ratio. These include fluoroetanidazole (FETA), fluoroerythronitroimidazole (FETNIM), fluoroazomycinarabinofuranoside (FAZA), and HX4[106]. Despite ongoing clinical trials for multiple radiolabelled 2-nitroimidazoles, many agree that

head-to-head comparisons will be required to determine if any radiotracer is superior to another, and this may have to be conducted on a site-by-site basis[106,192].

1.5.4 HIF and endogenous hypoxia markers

The 2-Nitroimidazoles pimonidazole and EF5 provide a means to assess hypoxia in microscopy, allowing for researchers to relate hypoxia with other features of tumour biology in pre-clinical and clinical samples. However, 2-nitroimidazole labelling itself is not necessarily identifying all cells that are responding to low oxygenation. The primary and most well characterized cellular response to poor oxygenation is formation of the hypoxia inducible factor (HIF) transcription factor. HIF is a heterodimer of an alpha and beta subunit. Mammalian cells constitutively transcribe and translate both HIF1α, HIF2α, and HIF1β. The formation of HIF is controlled by regulating the degradation of the alpha subunits. The enzymes primarily responsible for regulation of HIF alpha subunit degradation are iron, 2-oxoglutarate, and oxygen dependent prolyl hydroxylase (PHD) 1-3 enzymes[193,194]. In oxygenated conditions, PHD enzymes consume oxygen to hydroxylate two proline sites of the oxygen degradation domain present in both HIF1α and HIF2α. This hydroxylation creates a binding site on HIF1α and HIF2α for the ubiquitin ligase protein Von Hippel Lindau tumour suppressor protein (VHL). VHL activity directs the ubiquitination of the HIF subunits, which targets the proteins for proteasomal degradation. The activity of PHD enzymes is inhibited in hypoxia, thus, in hypoxia HIF1α and HIF2α are not targeted for degradation and can instead dimerize with HIF1β to initiate transcriptional activity[195]. While not regulating HIF subunit degradation, HIF activity is also regulated in an oxygen dependent manner by the factor inhibiting HIF (FIH) protein. FIH carries out oxygen-dependent hydroxylation of an asparagine in either HIF1α or HIF2α, which inhibits dimerization with HIF1β[194]. Some evidence suggests greater affinity of FIH for HIF1α compared with HIF2α, providing a mechanism for differential regulation of the alpha subunits[196]. The majority of research on focuses on HIF1α rather than HIF2α. The oxygen tension leading to stabilization of HIF1α varies between cell lines, although HIF1α protein or its transcription targets are often detectable in cells cultured in up to 2% O_2[106]. The number of genes induced by HIF1 is recently reported to be greater than 1500[197]. HIF1 binds to hypoxia responsive elements (HREs) in gene promoters that contain the sequence NCGTG (N is either A or G), directly upregulating the expression of proteins that aid in cell survival under hypoxia and nutrient

deprivation, including anaerobic metabolism, pH regulation, angiogenesis, and autophagy[197]. Thus, HIF1 and its transcriptional targets provide potential endogenous markers of cells that are experiencing hypoxia. HIF1α itself, carbonic anhydrase IX (CAIX), and glucose transporter 1 (GLUT1) in particular have been widely assessed in microscopy of pre-clinical and clinical tumours to quantify hypoxia[106]. Across solid tumours, it is clear that the majority of 2-nitrimidazole labelled cells are also positive for HIF1α or its transcription targets[115,132]. However, HIF1α and its transcription targets are also reliably found a few tumour cell layers more proximal to perfused blood vessels than 2-nitroimidazole positive cells, thus confirming the *in vitro* observations of HIF1α stabilization at oxygen concentrations greater than 2-nitroimidazole labelling, approximately 1-2% O_2 and 0.5-1% O_2 respectively[115,132,198]. Overall, HIF1α and its transcription targets indicate cellular response to hypoxia, but this occurs at higher oxygen concentrations than 2-nitroimidazole detection.

In summary, tumour hypoxia refers to tumour regions with poor oxygenation. Traditional methods of radiation-based assays likely relate to oxygenation well below 5 mmHg pO_2 (~0.65%). However, biological responses to hypoxia begin altering cell activity below approximately 15 mmHg pO_2 (~2%). 2-Nitroimidazoles mildly label cells below 10 mmHg pO_2 (~1.3%) and strongly label cells below approximately 5 mmHg pO_2 (~0.65%). The use of oxygen-detecting electrode probes, exogenous hypoxia reporters, or endogenous hypoxia reporters has overwhelmingly and reliably found hypoxia to predict poor patient outcome across tumour sites, whether patients receive curative intent surgery, radiotherapy, or chemotherapy[106,133,164–166,199–201], suggesting each method has some degree of validity in identifying clinically relevant hypoxia.

The interest of this thesis with regards to hypoxic tumour cells is tilted towards the response of tumour cells to radiation. However, radiation-based assays are limited by an inability to concurrently assess the hypoxic fraction while investigating tumour biology. Therefore, this thesis work will generally define hypoxic tumour cells as cells that label positive for 2-nitroimidazoles. The benefits of this include restricting the hypoxic cell population to cells viable at the time of 2-nitroimidazole exposure, the strong correlation between 2-nitroimidazoles and radiation response, the well understood if somewhat mismatched relation between 2-nitroimidazole labelling and HIF1α stabilization, and the ability to differentially detect

pimonidazole and EF5. The latter point allows for determination of a cell's oxygenation at different points in time by separating pimonidazole and EF5 administration.

1.6 Tumour perfusion modifying interventions

The impact of oxygen content on tumour response to radiation has inspired a number of interventions aiming to increase tumour oxygenation. Not discussed here include interventions to increase the oxygen carrying capacity of the blood (e.g. erythropoietin)[202] or to decrease tumour cell oxygen consumption (e.g. metformin)[203,204]. Instead, this section will discuss interventions aiming to improve tumour perfusion and therefore oxygen delivery. Two distinct groups of interventions are clear: (1) those that are short lasting and are delivered just prior to irradiation, and (2) those that attempt to modify the tumour microenvironment to stably reduce the hypoxic fraction. Regarding the former, this thesis will focus on pentoxifylline (Chapters 2, 3, & 4), and regarding the latter this thesis will focus on angiotensin system inhibitors (Chapter 4).

1.6.1 Short-term interventions and pentoxifylline

Short-term improvement of solid tumour perfusion is challenging because of the dysfunctional nature of the tumour vasculature and microenvironment (Chapter 1.1). For example, classic vasodilators are an intuitive strategy to briefly increase flow and oxygen delivery to peripheral tissue. However, administration of hydralazine to mice bearing spontaneous or implanted human or murine tumours has the opposite effect of nearly eliminating tumour perfusion and significantly increasing tumour hypoxia[52,205–208]. Hydralazine-induced loss of tumour perfusion is attributed to vasodilation of local healthy tissue vessels and an inability of tumour blood vessels to dilate. This combination favours blood flow to the adjacent normal tissue at the expense of tumour perfusion and is referred to as the 'steal effect', which is so significant that hydralazine has instead been tested for ability to increase activity of hypoxia-activated pro-drugs[209]. Overall, work with hydralazine has led to the conclusion that traditional vasodilators are not viable options to acutely improve tumour perfusion.

Returning to the causes of tumour vascular dysfunction, another source of vascular resistance to target is the heightened blood viscosity in tumours (Chapter 1.1.1.2). Pentoxifylline is a phosphodiesterase inhibitor that increases erythrocyte deformability with the functional effect of decreasing blood viscosity, attributed to an increase in erythrocyte cAMP signaling[37–39].

Pentoxifylline-induced cAMP signaling leads to protein kinase A (PKA) activation. In erythrocytes, PKA signaling stimulates glycolysis, leading to increased activity of cellular membrane ion pumps that maintain homeostatic cell volume to optimize deformability[210]. Activated PKA may also directly phosphorylate cytoskeletal elements that may result directly in increased erythrocyte deformability[211]. Pentoxifylline-induced PKA activation has been observed to reduce NFκB activation in human mononuclear cells, leading to reduced production of inflammatory cytokines such as tumour necrosis factor α (TNFα)[212]. Despite some potential off-target effects on glycolytic metabolism or inflammatory cytokines, pentoxifylline has been studied in a number of pre-clinical tumour models where it is observed that pentoxifylline increases tumour perfusion and reduces hypoxia[50,52,171,213–223]. This thesis makes repeated use of pentoxifylline and therefore the following paragraphs will delve deeper into the experimental evidence for the effects of pentoxifylline on tumour perfusion and tumour hypoxia.

The pharmacokinetics of pentoxifylline in mice suggest some saturation of clearance mechanisms, as the blood half-life of the parent compound increases with dose from ~5 min after 10 mg/kg up to ~7-9 min after 50 mg/kg, and ~10 min after 100 mg/kg, when administered intraperitoneally or intravenously[222,224–226]. Pentoxifylline is metabolized to an active metabolite that is at least similarly as effective in reducing erythrocyte viscosity as the parent compound[227,228]. The active metabolite of pentoxifylline has a similar half-life of ~6 min in mice, and may increase the blood 0-60 minute area under the curve of pentoxifylline activity by up to 30%[224–226]. Pentoxifylline is demonstrated to exhibit significant reductions in erythrocyte viscosity at concentrations as low as 1-2 μg/mL for healthy donor erythrocytes, and as low as 0.03 μg/mL for stiffened erythrocytes[227,228]. In pre-clinical study of tumour-bearing mice or rats, pentoxifylline dosage is commonly 50 mg/kg by intraperitoneal injection[50,52,171,213–223], which reportedly results in a maximum blood concentration of ~50-70 μg/mL 5 minutes after injection. With an 8 min half-life, pentoxifylline would therefore be expected to exhibit blood viscosity-reducing effects for healthy erythrocytes for ~5 half-lives, or ~40 min, without consideration of active metabolites. Overall, for pre-clinical study of 50 mg/kg doses of pentoxifylline it should be expected that the drug will reduce blood viscosity in mice for at least 40 minutes.

The reduced blood viscosity provided by pentoxifylline treatment should be expected to reduce vascular resistance in solid tumours and impact tumour perfusion. Pentoxifylline treatment increases erythrocyte flux in LDF plots for murine tumours[213,221], rat tumours[213,216],

and clinical tumours from mixed sites[220]. Increased erythrocyte flux was often observed as early as 10-15 minutes post-injection and did not appear to decrease 60 minutes post-injection in any study. These data indicate that pentoxifylline is having a prolonged effect on tumour perfusion, but, are collected from only a few LDF probe measurements per tumour. Bulk tumour perfusion has been reported following pentoxifylline treatment using multiple radioactive perfusion reporters. Human tumour xenografts[50,52] and murine tumours[213,215,222,223] show mixed responses to pentoxifylline. The average case appears to be an approximate 50% increase in tumour perfusion peaking 15 minutes after pentoxifylline[50]. Overall, pentoxifylline increases erythrocyte flux and bulk tumour perfusion, although the bulk tumour perfusion response is brief and the increase in erythrocyte flux is prolonged.

WiDr human colorectal adenocarcinoma tumours are previously characterized to exhibit a relatively high rate of microregional perfusion fluctuations and transient hypoxia within the time frame of 10-40 minutes described in previous sections (Chapter 1.2.1)[50,67,229]. Thus, it is also of interest to determine the effect of pentoxifylline on the perfusion status of individual blood vessels throughout WiDr tumours. To investigate this, previous researchers administered Hoechst 33342 followed by $DiOC_7$ 35 minutes later, with pentoxifylline administered 15 or 30 minutes prior to $DiOC_7$. Pentoxifylline 30 minutes prior to $DiOC_7$ increased the fraction of vessels that experienced an increase in perfusion dye fluorescence, with a trending decrease in the fraction of vessels that experienced a decrease in perfusion dye fluorescence[50]. These data suggest that pentoxifylline increased the perfusion of a significant fraction of tumour blood vessels, above what would occur naturally due to perfusion fluctuations. The bulk perfusion response of WiDr tumours was a sharp increase 15 minutes post-injection of pentoxifylline that returned to baseline 30 minutes post-injection[50]. Thus, the WiDr data reiterate the LDF observations in that individual blood vessels may exhibit a prolonged increase in blood flow without the presence of a concurrent increase in bulk tumour perfusion. Together, these data are conceptualized as increased distribution of perfusion to more tumour regions and represent the first suggestion that pentoxifylline may affect transient hypoxia.

Increased erythrocyte flux, increased tumour perfusion, and improved microregional perfusion suggest that pentoxifylline may increase oxygen delivery to solid tumours. Firstly, it is worth noting that pentoxifylline treatment does not alter rat or mouse subcutaneous tissue (location of most model tumours) blood flow or oxygen electrode readings, and does not affect

arterial oxygen content[218,219,222]. These observations suggest that any effects on tumour oxygenation are due to a change in local perfusion and not increased vascular oxygen content. The effect of pentoxifylline on tumour oxygen electrode readings is largely reliable. Noting that the median pO_2 reading for many model tumours is below 10 mmHg, in the majority of tumours pentoxifylline treatment reduces the number of pO_2 readings in the most hypoxic data bin (usually <5 mmHg), but the median pO_2 reading remains below 10 mmHg[171,216–219,221,223]. These data agree with reports that pentoxifylline does not increase vascular oxygen content, but instead that pentoxifylline improves microregional perfusion to reduce the population of severely hypoxic tumour cells. These observations would be consistent with pentoxifylline-induced reoxygenation of transiently hypoxic tumour cells.

If pentoxifylline is reducing the population of severely hypoxic tumour cells, then pentoxifylline should increase tumour sensitivity to radiation. As previously discussed in Chapter 1.4, half-maximal radiation resistance occurs at approximately 3.8 mmHg. Therefore, even if pentoxifylline does not increase the median pO_2 reading in tumours it may still be significant to reduce the population of tumour cells below 5 mmHg. Multiple studies have indeed found pentoxifylline to reduce tumour cell clonogenic survival following single-dose x-irradiation, including in tumours where there was no significant change in median pO_2 reading[50,217,222]. This latter observation is particularly suggestive of transient hypoxia reoxygenation in that radiation response may be modified by re-distributing tumour oxygen delivery without increased blood oxygen carrying capacity.

The specificity of pentoxifylline-induced reoxygenation and radio-sensitization for transient hypoxia may be further investigated by sorting cells based on distance from perfused blood vessels. As described in previous sections (Chapter 1.2), tumour cord structure is layered outwards from perfused blood vessels as follows: normoxic cells, transiently hypoxic cells if present, and chronically hypoxic cells most distal from blood vessels. To parse the responses of each population to pentoxifylline, cellular fluorescence of intravenously injected Hoechst 33342 may be applied as a means to sort viable tumour cells based on distance from perfused blood vessels[50,69,230]. Sorted cell populations are referred to as “sort fractions”. To confirm the accuracy of this method, hypoxic cells labelled by pimonidazole may be compared with cells labelled by exogenous uridine analogues as an indicator of cells that are currently normoxic and proliferating. In WiDr tumours, pimonidazole labels a greater number of cells with increasing

distance from perfused blood vessels[68,127,229,230]. Conversely, the uridine analogue iododeoxyuridine (IdUr) labels a decreasing number of cells with increasing distance from perfused blood vessels[68,127,230]. When co-administered, very few cells are double-positive for pimonidazole and IdUr[68,127]. This is the baseline experimental condition that confirms tumour cells are not likely to be proliferating while concurrently hypoxic. A second set of experiments repeatedly administered pimonidazole over a 38-hour period, followed by a single dose of IdUr. This experimental approach increases the likelihood that a transiently hypoxic cell will be hypoxic at some point in time during the repeated pimonidazole doses, but also be reoxygenated and proliferating at the time of IdUr administration. In WiDr tumours, there is a clear appearance of a double-positive tumour cell population in cells at intermediate distances from perfused blood vessels, with very few double-positive cells in either the most proximal or most distal sort fractions[68]. The inverse experiment, repeatedly administering IdUr followed by a single dose of pimonidazole, yields similar results (unpublished data at BCCRC by Durand RE). These data support that transiently hypoxic tumour cells occupy cell layers at intermediate distances from Hoechst 33342 perfused blood vessels in WiDr tumours.

If pentoxifylline-induced reoxygenation is specific to transient hypoxia then it should be specific to WiDr tumour cells at intermediate Hoechst 33342 sort fractions. WiDr tumour-bearing mice were therefore treated with pentoxifylline, followed by 10 Gy x-irradiation, followed immediately by Hoechst 33342 and tumours harvested 20 minutes thereafter. As expected, there was reduced clonogenic survival in tumour cells from bright sort fractions (i.e. well-oxygenated cells close to blood vessels) compared to dim sort fractions. Pentoxifylline significantly reduced the clonogenic survival of tumour cells, specifically in intermediate sort fractions with no effect on survival of tumour cells in the most proximal or distal sort fractions[50]. These data indicate that pentoxifylline reoxygenates specifically tumour cells at intermediate sort fractions in WiDr tumours, the same sort fractions demonstrated to contain transient hypoxia.

Collectively, pentoxifylline may briefly increase bulk tumour perfusion but induce more prolonged increases in microregional tumour perfusion. This is accompanied by a reduction in the fraction of severely hypoxic (<5 mmHg) pO_2 readings and a reduction in tumour cell survival following irradiation, with minimal or no increase in median pO_2. These observations are consistent with pentoxifylline-induced reoxygenation of transiently hypoxic tumour cells via reduced flow resistance and improved flow to blood vessels that would otherwise be non-

perfused or more poorly perfused, increasing oxygen delivery without increasing blood oxygen carrying capacity. The radiosensitization of tumour cells at intermediate distances from Hoechst 33342 positive blood vessels, and not cells distal to Hoechst 33342 positive vessels, supports that the reoxygenation induced by pentoxifylline is specific to transiently hypoxic tumour cells and excludes chronically hypoxic tumour cells.

1.6.2 Angiotensin system inhibitors

The renin angiotensin system (RAS) is a signaling cascade that maintains blood pressure homeostasis. The RAS precursor angiotensinogen is continuously secreted into the blood by the liver. The detection of low blood pressure stimulates glomerular cells in the kidney to convert circulating pro-renin into the active enzyme renin[231]. Renin cleaves circulating angiotensinogen into the decapeptide Angiotensin I, followed by cleavage into the octapeptide angiotensin II (AngII) via angiotensin converting enzyme (ACE) on the luminal surface of endothelial cells[231]. AngII binds to Angiotensin II type 1 receptors (AT1R) throughout the body to increase blood pressure both directly by stimulating vasoconstriction, and indirectly by promoting aldosterone production, which in turn promotes fluid retention[231]. The potent blood pressure-increasing activity of AngII may be naturally antagonised by expression of angiotensin II type 2 receptors (AT2R), which induce vasodilation, and by ACE2, which cleaves AngII into the heptapeptide Ang(1-7). Ang(1-7) stimulates Mas receptors (MasR), which are also vasodilatory[231]. However, expression levels of AT2R, MasR, and ACE2 in adults are significantly lower compared to the AT1R signaling axis, resulting in AngII being a potent blood pressure increasing signal. Angiotensin system inhibitors have been developed for treatment of hypertension, including renin inhibitors[232], ACE inhibitors (ACEi)[233], and AT1R blockers (ARB)[234]. ARBs and ACEi have already been successful with approved indications including hypertension, heart failure, diabetes, atrial fibrillation, and cardiovascular disease risk reduction. In addition, angiotensin system inhibitors are more recently demonstrated to have anti-fibrotic and anti-inflammatory effects with potential for treatment against a variety of fibrotic diseases.

A series of articles recently found the ARB losartan to reduce the activity of cancer associated fibroblasts (CAFs) in solid tumours. CAFs isolated from tumours may become activated and express αSMA via autocrine TGFβ signaling[85]. However, treatment of CAFs in culture with losartan inhibited the cleavage and activation of TGFβ, reduced CAF expression of

αSMA, and reduced CAF Col1 production[85]. These effects have been replicated in murine and human tumour xenografts where losartan treatment reduced the abundance of αSMA positive CAFs, reduced Col1 in tumours, reduced mechanical compression of tumour blood vessels, and improved drug delivery to the tumour[85,86,88–90]. The improvement in drug delivery is indicative of increased tumour perfusion. Importantly, the anti-fibrotic effect of losartan was lost in AT1R-null mice, but unaltered in AT2R-null mice, supporting that losartan activity is acting through AT1Rs on host cells[85]. Thus, αSMA positive cells in solid tumours are sources of tumour fibrosis, largely constituted by Col1, and treatment with ARBs is able to reduce Col1 deposition by CAFs to reduce tumour fibrosis and improve tumour perfusion.

A benefit of studying angiotensin system inhibitors is the potential for retrospective analysis as it can be expected that a sub-set of patients will be coincidentally taking these drugs at the time of cancer diagnosis and throughout treatment. To this point, a 2017 meta-analysis summarized 55 retrospective studies covering over 170,000 cancer patients across tumour sites, stages, and treatments. In the majority of retrospective trials assessed, ACEi/ARB users represented 15-30% of all patients. This meta-analysis found a global hazard ratio of 0.82 favouring ACEi/ARB users compared with non-users[235]. Based on the pre-clinical data that ARB treatment may improve drug delivery to tumours and these retrospective data indicating that angiotensin system inhibition provides a survival benefit, a prospective clinical trial is currently underway testing losartan in pancreatic cancer patients[236]. However, implications of ARB treatment on tumour hypoxia are poorly characterized and it remains unknown if ARB treatment will be beneficial for radiotherapy. Chapter 4 of this thesis investigates the effects of ARB treatment on the tumour microenvironment, tumour hypoxia, and tumour radiation response.

1.7 Research objectives

The overarching **hypothesis of this thesis is that poor and dysfunctional tumour perfusion is a significant source of tumour resistance to radiation and that fluctuating microregional perfusion in solid tumours produces transient hypoxia that increases the radiation resistant population.** The field currently has a poor understanding of nature of transiently hypoxic tumour cells *in vivo*, which has resulted in highly varied methods for modeling transient hypoxia in pre-clinical work. Further, there are currently no specific factors identified that predict or identify tumours that will exhibit microregional perfusion fluctuations

and transient hypoxia. In turn, there are no drugs that have been demonstrated to stably eliminate the development of transient hypoxia for pre-clinical or clinical applications. Investigation on the fundamental biology of transient hypoxia will significantly advance the field of radiation biology by providing greater understanding of the nature of transiently hypoxic tumour cells *in vivo*. The development of an intervention to improve and provide long-term stabilization to tumour perfusion, as well as new methods to quantify drug-induced changes to tumour perfusion, represents useful advancement for both pre-clinical study of solid tumour perfusion and transient hypoxia with the potential for clinical translation.

1.7.1 Specific aims

I. To quantify the lifetime of hypoxic tumour cells in solid tumour xenografts while distinguishing between chronic and transient hypoxia. This aim will provide specific information that can be applied in pre-clinical modeling of transient hypoxic populations and provide broader insight into the environment that different hypoxic cells experience *in vivo*.

II. To validate 2-^{18}F-fluoroethanol as a novel reporter of solid tumour perfusion. This aim will validate the first ^{18}F based reporter of solid tumour perfusion and demonstrate the ability of this reporter to quantify tumour response to perfusion modifying drugs.

III. To test the effects of angiotensin II type 1 receptor blockers on transient hypoxia and radiation response. This aim hypothesizes that reducing Col1 deposition in solid tumours represents a method to not only increase solid tumour perfusion but to stabilize microregional perfusion, reduce the development of transient hypoxia, and improve tumour radiation response. This aim will further investigate the potential utility of ARBs in cancer treatment by testing these drugs for efficacy with radiation treatment.

1.7.2 Thesis overview

The subsequent chapters will address each of the specific aims listed above. Chapter 2 will apply 2-nitroimidazoles to quantify the lifetime of hypoxic tumour cells. This chapter will strategically apply pentoxifylline to differentiate between hypoxic cell loss that may be attributed to chronic and transient hypoxia in order to reach conclusions on the order and rate in which hypoxic cells turnover. This chapter will compare two tumour models that have been well

characterized in our group[50,67,68,128,229,230,237,238], the WiDr human colorectal adenocarcinoma and SiHa human cervical squamous cell carcinoma. As subcutaneous tumours, WiDr tumours develop with significantly more microregional perfusion fluctuations and transient hypoxia than SiHa tumours. Thus, for this thesis WiDr tumours will be tested as the model containing both chronic and transient hypoxia, while SiHa tumours will be tested as the model containing only chronic hypoxia. Chapter 2 will reach conclusions on the *in vivo* lifetime of chronically and transiently hypoxic tumour cells, which will provide novel recommendations on the maximum length of time that cells should be exposed to cycling hypoxia in pre-clinical study in order to appropriately model the *in vivo* experience of transiently hypoxic tumour cells.

Chapter 3 will validate 2-^{18}F-fluoroethanol as a reporter of solid tumour perfusion. This chapter will compare two well characterized tumour models, the well-perfused 67NR murine mammary carcinoma and the syngeneic poorly perfused 4T1 mammary carcinoma. This chapter will directly compare 2-^{18}F-FEtOH with an established reporter of tumour perfusion, ^{14}C-iodoantipyrine, in tumour and healthy tissue. This chapter will further test for the response of 67NR and 4T1 tumours to short-term perfusion modifying drugs including pentoxifylline, nicotinamide, and hydralazine.

Chapter 4 will test the ARBs losartan and telmisartan for effects on tumour perfusion and transient hypoxia. This chapter will apply 2-^{18}F-FEtOH PET to quantify bulk tumour perfusion and again will compare WiDr and SiHa tumours. Losartan and telmisartan will be first investigated for effects on CAFs and Col1 in each tumour to confirm that ARB activity in our models agree with the proposed mechanisms published elsewhere. This chapter will then investigate the effects of ARB treatment on microregional perfusion stability, transient hypoxia, and radiation response.

Chapter 5 will provide a thesis summary, discuss the significance of the advancements offered by the work within this thesis, and discuss potential future directions for research within the field of solid tumour perfusion and radiation biology.

Chapter 2: The lifetime of transiently hypoxic cells in solid tumours.

The contents of this chapter have been submitted for publication as: Brennan J Wadsworth, Che-Min Lee, Kevin L Bennewith. "The lifetime of transiently hypoxic tumour cells in solid tumour xenografts"

SYNOPSIS

Solid tumours develop regions of hypoxia where tumour cells reside beyond the oxygen diffusion limit of local vasculature, referred to as diffusion-limited or chronic hypoxia. Unstable microregional perfusion in solid tumours exposes some tumour cells to cycles of hypoxia and reoxygenation, termed transient hypoxia. The lifetime of hypoxic cells in solid tumours is poorly characterized, and any differences between chronic and transient hypoxic cell turnover is unknown. To improve the fundamental understanding of tumour hypoxia, this study investigated the rate of hypoxic cell turnover while distinguishing between chronic and transient hypoxia.

Hypoxic cells were labelled using 2-nitroimidazoles and turnover quantified as the loss of labelled cells over time. The perfusion-modifying drug pentoxifylline was applied to reoxygenate transiently hypoxic cells prior to 2-nitroimidazole administration, causing 2-nitroimidazoles to specifically label chronically hypoxic cells. In the pentoxifylline-treated experiments, loss of 2-nitroimidazole positive cells could therefore only be attributed to loss of chronically hypoxic cells. The rate of turnover of transiently hypoxic cells was determined by comparison between control and pentoxifylline-treated mice.

The majority of hypoxic cell loss occurred within 72 hours after labelling. In pentoxifylline treated tumours the rate of hypoxic cell loss was similar to untreated tumours for the first 48 hours after 2-nitroimidazole labelling, indicating that primarily chronically hypoxic cells are lost in the first 48 hours. In pentoxifylline-treated tumours, the rate of hypoxic cell loss was reduced 72 hours after labelling, indicating that transiently hypoxic cells are lost between 48 and 72 hours after 2-nitroimidazole labelling.

Our observations suggest that the majority of hypoxic cells *in vivo* turnover within 72 hours. We observe ordered hypoxic cell loss; chronically hypoxic cells in the first 48 hours after labelling, followed by transiently hypoxic cells between 48 and 72 hours after labelling. These data suggest a maximum lifetime of 72 hours for transiently hypoxic tumour cells.

2.1 Introduction

Solid tumours often develop regions with low oxygen content (i.e. hypoxia). The presence of hypoxia in tumours is associated with resistance to radiation and chemotherapies[239,240], while exposure of tumour cells to hypoxia either *in vitro* or *in vivo* increases many pro-metastatic phenotypes[241,242]. These observations have provided rationale for the development of hypoxia-activated prodrugs[243], exogeneous reporters to quantify hypoxia in tumours[244], and models for predicting the impact of hypoxia on radiation response[174]. Implicit in these directions of study is that hypoxic cells live long enough to be detected and to be therapeutically relevant.

Hypoxia occurs where tumour cells reside in areas of limited oxygen supply. Oxygen diffuses effectively from functioning blood vessels in solid tumours through 70-100 μm of metabolically active tumour tissue[109,110], beyond which cells are provided low levels of oxygen (i.e. less than 0.5% O_2). Hypoxia produced as a result of this limiting oxygen gradient from functioning blood vessels is termed diffusion-limited or chronic hypoxia. In recent decades tumour oxygenation has been described as more dynamic due to observations of perfusion that is unstable over time[245]. Unstable perfusion is reported in studies employing fluorescent markers of vessel function in murine tumours[63,71], and using laser doppler flowmetry to monitor erythrocyte flux combined with oxygen electrode probes in rat tumours[118], spontaneous canine tumours[121], and human tumours[117]. The period for blood flow and oxygen fluctuations is relatively consistent across organisms with the most common hypoxic period lasting between 10-40 minutes. These observations led to the description of perfusion-limited or transient hypoxia as a second population of hypoxic cells that are hypoxic only during periods of poor oxygen delivery and exist at intermediate distances from perfused blood vessels[68,229]. Study of tumour cell response to cycles of hypoxia and reoxygenation *in vitro* and *in vivo* have found increased expression of metastasis related genes[246] and increased metastatic growth compared to chronic exposures of hypoxia[242,247]. Further, the observation that transiently hypoxic tumour cells may be more resistant to radiation than chronically hypoxic tumour cells[248] highlights the potential therapeutic importance of transient hypoxia.

The spatial relationship of chronically and transiently hypoxic tumour cells comes from previous studies that have sorted tumour cells using fluorescence activated cell sorting (FACS) based on fluorescence intensity for intravenously injected Hoechst 33342 fluorescent dye. With

this method, tumour cells proximal to perfused blood vessels *in vivo* label brightly, and those distal from perfused blood vessels are dim. If Hoechst 33342 is intravenously injected immediately prior to irradiation, then tumour cell survival irradiation is inversely correlated with Hoechst 33342 fluorescence[64,65,69], indicating greater survival of tumour cells distal from perfused blood vessels. In tumours demonstrated to exhibit transient hypoxia, if Hoechst 33342 is intravenously injected 20 or 30 minutes prior to irradiation, then Hoechst-bright and Hoechst-dim populations exhibit similar survival[64,65,69]. This demonstrates that tumour cells with a stable radiation-resistant phenotype are those that are distal to perfused blood vessels, while tumour cells with a dynamic radiation-resistant phenotype reside more proximal to perfused blood vessels, i.e. chronically and transiently hypoxic cells respectively.

Further characterization applying Hoechst 33342 has split tumour cells into six or eight 'sort fractions' based on Hoechst 33342 fluorescence. From these studies it is clear that tumour cells distal to perfused blood vessels label strongly with hypoxia reporters such as 2-nitroimidazoles and are radiation resistant[68,129,229,249]. In turn, tumour cells more proximal to blood vessels are sensitive to radiation and are more likely to be proliferating, indicated by labelling by detectable nucleosides, such as iododeoxyuridine (IdUr)[68,111]. Tumour cells are unlikely to be dual labelled for simultaneously administered pimonidazole and iododeoxyuridine[68]. Thus, tumour cells are unlikely to be concurrently hypoxic and proliferative. However, if the 2-nitroimidazole pimonidazole is administered repeatedly over a 38-hour period followed by a single dose of IdUr just prior to harvest, this increases the likelihood that a transiently hypoxic cell will be hypoxic at some point in time during the repeated pimonidazole doses, but also be reoxygenated and proliferating at the time of IdUr administration. In tumours demonstrated to exhibit transient hypoxia, there is a clear appearance of a double-positive tumour cell population in cells at intermediate distances from perfused blood vessels, with very few double-positive cells in either the most proximal or most distal sort fractions[68]. Thus, transiently hypoxic tumour cells occupy cell layers more proximal to perfused blood vessels than chronically hypoxic cells.

Necrosis is often observed beyond approximately 150 μm from perfused blood vessels in solid tumours, where nutrients become too limiting for tumour cell survival[109–113]. Thus, tumours can be modelled as units of cylindrical 'tumour cords' with cells layered as follows: central blood vessel, well-oxygenated proliferating cells, transient hypoxia if present, chronic hypoxia,

and necrosis[250]. Studies monitoring cells labelled by IdUr, 2-nitroimidazoles, or hypoxia-induced luciferase over time each independently demonstrate that tumour cells typically 'flow' radially outwards from perfused blood vessels based on cell proliferation (further detail in Chapter 1.3)[111,128,129,132], i.e. as a normoxic tumour cell divides one of the daughter cells is pushed outwards, pushing a 'downstream' cell into a region of chronic hypoxia, and in turn a chronically hypoxic cell into a region of necrosis. Thus, tumour cell turnover occurs by proliferation causing necrosis of hypoxic tumour cells.

Hypoxic tumour cells may be labelled *in vivo* by administration of 2-nitroimidazoles such as pimonidazole[182] and EF5[177]. Cellular reductive metabolism reduces 2-nitroimidazoles to metabolites that covalently bind intracellular macromolecules, although this process is strongly inhibited by oxygen[178,251,252]. The circulation half-lives of pimonidazole and EF5 (in mice 30 minutes[253] and 40 minutes[254] respectively) allows for time-integrated labelling of hypoxic cells, including the majority of rapidly cycling (i.e. fluctuations within 1 hour) transiently hypoxic cells[229]. Turnover of tumour cells *in vivo* has been quantified by the rate of disappearance of labelled cells after administration of proliferation indicators or 2-nitroimidazoles[129,111,128]. Past studies have observed relatively rapid turnover of hypoxic cells with a majority of 2-nitroimidazole labelled hypoxic cells disappearing from tumours within 24 or 48 hours[129,132]. In tumour lines with a cell cycle time close to 24 hours this suggests that at any time a large portion of hypoxic cells may be on the edge of being pushed into necrosis.

Alternatively, as transiently hypoxic cells are understood to exist more proximal to perfused blood vessels and further from regions of necrosis compared to chronically hypoxic cells, we hypothesized that transiently hypoxic cells would have an extended lifetime in untreated tumours compared to chronically hypoxic cells. An extended exposure to hypoxia *in vivo* could result in greater cumulative expression of hypoxia-induced and pro-metastatic genes that would further identify transient hypoxia as an important population of cells for contributing to the association between tumour hypoxia and poor patient outcome. In this study we follow hypoxic cells over time by administering pimonidazole and EF5 separated in time to tumour bearing mice. We find *in vitro* that pimonidazole-labelled cells can be detected above background after 3-4 cell divisions and conclude that dilution via proliferation of hypoxic cells is unlikely to be a source of labelled cell loss. *In vivo* we distinguish between transient hypoxia and chronic hypoxia by applying the perfusion modifying drug pentoxifylline, which is previously

characterized to specifically reoxygenate transiently hypoxic cells[50]. We compare two tumour models that we have previously characterized for transient hypoxia; SiHa tumours that contain chronic hypoxia, and WiDr tumours that contain both chronic hypoxia and transient hypoxia[50,229]. Our data indicate that in WiDr tumours there is indeed a delay in the turnover of transiently hypoxic cells compared to some chronic hypoxia populations. Overall, transient hypoxia may represent a relatively long-lived population of hypoxic tumour cells worthy of further focus in research on the impact of tumour hypoxia on cancer biology.

2.2 Materials and methods

2.2.1 Cells and mice

10-week-old male NOD/SCID-gamma mice were housed under specific pathogen-free conditions. WiDr[255], human colorectal adenocarcinoma, and SiHa[256], human cervical squamous cell carcinoma, cell lines were maintained in minimal essential medium +10% fetal bovine serum and used within 25 passages. Tumours were produced by subcutaneous injection of $1x10^6$ cells in 100 µl into mouse flanks. All experiments were performed in accordance with institutional and Canadian Council on Animal Care guidelines. For irradiation experiments, mice were fixed in a lead jig such that only the tumour was subjected to x-irradiation delivered at 250 keV with a dose rate of approximately 3 Gy/min (X-RAD320, Precision X-ray). Upon mouse sacrifice, tumours were removed and cut in half. One half was embedded in optimal cutting temperature medium (Tissue Tek) and frozen for sectioning and microscopy. The remaining half was processed into single cell suspension as previously described[229] for flow cytometry and clonogenic assays. For clonogenic assays, cells were counted, plated in triplicate at multiple dilutions, incubated for two weeks in standard culture conditions, and then stained with malachite green for colony counting. Data displayed are the ratio of observed colonies over the number of cells plated, after correction for plating efficiency of cells isolated from non-irradiated tumours.

For *in vitro* experiments, cells were cultured at 37 °C 5% CO_2 in either standard cell culture incubators (ThermoFisher Scientific), a hypoxia chamber maintained at 1% O_2, or in a bench top incubator for cycling hypoxia experiments. To cycle O_2 *in vitro,* cells were plated in T25 flasks (Corning) and individually gassed with variable O_2, 5% carbon dioxide, balance N_2 gas mixtures (Praxair). Cycling hypoxia exposures were 25 minutes of 0.5% O_2 followed by 25 minutes of 5% O_2. To ensure rapid oxygen equilibration, culture flasks were on a table-top

rocker within the incubator. O_2 concentration was measured in parallel flasks with contactless optical oxygen sensor spots and FireStingO2 (FSO2-2) meter (Pyroscience). Upon switching the input O_2, the measured O_2 tension was found to reach within 95% of the target O_2 setting within 5 minutes.

For *in* vitro growth rate experiments, growth rate was calculated as:

$$g = \frac{\left(log_2\left(\frac{N_f}{N_i}\right)\right)}{t}$$

Where g is the reported growth rate, N_i and N_f are the initial and final number of cells respectively, and t is the time elapsed in hours. Cells counts were made by trypsinization of cell culture and counting of single-cell suspensions using Beckman Z2 Cell and Particle Counter (Beckman). Growth rate may be interpreted as the number of population doublings per hour. *In vitro* cell viability was quantified using automated Trypan Blue assay on Vi-Cell Cell Viability Analyzer (Beckman).

2.2.2 Chemicals

The following agents were administered to mice by intraperitoneal injection: 50mg/kg pentoxifylline (Millipore Sigma), 100mg/kg pimonidazole (Hypoxyprobe), and 60mg/kg EF5 (Millipore Sigma). Intravenous injection of 1mg Hoechst 33342 10 minutes prior to mouse sacrifice was used to label cells surrounding functional perfused blood vessels[63,66]. For *in vitro* experiments cells were labelled with pimonidazole in media at a concentration of 200 μM for three hours in 1% O_2. The cyclin dependent kinase 4/6 (CDK) inhibitors Abemaciclib (MedChemExpress) and Palbociclib (MedChemExpress) were used to induce G1 cell cycle arrest for *in vitro* experiments at concentrations of 10 and 50 μM respectively.

2.2.3 Flow cytometry and immunofluorescent microscopy

For tumours from mice injected with Hoechst 33342, slides were imaged for Hoechst 33342 immediately following sectioning and then placed overnight in phosphate-buffered saline (PBS) with 2% fetal bovine serum and 0.1% triton X-100 for blocking, cell permeabilization, and to wash out the fluorescent dye signal prior to staining for other markers. Pimonidazole was detected using monoclonal antibody (Hypoxyprobe) conjugated to fluorescein isothiocyanate

(FITC). EF5 was detected using the ELK3-51 antibody conjugated to Cy5 (Millipore Sigma). Slides were stained for CD31 (Novus Biologicals) or carbonic anhydrase IX (CAIX, Novus Biologicals), with secondary antibody conjugated to Alexa 594 (Life Technologies). Slides were stained with 2 μM 4,6-diamidino-2-phenylindole (DAPI) to label cell nuclei. Immunofluorescent microscopy image acquisition system consisted of a robotic fluorescence microscope (Zeiss Axiomager Z1), a cooled, monochrome CCD camera (Retiga 4000R, QImaging), a motorized slide loader and x-y stage (Ludl Electronic Products), and customized ImageJ software (public domain program developed at the U.S. National Institutes of Health). Images were acquired with a resolution of 1.5 μm/pixel. Individual fields of view were automatically stitched together to create images of full tumour sections for analysis. Three sections cut 150-200 μm apart were imaged for technical replicates of each tumour. Images were analyzed using in-house macros with ImageJ software. Positive pixels were identified using automatic thresholding following background correction. Regions of necrosis were manually removed from analysis based upon DAPI and hypoxia marker staining.

For flow cytometry, permeabilized cells were labelled with 100 μM propidium iodide to measure DNA content for cell cycle analysis. To track cell divisions *in vitro,* cell cultures were provided a 20-minute exposure of 10 μM CellTrace Yellow (CTY) (ThermoFisher Scientific) in phosphate buffered saline. Flow cytometry was conducted using either a FACSCalibur (BD Biosciences) or Fortessa (BD Biosciences) flow cytometer. Flow cytometry analyses were conducted using FlowJo 7.6 software (Tree Star, Inc).

2.2.4 Statistical analysis

Statistical hypothesis testing was performed using Graphpad Prism 8 software, p values less than 0.05 were considered significant. Specific statistical tests used are listed in figure legends.

2.3 Results

2.3.1 Pimonidazole fluorescence *in vitro*

We planned to utilize 2-nitroimidazoles to label hypoxic tumour cells and track the loss of labelled cells over time. However, the loss of 2-nitroimidazole labelled cells over time could be due proliferation of labelled cells diluting the number of 2-nitroimidazole adducts per

daughter cell, eventually preventing detection of the 2-nitroimidazole positive cells compared against background cells. We thus first aimed to quantify the rate of pimonidazole fluorescence loss over time *in vitro*. Cells were synchronized overnight by serum starvation prior to labelling with pimonidazole in 1% O_2, followed by labelling with CTY to model proliferation associated loss of fluorescence signal. Cells were then incubated in either standard culture conditions (21% O_2) or a 1% O_2 hypoxia chamber for 24, 48, 72, or 96 hours before flow cytometry analysis. WiDr and SiHa cell CTY and pimonidazole mean fluorescence intensity (MFI) decreased over time in both 21% O_2 and 1% O_2 culture (Figure 2.1A-H). Pimonidazole MFI was significantly greater than background control cells, which were not provided pimonidazole but were stained with the pimonidazole detection antibody, for up to 72 hours for cells in 21% O_2 and throughout the 96-hour experimental protocol for cells in 1% O_2 (Figure 2.1E-H). In Figure 2.1 MFI is $\log_2$-transformed so that changes by a factor of 2, as expected for marker dilution due to cell division, may be observed more clearly. The change in CTY MFI indicates that WiDr cells had undergone ~3.5 divisions after 72 hours in 21% O_2 and ~4.8 divisions after 96 hours in 1% O_2, while SiHa cells had undergone ~3.7 and ~ 4.3 divisions in similar conditions and time frames (Figure 2.1A-D). These data suggest that labelled cells retained fluorescence greater than background for 72-96 hours, or 3-4 cell divisions.

To determine if the loss of pimonidazole MFI over time correlates with cell division, we asked if there was a linear relationship between pimonidazole MFI and CTY MFI. Log-transformed MFI of pimonidazole versus CTY (Figure 2.1I,J) indicated a strong linear relationship with significantly non-zero slope in both normoxia and hypoxia for WiDr (mean ± SEM; normoxia slope = 0.90 ± 0.08, r^2 = 0.90, hypoxia slope= 0.78 ± 0.11, r^2=0.80) and SiHa cells (mean ± SEM; normoxia slope = 0.96 ± 0.06, r^2 = 0.95, hypoxia slope = 0.86 ± 0.07, r^2 = 0.92). These data indicate that the decrease in pimonidazole over time occurred in proportion to cell division. The difference between pimonidazole-CTY slopes in normoxia and hypoxia was not significant, suggesting that pO_2 is not strongly modifying the relationship between pimonidazole MFI and cell division.

The data in Figure 2.1 indicate that pimonidazole MFI may decrease over time in proportion to cell division. We next aimed to determine if that decrease in pimonidazole MFI over time was dependent on cell division and not simply coincident with cell division. To address this possibility, we next asked whether or not addition of a cytostatic agent to arrest cells

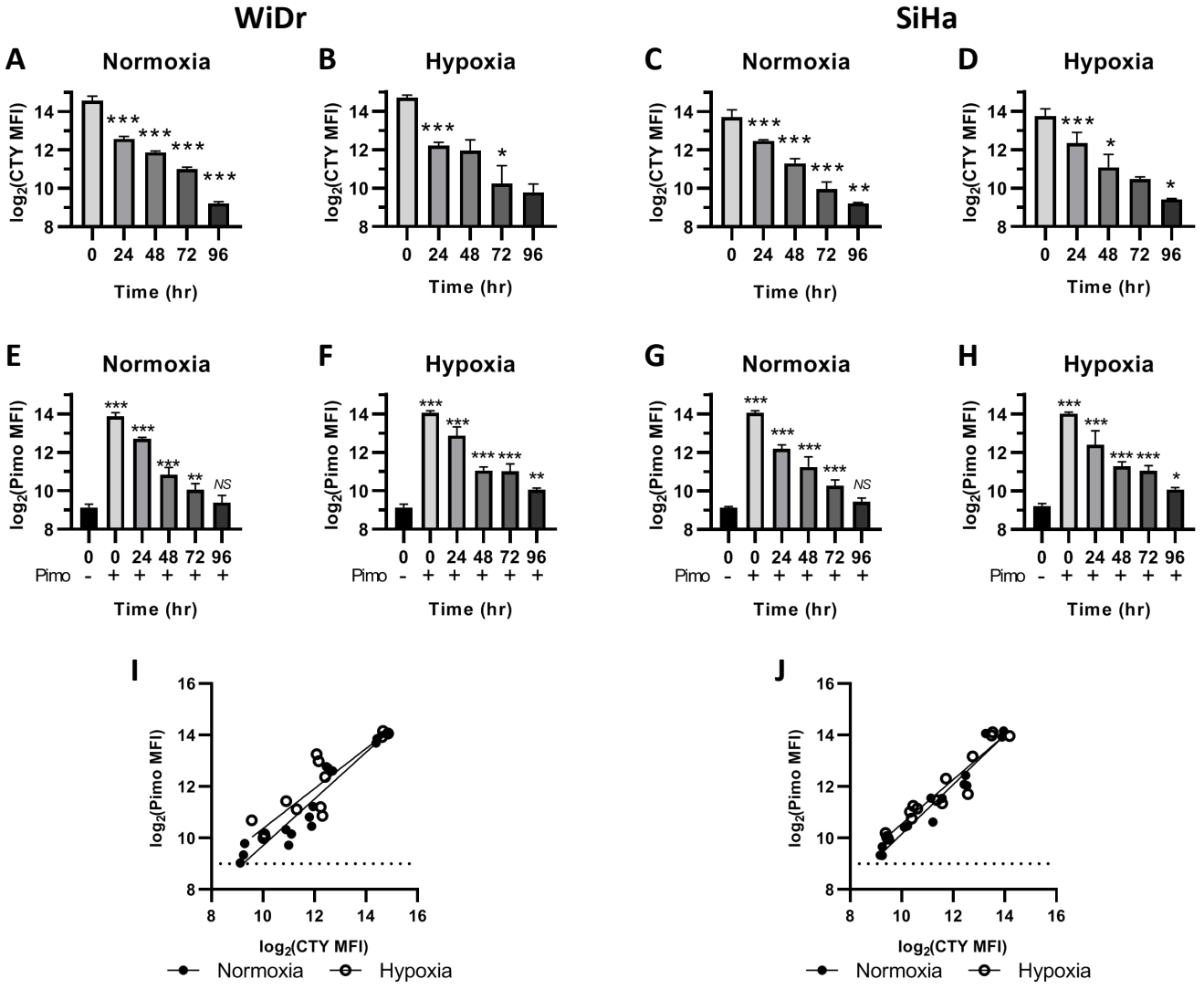

Figure 2.1 Pimonidazole loss in *in vitro* tracks with cell divisions.

CTY MFI for WiDr cells cultured in (A) normoxia (21% O_2) and (B) hypoxia (1% O_2), and SiHa cells cultured in (C) normoxia and (D) hypoxia. Sidak's multiple comparisons test results indicated comparing each time point to the preceding time point, * $p < 0.05$, ** $p < 0.01$, *** $p < 0.001$, N = 3, mean ± SD. Pimonidazole MFI for WiDr cells cultured in (E) normoxia and (F) hypoxia, and SiHa cells cultured in (G) normoxia and (H) hypoxia . Dunnett's multiple comparison test results indicated comparing each time point to the no-pimonidazole control: * $p < 0.05$, ** $p < 0.01$, *** $p < 0.001$, *NS* $p > 0.05$, N = 3, mean ± SD. (I) WiDr and (J) SiHa $\log_2$(pimonidazole MFI) plotted against $\log_2$(CTY MFI). Dotted line indicates the average MFI of control cells that were not exposed to pimonidazole but were stained with pimonidazole detection antibody. Linear regression lines displayed, statistics reported in the main text.

in G1 would block loss of pimonidazole MFI over time. We labelled cells with pimonidazole and CTY as above and treated WiDr cells with one of two cyclin CDK inhibitors, Abemaciclib or Palbociclib. Inhibitors were added to the media after pimonidazole and CTY labelling and maintained in the media until harvest. We observed no difference in viability for cells treated with CDK inhibitors compared to dimethyl sulfoxide (DMSO) controls (Figure 2.2). DNA content indicated by propidium iodide fluorescence confirmed that in normoxia and hypoxia both Abemaciclib and Palbociclib were able to significantly reduce the proportions of cells in S and G2/M cell cycle phases at all time points (Figure 2.3A,B). The rate of pimonidazole loss was slowed by addition of either Abemaciclib or Palbociclib in both normoxia and hypoxia, as evidenced by a significant reduction in slope of the linear regression lines from the $\log_2$(pimonidazole MFI) versus time plots (Figure 2.3C,D). The inhibition of pimonidazole loss over time by cytostatic treatments supports that loss in fluorescence intensity of pimonidazole over time could largely be attributed to dilution via proliferation. However, collectively the data of Figure 2.1 and Figure 2.3 suggest that fluorescence intensity of pimonidazole labelled tumour cells may remain greater than background for at least 72-96 hours, or 3-4 cell divisions.

2.3.2 WiDr growth rate *in vitro*

The design and interpretation of further experiments therefore depends on the number of cell divisions that could be expected of hypoxic tumour cells *in vivo*. Therefore, we further investigated the effect of O_2 tension on cell proliferation. Within cell type, the growth rate for both WiDr and SiHa cells was similar for cells cultured in 5% and 1% O_2 (Figure 2.4A,B). However, culture in 0.5% O_2 significantly reduced SiHa cell proliferation and halted WiDr cell proliferation (Figure 2.4A,B). This is in agreement with many data that severe hypoxia induces a G1 cell cycle arrest and that hypoxic cells (e.g. 2-nitroimidazole-positive) *in vivo* are unlikely to be proliferating[111,113,128]. Cell labelling with 2-nitroimidazoles *in vivo* is demonstrated to increase most dramatically in cells below 0.5% oxygen[178,179], thus, it is unlikely that any sizeable population of chronically hypoxic tumour cells labelled with 2-nitroimidazoles will undergo multiple cell divisions in the days following 2-nitroimidazole labelling.

We were next concerned with the possibility of transiently hypoxic tumour cells undergoing multiple cell divisions. Cells were cultured while cycling between 25 minutes of 5% O_2 and 25 minutes of 0.5% O_2. We found that the growth rate of the oxygen-cycling WiDr cells

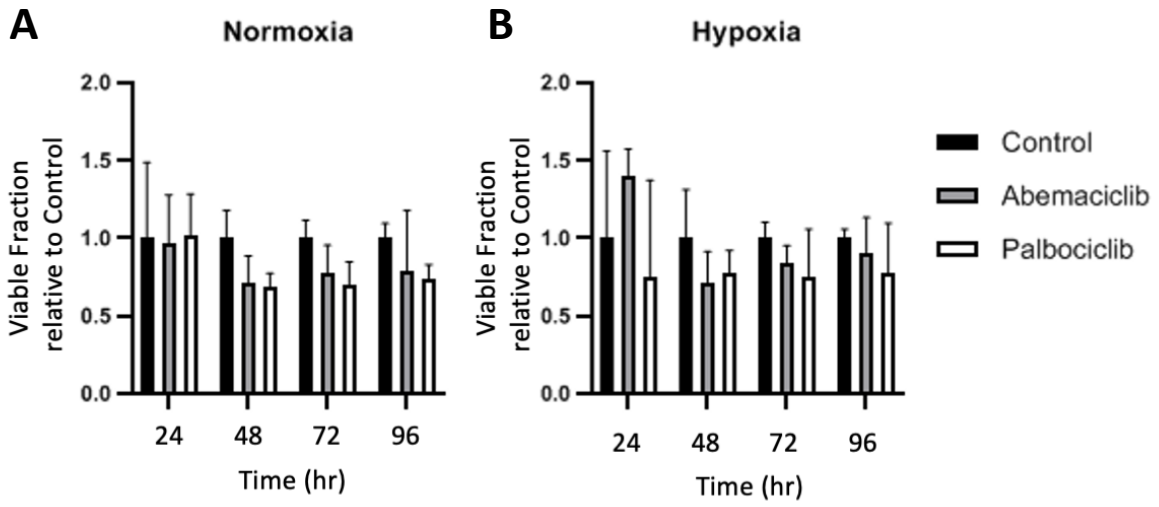

Figure 2.2 Cell viability over time with CDK4/6 inhibitors

WiDr cell viability in trypan blue assay following culture in (A) normoxia or (B) hypoxia, with media containing either 10 μM Abemaciclib, 50 μM Palbociclib, or DMSO control, for the indicated time period. Viability expressed relative to time matched DMSO controls. N = 6, mean ± SD. Dunnett's multiple comparisons test comparing treatment groups within time points, no significant differences were observed at any time points.

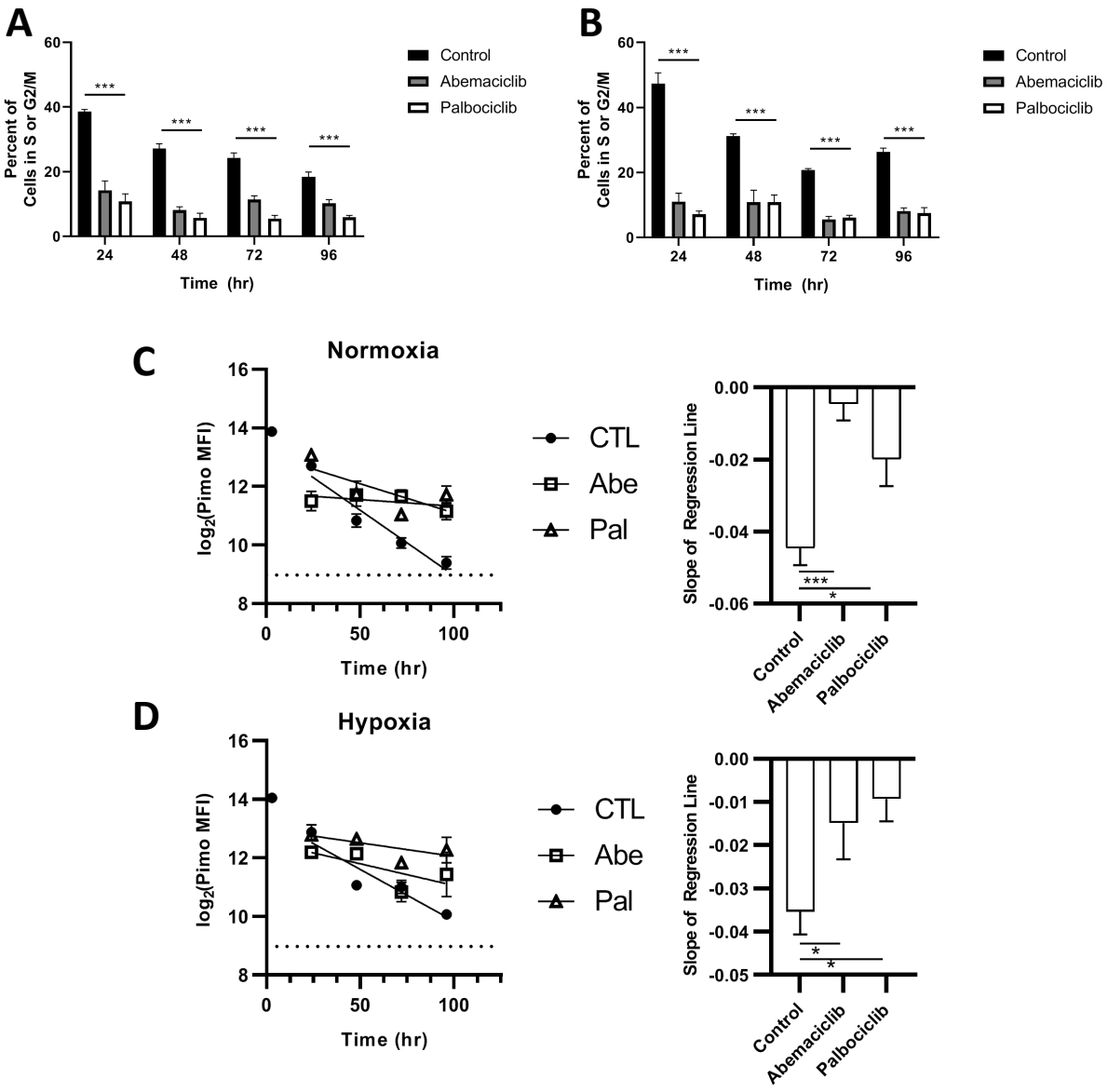

Figure 2.3 Loss of pimonidazole *in vitro* can be inhibited by cytostatic agents.

WiDr cells were labelled with pimonidazole and CTY as in Figure 2.1, but cultured with either 10 μM Abemaciclib, 50 μM Palbociclib, or DMSO control for the remainder of the experiment. To assess ability of the inhibitors to cause a cell cycle arrest we quantified the percentage of cells in S or G2/M cell cycle phases by propidium iodide flow cytometry. For each treatment group the percentage of cells in either S or G2/M cell cycle phases are displayed for (A) cells in normoxia (21% O_2) and (B) cells in hypoxia (1% O_2). The rate of loss in pimonidazole fluorescence is shown in plots of $\log_2$(pimonidazole MFI) versus time with linear regression lines displayed for each treatment group in (C) normoxia and (D) hypoxia culture conditions. Closed circles represent DMSO controls, squares Abemaciclib treated cells, and triangles Palbociclib treated cells. Also displayed are plots of statistical comparison of slopes for each line. Dunnett's multiple comparison test results are shown comparing each group to DMSO control, *** $p < 0.001$, ** $p < 0.01$, * $p < 0.05$. N = 3, mean ± SEM.

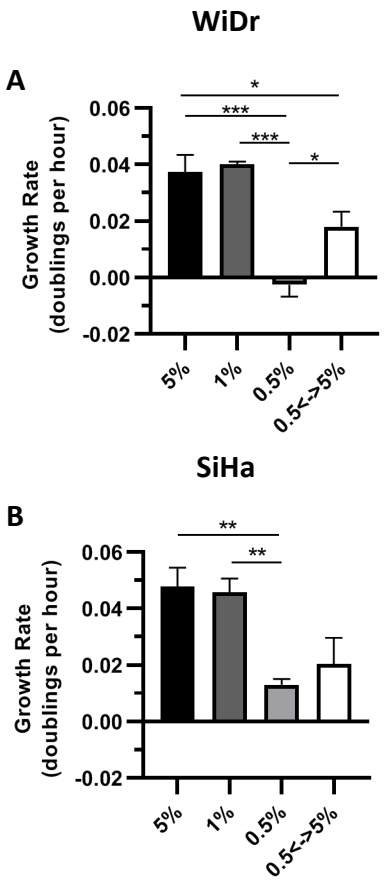

Figure 2.4 Cells cycling between hypoxia and normoxia exhibit intermediate growth rates.

(A) WiDr and (B) SiHa cells were cultured in flasks individually gassed with either 5% O_2, 1% O_2, 0.5% O_2, or 25 minutes of 5% O_2 followed by 25 minutes of 0.5% O_2 for 48 hours. The growth rate values reported should be interpreted as the number of times that the cell population doubles per hour. N = 6 mean ± SEM, Tukey multiple comparisons test results displayed, * $p < 0.05$, ** $p < 0.01$, *** $p < 0.001$.

was intermediate of the growth rates for cells cultured chronically in 5% and 0.5% O_2 (Figure 2.4A). This is in agreement with our previous reports on WiDr tumours observing that cells *in vivo* are unlikely to be dual labelled by simultaneously administered pimonidazole andiododeoxyuridine[68]. Overall, these data support that transiently hypoxic WiDr tumour cells are likely only proliferative during phases of normoxia and that their rate of proliferation *in vivo* will be reduced relative to normoxic cells. Durand et al found the *in vivo* cell cycle time of WiDr cells labelled by iododeoxyuridine to be approximately 24 hours[128]. If transiently hypoxic tumour cells proliferate at half this rate, the limit of any experiment studying the loss of 2-nitroimidazoles in these cells may therefore be as long as 144 hours to allow for no more than three cell divisions from any cell in this population. Further, published reports suggest that tumour cells are pushed into layers further from functional blood vessels over time due to normoxic cell proliferation. This flow of cells outwards from blood vessels will push tumour cells into regions of more severe hypoxia and therefore progressively less supportive of proliferation with time[129,132,249,250]. Overall, our data and reasoning from published data support that multiple cell divisions capable of diluting pimonidazole below the level of detection against background is unlikely to occur within either chronically or transiently hypoxic tumour cells within 144 hours after initial labelling. Previous reports observe rapid loss of hypoxic cells within 48 hours followed by a plateau[129], suggesting the majority of hypoxic cell loss may be captured well within 144 hours. We therefore moved forward with a limit of 96 hours between pimonidazole administration and tumour harvest, which our data suggests is well within the time frame to exclude the possibility of significant pimonidazole adduct dilution in labelled chronically or transiently hypoxic tumour cells.

2.3.3 Stabilization of hypoxic fraction *in vivo*

In order to quantify the lifetime of hypoxic tumour cells *in vivo* we next investigated growth of WiDr and SiHa tumours in NSG mice to select the optimal 96-hour window. In previous experiments from tumours grown in NSG mice we have harvested SiHa tumours either 21, 25, or 29 days post-implant, while we have harvested WiDr tumours at various points between 21- and 45-days post-implant. Gompertzian growth curves indicate that in a four day period a 300 mg SiHa tumour will increase in mass by approximately 50% and a 300 mg WiDr tumour will increase in mass by approximately 25% (Figure 2.5A,B). With this change in tumour

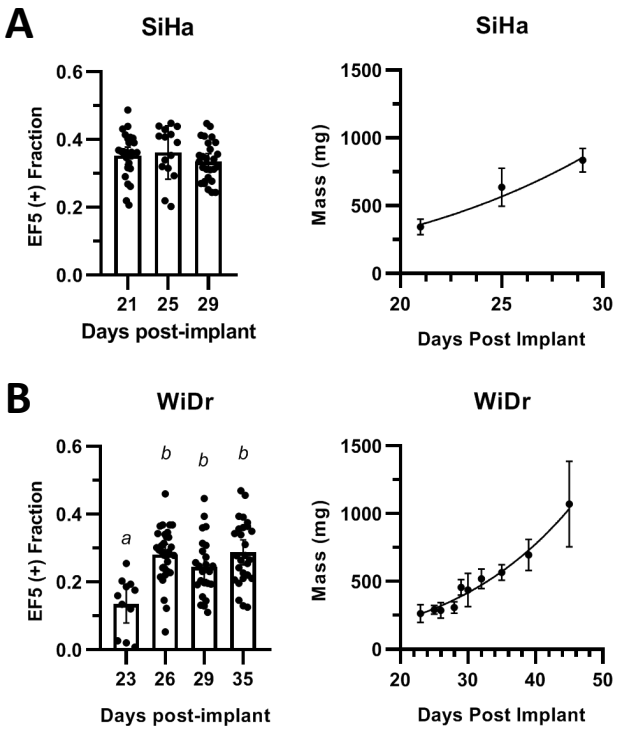

Figure 2.5 Hypoxic fraction stabilizes during tumour growth

Fraction of tumour area positive for EF5 and tumour mass as functions of harvest date post-implant for (A) SiHa and (B) WiDr tumours. N = 11-29, mean ± 95% CI, Tukey multiple comparisons test results displayed, *a* vs *b* $p < 0.01$. No significant differences in SiHa hypoxic fraction data.

mass we next asked if there was a change in the average hypoxic fraction. In tumours administered EF5 3 hours prior to sacrifice, we observed no change in the total EF5 positive hypoxic fraction in SiHa tumours across harvest time points. In WiDr tumours the hypoxic fraction was stable beginning at least 26 days post-implant. Stabilization of the hypoxic fraction is in agreement with past studies employing a variety of hypoxia detection methods[257–260]. Based on these observations, further experiments were conducted within 96-hour time frames of a stable hypoxic fraction. SiHa tumours were harvested 29 days post-implant, with 2-nitroimidazole injections as early as 25 days post-implant. WiDr tumours were harvested 32 days post-implant with 2-nitroimidazole injections as early as 28 days post-implant.

2.3.4 Pimonidazole and EF5 positive tumour area over time

With the time frame and days post-implant specified we next conducted experiments tracking the rate of loss of 2-nitroimidazole labelled tumour cells in order to quantify the rate of hypoxic cell turnover. Our experimental design was to administer pimonidazole between 3 and 96 hours prior to mouse sacrifice and EF5 always 3 hours prior to sacrifice (Figure 2.6A). As predicted by the data in Figure 2.5A-B, we found that the EF5 positive tumour area was consistent within tumour types (Figure 2.6B-D). Also as expected, the area positive for pimonidazole decreased as separation between pimonidazole administration and sacrifice increased (Figure 2.6B-D). When pimonidazole and EF5 are co-administered 3 hours prior to mouse sacrifice we observed strong agreement between the two markers, with 4-6% of tumour area singly-labelled for pimonidazole or EF5 in either WiDr or SiHa tumours (Figure 2.7A,B). As separation between pimonidazole administration and mouse sacrifice increased, the area singly-labelled for EF5 increased and the area singly-labelled for pimonidazole decreased or did not change, in both WiDr and SiHa tumours (Figure 2.7A,B).

Based on the observations of Figure 2.5 indicating that the EF5 positive hypoxic fraction is stable over time and the agreement between co-administered pimonidazole and EF5 (Figure 2.6C,D), we interpreted the EF5 positive tumour fraction as an estimate of the hypoxic fraction that was present at the time of pimonidazole administration. Thus, calculating the difference in the fraction of tumour area positive for EF5 and pimonidazole provides a change-from-baseline quantification of pimonidazole positive tumour area that was lost. This value was interpreted to indicate dying of pimonidazole labelled cells. This value of pimonidazole cell loss is displayed

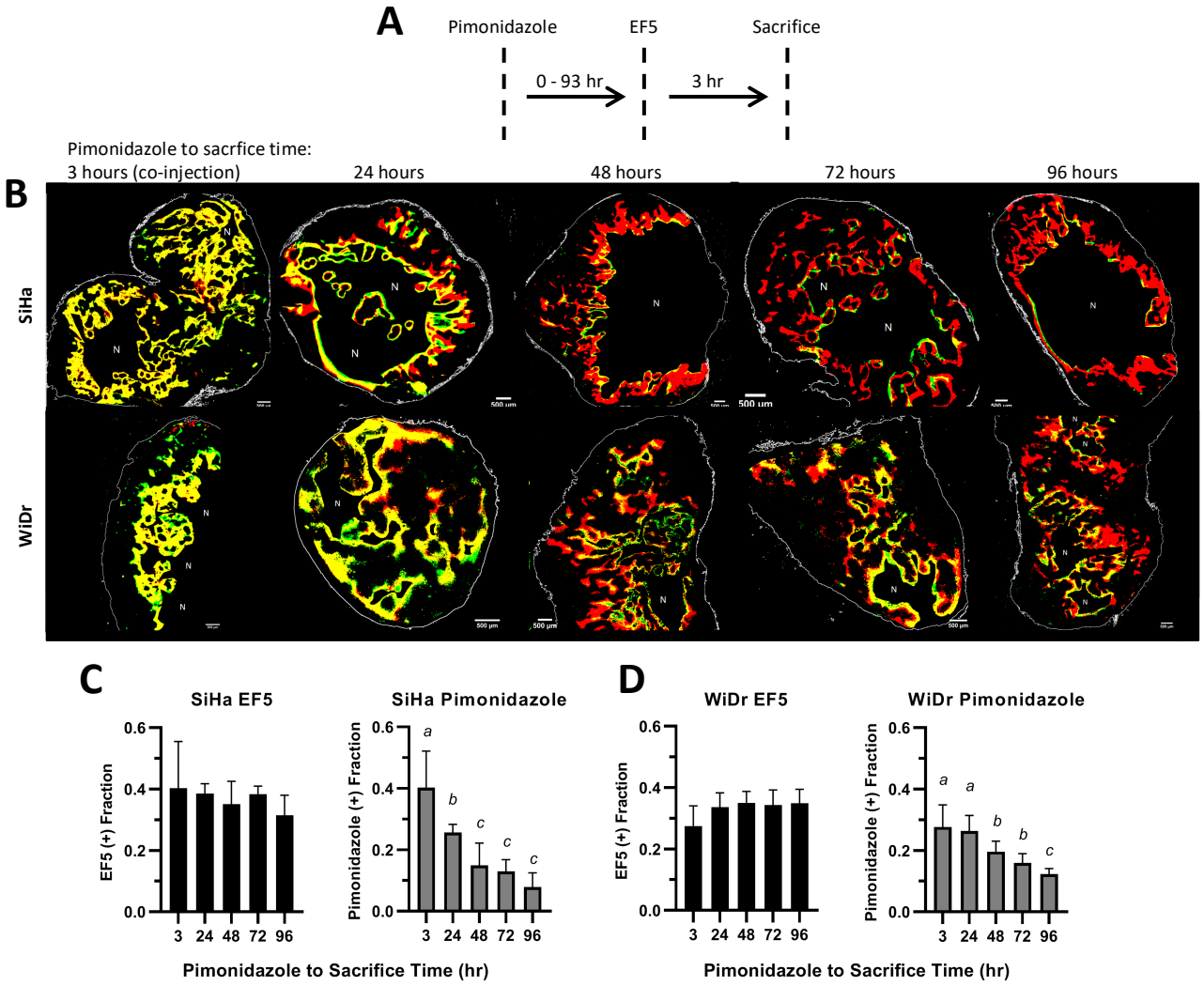

Figure 2.6 2-Nitroimidazole positive tumour area over time

(A) Timeline of *in vivo* experiments. (B) Representative images of SiHa and WiDr tumours for indicated pimonidazole to sacrifice separation times. Pimonidazole is shown as green, EF5 as red, overlap of the two is yellow, the tumour outline is indicated in white, and a 500 µm scale bar is displayed for each image. Images are displayed as they would be analyzed, each channel is binarized and regions of overt necrosis (N) have been removed. The fraction of tumour area positive for EF5 and pimonidazole is displayed for (C) SiHa and (D) WiDr tumours. The average EF5 positive fraction was consistent across all groups for both tumour types, while pimonidazole decreased over time in both groups. N = 9-12, mean ± 95% CI, Tukey multiple comparisons test results displayed, *a* vs *b* $p < 0.05$, *a* vs *c* $p < 0.001$, *b* vs *c* $p < 0.01$.

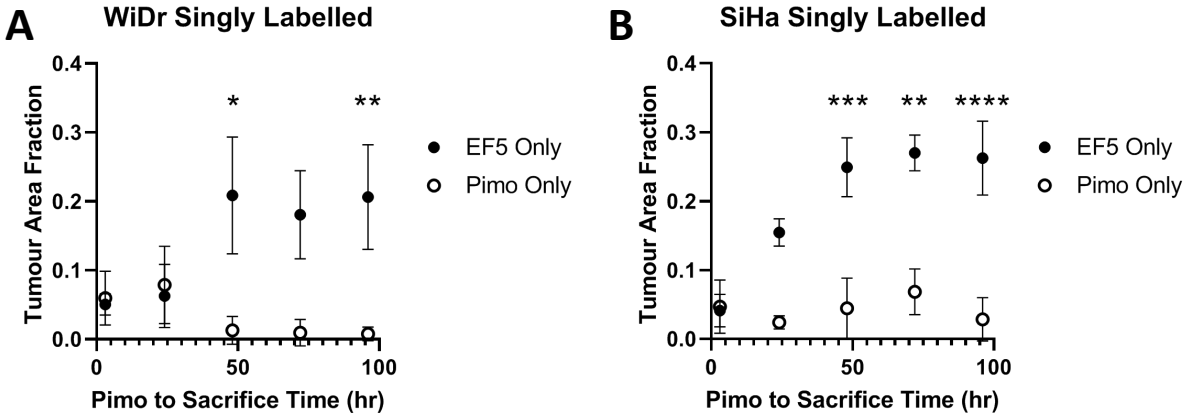

Figure 2.7 Pimonidazole and EF5 singly-labelled tumour area over time

The fraction of tumour area positive for only a single hypoxia marker plotted versus the time between pimonidazole administration and mouse sacrifice for (A) WiDr and (B) SiHa tumours. N = 9-12, mean ± SD, Kruskal-Wallis test results displayed. Statistics were calculated comparing each data point with the 3-hour time point within hypoxia marker groups, * $p < 0.05$, ** $p < 0.01$, *** $p < 0.001$, **** $p < 0.0001$.

for SiHa and WiDr tumours for each time point (Figure 2.8B,C, closed circles). Our data indicate a half-life for pimonidazole-labelled tumour cells of 42 hours and 54 hours for SiHa and WiDr tumours respectively.

2.3.5 Pentoxifylline reoxygenation of transient hypoxia

We were next interested in distinguishing between the loss of chronically hypoxic cells and transiently hypoxic cells. To do so, we applied the acute perfusion modifying drug pentoxifylline. Pentoxifylline is an anti-hypertensive hemorheologic agent that reduces blood viscosity by increasing erythrocyte deformability[39]. In the context of solid tumours this has the functional effect of increasing the fraction of perfused blood vessels and reoxygenating transient hypoxia. We have previously characterized WiDr tumours, and not SiHa tumours, to exhibit rapid mismatch of vessel perfusion status consistent with timelines of transient hypoxia[67]. Accordingly, pentoxifylline increases the perfusion indicator Hoechst 33342 labelling of blood vessels in WiDr but not SiHa tumours[50]. Further, we have previously found pentoxifylline to improve radiation response of tumour cells at intermediate distances from perfused blood vessels in WiDr tumours with no effect on cells at greater distances from blood vessels, and no effect in SiHa tumours[50]. These past data indicate that pentoxifylline specifically reoxygenates transiently hypoxic cells in WiDr tumours.

To validate that pentoxifylline was functioning to reduce 2-nitroimidazole labelling of transiently hypoxic tumour cells in this study, we administered pentoxifylline 15 minutes prior to EF5 (Figure 2.9A). As expected, when pentoxifylline is administered 15 minutes prior to EF5 we observe no difference in the EF5 positive fraction of SiHa tumours (Figure 2.9B). However, we observed a 26% decrease in the fraction of EF5 positive tumour area in WiDr tumours treated with pentoxifylline compared with controls (Figure 2.9B). This indicates that transiently hypoxic tumour cells constitute approximately 26% of the hypoxic fraction in WiDr tumours. Further, we compared EF5 labelling with the well characterized hypoxia-induced protein carbonic anhydrase IX (CAIX). CAIX has been used as an endogenous reporter of hypoxia that is expressed by chronic and transiently hypoxic cells[246] in part because it has a long expression half-life even upon reoxygenation (approximately 40 hours)[261]. Thus, tumour regions positive for CAIX but negative for an administered 2-nitroimidazole may indicate reoxygenated tumour cells. There was no effect of pentoxifylline treatment on the fraction of tumour area positive for CAIX

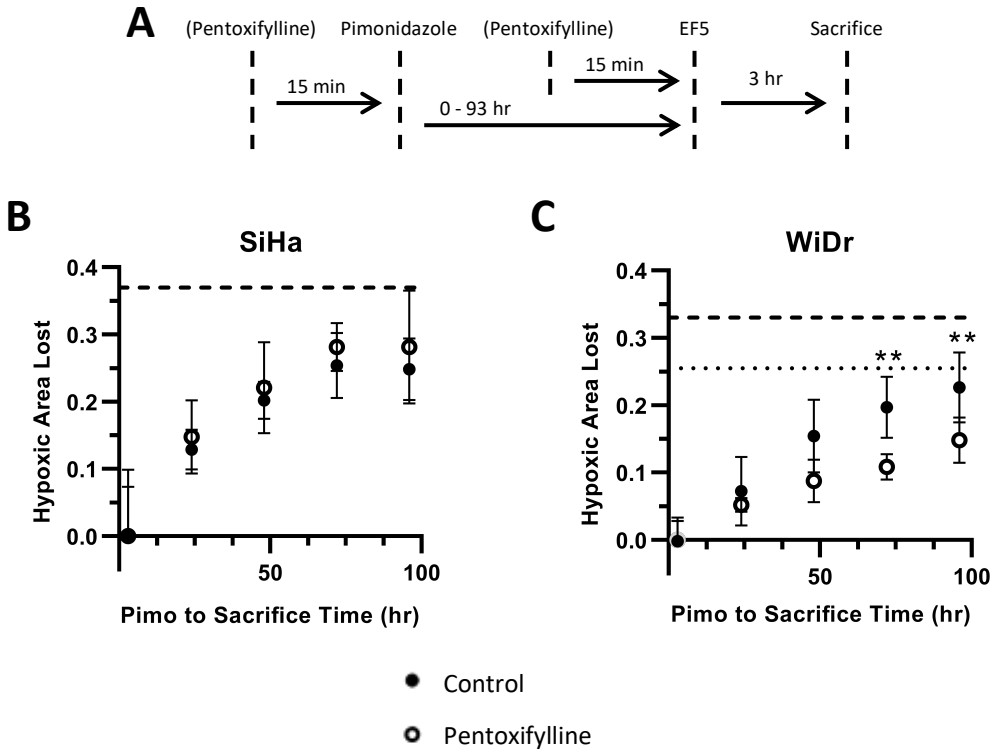

Figure 2.8 Time course of hypoxic area lost

(A) Experiment timeline. For (B) SiHa and (C) WiDr the difference between EF5 and pimonidazole positive tumour fraction was calculated to indicate the loss of pimonidazole-labelled hypoxic tumour area. The average EF5 positive tumour fraction across all time points is displayed as the dashed line for controls and the dotted line for pentoxifylline-treated mice. For the SiHa plot only the dashed line is shown as this overlaps with the average EF5 area for pentoxifylline treated SiHa tumours. Comparisons were made between control and pentoxifylline groups within time points, N = 9-12 mean ± 95% CI, Sidak multiple comparisons test results are displayed, ** $p < 0.01$.

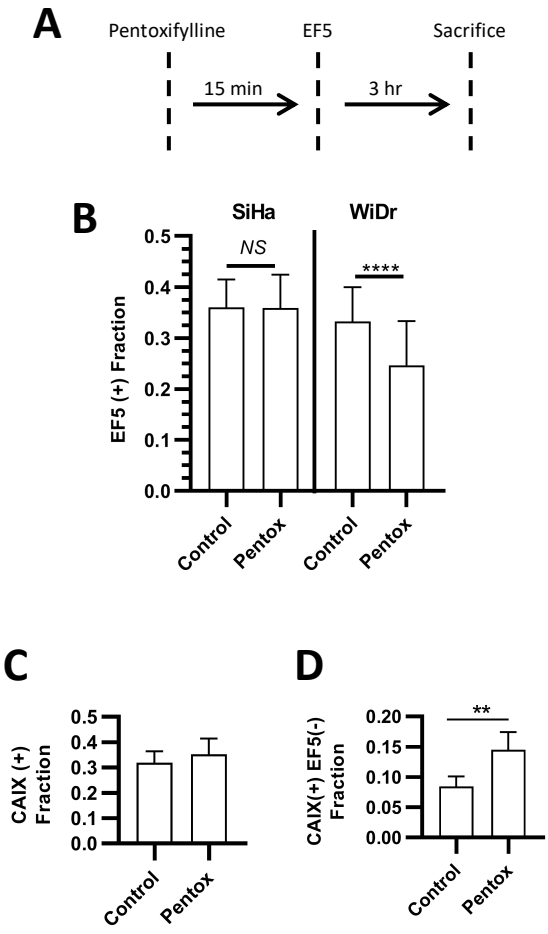

Figure 2.9 Perfusion limited hypoxia in WiDr tumours is reoxygenated by pentoxifylline.

(A) Experiment timeline. (B) EF5 positive tumour area is reduced in WiDr tumours, but not SiHa, when pentoxifylline is administered 15 minutes prior to EF5. N = 19-46 mean ± 95% CI, Mann-Whitney test **** $p < 0.0001$. Pentoxifylline does not reduce (C) CAIX positive tumour area in WiDr tumours but does increase the mismatch between EF5 and CAIX as indicated by the change in (D) tumour area positive for CAIX and negative for EF5. N = 15-20 mean ± 95% CI, Mann-Whitney test ** $p < 0.01$.

(Figure 2.9C). In WiDr tumours we observe some CAIX-positive EF5-negative tumour area in control mice, which is in agreement with past data that demonstrate hypoxia inducible factor 1α stabilizes at oxygen tensions greater than 2-nitroimidazole labelling (Chapter 1.5)[132]. However, pentoxifylline treatment significantly increased the amount of CAIX-positive EF5-negative tumour area (Figure 2.9D). These data demonstrate that pentoxifylline treatment is reoxygenating previously hypoxic CAIX positive tumour cells, resulting in reduced EF5 labelling of transiently hypoxic tumour cells.

2.3.6 Rate of chronic and transient hypoxic cell loss

We next applied pentoxifylline to distinguish between the rate of cell loss in chronic versus transient hypoxia. We compared experiments tracking the loss of pimonidazole positive tumour area over time with and without administering pentoxifylline 15 minutes prior to both pimonidazole and EF5 (Figure 2.8A). Pentoxifylline administered prior to both pimonidazole and EF5 reoxygenates the transiently hypoxic population and therefore removes this population from the time course, i.e. the loss of pimonidazole in pentoxifylline treated mice could not indicate loss of transiently hypoxic cells as they were never labelled and therefore the loss of pimonidazole must be attributed to chronically hypoxic cells. Thus, the difference in the rate of pimonidazole loss between control and pentoxifylline treated mice indicates loss of transiently hypoxic cells. Pentoxifylline treatment prior to pimonidazole and EF5 did not affect the total EF5 positive fraction or the loss of pimonidazole positive cells in SiHa tumours at any time point compared with control mice (Figure 2.8B). From this data we conclude that transiently hypoxic tumour cells do not contribute to pimonidazole loss in SiHa tumours. This data agrees with our past characterization that SiHa tumours do not exhibit rapid oxygen cycling[50,67,229]. Pentoxifylline treatment reduced the total EF5 positive fraction in WiDr tumours (Figure 2.8C). Pentoxifylline treatment prior to both pimonidazole and EF5 did not affect the loss of pimonidazole positive cells in WiDr tumours compared with control mice when pimonidazole was administered 24 or 48 hours prior to sacrifice (Figure 2.8C). This observation indicates that the major population of hypoxic cells lost in the first 48 hours after labelling are chronically hypoxic cells. However, pentoxifylline treatment significantly reduced the loss of pimonidazole positive cells at all later time points (Figure 2.8C). These data suggest that transiently hypoxic

cells are protected from cell loss in the first 48 hours after labelling but begin dying in the third day after labelling.

In WiDr tumours we observe that chronically hypoxic tumour cells outnumber transiently hypoxic cells significantly, approximately 3:1 indicated by the fraction of tumour area labelled by EF5 in control mice (0.33 ± 0.07, mean ± SD; chronic + transient hypoxia) and pentoxifylline treated mice (0.25 ± 0.09, mean ± SD; chronic hypoxia alone), i.e. transient hypoxia constitutes a fraction of approximately 0.08 of the tumour area (Figure 2.9B). Comparing the pimonidazole area lost in WiDr tumours between control and pentoxifylline-treated mice with 72 hours of separation between pimonidazole and sacrifice (control = 0.20 ± 0.06, pentoxifylline = 0.11 ± 0.03, mean ± SD) and 96 hours of separation (control = 0.23 ± 0.08, pentoxifylline = 0.15 ± 0.05, mean ± SD; Figure 2.8C) suggests that approximately 0.08-0.09 of the pimonidazole area lost can be attributed to transient hypoxia. Thus, these data suggest that transiently hypoxic tumour cells are completely lost within 72 hours after pimonidazole labelling.

2.3.7 Radiation-induced vascular failure

A major implication of tumour hypoxia is the survival of hypoxic tumour cells following irradiation. We have previously found that pentoxifylline-sensitive transiently hypoxic tumour cells contribute to tumour radiation resistance when tumours are harvested shortly after irradiation for clonogenic assay[50]. However, radiation doses greater than ~8 Gy cause endothelial cell apoptosis that leads to additional tumour cell death[169,170]. It is currently unknown whether radiation-induced vascular destruction preferentially kills chronically or transiently hypoxic tumour cells. To investigate the response of hypoxic populations to both direct radiation cell killing and indirect cell killing via vascular destruction, we compared multiple irradiation protocols and two harvest time points. Tumours were either irradiated with a single dose of 5 Gy or a single dose of 10 Gy (Figure 2.10A), and based on previous studies we predicted that only the latter would induce vascular destruction[169]. For comparison of equivalent cumulative doses, parallel tumours were irradiated with two doses of 5 Gy administered 6 hours apart (Figure 2.10A). The separation time was provided to allow for repair of DNA damage induced by the first dose. Radiation-induced endothelial cell apoptosis following large single radiation doses takes 4-6 hours to occur, and additional time is required for subsequent tumour cell starvation[169,170]. Thus, to investigate the response of the tumour microenvironment to each

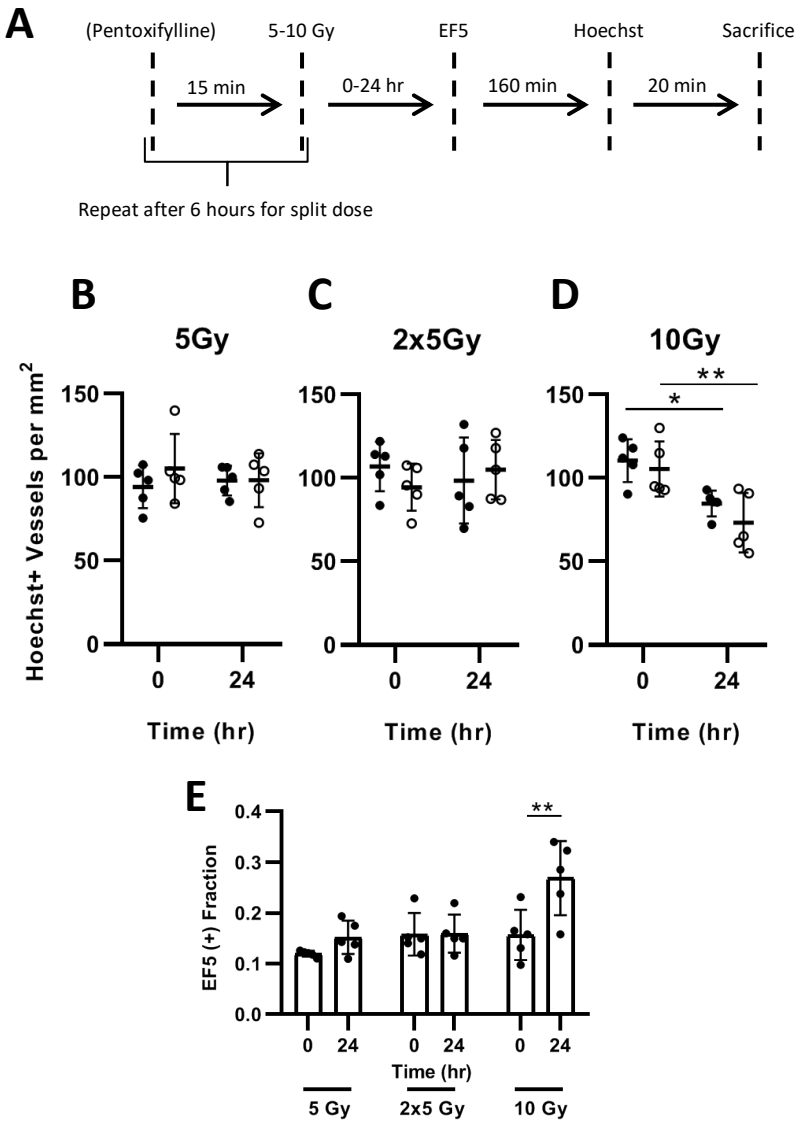

Figure 2.10 Radiation-induced vascular failure

(A) Experiment timeline. The density, per square mm, of perfused blood vessels identified by immunofluorescent microscopy detection of Hoechst 33342-positive CD31-positive vessel objects within viable tumour regions is displayed for WiDr tumours subject to (B) a single dose 5 Gy, (C) two doses of 5 Gy 6 hours apart, and (D) a single dose of 10 Gy. Closed circles indicate control tumours, open circles indicate pentoxifylline treated tumours. (E) The fraction of tumour area positive for EF5 in control tumours.

radiation exposure, we compared tumours harvested 3 hours after the final radiation dose and 27 hours after their final dose (Figure 2.10A).

We first investigated the response of the tumour microenvironment to each irradiation protocol. All mice were administered EF5 3 hours prior to sacrifice and Hoechst 33342 20 minutes prior to sacrifice (Figure 2.10A). For mice sacrificed 3 hours following irradiation EF5 was administered immediately following irradiation. We quantified the density of Hoechst 33342 positive CD31 positive blood vessels in WiDr tumours as an indicator of microregional vessel function. There was no effect of harvest time on the density of Hoechst 33342 positive vessels in the tumours exposed to 5 Gy or 2x5 Gy (Figure 2.10B,C). These data indicate that neither 5 Gy or 2x5 Gy radiation treatments induced destruction of tumour vasculature. However, we observed a significant reduction in the density of Hoechst 33342 positive CD31 blood vessels in the tumours harvested 27 hours following 10 Gy irradiation compared to those harvested 3 hours post-irradiation (Figure 2.10D). These data are in agreement with past studies reporting that single doses of x-irradiation greater than 8 Gy are sufficient to induce vascular failure within 24 hours of irradiation[169,170]. Pentoxifylline treatment 15 minutes prior to irradiation did not affect Hoechst 33342 positive vessel density for any radiation treatment (Figure 2.10B-D). We hypothesized that a functional effect of the vascular failure would be an increase in tumour hypoxia. To investigate this, we quantified the fraction of tumour area positive for EF5. Further in agreement with vascular dysfunction, we observed a significant increase in the fraction of tumour area positive for EF5 when tumours were harvested 27 hours following 10 Gy irradiation compared to 3 hours post-irradiation (Figure 2.10E). There was no effect of harvest time on the fraction of tumour area positive for EF5 in the tumours subject to 5 Gy or 2x5 Gy (Figure 2.10E), consistent with no change in the density of perfused blood vessels. These data indicate that a single dose of 10 Gy x-irradiation induces vascular destruction in WiDr tumours, while 5 Gy and 2x5 Gy doses do not[169,170].

2.3.8 Hypoxic cell survival following irradiation

Tumour cell survival was quantified via clonogenic assay. As expected, 10 Gy x-irradiation induced greater cell kill than either 5 Gy or 2x5 Gy (Figure 2.11A-C). Mice receiving pentoxifylline 15 min prior to each radiation dose were compared with controls. Clonogenic survival of WiDr tumour cells harvested 3 hours after the final dose of irradiation was decreased

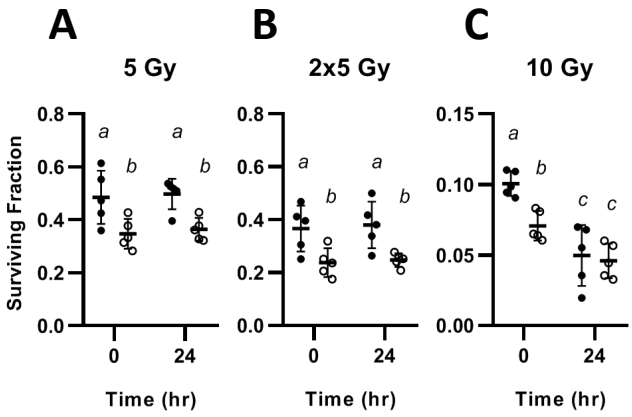

Figure 2.11 Hypoxic cell response to direct and indirect effects of irradiation.

Clonogenic survival of WiDr tumour cells from (A) a single dose 5 Gy, (B) two doses of 5 Gy 6 hours apart, and (C) a single dose of 10 Gy are displayed. Note the different range in the y-axis used for (C). Closed circles represent control tumours, open circles represent pentoxifylline treated tumours. Clonogenic survival data shown are after correction from plating efficiency calculated from 5 non-irradiated tumours of each group. N=5, mean ± SD, Tukey multiple comparisons test results displayed; *a* vs *b* $p < 0.05$, *a* vs *c* $p < 0.001$, *b* vs *c* $p < 0.05$.

by pentoxifylline for all radiation schedules (Figure 2.11A-C), indicating that transiently hypoxic cells are resistant to direct radiation cell killing. Pentoxifylline reduced tumour cell survival by approximately 28%, 35%, and 30% for tumours irradiated with 5 Gy, 2x5 Gy, and 10 Gy respectively. These data suggest that transiently hypoxic tumour cells represent between 28-35% of radiation-resistant tumour cells. As we found transiently hypoxic cells to represent approximately 26% of the hypoxic population in WiDr tumours (Figure 2.8, Figure 2.9), these data suggest similar resistance to radiation between chronic and transiently hypoxic tumour cells.

For control tumours administered a single dose of 5 Gy or 2x5 Gy, clonogenic survival of tumour cells was similar whether tumours were harvested 3 hours post-irradiation or 27 hours post-irradiation (Figure 2.11A,B). Further, clonogenic survival was similar at both harvest time points for pentoxifylline-treated tumours administered 5 Gy or 2x5 Gy. These data indicate that there was no significant indirect radiation-induced cell killing of either chronically or transiently hypoxic tumour cells following either 5 Gy or 2x5 Gy, consistent with no change in perfused vessel density and hypoxic fraction (Figure 2.10).

However, we observe a significant reduction in the clonogenic survival of control WiDr tumour cells 27 hours after a single dose of 10 Gy compared to 3 hours post-irradiation (Figure 2.11C). This indicates the loss of some hypoxic cells due to an indirect effect of irradiation, consistent with our observation of vascular destruction following 10 Gy irradiation (Figure 2.10). In the 24-hour period after 10 Gy irradiation, the surviving fraction in control tumours dropped from 0.101 ± 0.004 to 0.050 ± 0.010 (mean ± SEM). This data indicates killing of tumour cells due to an indirect effect of irradiation, consistent with our observation of vascular destruction following 10Gy. This indicates that the fraction of cells that survived the direct effects of irradiation but died to the indirect effects was ~0.051.

To determine the contribution of chronic and transient hypoxia to the fraction of tumour cells that was lost to the indirect effects of irradiation we compared the survival of control tumours with pentoxifylline-treated tumours. In pentoxifylline treated tumours, we again observe a significant decrease in tumour cell survival when tumours were harvested 27 hours post-irradiation compared with 3 hours post-irradiation (Figure 2.11). This indicates loss of specifically chronically hypoxic tumour cells due to an indirect effect of irradiation. In the 24-hour period after 10 Gy irradiation, the surviving fraction in pentoxifylline-treated tumours dropped from 0.071 ± 0.005 to 0.046 ± 0.005 (mean ± SEM). These data indicate that the

majority (0.046/0.071 = 64%) of chronically hypoxic tumour cells that survive the direct effects of irradiation also survive the 24-hour period following 10 Gy. These data further indicate that the fraction of tumour cells that were chronically hypoxic at the time of irradiation, survived the direct effects of irradiation, and died in the 24-hour period following 10 Gy was equal to ~0.025.

Thus, death of chronically hypoxic cells in the pentoxifylline-treated group cannot fully account for the death of tumour cells due to indirect effects of irradiation. The remaining fraction of tumour cells that survived the direct effects of irradiation but died in the 24-hour period following 10 Gy irradiation is equal to approximately ~0.026 and must be attributed to transiently hypoxic tumour cells. Our data indicate that the fraction of tumour cells that were transiently hypoxic cells at the time of irradiation and survived the direct effects of radiation was ~0.030 (0.101 ± 0.004 vs 0.071 ± 0.005, mean ± SEM, 3-hour harvest control vs pentoxifylline). Thus, these data indicate that the majority (0.026/0.030 = 87%) of transiently hypoxic tumour cells that are radiation resistant die due to 10 Gy radiation-induced vascular destruction.

The data from the irradiation studies suggest that pentoxifylline-sensitive transiently hypoxic cells are sufficiently hypoxic during periods of low oxygenation to exhibit resistance to the direct effects of 5 Gy, 2x5 Gy, and 10 Gy x-irradiation. We observe no significant loss of transient hypoxia or chronic hypoxia clonogens in the day following 5 Gy or 2x5 Gy, indicating that the rate of loss for both populations observed in untreated tumours is inhibited by low doses of irradiation. The data also suggest that both hypoxic populations are sensitive to cell loss attributable to 10 Gy radiation-induced vascular dysfunction, although transiently hypoxic tumour cells appear particularly sensitive.

2.4 Discussion

Research interested in the phenomenon of fluctuating microregional perfusion and oxygen supply is widely varied in terms of the methodology used for hypoxia-reoxygenation cycle frequency, pO_2 range, and total duration. The variability in methodology is due in part to a poor understanding of the *in vivo* experience of transiently hypoxic cells. In this study, we present evidence on the basic understanding of transient hypoxia in solid tumours by investigating the turnover of these cells in untreated and irradiated tumours. We hypothesized that transiently hypoxic cells would have a greater lifetime than chronically hypoxic cells based on relative distance to necrosis. In WiDr tumours, we observed loss of preferentially chronically

hypoxic cells in the first 48 hours after labelling with pimonidazole, followed by loss of transiently hypoxic cells between 48 and 72 hours after labelling (Figure 2.8). Further, we observe that the amount of hypoxic cell loss that could be attributed to transiently hypoxic cells was similar to the total amount of transiently hypoxic cells estimated to exist in WiDr tumours (Figure 2.8), suggesting that the majority of transiently hypoxic cells were lost in this time period. These data would therefore recommend that future studies modelling transient hypoxia limit the total experimental protocol duration to 72 hours[129].

However, for modelling of transient hypoxia, it is also relevant that transiently hypoxic tumour cells are likely to eventually occupy sites of chronic hypoxia. In this study we observe loss of chronically hypoxic cells followed in sequence by transiently hypoxic cells (Figure 2.8) in support of the ordered layering of tumour cells outward from blood vessels; normoxic, transiently hypoxic cells, chronically hypoxic cells, and necrosis. If or when transiently hypoxic cells transition into layers of chronic hypoxia is currently unclear, the study of which would benefit from a method that positively labels transient hypoxia cells as opposed to the negative selection in this study. However, our data suggest that it takes 48 hours to deplete the chronically hypoxic tumour cells layers in tumour cords prior to loss of initially transiently hypoxic cells (Figure 2.8). Therefore, it should be expected that initially transiently hypoxic cells will take 48 hours to traverse the chronically hypoxic cell layers as well. Therefore, the results of this study would recommend that future studies modelling transient hypoxia limit the duration of hypoxia cycles to 24 hours with the possibility for exposure to chronic hypoxia for up to 48 hours afterwards.

The next question in improving the modelling of transient hypoxia is the degree of hypoxia. Transiently hypoxic cells, as this study demonstrates, are capable of being labelled by 2-nitroimidazoles (Figure 2.9) and exhibit significant radiation resistance up to at least 10 Gy x-irradiation (Figure 2.11), which is in agreement with past study of transient hypoxia[50]. Studies monitoring erythrocyte flux concurrently with local oxygen tension have found that cycles of oxygen delivery fitting with timelines of transient hypoxia match with a wide range of changes in oxygen tension, although the majority of these fluctuations are within 5-10 mmHg, or approximately 1% pO_2[118]. Further, oxygen supply to tumour cells directly at the blood vessel wall have been estimated as low as 2-5% pO_2[262,263]. Fluctuations of erythrocyte flux as opposed to complete vessel collapse are more consistent with observations that transiently hypoxic cells

exist at intermediate distances from perfused blood vessels[50] and the rapid switch from loss of chronically hypoxic cells to transiently hypoxic cells observed in this study (Figure 2.8). Transiently hypoxic cells therefore likely experience some intermediate oxygenation below the pO_2 at the vessel wall during periods of oxygen delivery, which would allow for a drop in oxygen supply of only 5-10 mmHg to drop these cells to an oxygen tension sufficient to both strongly label with 2-nitroimidazoles and exhibit radiation resistance. Therefore, the upper limit for O_2 exposure to transiently hypoxic cells should be kept below 5% O_2, as opposed to the hyper-oxic 21% O_2 exposures applied in some studies[264]. The O_2 content during 'hypoxic' phases should reflect the radiation resistance (Figure 2.11)[50], 2-nitroimidazole labelling (Figure 2.8), and lack of proliferation (Figure 2.4)[68] of transiently hypoxic cells, and should therefore be kept at or below 0.5% O_2.

Further understanding of transient hypoxia that is currently unclear in the literature is the *de novo* generation of transient hypoxia. In WiDr tumours we observe that chronically hypoxic tumour cells outnumber transiently hypoxic cells significantly, approximately 3:1 indicated by the fraction of tumour area labelled by EF5 in control mice and pentoxifylline treated mice (Figure 2.9), and that the majority of transiently hypoxic tumour cells die within 72 hours after labelling with pimonidazole (Figure 2.8). This suggests that transient hypoxia does not contribute to the population of hypoxic cells that survived the 96-hour experiment and that transient hypoxia likely develops primarily in tumour regions with necrosis. Transiently hypoxic tumour cells residing exclusively in tumour cords that also contain chronic hypoxia and necrosis agrees with previous reports finding that tumour cord oxygenation is most sensitive to perfusion fluctuations in regions with low vascular density[119]. In turn, the chronically hypoxic population contributes both to the hypoxic cells that are lost early after labelling and to the hypoxic cells that survive the 96-hour experiment. These data indicate that chronically hypoxic cells likely reside both in tumour cords with necrosis, where they are in cell layers between transiently hypoxic cells and necrosis, and tumour cords without necrosis. Studies investigating a wider time range than the current study may be necessary to investigate the kinetics of how, or if, tumour cords with chronic hypoxia but no necrosis develop into tumour cords with transient hypoxia and/or necrosis.

We find that both chronically and transiently hypoxic tumour cells contribute to tumour cell survival following each radiation schedule tested, 1x5Gy, 2x5Gy, and 1x10Gy, in similar

proportion to their estimated abundance in WiDr tumours (Figure 2.9, Figure 2.11). This further supports the existing evidence that transiently hypoxic tumour cells are important considerations for tumour radiation resistance[50,106,108,202,214,244]. We further find that 10 Gy of x-irradiation induced a decrease in the density of Hoechst 33342 perfused CD31-positive blood vessels 24 hours post-irradiation, leading to an increase in tumour hypoxia and induction of tumour cell killing (Figure 2.10, Figure 2.11). This was not observed with either a single dose of 5 Gy or two doses of 5 Gy 6 hours apart. These observations are in agreement with past reports that endothelial cell apoptosis is induced by single doses of irradiation greater than ~8 Gy[169,170]. Importantly, we observed that transiently hypoxic tumour cells were disproportionately affected by radiation-induced vascular destruction compared with chronically hypoxic tumour cells, and only a small minority (<15%) of transient hypoxia-derived clonogens survived the indirect cell killing following 10 Gy (Figure 2.11). This suggests that transiently hypoxic tumour cells may be killed by large single doses of radiation that induce vascular destruction.

The killing of transiently hypoxic tumour cells by radiation-induced vascular destruction has implications for studies investigating interventions aiming to reoxygenate transiently hypoxic tumour cells. The majority of North American radiotherapy protocols apply fractionated radiotherapy with individual doses below the observed threshold to induce vascular destruction (often 2 Gy), while the majority of pre-clinical studies apply large single doses (often ≥ 10 Gy) in order to assay the population of severely hypoxic tumour cells. The goal for an intervention aiming to reoxygenate transiently hypoxic tumour cells, such as nicotinamide or pentoxifylline, is to increase the direct cell killing of radiation as this will be the main form of cell death induced by radiation in fractionated protocols. Direct radiation-induced cell killing will be captured if tumours are harvested soon after irradiation for clonogenic survival assays[50], but the effect of any reoxygenating intervention may be masked by death due to vascular destruction if tumours are not harvested and instead monitored in a tumour control or growth delay assay[265]. Therefore, studies aiming to reoxygenate transiently hypoxic tumour cells at the time of radiation should consider the potential effects of cell killing due to vascular destruction.

Overall, we observe that transiently hypoxic tumour cells survive in untreated WiDr tumours for up to 72 hours after labelling with pimonidazole. Transiently hypoxic tumour cells survive longer than neighbouring chronically hypoxic cells, which die within the first 48 hours after pimonidazole labelling. However, the longest-lived hypoxic cells in WiDr tumours are

likely chronically hypoxic cells that reside in tumour cords without necrosis. We find that transiently hypoxic tumour cells are resistant to radiation, confirming that these cells are important targets to modify tumour radiation response. However, the potential to induce transient hypoxic cell death due to radiation-induced vascular destruction must be considered when interpreting the effects of interventions aiming to reoxygenate transiently hypoxic cells at the time of radiation.

Chapter 3: 2-^{18}F-Fluoroethanol is a novel positron emission tomography reporter of solid tumour perfusion

The contents of this chapter are published: Brennan J Wadsworth, Jinhe Pan, Iulia Dude, Nadine Colpo, Momir Bosiljcic, Kuo-Shyan Lin, Francois Benard, and Kevin L Bennewith. (2017) 2-^{18}F-Fluoroethanol is a PET reporter of solid tumor perfusion. J Nucl Med. 58:815-820.

SYNOPSIS

Solid tumour perfusion is a proven variable of interest for predicting cancer aggression and response to therapy. Current methods for non-invasively imaging tumour perfusion with positron emission tomography (PET) are limited by restricted accessibility and short half-lives of perfusion radiotracers. This study presents 2-^{18}F-fluoroethanol (2-^{18}F-FEtOH) as a perfusion reporter that can distinguish between tumours of varying perfusion levels and can be applied to screening drugs that modify tumour perfusion.

Uptake of 2-^{18}F-FEtOH in 4T1 and 67NR murine mammary carcinoma tumours grown in mice was measured using *ex vivo* radiography as well as static and dynamic PET imaging. Uptake of 2-^{18}F-FEtOH was directly compared with the ^{14}C-Iodoantipyrine perfusion reporter and perfusion-modifying drugs nicotinamide, pentoxifylline, and hydralazine were utilized to manipulate tumour perfusion before 2-^{18}F-FEtOH quantification.

Uptake of 2-^{18}F-FEtOH was greater in 67NR tumours compared with 4T1 tumours, consistent with known perfusion differences within and between these tumours. Uptake of 2-^{18}F-FEtOH corresponded well with ^{14}C-Iodoantipyrine with a strong dynamic range to distinguish between 4T1 tumours, 67Nr tumours, and brain tissue. Uptake of 2-^{18}F-FEtOH was increased in tumours following treatment with either nicotinamide or pentoxifylline, and uptake was reduced by treatment with hydralazine.

These data indicate that 2-^{18}F-FEtOH is a novel ^{18}F-based radiotracer for investigating tumour perfusion with PET imaging. Quantification of 2-^{18}F-FEtOH uptake can be used to distinguish between tumours of varying perfusion, and to screen the efficacy of blood flow modifying drugs for use as adjuvants to existing cancer therapies.

3.1 Introduction

Non-invasive imaging modalities are critical components of cancer care that can visualize the varied and widespread nature of cancer. PET is a workhorse technique for non-invasive imaging. The utility of PET has evolved from detecting metabolically active tumours with 2-^{18}F-fluorodeoxyglucose towards a broader ability to characterize the tumour microenvironment. Within this trend are radiotracer indicators of tumour hypoxia (i.e. regions of low oxygen content), such as ^{18}F-fluoromisonidazole, ^{18}F-fluoroazomycin arabinoside, and ^{18}F-EF5. Tumour hypoxia is associated with reduced overall survival and poor prognosis in multiple cancer types[106] because hypoxic cells are resistant to therapy and exhibit multi-faceted support of metastasis[266]. Successes of PET hypoxia reporters in patient studies include distinguishing aggressive high-grade glioblastoma multiform from less aggressive astrocytoma and oligodendrioma[267] as well as prediction of resistance to primary endocrine therapy in breast cancer[268].

Hypoxia develops in tumours from a combination of high metabolic demand and insufficient delivery of oxygenated blood (Chapter 1.2). Tumour vasculature is typically abnormal, exhibiting low vascular density and a dysfunctional architecture prone to leakiness and regional perfusion loss (Chapter 1.1)[245]. Tumour perfusion itself is also a primary variable of interest with potential effects on tumour metabolism and delivery of chemotherapeutics[85,90]. Measuring tumour perfusion either at baseline or before and after a therapy cycle has predicted disease free survival in patients with breast cancer[59,269], response to chemotherapy in head and neck cancer[270], response of cervical cancer to radiation therapy[271], and response of glioblastoma to anti-angiogenic therapy[272]. In addition to complementing hypoxia reporters and independently providing prognostic data, non-invasive imaging of tumour perfusion could be used pre-clinically to study strategies for modifying tumour perfusion for either radio-sensitization or manipulating chemotherapy delivery.

The gold standard in PET based imaging of perfusion is ^{15}O-H_2O (half-life: 2 minutes). The initial development of ^{15}O-H_2O was for myocardial perfusion imaging[42,45] and cerebral perfusion imaging[46], although ^{15}O-H_2O has recently been used for imaging tumour perfusion[57–59]. The main challenge with using ^{15}O-H_2O and other established PET reporters of perfusion with rapid half-lives, such as ^{15}O-butanol[47] and ^{13}N-NH_3[48] (half-life: 10 minutes), is the requirement of an on-site cyclotron for production and nearby administration. Rubidium-82 (^{82}Rb, half-life:

1.25 minutes) is a validated perfusion reporter[49] that can be produced using a $^{82}Sr/^{82}Rb$ generator, thus alleviating the need for an on-site cyclotron. However, ^{82}Rb suffers from a long positron range[60], which reduces PET resolution. ^{82}Rb also exhibits relatively low tissue extraction from the blood, at least in myocardium studies, which results in poor contrast between well-perfused and poorly-perfused regions[53]. Development of an ^{18}F (half-life: 110 minutes) based reporter of tumour perfusion will provide both logistical and accessibility benefits, while possessing the shortest positron range (and therefore highest PET resolution) of the radioisotopes discussed[60].

This study presents 2-^{18}F-fluoroethanol (2-^{18}F-FEtOH) as a novel reporter of tumour perfusion. We have previously shown that 2-^{18}F-FEtOH indiscriminately labels well-perfused organs in the body, exhibits relatively low rates of defluorination, and provides a large window of time for imaging due to an extended plateau of activity that is protected from biological clearance[273]. This plateau is believed to arise from intracellular conversion of 2-^{18}F-FEtOH to ^{18}F-fluoroacetate followed by conversion to ^{18}F-fluoroacetylCoA and ^{18}F-fluorocitrate, both of which are trapped inside cells[274]. We predict that this 2-^{18}F-FEtOH-mediated accumulation of ^{18}F inside well-perfused cells will enhance contrast against poorly perfused cells to provide strong resolution of intra-tumoural regional differences in perfusion status and allow for imaging of tumour perfusion well after the injection of the radiotracer.

We aimed to validate 2-^{18}F-FEtOH as a reporter of tumour perfusion using PET in murine tumour models. We assessed if 2-^{18}F-FEtOH uptake would discriminate between tumours with differing perfusion phenotypes by comparing 67NR and 4T1 murine mammary carcinomas[275]. To determine if 2-^{18}F-FEtOH uptake is specific to perfusion status we conducted direct comparison to the established perfusion reporter ^{14}C-iodoantipyrine (^{14}C-IAP)[43], we conducted kinetic analysis of dynamic PET scans to ensure 2-^{18}F-FEtOH uptake was dependent on plasma input, and we manipulated tumour perfusion with the blood flow modifying agents nicotinamide, pentoxifylline, and hydralazine. Our data indicate that 2-^{18}F-FEtOH is a novel radiotracer applicable to quantifying native or drug-induced changes in tumour perfusion by PET.

3.2 Materials and methods

3.2.1 2-^{18}F-Fluoroethanol synthesis

2-^{18}F-FEtOH was synthesized as described previously[273].

3.2.2 Gamma counting and liquid scintillation counting

^{14}C-Iodoantipyrine and 2-^{18}F-FEtOH were co-injected into anesthetized mice, which were sacrificed 2 minutes post-injection for tissue harvest. Harvested tissue was subject to gamma counting for detection of ^{18}F activity using a Wizard2 2480 automatic gamma counter (Perkin Elmer) followed by ^{14}C counting using a RackBeta1219 liquid scintillation counter (LKB Wallac).

3.2.3 Tumour models

10 week old female BALB/c mice were purchased from Taconic (Germantown, NY) and housed in the Animal Resource Centre at the BC Cancer Agency Research Centre under specific pathogen-free conditions. 67NR and 4T1 murine mammary carcinoma cell lines (gifts from Dr. Fred Miller, Karmanos Cancer Institutes, Detroit, MI) were maintained in RPMI 1640 medium + 10% FBS and used within 20 passages. All animal experiments were performed in accordance with Institutional and Canadian Council on Animal Care guidelines.

3.2.4 Antibodies

Tumour sections were stained with unconjugated CD31 antibody (BD Pharmingen) with Alexa 594 secondary antibody (Invitrogen), and FITC-conjugated antibody against pimonidazole (Hypoxyprobe). 100mg/kg pimonidazole was injected intraperitoneally 1.5 hours prior to mouse sacrifice. Images were captured with a Retiga EXi camera (QImaging) using an Axiovert S100 microscope (Carl Zeiss Canada).

3.2.5 *Ex vivo* radiography experiments

Mice received tail vein injections of 20 MBq 2-^{18}F-FEtOH followed 55 minutes later by tail vein injection of 50 µL of 10 mg/mL Hoechst 33342 (Thermo Fisher Scientific). Drug treated mice received either 500 mg/kg nicotinamide (Sigma-Aldrich) 30 min prior to 2-^{18}F-FEtOH, 10 mg/kg hydralazine (Sigma-Aldrich) 15 min prior to 2-18F-FEtOH, or 50 mg/kg pentoxifylline (Sigma-Aldrich) 15 min prior to 2-^{18}F-FEtOH. Tumours were harvested and immediately embedded in OCT, sectioned onto microscope slides, and incubated on a phosphor screen for 90 min before detection using a Typhoon FLA 9500 scanner (GE Life Sciences).

Phosphor images were analyzed using ImageJ software. Activity histograms were gathered from regions of interest drawn around individual tumours. The line profile function on ImageJ was used to quantify regional differences in 2-^{18}F-FEtOH activity. This tool returns the pixel intensity at each point along a line drawn across the full width of each tumour radiography image. To quantify the presence of central ischemia, the intensity of ^{18}F activity at the centre of each tumour was calculated as the average of the 11 pixels closest to the mid-point of each line. Tumour-centre intensity values were divided by the maximum intensity value of the entire tumour to express the tumour-centre values as a fraction of the maximum. Three line profiles were drawn and data averaged for each tumour image.

3.2.6 PET imaging experiments

PET imaging was conducted as previously published[273]. Rate of irreversible 2-^{18}F-FEtOH uptake was determined with the Patlak method[276] using image-derived input functions from the vena cava as previously published[55] and analysis conducted with MatLab software (MathWorks).

3.3 Results

3.3.1 2-^{18}F-FEtOH uptake depicts regional perfusion differences

Immunofluorescent images of 67NR and 4T1 (Figure 3.1A) tumours grown orthotopically in contralateral mammary fat pads show distinct phenotypes of vascular density and blood vessel function. CD31 vascular endothelium staining was significantly more prevalent in 67NR than in 4T1 tumours (Figure 3.1B; tumour area positive for CD31 equal to 10.0 ± 0.7% in 67NR vs 4.4 ± 0.2% in 4T1; mean ± standard error of the mean (SEM)), indicating greater vascular density in 67NR tumours. We also assessed uptake of intravenously administered Hoechst 33342 fluorescent dye, which diffuses out of perfused blood vessels to intercalate into cellular DNA. Nearly twice as much tumour area stained positive for Hoechst 33342 in 67NR vs 4T1 tumours (Figure 3.1B; 10.3 ± 0.7% vs 5.8 ± 0.6% mean ± SEM) indicating that 67NR tumour blood vessels are relatively well-perfused. Consistently, we observed greater staining of the exogenous hypoxia reporter pimonidazole in 4T1 tumours than in 67NR tumours (Figure 3.1B; 23.0 ± 2.5% vs 0.5 ± 0.2% mean ± SEM). Overall, the 4T1 tumours were found to exhibit low blood vessel density, poor perfusion, and large amounts of hypoxia, which opposes their syngeneic counterpart 67NR tumours and agrees with past research[277,278].

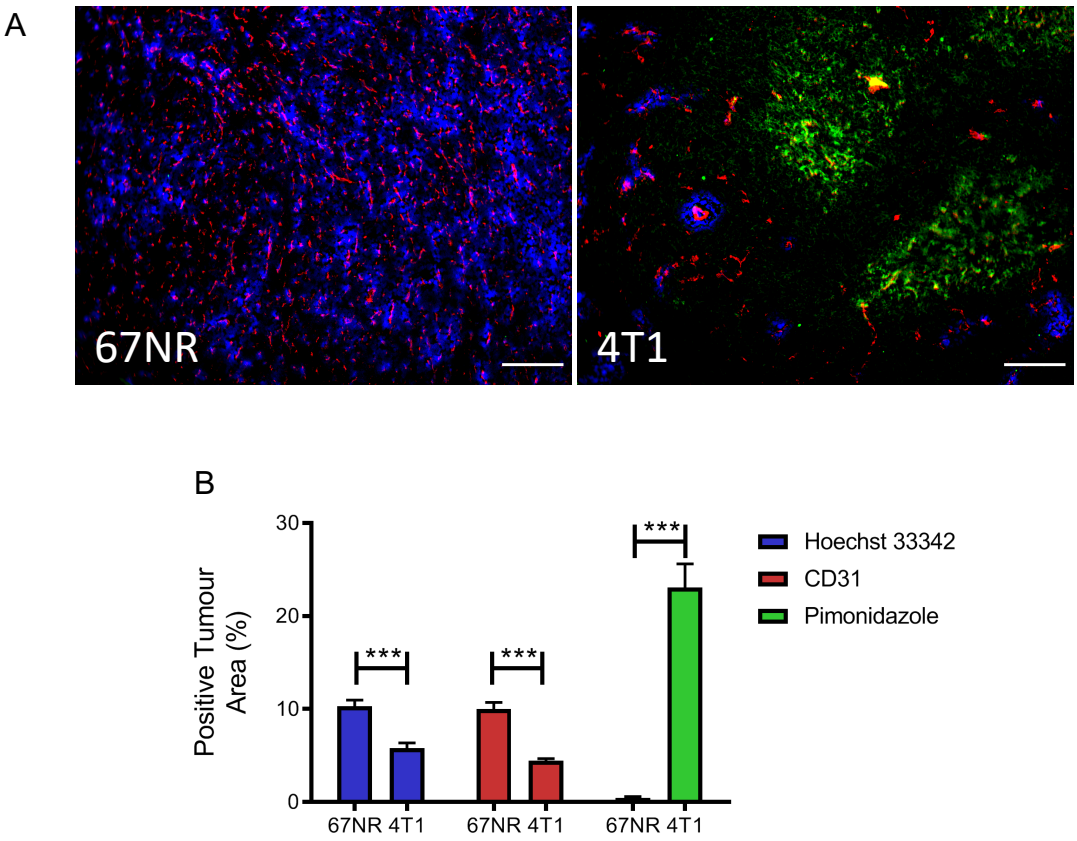

Figure 3.1 4T1 and 67NR hypoxia and vascularity

(A) Immunofluorescent images of 67NR and 4T1 tumours; perfusion indicated by Hoechst 33342 (blue), vascular endothelium by CD31 (red), and hypoxia by pimonidazole (green). Scale bar 250 μm. (B) Percent tumour area positive for Hoechst 33342, CD31, and pimonidazole (N=8, mean ± SEM, unpaired t-test, ***p<0.0001).

The microenvironment of 4T1 tumours provides a model for assessing regional perfusion differences. The peripheral regions of 4T1 tumours contain perfused blood vessels, indicated by Hoechst 33342 staining, while the centres of 4T1 tumours are poorly perfused and do not contain viable tissue, as indicated by a lack of Hoechst 33342 staining (Figure 3.2A). This is again in contrast to 67NR tumours that display perfusion throughout the tumour (Figure 3.2A). We exploited this feature as a first test for 2-^{18}F-FEtOH as a reporter of tumour perfusion, hypothesizing that the radiotracer would be present only in the periphery of 4T1 tumours and throughout 67NR tumours.

Ex vivo radiography of 2-^{18}F-FEtOH conducted on tumours excised 55 minutes post-injection displayed similar patterns to Hoechst 33342; low activity was observed in central regions of 4T1 tumours, moderate activity in the periphery of 4T1 tumours, and high activity throughout 67NR tumours (Figure 3.2B). To quantify these observations, the pixel intensities were assessed in line profiles drawn across the width of each tumour's radiography image (Figure 3.3). Values of the 11 pixels closest to the midpoint of the line profile were averaged to represent the 2-^{18}F-FEtOH activity in the tumour centre. These values were compared to the maximum intensity in the entire associated tumour image. We observed that pixel intensities in the centre of 67NR tumours were 88 ± 2.0% the value of the maximum 67NR intensity, while the centre of 4T1 tumours were only 65 ± 5.7% of tumour maximums (Figure 3.2C). These results suggest that 2-^{18}F-FEtOH uptake provides intra-tumoural resolution of perfusion status that is in agreement with blood vessel density, perfusion status, and hypoxia in 4T1 and 67NR tumours.

3.3.2 2-^{18}F-FEtOH uptake agrees with ^{14}C-iodoantipyrine

To link 2-^{18}F-FEtOH uptake with tissue perfusion, we co-injected 2-^{18}F-FEtOH with ^{14}C-IAP, which is a validated perfusion reporter used to study cerebral and tumour perfusion[279–281]. We found that 2-^{18}F-FEtOH and ^{14}C-IAP radioactivity in brain tissue and in 67NR and 4T1 tumours provided clear distinction of each tissue type, with a general progression from poorly perfused 4T1 tumours through 67NR tumours, and up to well perfused brain tissue. Activity of 2-^{18}F-FEtOH and ^{14}C-IAP were significantly correlated, and the dynamic range of 2-^{18}F-FEtOH activity was greater than ^{14}C-IAP with a slope of 1.16 ± 0.14 %ID/g across all tissues analyzed (Figure 3.4).

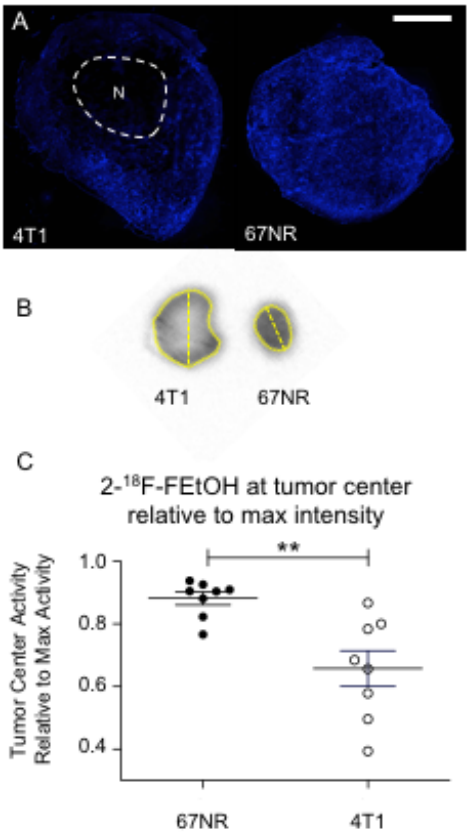

Figure 3.2 Comparison of 2-^{18}F-FEtOH *ex vivo* radiography with Hoechst 33342

(A) Fluorescent microscopy of Hoechst 33342 in 4T1 and 67NR tumours, identifies central necrosis (N) in 4T1 tumours. Scale bar 1000 µm. (B) 2-^{18}F-FEtOH radiography of untreated tumours, solid yellow line defines tumour border, dashed lines are examples of where line profiles are drawn. (C) Tumour-centre ^{18}F intensity expressed relative to tumour-max intensity displays the low 2-^{18}F-FEtOH uptake in the centre of 4T1 tumours (N=7, t-test *$p<0.05$).

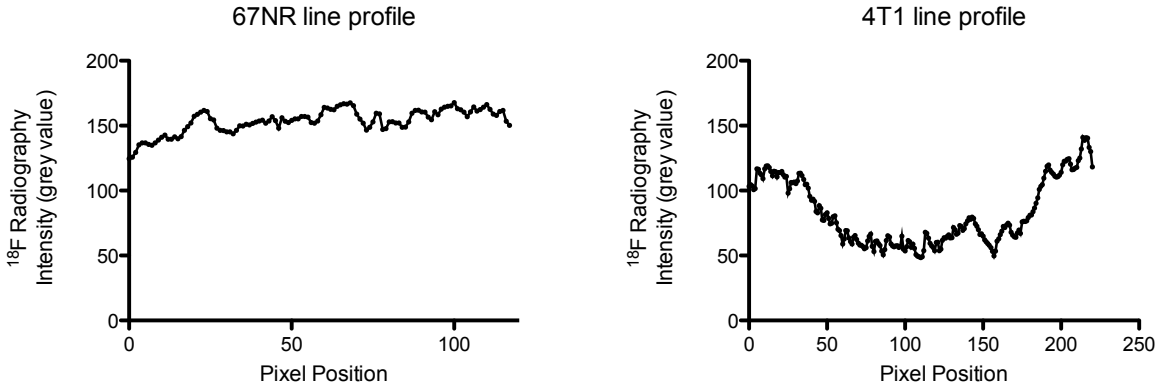

Figure 3.3 Sample line profiles

Sample line profile data for 67NR and 4T1 tumours from the radiography images displayed in Figure 3.2.

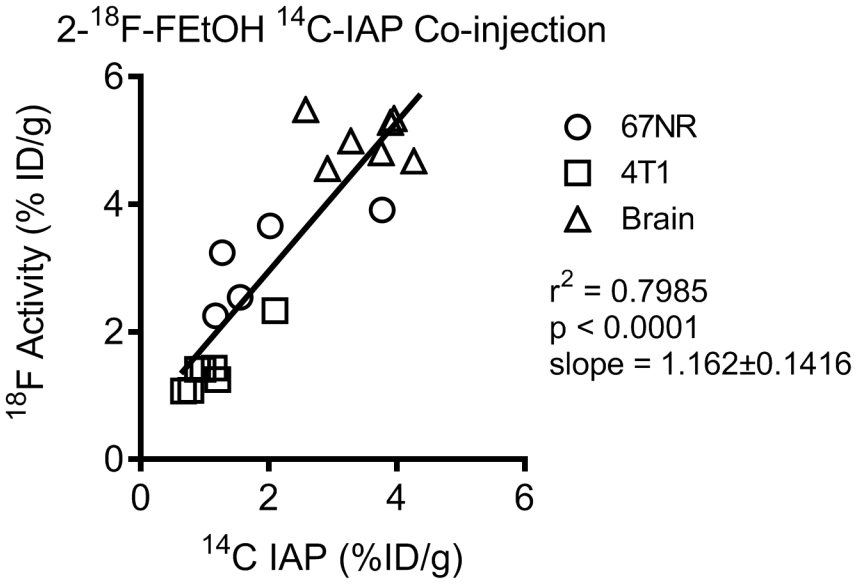

Figure 3.4 Comparison of 2-^{18}F-FEtOH uptake with ^{14}C-IAP

2-^{18}F-FEtOH was co-injected with ^{14}C-IAP and bulk tissue radioactivity measured to determine uptake of each radiotracer. Linear regression trend line across all three tissues is displayed in black with associated statistical data displayed to the right of the figure.

3.3.3 2-^{18}F-FEtOH provides distinction between 67NR and 4T1 tumours

We measured 2-^{18}F-FEtOH uptake in 67NR and 4T1 tumours for 55 minutes post-injection using dynamic PET imaging. Based upon previous work showing stable uptake of 2-^{18}F-FEtOH into cells[274], we hypothesized that 2-^{18}F-FEtOH activity would reach plateaus reflective of tumour perfusion status. In baseline scans, 2-^{18}F-FEtOH uptake into 67NR tumours plateaued at approximately 5.8 %ID/g after 2 minutes and activity did not significantly change over the remaining protocol (Figure 3.5A). In 4T1 tumours, 2-^{18}F-FEtOH activity did not reach a plateau until 30 minutes post-injection at approximately 4.5 %ID/g, after which no further increase was observed (Figure 3.5A). In 67NR tumours, 2-^{18}F-FEtOH activity was significantly greater than 4T1 from 1 minute until 12 minutes post-injection (Figure 3.5A). We performed static PET scans 55 minutes post-injection of 2-^{18}F-FEtOH to further assess this late time point in mice not anesthetized during tracer uptake (Figure 3.5B). Pairwise assessment of mean 2-^{18}F-FEtOH activity in each tumour revealed greater activity in 67NR versus the same-mouse 4T1 tumours in eleven out of twelve mice (Figure 3.5C). Further analysis computed static PET data into cumulative frequency plots to calculate the 2-^{18}F-FEtOH activity level representative of the 50th and 90th voxel percentiles. Results showed that both the 50th and 90th percentile activity levels were greater in the 67NR tumours (7.8 ± 0.2 %ID/g vs 6.6 ± 0.3 %ID/g, and 9.3 ± 0.2 %ID/g vs 7.7 ± 0.2 %ID/g respectively, mean ± SEM $p<0.05$). These data confirm that the 2-^{18}F-FEtOH radiotracer successfully distinguishes 67NR and 4T1 tumours using dynamic PET imaging or static PET imaging, including the potential for 2-^{18}F-FEtOH to report perfusion for a longer period of time compared to previously published PET-based perfusion reporters.

3.3.4 Irreversible uptake rate of 2-^{18}F-FEtOH is dependent on perfusion

We hypothesized that 2-^{18}F-FEtOH is irreversibly taken up into cells, fitting with a two tissue compartment model. While this allows for the signal stability displayed in Figure 3.5, it poses the risk of having 2-^{18}F-FEtOH uptake select for cells and tissues better able to metabolize FEtOH. To address this concern we conducted Patlak modeling[276] of 2-^{18}F-FEtOH uptake into 67NR and 4T1 tumours using image-derived input functions (sample in Figure 3.6) based on voxels of ^{18}F activity derived from dynamic PET images of the mouse vena cava[55] after injection of 2-^{18}F-FEtOH. The Patlak method outputs an irreversible uptake rate constant 'Ki' that is dependent on both metabolism of the radiotracer and its concentration in the plasma. Thus, Ki

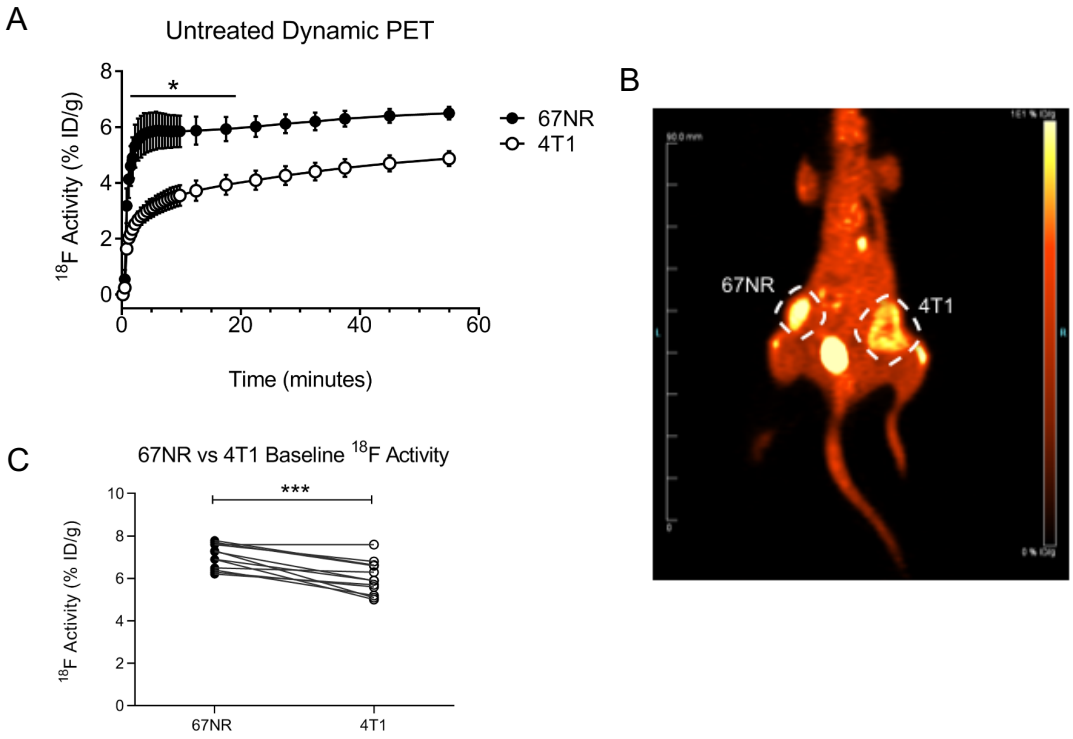

Figure 3.5 2-^{18}F-FEtOH PET uptake distinguishes between 4T1 and 67NR tumours

2-^{18}F-FEtOH distinguishes 67NR from 4T1 tumours. (A) Mean tumour 2-^{18}F-FEtOH activity during dynamic PET (N=4, mean ± SEM, two-way ANOVA with Bonferroni multiple comparisons 67NR vs 4T1 *p<0.05). (B) Sample whole body static PET image 55 minutes post-injection. (C) Mean tumour 2-^{18}F-FEtOH activity from static PET (N=12, paired t-test ***p<0.0001).

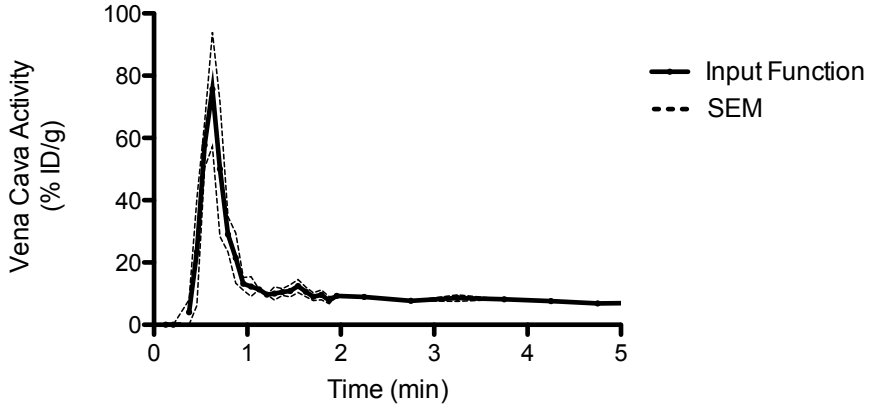

Figure 3.6 Sample arterial input function

Image derived input functions were produced based on the voxels within the Vena Cava, identified during the first pass of the 2-^{18}F-FEtOH bolus after the tail vein injection. Displayed is the input function averaged across four dynamic scans from untreated mice. Data points were produced every 5 seconds across the first 2 minutes, then every 30 seconds up until 5 minutes post-injection, and finally every 5 minutes until the end of the 60-minute PET scan.

Reflects both possible intrinsic differences between cells and the delivery of 2-^{18}F-FEtOH through perfused vasculature. When Ki values were determined based on tissue activity curves of full tumour volumes, the Ki was significantly greater in 67NR tumours than 4T1 tumours (1.6-fold difference, data not shown). However, regions of interest drawn in well-perfused peripheral 4T1 regions produced similar Ki values as whole 67NR tumours (Figure 3.7). In contrast, the poorly perfused center 4T1 regions possessed Ki values that were significantly lower than 67NR tumours or peripheral regions of 4T1 tumours. These data support that differences in 2-^{18}F-FEtOH uptake are due to perfusion differences and not differences in FEtOH metabolism.

3.3.5 2-^{18}F-FEtOH uptake is modified by perfusion-modifying drugs

We next tested three blood flow modifying agents to observe if 2-^{18}F-FEtOH uptake into 4T1 and 67NR tumours would reflect the perfusion changes. We utilized two agents to increase tumour blood flow, nicotinamide[65] and pentoxifylline[50], and used hydralazine as an agent to reduce tumour blood flow[205]. Mice were treated with one drug prior to 2-^{18}F-FEtOH injection and tumours were harvested 55 minutes later for *ex vivo* radiography. Nicotinamide increased 2-^{18}F-FEtOH uptake in both 67NR and 4T1 tumours, indicated by the rightward shifts towards greater pixel intensity on histograms (Figure 3.8A). This is consistent with the known activity of nicotinamide to improve solid tumour perfusion. Similarly, pentoxifylline increased 2-^{18}F-FEtOH uptake in both tumours (Figure 3.8B), with a more modest rightward shift compared to nicotinamide. Hydralazine induced a leftward shift in 4T1 tumour histograms (Figure 3.8C), indicating a reduction in perfusion that is consistent with the known activity of hydralazine. However, 67NR tumours did not display a reliable shift in response to hydralazine at this time point when tumours were harvested 55 minutes after 2-^{18}F-FEtOH injection (Figure 3.8C).

To further investigate the responses of 67NR and 4T1 tumours to hydralazine, we performed dynamic PET imaging of 2-^{18}F-FEtOH uptake after hydralazine administration compared to baseline images (sample images in Figure 3.9). 67NR tumours treated with hydralazine displayed a significant reduction in 2-^{18}F-FEtOH activity over the first 10 minutes of dynamic PET imaging (Figure 3.10A). 67NR 2-^{18}F-FEtOH activity in control and hydralazine groups converged within 55 minutes, agreeing with the *ex vivo* radiography data (Figure 3.8B). The mean 2-^{18}F-FEtOH activity in 4T1 tumours was reduced throughout the dynamic scan

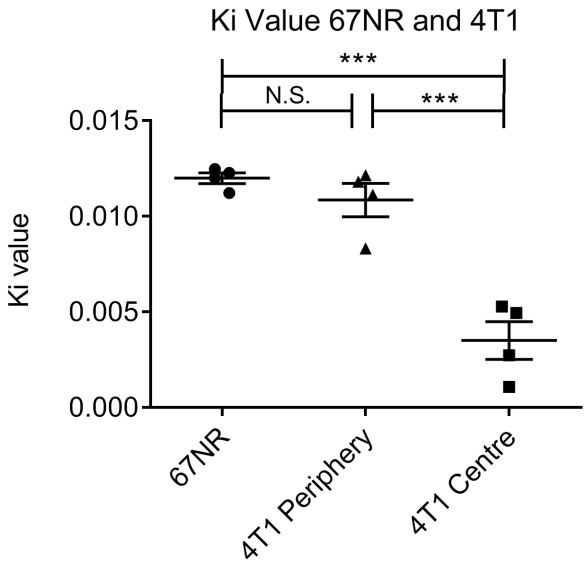

Figure 3.7 Patlak modeling of dynamic 2-^{18}F-FEtOH uptake

Patlak irreversible rate constant 'Ki' was computed for whole 67NR tumour volumes and compared to select regions of 4T1, the poorly perfused tumour center and well-perfused periphery. (N=4, one-way ANOVA with Tukey multiple comparisons test, ***$p<0.0001$)

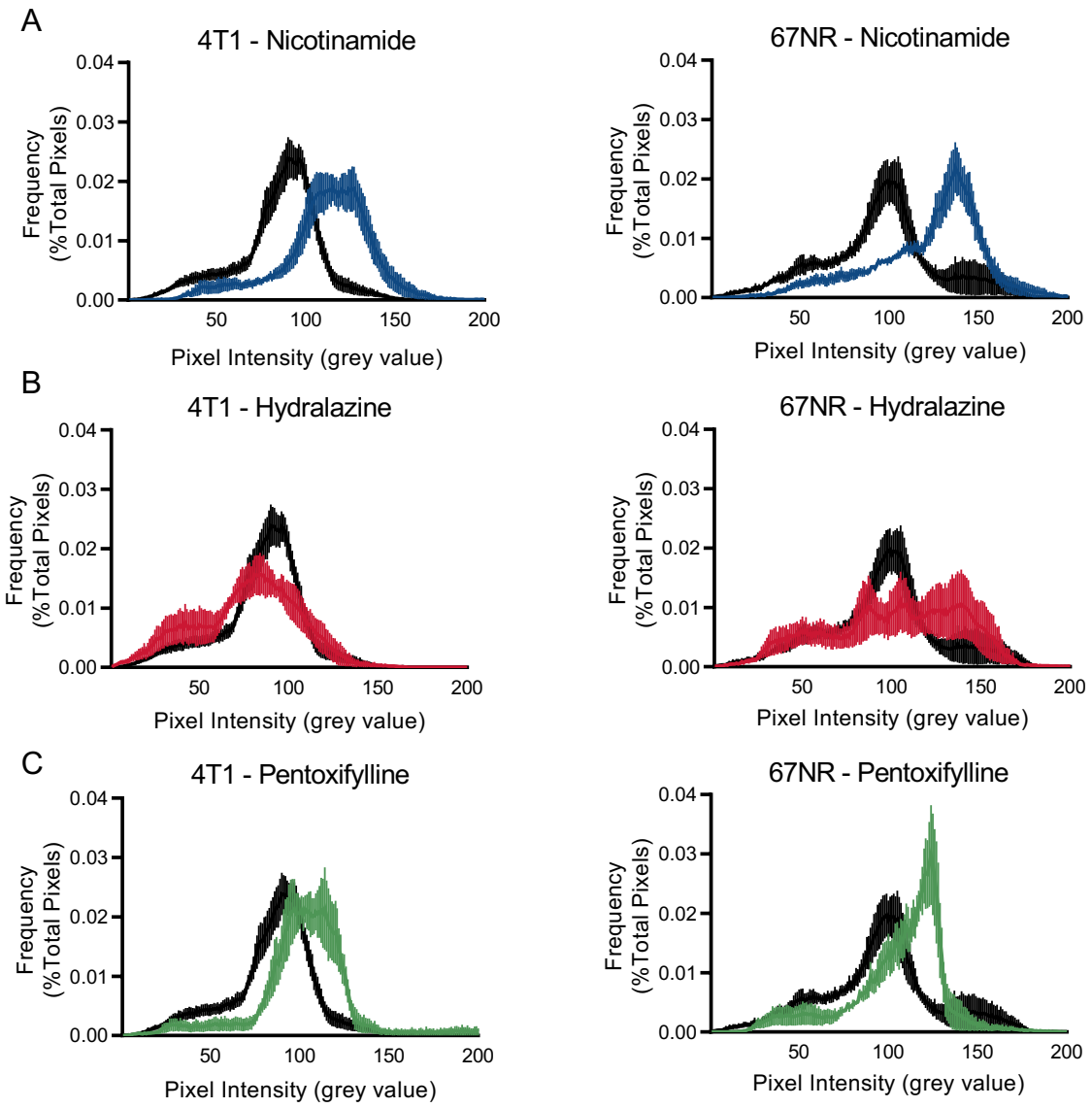

Figure 3.8 2-^{18}F-FEtOH uptake in response to perfusion modifying drugs

Perfusion modifying drugs alter 2-^{18}F-FEtOH uptake into 4T1 and 67NR tumours. Mice were administered one of (A) nicotinamide, (B) pentoxifylline, or (C) hydralazine prior to 2-^{18}F-FEtOH injection. Radioactivity was detected using radiography and expressed as histograms. (N=5, mean ± SEM). Control histogram is indicated in black, drug-treated histogram is overlaid in colour with the drug indicated in individual figure titles.

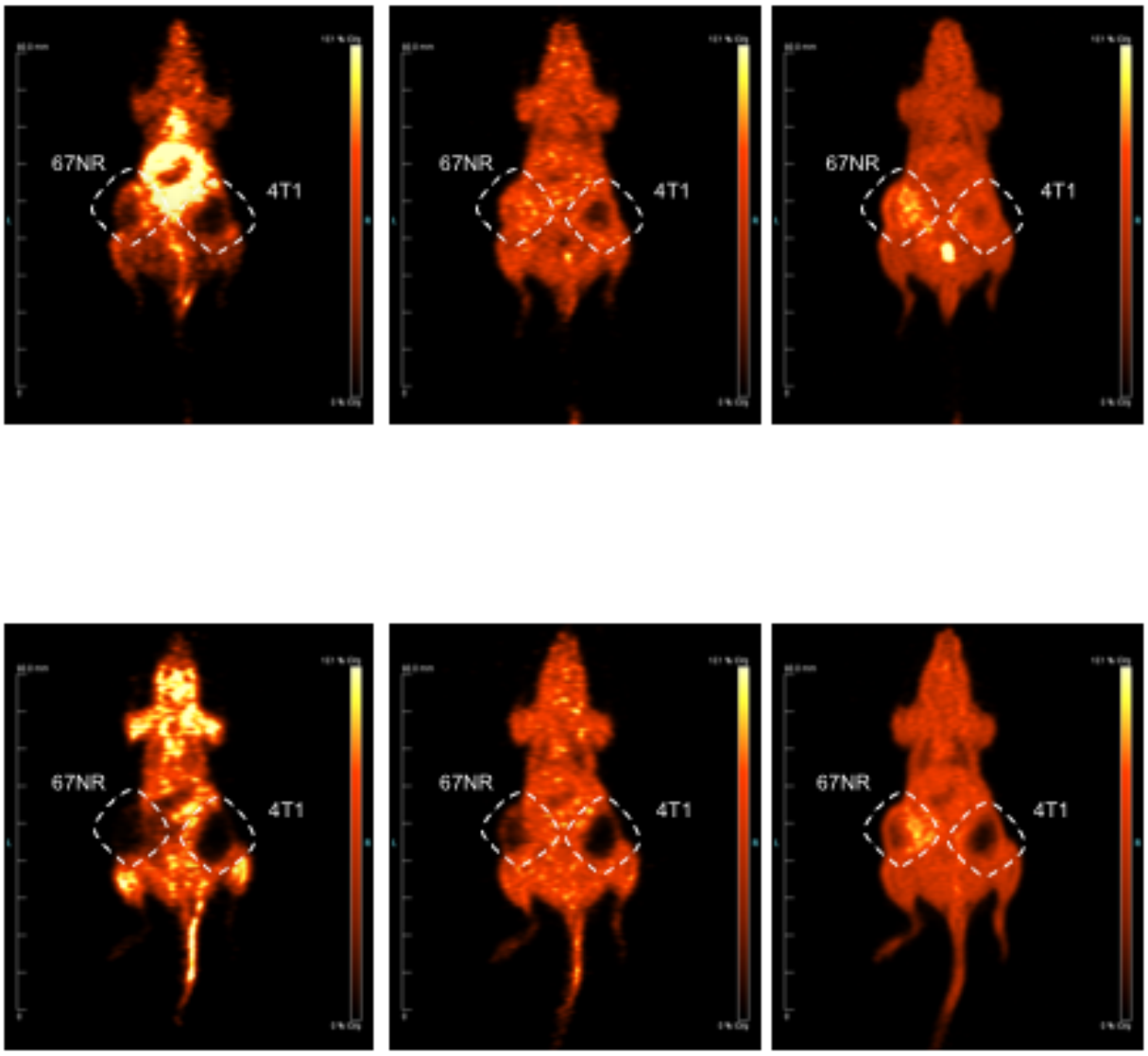

Figure 3.9 Sample 2-^{18}F-FEtOH images from dynamic PET

Representative images from dynamic PET scans of the same mouse imaged for untreated baseline images (top) on the first day, and images following hydralazine treatment on the subsequent day (bottom). Images left to right are 1-minute post-injection of 2-^{18}F-FEtOH, 10 minutes post-injection, and 55 minutes post-injection.

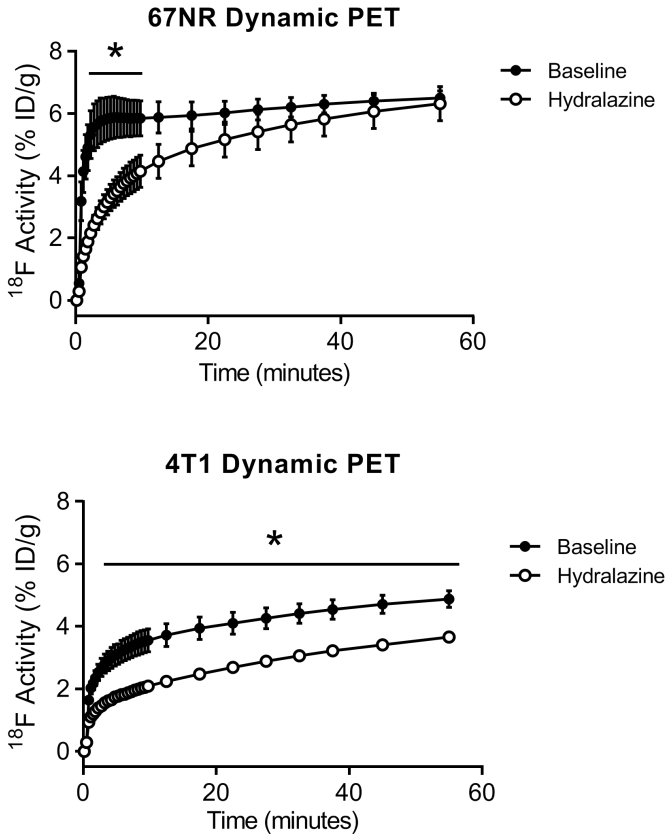

Figure 3.10 Response of 2-^{18}F-FEtOH uptake to hydralazine in dynamic PET

Hydralazine slows 2-^{18}F-FEtOH delivery. 2-^{18}F-FEtOH mean activity in dynamic PET comparing baseline (closed circles) scans and hydralazine (open circles) scans for (A) 67NR and (B) 4T1. (N=4, mean ± SEM, Bonferroni multiple comparisons *$p<0.05$).

(Figure 3.10B). These data indicate that response of tumour perfusion to blood flow modifying drugs is best reflected by 2-^{18}FEtOH uptake within 10 minutes post-injection.

3.4 Discussion

This study presents 2-^{18}F-FEtOH as a novel radiotracer for measuring tumour perfusion. We have found that uptake of 2-^{18}F-FEtOH is dependent on regional perfusion status, with 2-^{18}F-FEtOH uptake in agreement with the intra-tumoural heterogeneity of Hoechst 33342 staining (Figure 3.2). Uptake of 2-^{18}F-FEtOH also accurately reflected the perfusion statuses of two tumour models with distinct vascular and hypoxic phenotypes (Figures 3.1 – 3.4). There was strong agreement between uptake of 2-^{18}F-FEtOH and ^{14}C-IAP into 67NR tumours, 4T1 tumours, and brain tissue, while 2-^{18}F-FEtOH uptake displayed a greater dynamic range in distinguishing each tissue (Figure 3.4).

We also show that 2-^{18}F-FEtOH uptake can be used to measure the effects of pharmacological agents that modify tumour perfusion (Figure 3.8 and Figure 3.10). We tested two vasoactive drugs (nicotinamide and hydralazine) as well as pentoxifylline, which improves perfusion by improving the flexibility of red blood cells to facilitate their flow through tortuous tumour vessels[39,171]. Further experiments with hydralazine displayed that the effects of perfusion-modifying agents are best quantified by 2-^{18}F-FEtOH within 10 minutes of radiotracer injection (Figure 3.10). Taken together, our data show the potential for 2-^{18}F-FEtOH uptake quantified by dynamic PET imaging to be used to screen blood flow-modifying agents for use as therapeutic adjuvants to existing cancer therapies.

The extended half-life of the ^{18}F isotope relative to other isotopes used in PET perfusion reporters provides 2-^{18}F-FEtOH with the benefits of accessibility and eased protocol timelines. It is previously observed that 2-^{18}F-FEtOH is also stably taken up into cells and produces an activity plateau in many well-perfused healthy tissues[273]. An extended half-life and activity plateau provides a unique opportunity to detect perfusion at later time points post-injection, with activity plateaus lasting up to 30 minutes and later time points exhibiting only a small increase in activity (Figure 3.5 and Figure 3.10).

The data displayed in this study presents the utility of 2-^{18}F-FEtOH as a general indicator of tumour perfusion, distinguishing well-perfused and poorly perfused regions. To support that perfusion is the driving factor in 2-^{18}F-FEtOH uptake in this study and not cellular differences in

metabolic trapping, we applied the Patlak method to determine the irreversible uptake rate constant Ki. The value of Ki is reflective of both the concentration of 2-^{18}F-FEtOH delivered to a tissue and the ability for the tissue to metabolize the radiotracer into cell impermeable metabolites. In this study, Ki values did not vary between 67NR tumours and well-perfused regions of 4T1 tumours in the same animal (Figure 3.7), suggesting no significant difference in metabolic trapping between tumour types. Rather, Ki values varied strongly within 4T1 tumours in a regional manner, with the lowest Ki values associated with 4T1 tumour centres (Figure 3.7), which we also showed to be poorly perfused (Figure 3.2). Together these observations suggest that differences in 2-^{18}F-FEtOH uptake are due to the concentration of 2-^{18}F-FEtOH delivered to tumour tissue, i.e. regional tumour perfusion. These modeling data are somewhat limited by the use of an image derived input function instead of direct blood draws to assess 2-^{18}F-FEtOH in the bloodstream, although image analysis methods have fared well when directly compared to blood collection methods[55]. Future kinetic modelling of 2-^{18}F-FEtOH should include analysis of FEtOH metabolites and assessment of enzymes that will relate to enhanced metabolic trapping.

Future studies should evaluate 2-^{18}F-FEtOH uptake as a measure of tumour perfusion in other solid tumour types. Of additional interest will be investigating the oxygenation of tumour regions with low 2-^{18}F-FEtOH activity to distinguish between poorly perfused and poorly oxygenated tumour regions. Of additional interest is comparison of 2-^{18}F-FEtOH perfusion and PET-based hypoxia measurements to predict patient response to radiation therapy and particularly chemotherapy, where other perfusion reporters have provided strong prognostic data on tumour response. The accessibility benefit of 2-^{18}F-FEtOH over ^{15}O perfusion reporters and the ability to image 2-^{18}F-FEtOH 55 minutes post-injection would also make 2-^{18}F-FEtOH an appealing candidate to monitor tumour response during therapy to determine how tumour perfusion responds to therapy. Previous work showing 2-^{18}F-FEtOH uptake in normal tissues[273] suggest that 2-^{18}F-FEtOH-based perfusion measurements may have applicability beyond solid tumours, with potential for measuring tissue perfusion in other disease states. Taken together, our data support the further development and application of 2-^{18}F-FEtOH as a PET-based marker of tissue and solid tumour perfusion.

These data demonstrate that 2-^{18}F-FEtOH uptake provides intra-tumour resolution of perfusion, discriminates well-perfused and poorly perfused tumours, responds to tumour-perfusion modifying pharmaceuticals, and provides an extended window of detection compared

to current PET perfusion reporters. We will apply 2-^{18}F-FEtOH to quantify bulk tumour perfusion in response to ARB treatment in Chapter 4.

Chapter 4: Angiotensin II type 1 receptor blocker telmisartan inhibits the development of transient hypoxia and improves response to radiation.

Parts of this chapter have been submitted for publication as: Brennan J Wadsworth, Rachel A Cederberg, Che-Min Lee, Natalie S Firmino, S Elizabeth Franks, Jinhe Pan, Nadine Colpo, Kuo-Shyan Lin, Francois Benard, Kevin L Bennewith. "Angiotensin II type 1 receptor blocker telmisartan inhibits the development of transient hypoxia and improves tumour response to radiation."

SYNOPSIS

Hypoxic tumour cells are resistant to radiation therapy and are associated with poor therapeutic outcome. Solid tumours can contain regions with unstable tumor perfusion, exposing tumor cells to varying oxygen tensions over time and creating "transiently" hypoxic cells. Transiently hypoxic tumor cells are thought to be important, yet poorly understood, limitations to cancer therapy and represent intriguing therapeutic targets. Recent evidence suggests that angiotensin II type 1 receptor blockers (ARBs) can improve tumour perfusion by reducing collagen deposition from cancer associated fibroblasts (CAFs). However, the influence of ARBs on transient tumour hypoxia and response to radiation therapy is unknown.

We tested how the ARBs losartan and telmisartan affected the microenvironment in human tumor xenografts, using fluorescent perfusion dyes and positron emission tomography to quantify tumour perfusion, and a combination of hypoxia markers and the hemorheological agent pentoxifylline to assess transient tumour hypoxia. We found CAF-containing tumors have significantly reduced collagen I levels in response to the ARB telmisartan, but not losartan. Telmisartan significantly increased tumour blood flow, stabilized tumor perfusion, and reduced the development of transient tumour hypoxia. Telmisartan-treated tumors were also more responsive to treatment with ionizing radiation, indicating that telmisartan reduces a therapeutically important population of transiently hypoxic tumour cells.

Our findings indicate telmisartan is capable of modifying the solid tumour microenvironment to stabilize tumour perfusion, reduce transient hypoxia, and significantly improve tumour radiation response.

4.1 Introduction

A hallmark of solid tumour growth is angiogenic signalling that tends to form immature, poorly functional blood vessels in an inefficient, low density network within the tumour. Dysfunctional tumour vasculature contributes to poor tissue perfusion[2], inhibited delivery of chemotherapeutics[85,86], and the development of regions within tumours with low oxygen content (i.e. hypoxia)[114]. Multiple studies have observed that perfusion, and indeed oxygen supply, is unstable in many solid tumours[63]. Fluctuations in oxygen supply can occur in repeated patterns of hypoxia and reoxygenation that result in populations of tumour cells being exposed to transient hypoxia[67,118,229]. This transient hypoxia is sufficient to induce expression of hypoxia-induced genes and increase metastasis[242,246]. It is well established that oxygenation at the time of radiation is a major modifier of radiation response[103,174], and transient hypoxia can contribute to radiation resistance[50,64]. Thus, modifying the tumour microenvironment to reduce the hypoxic tumour cell population and eliminate transient hypoxia could significantly improve tumour response to radiation therapy.

The solid tumour extracellular matrix (ECM) is a potentially modifiable source of tumour vascular dysfunction. Tumour regions with greater fibrillar type 1 collagen (Col1) deposition exhibit reduced perfusion and increased interstitial fluid pressure[98]. In turn, injection of ECM degrading enzymes into tumour xenografts has been shown to increase microregional perfusion[98]. An alternative strategy to stably improve tumour microregional perfusion is to inhibit Col1 deposition. A major source of Col1 deposition in solid tumours are alpha-smooth muscle actin (αSMA) positive cancer associated fibroblasts (CAFs)[72,282]. In recent years, angiotensin II type 1 receptor blockers (ARBs) have been applied to reduce CAF activation to ultimately reduce Col1 deposition in the tumour. ARBs have been shown to reduce the abundance of αSMA positive CAFs, reduce Col1, reduce vascular compression forces, increase perfusion, and increase delivery of chemotherapeutics across multiple murine tumours and human tumour xenografts[85,86,88]. However, the influence of ARBs on transient hypoxia or radiation response is unknown. We hypothesized that treatment of tumours with ARBs would eliminate transient hypoxia from solid tumours, leading to increased radiation response. To investigate transient hypoxia, we compared two human tumour xenograft models, the WiDr colorectal adenocarcinoma and SiHa cervical squamous cell carcinoma. WiDr tumours exhibit greater prevalence of rapidly fluctuating transient hypoxia while oxygenation in SiHa tumours is

relatively stable[50,67,229]. Herein, we show that the ARB telmisartan improves and stabilizes tumour perfusion, reduces the development of transient hypoxia, and significantly improves response to radiation.

4.2 Materials and methods

4.2.1 Cell lines and mice

WiDr[255] and SiHa[256] cells were maintained in standard culture conditions in minimal essential medium +10% FBS and used within 30 passages. Flanks of NOD/Rag-gamma (NRG) mice were inoculated by subcutaneous injection of 1 x 10^6 cells. All animal experiments were performed in accordance with institutional and Canadian Committee on Animal Care guidelines. Upon harvest, half of each tumour was embedded in optimal cutting temperature medium (Tissue Tek) and frozen for sectioning. The other half of each tumour was processed into single cell suspensions as previously described[229] for clonogenic assays and/or flow cytometry.

4.2.2 Drugs

50mg/kg of Pentoxifylline (Millipore Sigma) was administered by i.p. injection as indicated. Losartan (Millipore Sigma) was added to the drinking water of the mice at a concentration of 300 mg/L, while acidified drinking water (pH 2.5) was used for telmisartan (Millipore Sigma) treatment at a concentration of 75mg/L. Treated drinking water was provided to mice *ad libitum* beginning the day of tumour implant and maintained until animal sacrifice. Water bottles were weighed twice per week and the loss in mass attributed to mouse water consumption in order to estimate drug dosage. To label hypoxic tumour cells, mice were administered 100mg/kg of pimonidazole-HCl (Hypoxyprobe) by i.p. injection 90 minutes prior to mouse sacrifice. Intravenous injection of 1mg Hoechst 33342 or 0.25mg of $DiOC_7$ carbocyanine was performed to label cells surrounding perfused blood vessels[63].

4.2.3 Flow cytometry and immunofluorescent microscopy

For tumours from mice injected with Hoechst 33342, slides were imaged for Hoechst 33342 and $DiOC_7$ immediately following sectioning and then placed overnight in phosphate-buffered saline (PBS) with 2% fetal bovine serum and 0.1% triton X-100 for blocking, cell permeabilization, and to wash out the fluorescent dye signal prior to staining for other markers.

Pimonidazole was detected using monoclonal antibody conjugated to fluorescein isothiocyanate (FITC; Hypoxyprobe). Slides were stained for CD31 using (Pharmogen 553377) rabbit monoclonal antibody. α-Smooth muscle actin was detected using clone 1A4 mouse monoclonal antibody conjugated to FITC (Millipore Sigma). Collagen 1 was detected using LF-68 anti-collagen alpha-1 antibody (Kerafast, Boston, MA). Secondary antibodies conjugated to Alexa Fluor 488 or Alexa Fluor 594 (Life Technologies) were used to detect unconjugated primary antibodies. Slides were stained with 2 μM 4,6-diamidino-2-phenylindole (DAPI) to label cell nuclei. Immunofluorescent microscopy image acquisition system consisted of a robotic fluorescence microscope (Zeiss Axiomager Z1), a cooled, monochrome CCD camera (Retiga 4000R, QImaging), a motorized slide loader and x-y stage (Ludl Electronic Products), and customized ImageJ software (public domain program developed at the U.S. National Institutes of Health). Images were acquired with a resolution of 1.5 μm/pixel. Individual fields of view were automatically stitched together to create images of full tumour sections for analysis. Three sections cut 150-200 μm apart were imaged for technical replicates of each tumour. Images were analyzed using ImageJ software. Positive pixels were identified using automatic thresholding following background correction. Regions of necrosis were manually removed from analysis based upon DAPI and hypoxia marker staining. Flow cytometry was conducted using a FACSCalibur flow cytometer (BD Biosciences) and FlowJo software (Tree Star, Inc., Ashland, OR).

4.2.4 Mismatch of Hoechst 33342 and carbocyanine ($DiOC_7$)

To quantify microregional fluctuations in tumour perfusion we compared blood vessel fluorescence following intravenous injection of Hoechst 33342 and $DiOC_7$ 20 minutes apart based on established methods[50,67]. Briefly, fluorescence intensity of each dye was quantified for individual blood vessels in tumour sections and plotted as the ratio of fluorescence intensity, $DiOC_7$ over Hoechst 33342, and values below 1.0 were inversed. Fold change in fluorescence intensity was binned as either greater than 3.0, between 2.0 and 3.0, or between 1.0 and 2.0, the latter values classified as representing stable perfusion.

4.2.5 Clonogenic assay and radiation growth delay experiments

Mice were subject to x-ray irradiation delivered at 250 keV with a dose rate of approximately 3 Gy/min (X-RAD320, Precision X-ray). Mice were placed in a lead jig that shields the majority of the mouse, leaving exposed the rear dorsal region of the mouse where the tumours were inoculated. For clonogenic assays, upon harvest tumours were digested to a single cell suspension as described previously[229], incubated for two weeks in standard culture conditions, and then stained with malachite green for colony counting. For radiation growth delay experiments, mice were irradiated and returned to animal housing. Tumours were measured twice per week using digital calipers by animal facility staff blinded to irradiation treatment. Tumour volume was calculated from caliper measurements according to the equation $V = (L \times (W^2))/2$ where V is the volume in mm^3 and L and W are the length and width of the tumour in mm. Tumour length was always the larger of the two perpendicular measurements.

4.2.6 PET imaging

2-^{18}F-FEtOH synthesis[273], dynamic microPET/CT imaging, image reconstruction, and volume of interest analysis were conducted as previously described[52].

4.2.7 Statistical analysis

Data are expressed as the arithmetic mean with variance as indicated. Statistical hypothesis testing was performed using Graphpad Prism 5 or R software, with specific tests used as indicated. Differences of $p<0.05$ were considered significant.

4.3 Results

4.3.1 Telmisartan reduces Col1 in the tumour microenvironment

The ARBs losartan or telmisartan were administered to tumour-bearing mice via the drinking water with estimated doses of 29 mg/kg/day and 8 mg/kg/day respectively (Figure 4.1A,B). Mice maintained on these doses for up to 28 days during tumour growth showed no signs of weight loss compared to mice drinking untreated water, and neither SiHa nor WiDr tumour masses were significantly different compared to controls at the time of harvest (Figure 4.1C-E). ARB treatment therefore did not significantly alter tumour growth.

To investigate whether ARBs altered the tumour microenvironment, we conducted

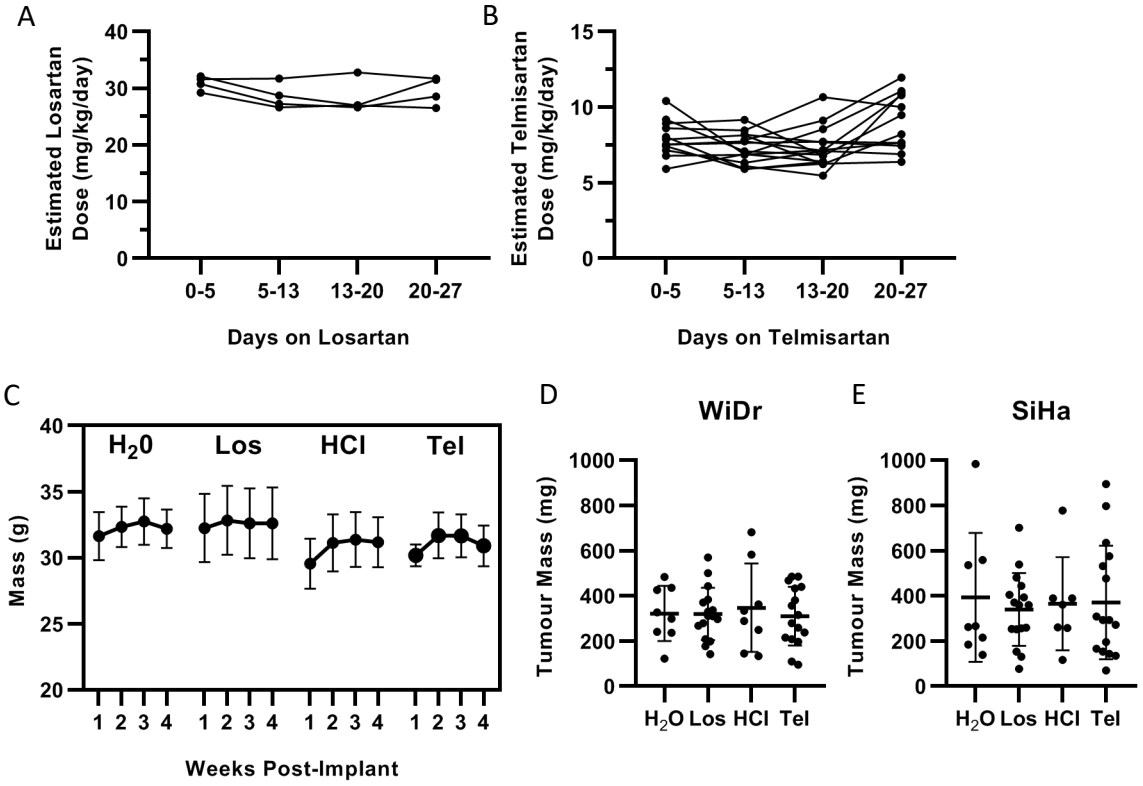

Figure 4.1 Consumption and growth effects of losartan and telmisartan.

(A) Estimated dosage of losartan over time for mice consuming water containing 300 mg/L losartan. Each data point represents one cage of mice. (B) Estimated dosage of telmisartan over time. Each data point represents one cage of mice. (C) Mouse mass was not affected by consumption of losartan or telmisartan treated water. (D) Tumour mass was not different between any groups for WiDr tumours harvested 28 days after implant or (E) SiHa tumours harvested 21 days after implant, both with treated water beginning day of implant. For C, D, & E; H_2O = water, Los = losartan, HCl = acidified water, Tel = telmisartan, N = 8-16 mice per treatment, mean ± SD.

immunofluorescent microscopy for Col1 and αSMA. We found 33 ± 5% (mean ± SD) of WiDr tumour area was positive for Col1 compared with 15 ± 6% (mean ± SD) of SiHa tumour area (Figure 4.2A-B). Losartan treatment did not significantly modify the Col1 abundance in either tumour (Figure 4.2A). Telmisartan treatment reduced Col1 in WiDr tumours to 17 ± 6% (mean ± SD) of tumour area, with no effect in SiHa tumours (Figure 4.2A). We next investigated if the reduction in Col1 occurred with a change in αSMA+ CAFs, which are major producers of Col1 in solid tumours[85,282]. Notably, αSMA+ CAFs were common in WiDr tumours and virtually undetectable in SiHa tumours (Figure 4.2). Losartan treatment did not affect the abundance of αSMA+ CAFs in WiDr tumours, while telmisartan treatment reduced the abundance of αSMA+ CAFs in WiDr tumours (Figure 4.2C). To determine whether the reduction in CAFs and Col1 within WiDr tumours was functionally significant, we quantified CD31+ blood vessel perfusion status based on fluorescent labelling of intravenously injected Hoechst 33342[63]. We observed no change in the fraction of Hoechst 33342 perfused CD31+ blood vessels in either WiDr or SiHa tumours of losartan-treated mice (Figure 4.2D). Telmisartan significantly increased the fraction of perfused CD31+ blood vessels in WiDr tumours, while telmisartan did not affect the fraction of perfused CD31+ blood vessels in SiHa tumours (Figure 4.2D). Overall, these data indicate telmisartan reduces the abundance of αSMA+ CAFs, reduces Col1 deposition, and increases the fraction of perfused blood vessels in WiDr tumours. Telmisartan did not affect CAFs, Col1, or perfusion in SiHa tumours that have inherently low levels of αSMA+ CAFs and Col1. In addition, these data indicate that telmisartan is superior to losartan in modifying the tumour microenvironment of WiDr tumours.

4.3.2 Telmisartan improves and stabilizes WiDr tumour perfusion

The increased fraction of perfused blood vessels in WiDr tumours treated with telmisartan suggests a wider distribution of blood flow throughout the tumour. An increase in blood flow distribution could occur with or without a net increase in whole tumour perfusion, as both have been observed previously with tumour perfusion modifying drugs[50]. To assess whole tumour perfusion, we used dynamic positron emission tomography (PET) to quantify tumour uptake of our newly developed 2-^{18}F-fluoroethanol (2-^{18}F-FEtOH) radiotracer (Chapter 3)[52]. We observed a significant increase in 2-^{18}F-FEtOH uptake in WiDr tumours of telmisartan-treated mice compared with controls (Figure 4.3A,B). There was no effect of telmisartan treatment on 2-

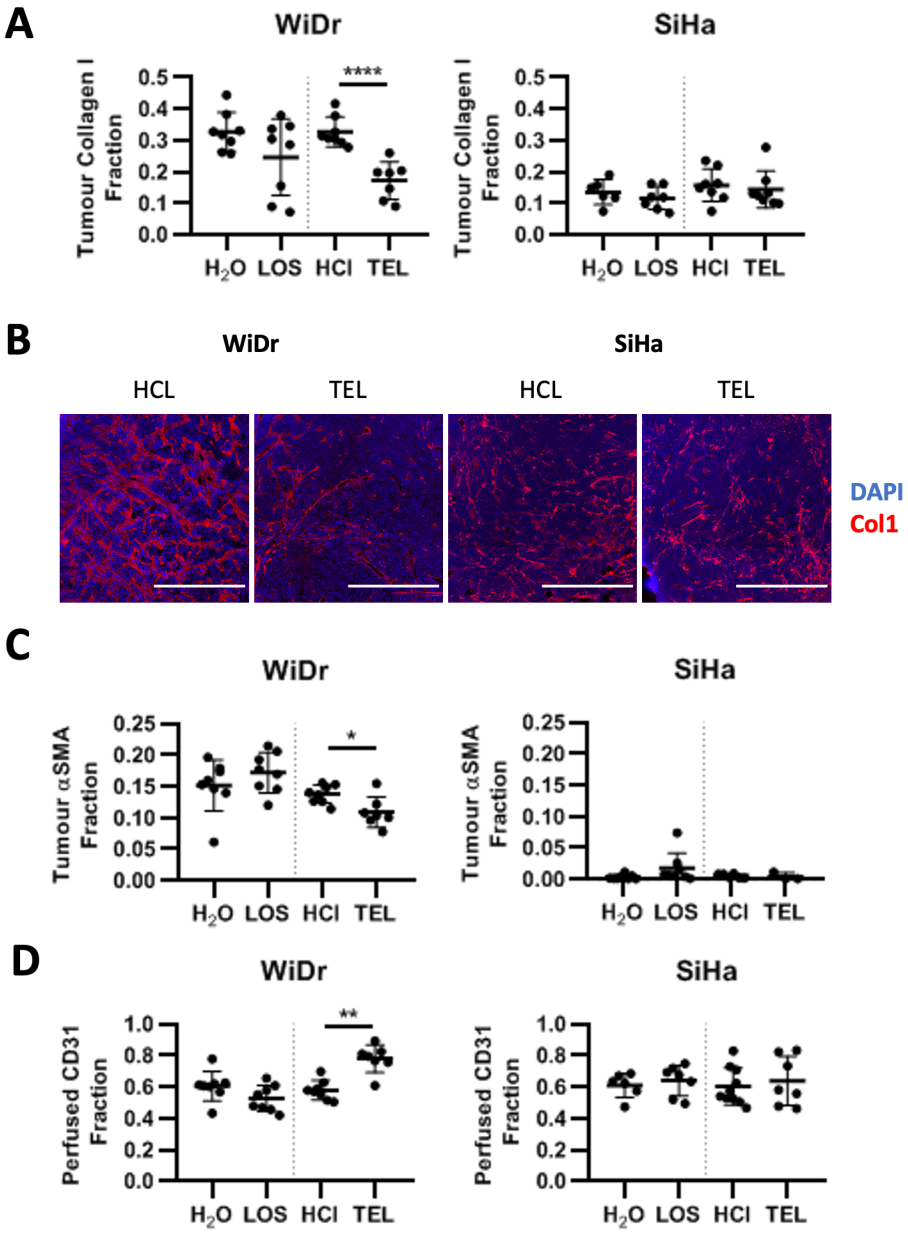

Figure 4.2 Telmisartan treatment alters the tumour microenvironment.

(A) Fraction of viable tumour area positive for Col1, with (B) sample fields of view for WiDr and SiHa tumours treated with telmisartan adjacent controls. (C) Fraction of viable tumour area positive for αSMA. (D) Fraction of CD31 blood vessels positive for Hoechst 33342. All data are mean ± SD, N = 6-8. Comparisons made using unpaired Student's t-test with only significant differences displayed; * $p < 0.05$, ** $p < 0.01$, **** $p < 0.0001$.

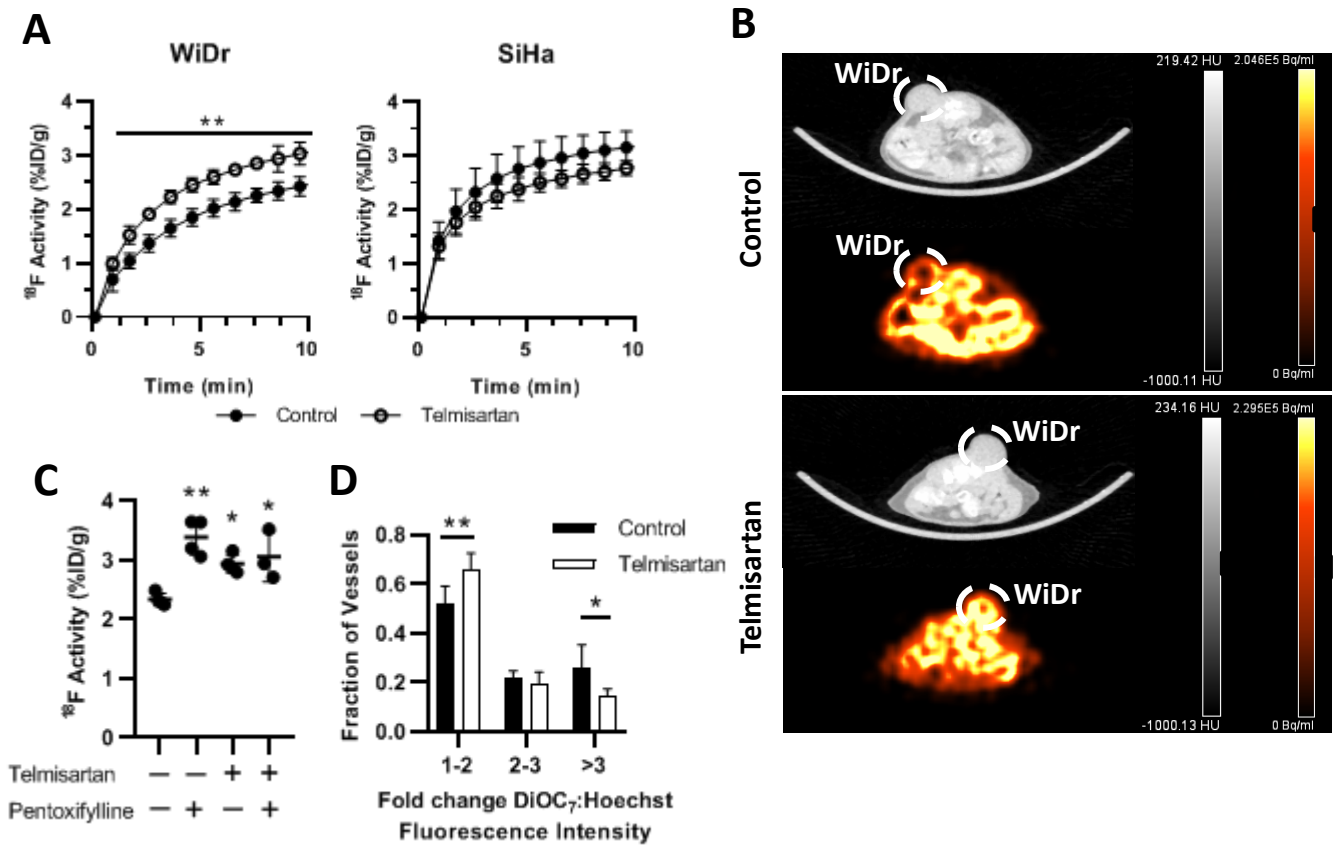

Figure 4.3 Telmisartan increases and stabilizes WiDr tumour perfusion.

(A) Tumour tissue activity curves during the first 10 minutes after intravenous injection of 2-^{18}F-FEtOH comparing. (B) Sample axial cross sections of computed tomography and PET images of WiDr tumour bearing mice at the level of tumour mid-point. WiDr tumour location is indicated on the back of the mouse. The imaging bed is visible below the mouse in the computed tomography image. (C) WiDr 2-^{18}F-FEtOH uptake averaged across time points 8-10 minutes after 2-^{18}F-FEtOH injection comparing controls with telmisartan treated mice with and without pentoxifylline 15 minutes prior to 2-^{18}F-FEtOH. All data are mean ± SD, N = 3-4. For A, Sidak's multiple comparison test comparing control versus telmisartan at individual time points, all comparisons indicated reach significance of ** $p < 0.01$. For C, Tukey multiple comparisons test concluded that the only significant differences present were in comparisons with the telmisartan(-)/pentoxifylline(-) group, * $p < 0.05$, ** $p < 0.01$. (D) After intravenous injection of Hoechst 33342 and DiOC$_7$ 20 minutes apart, the fold change in fluorescent perfusion dye intensity was measured for individual blood vessels. Blood vessels were binned as indicated with the percent of vessels in each bin shown. Sidak's multiple comparisons test between groups within bins, * $p < 0.05$, ** $p < 0.01$, N = 7.

^{18}F-FEtOH uptake in SiHa tumours (Figure 4.3A). Our data therefore indicate that WiDr tumours in telmisartan-treated mice have increased proportions of perfused blood vessels and increased overall tumour perfusion.

We have previously shown that WiDr tumours exhibit transient changes in perfusion and hypoxia over time[50,67,229], and we were curious whether telmisartan reduces perfusion fluctuations in these tumours. Pentoxifylline is a drug that increases erythrocyte deformability to reduce blood viscosity[39], allowing blood to more readily flow through constricted vasculature. We have previously shown that pentoxifylline temporarily reduces perfusion fluctuations and reoxygenates transient hypoxic cells in WiDr tumours[50], providing a tool to test whether telmisartan inhibits the development of transient perfusion and hypoxia. We first validated the effect of pentoxifylline on whole tumour perfusion by administering pentoxifylline 15 minutes prior to 2-^{18}F-FEtOH dynamic PET, consistent with the rapid effect of this drug on tumour perfusion[50]. Measurements of 2-^{18}F-FEtOH uptake were taken 8-10 minutes following radiotracer injection, as we previously established this time point is indicative of tumour response to perfusion modifying drugs[52]. We found that pentoxifylline significantly increased 2-^{18}F-FEtOH uptake in WiDr tumours (Figure 4.3C), consistent with our previous work[50]. Interestingly, the high level of WiDr perfusion in telmisartan-treated mice was not further increased by pentoxifylline (Figure 4.3C). We did not observe a significant effect of pentoxifylline on 2-^{18}F-FEtOH uptake in SiHa tumours (Figure 4.4), consistent with our past observations that SiHa tumours have minimal perfusion fluctuations and do not respond to pentoxifylline[50]. Taken together, these data indicate that telmisartan increases bulk WiDr tumour perfusion and suggest that telmisartan-treated WiDr tumours have a remodeled tumour microenvironment that may prevent the development of fluctuating perfusion.

We next investigated the effect of telmisartan on microregional perfusion fluctuations by comparing fluorescent intensity of intravenously injected fluorescent perfusion dyes Hoechst 33342 and carbocyanine ($DiOC_7$)[50,63,67]. Fluctuations in tumour perfusion commonly occur on the order of 10-40 minutes in length[118], and we therefore administered Hoechst 33342 and $DiOC_7$ 20 minutes apart. In control WiDr tumours only 52.3 ± 0.07 % (mean ± SD) of blood vessels had stable perfusion, with the other ~48% of vessels experienced greater than 2-fold changes in perfusion over the 20-minute span. Telmisartan significantly increased the proportion of stable vessels in WiDr tumours, to 65.7 ± 0.06 % (mean ± SD), while also reducing the

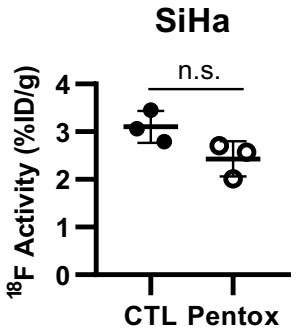

Figure 4.4 Pentoxifylline does not affect 2-^{18}F-FEtOH uptake in SiHa tumours

SiHa tumour 2-^{18}F-fluoroethanol uptake values averaged from imaging time points 8-10 minutes post-injection of the radiotracer. There is a no difference between control (CTL) and pentoxifylline (pentox) treated mice. N = 3, Student's t-test, $p > 0.05$.

proportion of vessels with large (greater than 3-fold) changes in perfusion (Figure 4.3D). These data indicate that telmisartan stabilizes perfusion in WiDr tumours.

4.3.3 Telmisartan reduces the development of transient hypoxia

We next investigated the effect of telmisartan on WiDr tumour hypoxia. Mice were administered the hypoxia marker pimonidazole[229] 90 minutes prior to sacrifice. Regions of chronic hypoxia could be easily identified in WiDr tumours from control and telmisartan-treated mice (Figure 4.5A). CD31+ blood vessels that were negative or weakly positive for Hoechst 33342 were commonly observed in control WiDr tumours (Figure 4.5A). In central tumour regions these blood vessels appeared proximal to pimonidazole labelled tumour cells (Figure 4.5A). We therefore mapped pimonidazole-labelled hypoxic cells based on distance from the nearest Hoechst 33342 perfused blood vessel. In control WiDr tumours, the median pimonidazole distance from perfused blood vessels was 35 ± 13 μm (Figure 4.5B). Telmisartan significantly increased the median distance between perfused blood vessels and pimonidazole positive hypoxic cells to 57 ± 7 μm (Figure 4.5B). There was no effect of telmisartan on the median distance between perfused blood vessels and pimonidazole positive hypoxic cells in SiHa tumours (Figure 4.5B). These data indicate that telmisartan preferentially increases oxygenation of tumour cells that are within 58 μm of perfused blood vessels. Our previous data indicate that transiently hypoxic tumour cells are present in similar proximities to functional vasculature[50,64,229], suggesting telmisartan may restrict the development of transient hypoxia in WiDr tumours.

To further investigate if the stabilized perfusion in telmisartan-treated WiDr tumours was indicative of reduced transient hypoxia, we administered pentoxifylline to WiDr tumour bearing mice 15 minutes prior to injection of pimonidazole. Consistent with our previous work, we observed a significantly reduced fraction of hypoxic tumour cells in pentoxifylline-treated tumours (Figure 4.5C)[50]. Telmisartan also reduced the fraction of hypoxic cells in WiDr tumours, however, there was no additive effect of administering pentoxifylline to telmisartan-treated mice (Figure 4.5C). Pimonidazole labelling in SiHa tumours was not affected by telmisartan or pentoxifylline treatment (Figure 4.5C). Thus, telmisartan decreases perfusion fluctuations in WiDr tumours and decreases tumour hypoxia by reducing development of transiently hypoxic cells known to be responsive to pentoxifylline.

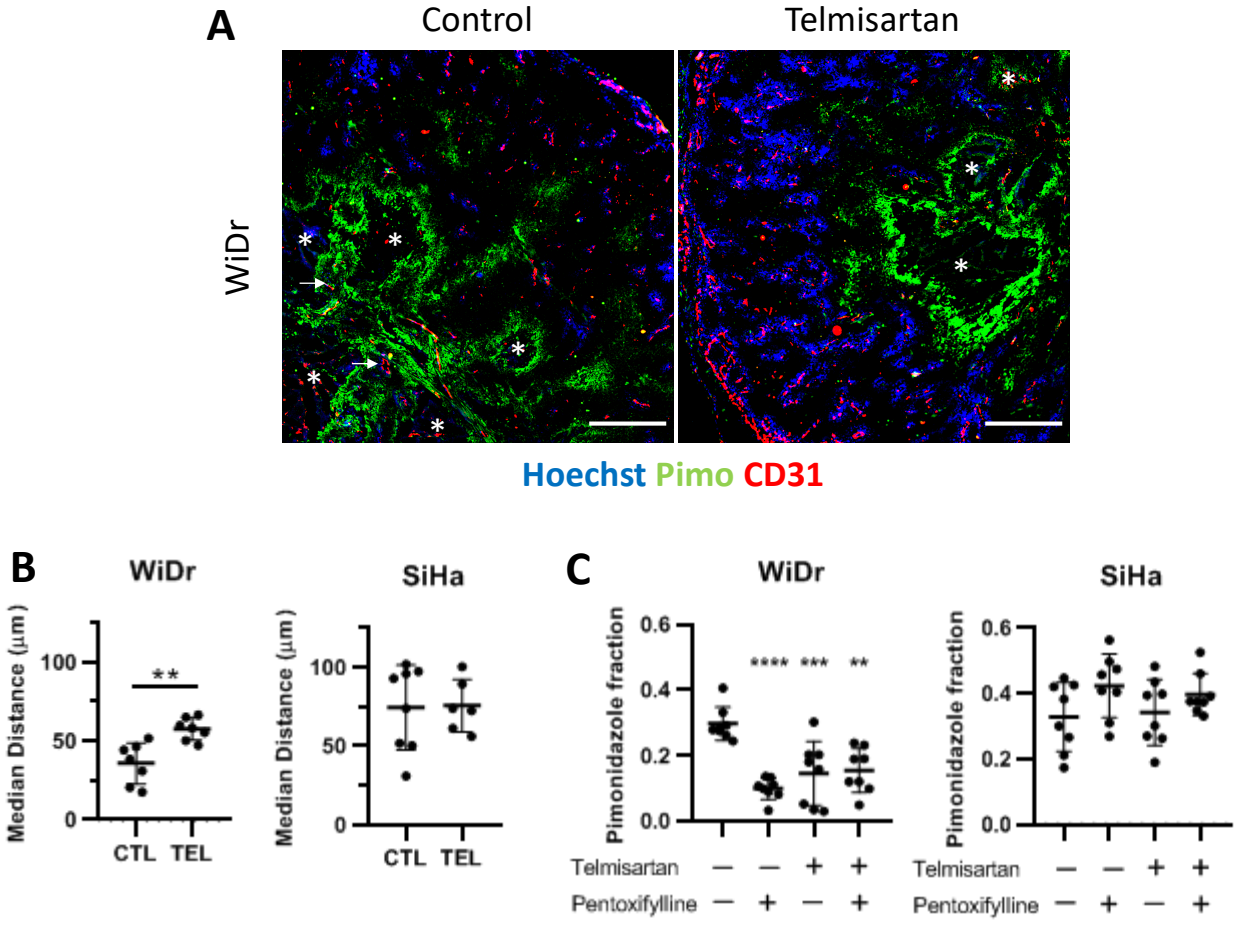

Figure 4.5 Telmisartan reduces WiDr tumour hypoxia.

(A) Sample immunofluorescent microscopy images of Hoechst 33342 (blue), pimonidazole (green), and CD31 (red) in WiDr tumours. Regions of necrosis indicated by '*'. Examples of CD31+ blood vessels in viable tumour regions with weak Hoechst 33342 staining are indicated by white arrows. Scale bars = 500µm. (B) In immunofluorescent microscopy, pimonidazole positive pixels were mapped based on distance from Hoechst 33342. From that analysis data plots display the median distance of all pimonidazole positive pixels in terms of distance to the nearest Hoechst 33342 pixel for both WiDr and SiHa tumours. CTL = control, TEL = telmisartan. Unpaired Student's t-test significant differences displayed, ** $p < 0.01$. (C) Fraction of tumour cells positive for pimonidazole in flow cytometry for WiDr and SiHa tumours. All data are mean ± SD, N = 6-8. Tukey multiple comparisons concluded that the only significant differences present were in comparisons with the telmisartan(-)/pentoxifylline(-) group, * $p < 0.05$, ** $p < 0.01$, *** $p < 0.001$, **** $p < 0.0001$.

4.3.4 Telmisartan improves WiDr tumour radiation response

To assess whether telmisartan is reducing the abundance of a radiation resistant population of hypoxic cells, we quantified clonogenic survival of tumour cells following irradiation with 10 Gy. Firstly, neither telmisartan nor pentoxifylline affected WiDr or SiHa cell survival when irradiated *in vitro*, indicating that neither drug is a direct radiation sensitizer (Figure 4.6). Clonogenic survival for WiDr tumours in mice treated with either pentoxifylline or telmisartan was reduced compared to controls, with no additive effect of combining telmisartan and pentoxifylline (Figure 4.7A). There was no effect of telmisartan or pentoxifylline on clonogenic survival of SiHa tumours (Figure 4.7B). These data indicate that telmisartan treatment is eliminating the hypoxic population that is targeted by pentoxifylline in WiDr tumours, and that this population would otherwise be sufficiently hypoxic to exhibit radiation resistance.

We next measured WiDr tumour growth delay induced by radiation for telmisartan-treated or control mice. Tumours were irradiated with 10 Gy 26-days post-implant when WiDr tumours measured 356 ± 106 mm^3 (mean ± SD). The growth curves for each group are displayed (Figure 4.8A), along with survival curves displaying time for all tumours in each group to exceed 1000 mm^3 (Figure 4.8B). Telmisartan did not affect the growth of non-irradiated WiDr tumours. In survival plots, 10 Gy irradiation of control tumours induced a significant growth delay of 14 days compared with non-irradiated tumours (Figure 4.8B). Irradiation of telmisartan-treated tumours with 10 Gy induced a 31-day growth delay compared with non-irradiated tumours (Figure 4.8B). These data indicate a significantly greater radiation-induced growth delay in telmisartan-treated WiDr tumours. Overall these data indicate that the reduction in hypoxia provided by telmisartan inhibits the development of a therapeutically significant radiation resistant population within WiDr tumours.

4.3.5 Improved radiation response from telmisartan treatment is dependent on altering the development of the tumour microenvironment

Clinical trials are currently ongoing testing the ARB losartan as an intervention for pancreatic ductal adenocarcinoma with the intention of increasing the delivery of chemotherapy to the tumour as was observed in pre-clinical study[85–89,236]. Patients selected to the losartan arm of the trial will receive losartan for a week prior to beginning chemotherapy[236]. We were

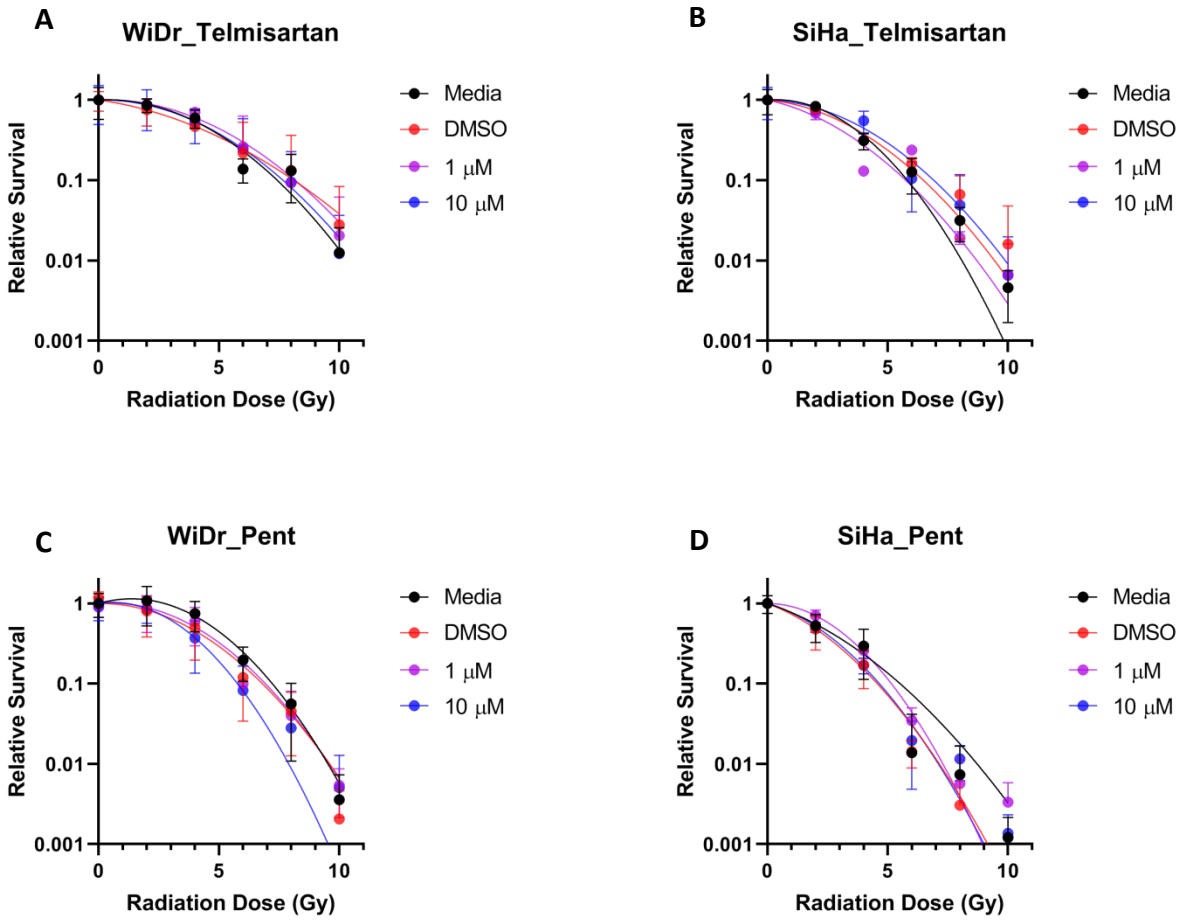

Figure 4.6 Telmisartan and pentoxifylline do not modify radiation sensitivity *in vitro*.

Clonogenic survival following x-irradiation is displayed for *in vitro* exposure of (A) WiDr cells to telmisartan, (B) SiHa cells to telmisartan, (C) WiDr cells to pentoxifylline, and (D) SiHa cells to pentoxifylline. WiDr and SiHa cells were plated and left to adhere to plates for four hours in normal MEM media +10% FBS before switching to either fresh media, media containing DMSO, or media containing DMSO with either 1μM or 10 μM of the indicated drug. Cells were incubated for 60 minutes prior to indicated doses of x-irradiation. After irradiation cells were switched to fresh media containing 10% FBS and penicillin-streptomycin, incubated for two weeks, stained with malachite green and colonies counted. Relative survival is plotted versus non-irradiated control within groups. Dunnett's multiple comparison test comparing each group to the DMSO group at each radiation dose concluded no significant differences in any experiment.

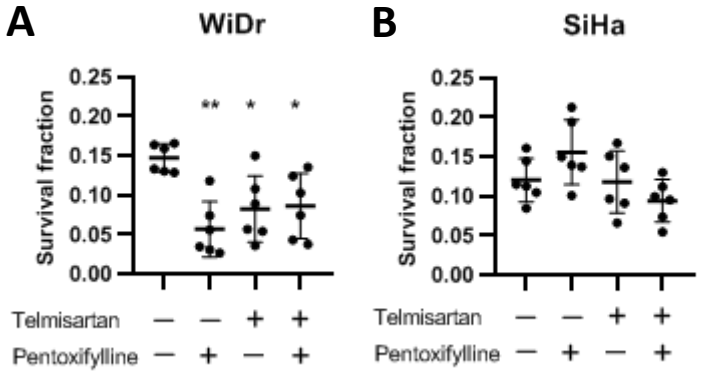

Figure 4.7 Telmisartan treatment reduces WiDr tumour cell survival following irradiation

Mice were subject to 10 Gy x-irradiation targeting the tumour. Plots display the clonogenic survival of (A) WiDr and (B) SiHa tumours after plating efficiency correction from parallel cohorts of mice that were not irradiated. All data are mean ± SD, N = 6-8. Tukey multiple comparisons concluded that the only significant differences present were in comparisons with the telmisartan(-)/pentoxifylline(-) group, * $p < 0.05$, ** $p < 0.01$, *** $p < 0.001$, **** $p < 0.0001$.

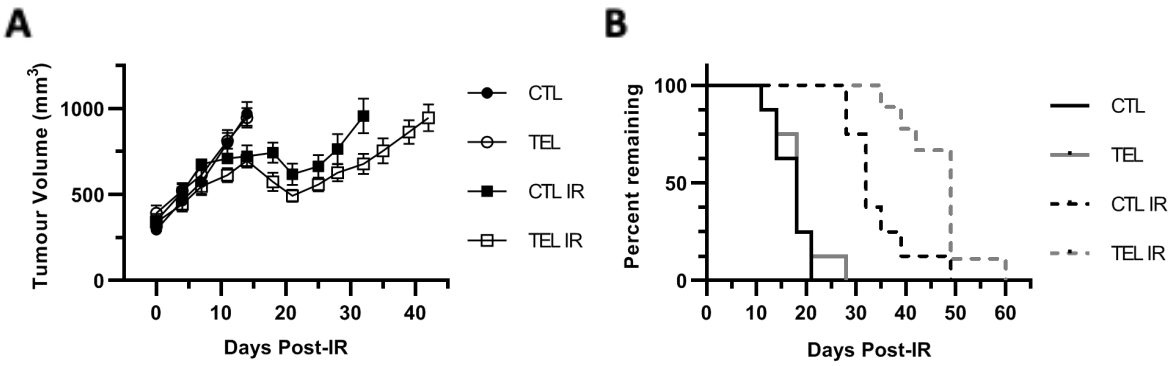

Figure 4.8 Telmisartan treated WiDr tumours exhibit a significant radiation growth delay.

(A) Growth curves from twice weekly caliper measurements and (B) survival plots with events defined as tumour volume reaching 1000 mm^3. CTL = control, TEL = telmisartan, IR = 10 Gy irradiated. N = 8-9 mice per group, growth curve plots display mean ± SEM. Statistical comparisons made on survival plot data using Log-rank test and correction for multiple comparisons made using Benjamini-Hochberg method with a false discovery rate of 5%; there was no difference in time to 1000 mm^3 for WiDr tumours in non-irradiated control versus non-irradiated telmisartan treated mice, all other comparisons were significant.

therefore interested in modeling our observed improvement in radiation response from telmisartan treatment based on the ongoing clinical trial with losartan.

To investigate the ability of telmisartan to improve radiation response as a therapeutic intervention, we again conducted a radiation growth-delay experiment irradiating WiDr tumours with 10 Gy x-irradiation 26 days post-implant. However, mice were not started on telmisartan until 18 days post-implant, thus mice were on telmisartan for a full week prior to irradiation (Figure 4.9A). At the time of randomization into control or telmisartan-treated groups, tumours were approximately 100 mm^3 (Figure 4.9). A parallel cohort of mice was not irradiated on day 26 and instead the tumours harvested to investigate the effects of delayed telmisartan treatment on the tumour microenvironment. Delayed telmisartan treatment did not significantly affect the Col1 content of WiDr tumours (Figure 4.9B). There was a trend ($p=0.07$) towards reduced tumour area positive for αSMA in telmisartan-treated WiDr tumours (Figure 4.9C). Delayed telmisartan treatment did not affect the fraction of CD31+ blood vessels labelled by intravenously injected Hoechst 33342 (Figure 4.9D). The fraction of WiDr tumour cells positive for pimonidazole in flow cytometry was similar between telmisartan-treated tumours and controls (Figure 4.9E). Tumour measurements were made twice per week (Figure 4.9F) and survival curves produced as before with events defined as when tumours reached 1000 mm^3 in volume (Figure 4.9G). We observed no difference in the time for WiDr tumour volume to reach 1000 mm^3 between control and telmisartan-treated mice. These data suggest that one week of telmisartan treatment is not sufficient to modify tumour radiation response. However, these data do support that the improvement in radiation response observed in Figure 4.8 was in fact dependent on the hypothesized mechanism of telmisartan-induced reduction in αSMA+ CAFs early in tumour development, reduced Col1 content, and improved tumour perfusion, leading to reduced hypoxia, and not due to an off-target mechanism of telmisartan.

4.4 Discussion

The current study identifies WiDr tumours as collagen-rich tumours with abundant αSMA+ CAFs that exhibit significant microregional perfusion fluctuations and hypoxia. Telmisartan significantly reduced both Col1 and αSMA+ cells in WiDr tumours (Figure 4.2), while improving whole tumour perfusion (Figure 4.3), stabilizing microregional perfusion (Figure 4.3), decreasing hypoxia (Figure 4.5), and improving radiation response (Figure 4.8).

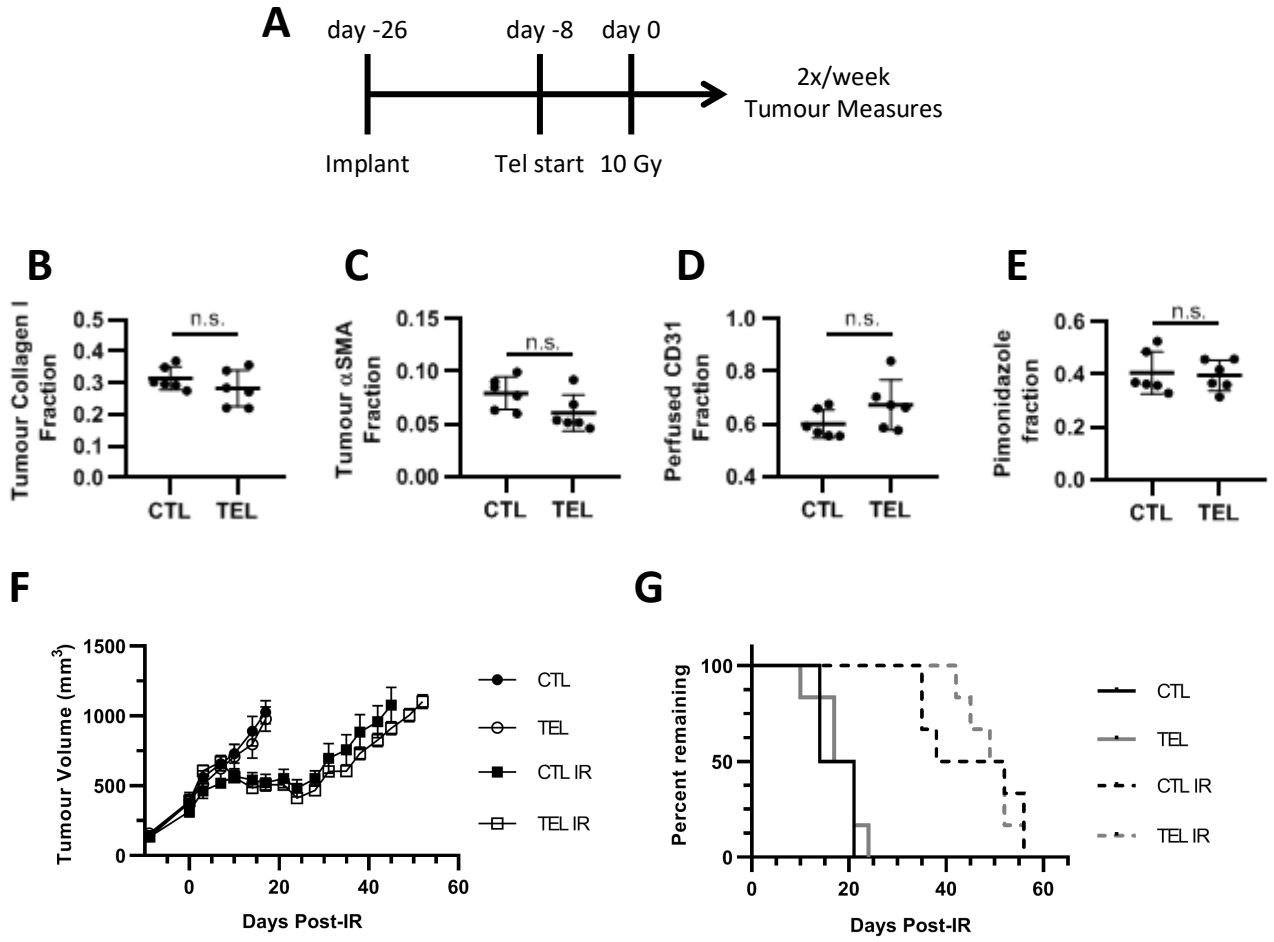

Figure 4.9 Delayed telmisartan treatment does not modify radiation response

(A) Experiment timeline. Parallel cohorts of mice were harvested at day 0 without irradiation exposure. Displayed are immunofluorescent microscopy quantification of the fraction of viable tumour area positive for (B) Col1 and (C) αSMA, as well as (D) the fraction of Hoechst 33342 perfused CD31 blood vessels. (E) The fraction of tumour cells positive for pimonidazole was quantified using flow cytometry. (F) Growth curves and (G) survival plots were constructed as described for Figure 4.8. For B-E, mean± SD, N =6, Student's unpaired t-test results are displayed, n.s. $p > 0.05$. For F and G, mean ± SEM N = 6, statistical comparisons are discussed in the main text.

This proposed mechanism is summarised in Figure 4.10. SiHa tumours were nearly devoid of αSMA+ cells, exhibited significantly less Col1, and neither tumour perfusion nor hypoxia responded to telmisartan treatment, consistent with previous work suggesting ARBs act specifically through reducing αSMA+ CAF activity[85]. We found that losartan was less effective in reducing Col1 than telmisartan, which agrees with telmisartan's greater affinity for angiotensin II type 1 receptors, greater antagonism of angiotensin II in vasoconstriction assays, and extended biological half-life compared to losartan[234]. While other studies have observed significant tumour microenvironment remodelling and perfusion changes induced by losartan[85,86,88–90], our observations are consistent with previous work showing telmisartan was superior to losartan in reducing Col1 and increasing perfusion in orthotopic A549 lung tumour xenografts[90]. The greater efficacy of telmisartan in our study highlights the need to test multiple ARBs in future pre-clinical and clinical interventions designed to modify the tumour microenvironment.

Blood vessel compression in collagen-rich tumours may be a source of microregional pressure deregulation that could be partially responsible for transient hypoxia. We previously showed that WiDr tumours, but not SiHa tumours, contain significant perfusion fluctuations and transient hypoxia, and that pentoxifylline temporarily stabilizes perfusion and decreases hypoxia[50]. The lack of an additive effect of administering pentoxifylline to telmisartan-treated WiDr tumours indicates that telmisartan reduces the development of transient hypoxia in these tumours. Telmisartan also significantly increased the median distance between perfused blood vessels and hypoxic cells (Figure 4.5), consistent with our previous work showing transiently hypoxic cells are in relatively close proximity to tumour blood vessels[50].

Collectively, the stabilization of microregional perfusion, lack of response to pentoxifylline, and reduced population of hypoxic cells proximal to blood vessels all suggest that telmisartan reduces the development of transient hypoxia in WiDr tumours. In turn, this suggests tumours with high abundance of Col1 and αSMA+ CAFs may be more likely to exhibit transient hypoxia. Interestingly, telmisartan dramatically altered the microenvironment in WiDr tumours without affecting tumour growth rates (Figure 4.8), indicating that tumour volume does not predict the level of hypoxia within a solid tumour. Moreover, telmisartan reduced hypoxia and improved radiation response of genetically identical WiDr tumours implanted into the same mouse strain, indicating that transient hypoxia and response to radiation are at least partly driven

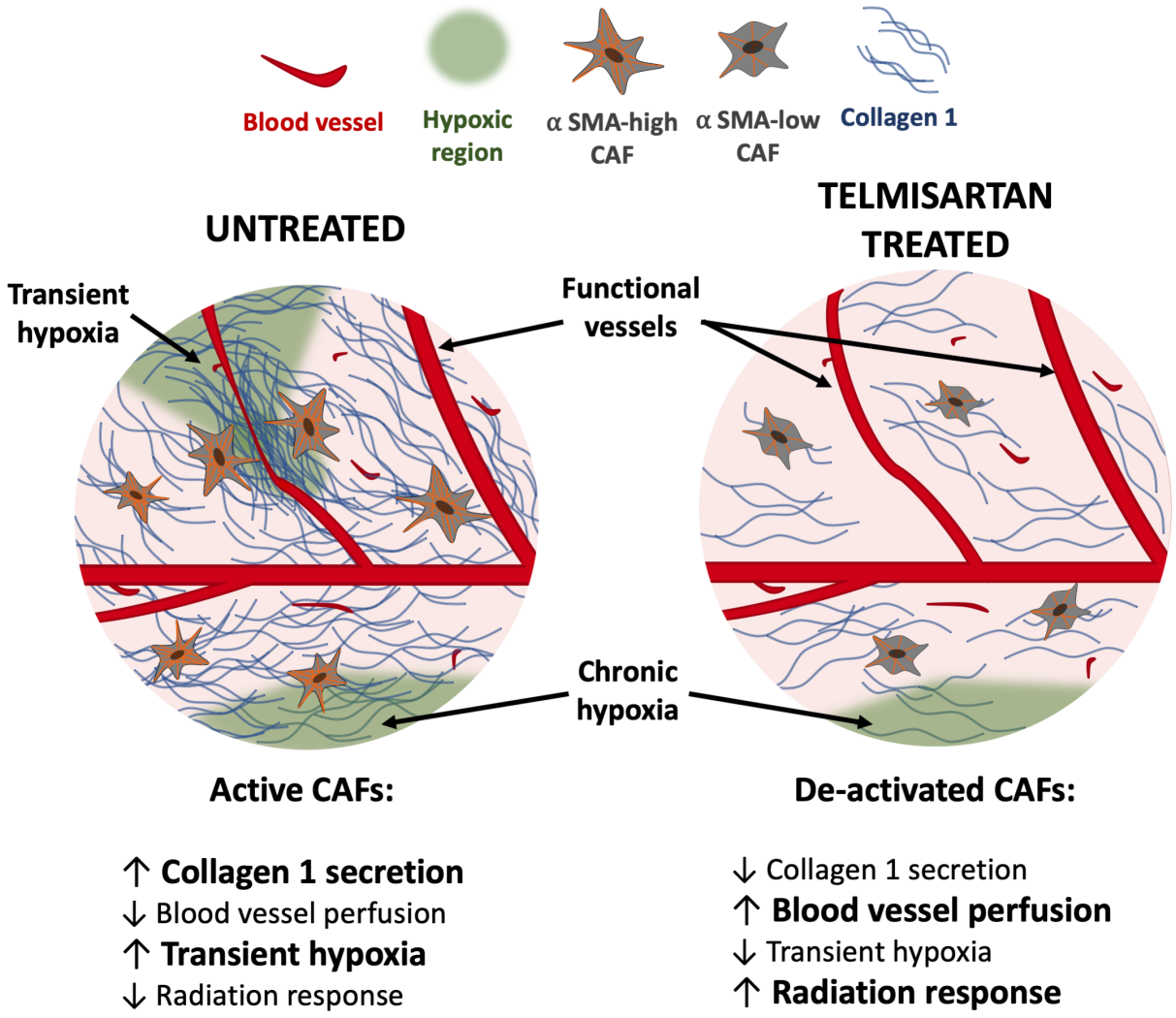

Figure 4.10 Proposed mechanism for the effect of telmisartan on the WiDr tumour microenvironment

Untreated WiDr tumours have high levels of αSMA+ CAFs and Col1 that compresses tumour blood vessels. Blood vessel compression causes reduced net tumour blood flow, unstable microregional perfusion, and transient tumour hypoxia that limits radiation response of the tumour. Telmisartan-treated WiDr tumours have fewer αSMA+ CAFs, decreased Col1, increased net tumour blood flow, improved microregional perfusion through functional blood vessels, decreased transient tumour hypoxia, and improved radiation response. Chronic hypoxia does not appear to be significantly affected by telmisartan treatment.

by CAF-mediated Col1 deposition during tumour development. Overall, this study identifies telmisartan as an intriguing tool for future pre-clinical study into transient hypoxia as the only intervention able to reduce the development of transient hypoxia in solid tumours.

ARBs are widely prescribed anti-hypertensive medications that are also used to reduce pathogenic fibrosis in patients. A recent meta-analysis designed to assess the effects of angiotensin II system inhibitors on cancer outcome showed that ARB or angiotensin II converting enzyme inhibitor (ACEi) users commonly represent between 15-30% of all cancer patients[235]. The influence of ARBs and ACEi on cancer therapy is an important clinical question, and this meta-analysis found a global hazard ratio of 0.82 significantly in favour of ARB and ACEi users across fifty-five studies including over 170,000 patients and various tumour sites[235]. The majority of our data, Figure 4.1 through Figure 4.8, essentially model this case where patients are coincidentally taking angiotensin system inhibitors at the time of cancer diagnosis and were presumably taking the drugs for some time prior, i.e. during tumour development. Pending confirmation of Col1 content and tumour perfusion in clinical tumours of ARB users and non-users, the retrospective data appears to agree with our data and pre-clinical data from others in that ARB usage favourably modifies tumour development. However, our observation of no benefit from delayed telmisartan treatment does highlight the potential pitfall of a mechanism reliant on modifying collagen deposition in that ARB intervention may either require a significant period of time to be effective or that ARB treatment must begin early in tumour growth. Further research will be required to determine exactly how ARBs should be applied as interventions for radiation therapy.

Our data show that the ARB telmisartan stabilizes microregional tumour perfusion, reduces the development of transient tumour hypoxia, and significantly improves radiation response in human tumour xenografts. Our study provides the first evidence that telmisartan improves radiation response, supporting further consideration of ARB usage in patients being treated with radiation therapy.

Chapter 5: Conclusions and future directions

5.1 Summary and contributions to the research field from Chapter 2

Chapter 2 of this thesis addressed the poor basic understanding of transient hypoxia by investigating the rate of hypoxic cell turnover and distinguishing between chronic and transient hypoxic cell loss. Briefly, we observed that chronically hypoxic tumour cells were the major contributor to hypoxic cell loss in the first 48 hours after labelling hypoxic cells with pimonidazole (Figure 2.8). Cells that could be classified as transiently hypoxic cells at the time of labelling were the major contributors to hypoxic cell loss between 48-72 hours after labelling (Figure 2.8). Further, we observe that the amount of hypoxic cell loss that could be attributed to transiently hypoxic cells was similar to the total amount of transiently hypoxic cells estimated to exist in WiDr tumours (Figure 2.8, Figure 2.9), suggesting that the vast majority of transiently hypoxic cells were lost in this time period. We also observe that radiation-induced vascular destruction preferentially kills transiently hypoxic tumour cells compared with chronically hypoxic tumour cells (Figure 2.11).

Firstly, these data support the hypothesized 'flow' of tumour cells outwards from blood vessels suggested by previous studies, progressively pushing tumour cells into regions of poorer oxygenation and ultimately into regions of necrosis[111,129,132]. Our observation of ordered cell loss, chronically hypoxic cells followed by transiently hypoxic cells, supports the tumour cord model depicting cells layered outwards from perfused blood vessels as: normoxic cells, transiently hypoxic cells, chronically hypoxic cells, and necrosis. This tumour cord model is the accepted view for the relative location of chronic and transient hypoxia[202].

These data provide a defined limit for the lifetime of transiently hypoxic tumour cells *in vivo* of 72 hours, that until now was unknown. Our lifetime data has clear implications for pre-clinical modeling of transient hypoxia. First, our data support that transiently hypoxic tumour cells likely reside at intermediate distances from perfused blood vessels, are sufficiently hypoxic during periods of poor flow to label with 2-nitroimidazoles (Figure 2.9), and contribute to tumour clonogenic survival following 10 Gy x-irradiation (Figure 2.11). These observations suggest that transiently hypoxic cells experience oxygenation at or below 0.5% O_2 during hypoxic periods. The published data observing only modest increases in tumour oxygenation following pentoxifylline treatment[171,216–219,221,223], along with the modest fluctuations in

perivascular oxygen content observed in intra-vital imaging experiments[119], together suggest that transiently hypoxic tumour cells experience moderate oxygenation (more likely 1-2% O_2 than 5% O_2) during periods of reoxygenation. The published data suggest that oxygen fluctuations occur on the order of 10-40 minutes in length[50,67–69,71,116–119,229]. Collectively, these data suggest that future studies modeling transient hypoxia should cycle tumour cells between 2% O_2 and 0.5% for 10-40 minute periods. The data from Chapter 2 would suggest a maximum protocol length of 72 hours. To further model the observed 'flow' of tumour cells outwards from blood vessels and into regions of more chronic and more severe hypoxia, it would likely be accurate to limit cell exposure to cycles of hypoxia to 24 hours and switch to chronic hypoxia for an additional 48 hours. However, the time at which transiently hypoxic cells come to occupy regions of chronic hypoxia is not perfectly clear and would be better investigated by methods that positively label transiently hypoxic cells as opposed to the negative selection employed in this thesis.

Chapter 2 provides further evidence to the lifetime of chronically hypoxic cells, that to date was directly investigated by only one study[129]. Similar to Ljungkvist et al., we find the total hypoxic cell half-life for human tumours is in the range of 48 hours (Figure 2.8)[129]. However, our data imply the existence of two populations of chronically hypoxic tumour cells in WiDr tumours. First, there is the population of chronically hypoxic tumour cells that are lost within the first 48 hours after labelling. We also observe a population of hypoxic cells that survives the 96-hour protocol. We estimate that the vast majority of the transiently hypoxic cells are lost between 48-72 hours after labelling, thus the hypoxic cells that survive the 96-hour protocol must have been chronically hypoxic cells at the time of labelling. As discussed in Chapter 2, this implies the existence of chronic hypoxia both in tumour cords that contain necrosis and in tumour cords that do not yet contain necrosis. However, in both SiHa and WiDr tumours harvested 72 or 96 hours after pimonidazole administration, we observe pimonidazole positive tumour cells to reside exclusively in tumour regions adjacent to necrosis. Together, this implies either the movement of chronically hypoxic cells from tumour cords without necrosis into tumour cords containing necrosis, or the development of necrosis at the edge of existing tumour cords. Additionally, our data suggest that transiently hypoxic tumour cells reside exclusively in tumour cords that contain necrosis as no transiently hypoxic tumour cells survived through the 96-hour protocol. This observation is in agreement with past predictions made from modelling blood flow and oxygen

in intra-vital imaging, which concluded that the oxygenation of tumour regions with low vascular density were most vulnerable to fluctuations in blood flow[119].

We find that both chronically and transiently hypoxic tumour cells contribute to tumour cell survival following each radiation schedule, in similar proportion to their estimated abundance in WiDr tumours (Figure 2.9, Figure 2.11). This further supports the existing evidence that transiently hypoxic tumour cells are important considerations for tumour radiation resistance[50,106,108,202,214,244]. We further find that 10 Gy of x-irradiation induced a decrease in the density of Hoechst 33342 perfused CD31-positive blood vessels 24 hours post-irradiation, leading to an increase in tumour hypoxia and induction of tumour cell killing (Figure 2.10, Figure 2.11). This was not observed with either a single dose of 5 Gy or two doses of 5 Gy 6-hours apart. These observations are in agreement with past reports that endothelial cell apoptosis is induced by single doses of irradiation greater than ~8 Gy[169,170]. Importantly, we observed that transiently hypoxic tumour cells were disproportionately affected by radiation-induced vascular destruction compared with chronically hypoxic tumour cells, and only a small minority (<15%) of transient hypoxia-derived clonogens survived the indirect cell killing following 10 Gy (Figure 2.11). This suggests that transiently hypoxic tumour cells may be killed by large single doses of radiation regardless of interventions aiming to reoxygenate transient hypoxia at the time of irradiation.

Our data therefore have implications for studies testing the efficacy of interventions that aim to reoxygenate transiently hypoxic tumour cells at the time of irradiation, such as nicotinamide or pentoxifylline, as the majority of pre-clinical studies apply large single doses of irradiation. The important distinction to make is between those studies that reach conclusions based on clonogenic assay of tumours harvested soon after irradiation[50], compared with studies that apply tumour control or growth delay assays where tumours are not harvested and therefore subject to indirect radiation cell killing such as that caused by vascular destruction[265]. Studies employing tumour control and growth delay assays may underestimate the effect of reoxygenating transiently hypoxic tumour cells on the direct radiation cytotoxicity, as this may be masked by death of transiently hypoxic cells due to vascular destruction. On the other hand, studies employing clonogenic assay will assess the effect of reoxygenating transient hypoxia on the direct cytotoxicity of radiation because there will be no opportunity for vascular destruction to cause indirect cell death. Tumour control or growth delay assays will better assess the effect of

reoxygenating transiently hypoxic tumour cells in producing a tumour response, making these assays better if translating the data to clinical practice applying hypo-fractionated radiotherapy. However, most North American clinical practice applies traditional fractionated radiotherapy. To translate to fractionated radiotherapy practice, it is arguably more important to understand the ability of an intervention to modify the direct radiation cytotoxicity to transiently hypoxic tumour cells, which would support use of clonogenic assays. Of course, the best pre-clinical model of fractionated radiotherapy would be to conduct fractionated radiotherapy and assess tumour control or growth delay. However, the response of the tumour microenvironment regarding microregional perfusion stability and transient hypoxia during fractionated radiotherapy is poorly characterized and future study in this direction may be informative before testing interventions against transient hypoxia in this manner.

Overall, our data indicate that transiently hypoxic tumour cells are radiation resistant cells that live longer than neighbouring chronically hypoxic tumour cells. However, our data indicate that the longest-lived hypoxic cells in solid tumours are likely chronically hypoxic cells in tumour cords without adjacent regions of necrosis.

5.2 Summary and contributions to the research field from Chapter 3

The aim of Chapter 3 was to validate 2-^{18}F-FEtOH as a novel PET-based reporter of solid tumour perfusion that could be used to investigate tumour response to perfusion-modifying interventions[52]. Briefly, Chapter 3 found that 2-^{18}F-FEtOH uptake agreed with the established perfusion reporter ^{14}C-IAP (Figure 3.4), distinguished between 67NR and 4T1 tumours based on differences in perfusion (Figure 3.5, Figure 3.7), and accurately responded to nicotinamide, pentoxifylline, and hydralazine (Figure 3.8, Figure 3.10). These data indicate that 2-^{18}F-FEtOH is a functional reporter of solid tumour perfusion.

While Chapter 3 focused on the 67NR and 4T1 murine mammary carcinoma tumour lines, further study of 2-^{18}F-FEtOH was later conducted on WiDr and SiHa human tumour xenografts (Figure 4.3, Figure 4.4, Figure 5.1, and data not included in this thesis). Experiments on WiDr and SiHa tumours further support the ability of 2-^{18}F-FEtOH to report tumour perfusion, including response to perfusion-modifying interventions. For example, the bulk tumour perfusion response of WiDr tumours to pentoxifylline treatment was previously published from the ^{82}RbCl assay as demonstrating a large increase 15 minutes post-injection of

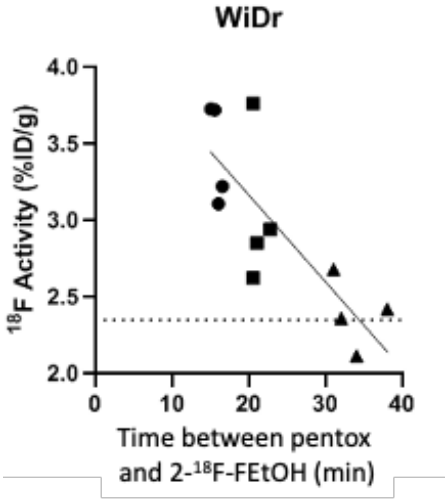

Figure 5.1 WiDr tumour 2-^{18}F-FEtOH uptake after pentoxifylline

Response of bulk WiDr tumour perfusion to pentoxifylline treatment is time dependent. WiDr tumour 2-^{18}F-FEtOH uptake averaged across 8-10 minutes after radiotracer injection, detected by dynamic PET scan. 50 mg/kg of pentoxifylline was administered at indicated times prior to 2-^{18}F-FEtOH. Different shapes correspond to different experiment dates.

pentoxifylline, and a return to baseline 30 minutes post-injection[50]. We have quantified 2-^{18}F-FEtOH uptake in WiDr tumours 15, 20, or 30 minutes after pentoxifylline and reproduced the same time dependent trend (Figure 5.1). As previously published, pentoxifylline treatment has no effect on SiHa tumour perfusion, and we observed no significant effect of pentoxifylline on SiHa tumour 2-^{18}F-FEtOH uptake (Figure 4.4)[50]. In chapter 4, we further find that telmisartan treatment significantly increased 2-^{18}F-FEtOH uptake in WiDr tumours (Figure 4.3). While we did not validate that telmisartan was improving bulk WiDr tumour perfusion by an independent method, the past research indicating that ARB-induced reduction in Col1 and αSMA+ CAFs leads to improved tumour perfusion supports that 2-^{18}F-FEtOH is again properly reporting increased WiDr tumour perfusion with telmisartan treatment. Further, we have attempted preliminary experiments quantifying 2-^{18}F-FEtOH uptake in losartan-treated WiDr tumours. In these experiments there was no effect of losartan treatment on 2-^{18}F-FEtOH uptake (data not shown), in agreement with the lack of effect from losartan on WiDr tumour Col1 or αSMA+ CAF content. Overall, these data support that tumour 2-^{18}F-FEtOH uptake is reporting bulk tumour perfusion and is responsive to perfusion-modifying interventions.

Therefore, 2-^{18}F-FEtOH represents an ^{18}F-based reporter of solid tumour perfusion, and 2-^{18}F-FEtOH remains the only validated ^{18}F-based reporter of solid tumour perfusion. The longer half-life of ^{18}F (~110 minutes) provides benefits compared to the majority of other validated PET perfusion reporters (e.g. ^{15}O-H_2O, half-life = ~2 minutes). First, it is possible to label molecules with ^{18}F (half-life ~110 minutes) and transport the radiotracer to distant locations without an on-site cyclotron[283]. Such accessibility is not possible for radioisotopes such as ^{15}O with very short half-lives. The extended half-life of ^{18}F also makes 2-^{18}F-FEtOH fit for detection via *ex vivo* radiography (extended half-life is required for processing time of tumour excision, mounting, sectioning, and detection). Current beta-imagers report resolution as low as 10 μm, approaching that of common fluorescent microscopes (1-2 μm). This means 2-^{18}F-FEtOH uptake may be quantified in a micro-regional manner that may be more meaningfully compared with fluorescent biomarkers of interest (e.g. pimonidazole) than would be possible with PET imaging alone. Overall, 2-^{18}F-FEtOH provides many benefits over current perfusion reporters and is an appealing option for future pre-clinical research interested in solid tumour perfusion.

5.3 Summary and contributions to the research field from Chapter 4

Chapter 4 aimed to investigate the effects of ARBs on the tumour microenvironment, with the hypothesis that ARB treatment would reduce transient hypoxia and improve tumour radiation response. The findings from Chapter 4 included, briefly, that telmisartan and not losartan treatment altered the development of the WiDr tumour microenvironment to reduce Col1 and αSMA+ CAF content (Figure 4.2), increase and stabilize tumour perfusion (Figure 4.3), reduce transient hypoxia (Figure 4.5), and increase tumour radiation response indicated by both clonogenic assay (Figure 4.7) and radiation growth delay (Figure 4.8). These data indicate that ARB treatment may improve tumour radiation response by reducing the development of transient hypoxia in solid tumours.

These data add to the growing mechanism of ARB modification to the tumour microenvironment. The currently proposed mechanism is that inhibition of AT1R receptors on CAFs prevents their ability to activate and respond to extracellular TGFβ, preventing further activation into αSMA+ CAFs[85]. This ARB-induced decrease in αSMA+ CAFs results in reduced Col1 deposition, which reduces tumour stiffness and decompresses blood vessels to increase tumour perfusion[85–89]. The data from Chapter 4 builds upon this mechanism by demonstrating that ARB-induced increases in tumour perfusion may also stabilize microregional perfusion (Figure 4.3) and reduce the development of transient hypoxia (Figure 4.5). These observations may further inform research and application of ARBs, but also provide predictive data for how other interventions modifying αSMA+ CAFs or Col1 deposition in solid tumours will affect tumour hypoxia.

The proposed and published applications of ARBs for cancer treatment are to increase chemotherapy delivery to solid tumours (i.e. increased tumour perfusion resulting in increased drug delivery)[86,89] and more recently to increase tumour response to immunotherapy[284]. This thesis work demonstrates that ARB-induced modifications to the tumour microenvironment are also of significant interest for radiotherapy. Recent estimates are that approximately 39% of Canadian cancer patients receive some form of radiotherapy[285]. Combined with the recent data suggesting that 15-30% of cancer patients coincidentally take angiotensin system inhibitors[235], it is clear that investigating the effect of ARB usage on radiotherapy may impact a large proportion of cancer patients. As our findings suggest that telmisartan usage is beneficial for radiotherapy response (Figure 4.8), our data do not suggest action is required for those patients coincidentally

taking ARBs at the time of diagnosis. However, we did observe that losartan was unable to reliably modify the WiDr tumour microenvironment, consistent with the known weaker activity of losartan compared with telmisartan[234]. While the majority of studies on ARBs and cancer have focused on losartan, our data is the second study to demonstrate that telmisartan is a much stronger option[90]. This has implications for the possible translation of ARBs in cancer, and our data would support two immediate changes to future research. Firstly, all future retrospective analyses of clinical data should record and report which specific ARBs patients were taking at the time of diagnosis, as well as any history of ARB usage. This recommendation may allow for sub-group analysis to eventually determine from clinical data if there is a difference between losartan and any newer generation ARB on patient outcome, which currently is not available in most reports. Second, future pre-clinical studies should continue to compare losartan with telmisartan or another newer generation ARB. In the scenario that early prospective clinical trials testing losartan treatment prior to initiating therapy (including the ongoing pancreatic ductal adenocarcinoma clinical trial[236]) are negative, data in support of further options for translating ARBs to cancer therapy will be required. Overall, Chapter 4 indicates that ARB usage in some form is likely beneficial for radiotherapy outcome. However, the work is not done to determine if or for whom losartan is sufficient versus more potent ARBs such as telmisartan.

Regarding the translation of ARBs into cancer treatment, our data are not in support of telmisartan as an intervention, as delayed telmisartan treatment failed to significantly affect any of αSMA+ CAFs, Col1, perfusion, hypoxia, or radiation response (Figure 4.9). While most studies treating tumour-bearing mice with ARBs treat for two weeks or more, at least one study has reported significant changes in solid tumour perfusion from as few as 5 days of losartan treatment[89]. Therefore, it may be possible for ARBs to be applied as interventions for some tumours and not others. Our negative observation should implore future studies to investigate factors that may make tumours more or less susceptible to ARBs, and to develop novel drugs that will improve our ability to target CAFs.

Finally, the research of Chapter 4 carries implications for the study of transient hypoxia. As mentioned in Chapter 1, prior to our work there were no specific factors demonstrated to predispose tumours to transient hypoxia and no interventions able to stably reduce transient hypoxia in solid tumours. The work of Chapter 4 demonstrates that ARB treatment is able to reduce the development of transient hypoxia in solid tumours. We display that ARB treated

WiDr tumours exhibit stabilized microregional perfusion (Figure 4.3), that the median distance of pimonidazole positive cells from perfused blood vessels is increased in telmisartan-treated tumours (Figure 4.5), and that the hypoxic fraction and radiation-resistant fraction of telmisartan-treated WiDr tumours can no longer be reoxygenated by pentoxifylline (Figure 4.5, Figure 4.7). All of these data strongly support that telmisartan reduces the development of transient hypoxia in solid tumours. This thesis therefore presents high αSMA+ CAFs and/or high Col1 content as a tumour microenvironmental feature that may cause or predispose tumours to experience transient hypoxia. This finding alone provides important insight into the development of transient hypoxia that was otherwise lacking and opens the door for investigation into the potential role of CAFs in the development of tumour hypoxia. Further, we demonstrate telmisartan treatment stably reduces the development of transient hypoxia in solid tumours without genetic manipulation of the tumour cells or a significant change to tumour growth. This identifies telmisartan an appealing tool for pre-clinical study interested in the role of transient hypoxia in tumour biology *in vivo*, which to date has only been investigated by the laborious and extreme intervention of gassing mice with cycles of low O_2 (~8%) and regular O_2 gas[242,247]. Overall, the data of Chapter 4 opens many doors for future research into the biology of transient hypoxia.

5.4 Future directions

This thesis largely focused on WiDr and SiHa human tumour xenografts grown in immunodeficient mice based upon thorough previous characterization of these tumours. Specifically, that WiDr tumours exhibit greater transient hypoxia compared with SiHa tumours[50,67,68,229,230]. Characterization of further tumour lines would aid in the characterization of transient hypoxia. Future study should investigate our novel findings regarding the lifetime of transiently hypoxic tumour cells and impact of αSMA+ CAFs on transient hypoxia. However, as of yet the only other tumour lines that are thoroughly characterized to exhibit transient hypoxia are the murine squamous cell carcinoma SCCVII line and murine KHT sarcoma line[63,64,69,71]. Murine tumour cells generally exhibit more rapid rates of proliferation and therefore may exhibit significantly different phenotypes regarding tumour cell turnover[128,129]. Thus, investigation into the lifetime of transiently hypoxic tumour cells in SCCVII and KHT tumours may be informative for the study of transient hypoxia in murine tumours, but overall further study of murine lines

may be limited in application to the study of human tumours relative to our data from WiDr tumours.

Therefore, another important avenue of future research will be the identification and characterization of further human tumour models that exhibit transient hypoxia. Of particular interest would be the identification of tumours that do and do not exhibit significant transient hypoxia within the same tumour site, instead of comparing a colorectal adenocarcinoma and cervical squamous cell carcinoma as in this thesis. However, prior to our work there were no reported specific causes of transient hypoxia and therefore no indicators to identify tumours that are most likely to exhibit transient hypoxia. Thus, this thesis presents a significant contribution to the field in that we have uncovered a potential cause of transient hypoxia in Chapter 4, high tumour Col1 content and/or high content of αSMA+ CAFs. Ongoing research within the Bennewith lab will be screening tumour xenografts produced from cervical and head and neck human tumour lines for Col1 and αSMA+ CAF content and characterizing these tumours for transient hypoxia. Cervical and head and neck sites will be studied because radiotherapy is commonly used to treat these sites, desmoplasia (i.e. tumour fibrosis) is associated with poor patient outcome, and αSMA+ CAFs are associated with poor patient outcome[102,286]. Tumour lines grown in mice will be assessed for perfusion, Hoechst 33342-$DiOC_7$ mismatch, and response of tumour hypoxia to pentoxifylline in order to correlate Col1 and αSMA+ CAF content with transient hypoxia phenotypes. Telmisartan treatment may then be applied to confirm that transient hypoxia phenotypes are indeed associated with αSMA+ CAFs and Col1 content. Identification of further human tumour lines that develop transient hypoxia in association with αSMA+ CAFs and Col1 will provide a greater resource to study the cause of transient hypoxia.

We hypothesize that transient hypoxia phenotypes will be associated with increased content of αSMA+ CAFs. It therefore may be possible to determine specific causes of transient hypoxia in terms of tumour cell mutations or gene expression by determining what causes tumour cells to recruit and/or activate fibroblasts. For instance, the abundance of αSMA+ CAFs in thyroid cancer has been associated with Braf and PTEN mutations in tumour cells[287]. Expression of mutant *KRAS* in pancreatic and colorectal cancer cells is observed to cause CAF-like activation of normal fibroblasts[288,289]. Thus, a search for specific factors leading to CAF activation and potentially the development of transient hypoxia may begin with *in vitro* assays

assessing CAF migration and activation in response to conditioned media from tumour cells transfected with siRNA against genes in epidermal growth factor receptor (EGFR) and phosphoinositide 3 kinase (PI3K) signaling pathways. Determining a specific cause, or set of causes, of transient hypoxia may provide a biomarker of tumours that are more likely to exhibit transient hypoxia and therefore more likely to benefit from interventions that will stabilize tumour perfusion, such as telmisartan. It should also be noted that environmental exposures may also regulate CAF activation, as researchers have found that exposure to smoke particles cause epigenetic alterations in fibroblasts that alter their ability to acquire an activated phenotype upon tumour implant[95,290]. Thus, CAF activation and the potential connection with the development of transient hypoxia could be influenced by environmental factors in addition to tumour cell genetics.

Identification of tumours that exhibit significant transient hypoxia would also be improved by biomarkers specific to transiently hypoxic cells. Currently there are no published biomarkers for transiently hypoxic tumour cells that distinguish them from chronically hypoxic cells. However, there is evidence of distinct biology. For example, exposure of tumour cells to cycles of hypoxia increases expression of many metastasis-related genes compared with exposure to chronic hypoxia[246], while extended exposure to hypoxia may reduce expression of many DNA repair genes compared to short hypoxic exposures[248]. Thus, it may be possible to produce at least a gene signature that could distinguish between tumour cells cultured in either chronic or cyclic hypoxia *in vitro,* for which this thesis provides specific guidelines in order to accurately model transient hypoxia (Chapter 2). To generate data derived from a solid tumour rather than *in vitro*, single-cell RNA-seq could be employed to identify sub-populations of hypoxic tumour cells. To ensure the genes identified are robust markers for specifically transient or chronic hypoxia, one could enhance the population of transient hypoxia by exposing mice to cycles of low (8% O_2) and normal oxygen content gas or reduce the transient hypoxia population via telmisartan treatment. Any identified candidate biomarkers could then be validated *in vivo* comparing the labelling of tumour cells for the biomarker versus 2-nitroimidazoles with and without pentoxifylline. Identifying a biomarker of transient hypoxia will be critical for clinical translation of research regarding transient hypoxia as no high throughput method exists to specifically investigate the presence of transient hypoxia in patient tumours.

This thesis did not delve into the intriguing connection between transient hypoxia and metastatic growth[242,246,247]. However, the data from Chapter 4 identifies telmisartan as a tool that may be capable of reducing the transient hypoxia population within tumours without completely removing hypoxia, genetically modifying tumour cells, or significantly altering tumour growth. Thus, genetically identical tumours of similar size may be assessed for metastatic propensity, with the knowledge that telmisartan-treated mice exhibit reduced transient hypoxia. For this research direction, the connection between telmisartan treatment and transient hypoxia would have to be teased apart from the intermediary steps, including potential for an off-target effect of telmisartan on tumour cell metastasis and confirming that the telmisartan-induced reduction in αSMA+ CAFs is not altering metastasis aside from effects on producing transient hypoxia. These studies may therefore require co-implanting tumour cells with genetically modified fibroblasts or mesenchymal stem cells (MSCs). Previous study demonstrates that co-implant of tumour cells with fibroblasts or MSCs significantly affects tumour growth and that modifying the fibroblasts or MSCs in culture prior to implant significantly modifies the CAF population found upon tumour harvest, overall supporting that the co-implanted fibroblasts become the dominant CAF population in the tumour[291–294]. With this experimental set-up, stable knockdown of AT1R protein expression in fibroblasts may be applied to investigate the specificity of telmisartan activity for modifying CAF activation, and stable knockdown of Col1 protein expression in fibroblasts may be applied to test the specificity for CAF activity as acting through Col1 production. This strategy would be an informative addition to the field of research implicating transient hypoxia as a promoter of metastatic growth, as well as again providing a link to clinical data. As mentioned previously, a 2017 meta-analysis of cancer patients coincidentally taking angiotensin system inhibitors (ARBs or ACEi) found a global hazard ratio of 0.82 in favour of angiotensin system inhibitor users[235]. The cause of this reduced hazard ratio for ARB/ACEi users may be due to improved chemotherapy delivery as suggested by previous studies[85–89,236] or improved radiotherapy response as suggested by the work in this thesis (Chapter 4). Based on our observation that ARB usage may reduce transient hypoxia, and past evidence that transient hypoxia promotes metastasis[242,246,247], one could also hypothesize that the improved outcome for ARB/ACEi users is due to reduced development of transient hypoxia and a resultant reduction in metastatic dissemination. Future research investigating the effects of telmisartan, or other ARBs,

on tumour metastasis may therefore provide a potential clinical link for translation of transient hypoxia research into clinical care.

Since 15-30% of cancer patients are taking ARBs/ACEi at the time of diagnosis it is impactful to study this population even if ARBs will not be an effective therapeutic intervention. However, it is worth noting that some data suggest short term ARB treatment may be sufficient to modify tumour perfusion[89]. Regardless, investigating ARBs provides a means to study how reducing Col1, reducing αSMA+ CAFs, improving tumour perfusion, and stably reducing transient hypoxia may affect outcome with the possibility to confirm with retrospective patient data based on coincidental ARB usage. Based upon the building evidence of benefit from ARB usage, future research may therefore investigate other strategies to, potentially more potently, reduce tumour Col1 and αSMA+ CAF. For example, ongoing research at BCCRC and UBC is investigating therapeutics to inhibit AT1R signaling in αSMA+ CAFs without the blood pressure-reducing effects of ARBs. Such a drug would allow for increased dose without risk of hypotension, possibly accelerating the effect of reducing CAF activation and improving the chance of drug efficacy as a true intervention. Response to Interventions aiming to reduce activity of CAFs could potentially be monitored non-invasively if the target CAF subtype is well-characterized and an appropriate radiotracer available. For example, non-invasive imaging agents against FAP have been recently produced[295,296] and could potentially identify tumours responding to ARB or other treatments. If FAP is identified as an indicator of response to ARBs, then patients could be monitored for response and potentially allow for decision making on whether a patient requires stronger ARBs such as telmisartan or if losartan is sufficient.

Overall, the literature suggests that transiently hypoxic tumour cells may be significant contributors to radiation resistance and metastatic growth. The major barriers to translation of research on transient hypoxia are the lack of a biomarker, poor fundamental understanding of transient hypoxia, highly varied pre-clinical modeling, a lack of connection with clinical data, and lack of interventions to stably modify transient hypoxia. This thesis work improves the fundamental understanding of transient hypoxia and provides data on the lifetime of transiently hypoxic tumour cells. This information may guide future pre-clinical modeling of transient hypoxia, resulting in further improvements in the ability to study this phenomenon and develop strong biomarkers for transiently hypoxic tumour cells. This thesis work also identifies specific potential tumour microenvironmental features associated with transient hypoxia, Col1 and

αSMA+ CAFs, which may be potential biomarkers for tumours that contain transient hypoxia that can be assessed in IHC of clinical samples. Further, we demonstrate that ARB treatment may reduce the development of transient hypoxia in solid tumours, providing a pre-clinical tool for stable reduction in the transient hypoxia population. If the connection between Col1 and αSMA+ CAFs with transient hypoxia is reproducible in further tumour lines, and the mechanism of ARB usage reducing Col1 and αSMA+ CAFs is reproducible in patients, then ARB usage also provides a connection between pre-clinical data modifying transient hypoxia with retrospective clinical data that may accelerate the translation of research on transient hypoxia.

References

1. Calzia E, Iványi Z, Radermacher P. Determinants of Blood Flow and Organ Perfusion. In: *Pinsky M.R., Payen D. (Eds) Functional Hemodynamic Monitoring. Update in Intensive Care and Emergency Medicine*. ; 2005:42. doi:10.1007/3-540-26900-2_3
2. Jain RK. Determinants of Tumor Blood Flow: A Review. *Cancer Res*. 1988;48(10):2641-2658.
3. Brody JS, Stemmler EJ, DuBois AB. Longitudinal distribution of vascular resistance in the pulmonary arteries, capillaries, and veins. *J Clin Invest*. 1968;47(4):783-799. doi:10.1172/JCI105773
4. Leunig M, Yuan F, Menger MD, et al. Angiogenesis, Microvascular Architecture, Microhemodynamics, and Interstitial Fluid Pressure during Early Growth of Human Adenocarcinoma LS174T in SCID Mice. *Cancer Res*. 1992;52(23):6553-6560.
5. Kut C, Mac Gabhann F, Popel AS. Where is VEGF in the body? A meta-analysis of VEGF distribution in cancer. *Br J Cancer*. 2007;97(7):978-985. doi:10.1038/sj.bjc.6603923
6. Liu SC, Alomran R, Chernikova SB, et al. Blockade of SDF-1 after irradiation inhibits tumor recurrences of autochthonous brain tumors in rats. *Neuro Oncol*. 2014;16(1):21-28. doi:10.1093/neuonc/not149
7. Brown JM. Vasculogenesis: A crucial player in the resistance of solid tumours to radiotherapy. *Br J Radiol*. 2014;87(1035). doi:10.1259/bjr.20130686
8. Kioi M, Vogel H, Schultz G, Hoffman RM, Harsh GR, Brown JM. Inhibition of vasculogenesis, but not angiogenesis, prevents the recurrence of glioblastoma after irradiation in mice. *J Clin Invest*. 2010;120(3):694-705. doi:10.1172/JCI40283
9. Bergers G, Hanahan D. Modes of resistance to anti-angiogenic therapy. *Nat Rev Cancer*. 2008;8(8):592-603.
10. Algire GH. Microscopic studies of the early growth of a transplantable melanoma of the mouse, using the transparent-chamber technique. *J Natl Cancer Inst*. 1943;4(1):13-20. doi:10.1093/jnci/4.1.13
11. Goodall CM, Sanders AG, Shubik P. Studies of vascular patterns in living tumors with a transparent chamber inserted in hamster cheek pouch. *J Natl Cancer Inst*. 1965;35(3):497-521. doi:10.1093/jnci/35.3.497

12. Peters W, Intaglletta M, Gross JF. Microcirculatory Studies in Rat Mammary Carcinoma. I. Transparent Chamber Method, Development of Microvasculature, and Pressures in Tumor Vessels. *JNCI J Natl Cancer Inst*. 1980;65(3):631-642. doi:10.1093/jnci/65.3.631
13. Vaupel P, Kallinowski F, Okunieff P. Blood Flow, Oxygen and Nutrient Supply, and Metabolic Microenvironment of Human Tumors: A Review. *Cancer Res*. 1989;49(23):6449-6465.
14. Konerding MA, Malkusch W, Klapthor B, et al. Evidence for characteristic vascular patterns in solid tumours: Quantitative studies using corrosion casts. *Br J Cancer*. 1999;80(5-6):724-732. doi:10.1038/sj.bjc.6690416
15. Hori K, Suzuki M, Abe I, Saito S, Sato H. New technique for measurement of microvascular pressure in normal and tumor vessels of rats. *Invasion and Metastasis*. Published online 1982.
16. Hori K, Suzuki M, Abe I, Saito S, Sato H. A micro-occlusion technique for measurement of the microvascular pressure in tumor and subcutis. *Gann*. 1983;74:122-127.
17. Wiig H. Microvascular pressures in DMBA-induced rat mammary tumours. *Scand J Clin Lab Invest*. 1982;42(2):165-171. doi:10.1080/00365518209168068
18. Pries AR, Höpfner M, Le Noble F, Dewhirst MW, Secomb TW. The shunt problem: Control of functional shunting in normal and tumour vasculature. *Nat Rev Cancer*. 2010;10(8):587-593. doi:10.1038/nrc2895
19. Carmeliet P, Jain RK. Molecular mechanisms and clinical applications of angiogenesis. *Nature*. 2011;473(7347):298-307. doi:10.1016/S0140-6736(01)91146-8
20. Winkler F, Kozin S V., Tong RT, et al. Kinetics of vascular normalization by VEGFR2 blockade governs brain tumor response to radiation. *Cancer Cell*. 2004;6(6):553-563. doi:10.1016/j.ccr.2004.10.011
21. Inai T, Mancuso M, Hashizume H, et al. Inhibition of vascular endothelial growth factor (VEGF) signaling in cancer causes loss of endothelial fenestrations, regression of tumor vessels, and appearance of basement membrane ghosts. *Am J Pathol*. 2004;165(1):35-52. doi:10.1016/S0002-9440(10)63273-7
22. Baluk P, Morikawa S, Haskell A, Mancuso M, McDonald DM. Abnormalities of Basement Membrane on Blood Vessels and Endothelial Sprouts in Tumors. *Am J Pathol*. 2003;163(5):1801-1815. doi:10.1016/S0002-9440(10)63540-7

23. Hashizume H, Baluk P, Morikawa S, et al. Openings between defective endothelial cells explain tumor vessel leakiness. *Am J Pathol*. 2000;156(4):1363-1380. doi:10.1016/S0002-9440(10)65006-7
24. Carmeliet P, Jain RK. Angiogenesis in cancer and other diseases. 2000;407:249-257. www.nature.com
25. Honkura N, Richards M, Laviña B, Sáinz-Jaspeado M, Betsholtz C, Claesson-Welsh L. Intravital imaging-based analysis tools for vessel identification and assessment of concurrent dynamic vascular events. *Nat Commun*. 2018;9:2746. doi:10.1038/s41467-018-04929-8
26. Tong RT, Boucher Y, Kozin S V., Winkler F, Hicklin DJ, Jain RK. Vascular normalization by vascular endothelial growth factor receptor 2 blockade induces a pressure gradient across the vasculature and improves drug penetration in tumors. *Cancer Res*. 2004;64(11):3731-3736. doi:10.1158/0008-5472.CAN-04-0074
27. Guo P, Fu BM. Effect of wall compliance and permeability on blood-flow rate in counter-current microvessels formed from anastomosis during tumor-induced angiogenesis. *J Biomech Eng*. 2012;134(4):19-26. doi:10.1115/1.4006338
28. Willett CG, Boucher Y, Di Tomaso E, et al. Direct evidence that the VEGF-specific antibody bevacizumab has antivascular effects in human rectal cancer. *Nat Med*. 2004;10(2):145-147. doi:10.1038/nm988
29. Lee CG, Heijn M, Di Tomaso E, et al. Anti-vascular endothelial growth factor treatment augments tumor radiation response under normoxic or hypoxic conditions. *Cancer Res*. 2000;60(19):5565-5570.
30. Boucher Y, Kirkwood JM, Opacic D, Desantis M, Jain RK. Interstitial Hypertension in Superficial Metastatic Melanomas in Humans. *Cancer Res*. 1991;51(24):6691-6694.
31. Padera TP, Kadambi A, Di Tomaso E, et al. Lymphatic metastasis in the absence of functional intratumor lymphatics. *Science (80-)*. 2002;296(5574):1883-1886. doi:10.1126/science.1071420
32. Leu AJ, Berk DA, Lymboussaki A, Alitalo K, Jain RK. Absence of functional lymphatics within a murine sarcoma: A molecular and functional evaluation. *Cancer Res*. 2000;60(16):4324-4327.
33. Secomb T, Pries A. Blood viscosity in microvessels: experiment and theory. *C R Phys*.

2013;14(6):470-478.

34. Fahraeus R, Lindqvist T. The viscosity of the blood in narrow capillary tubes. *Am J Physiol*. 1931;96:562-568.
35. Huisjes R, Bogdanova A, van Solinge WW, Schiffelers RM, Kaestner L, van Wijk R. Squeezing for life - Properties of red blood cell deformability. *Front Physiol*. 2018;9(JUN):1-22. doi:10.3389/fphys.2018.00656
36. Marie ES, Jain RK, Sevick EM. Effect of Red Blood Cell Rigidity on Tumor Blood Flow: Increase in Viscous Resistance during Hyperglycemia. *Cancer Res*. 1991;51(10):2727-2730.
37. Aifantis KE, Shrivastava S, Pelidou SH, Ngan AHW, Baloyannis SI. Relating the blood-thinning effect of pentoxifylline to the reduction in the elastic modulus of human red blood cells: An: in vivo study. *Biomater Sci*. 2019;7(6):2545-2551. doi:10.1039/c8bm01691g
38. Schubotz R, Mühlfellner O. The effect of pentoxifylline on erythrocyte deformability and on phosphatide fatty acid distribution in the erythrocyte membrane. *Curr Med Res Opin*. 1977;4(9):609-617. doi:10.1185/03007997709115279
39. Ehrly AM. The effect of pentoxifylline on the flow properties of human blood. *Curr Med Res Opin*. 1978;5(8):608-613. doi:10.1185/03007997809110195
40. Sevick EM, Jain RK. Viscous Resistance to Blood Flow in Solid Tumors: Effect of Hematocrit on Intratumor Blood Viscosity. *Cancer Res*. 1989;49(13):3513-3519.
41. Wagner H, Rhodes B, Sasaki Y, Ryan J. Studies of the circulation with radioactive microspheres. *Invest Radiol*. 1969;4:374-386.
42. Bergmann SR, Fox KAA, Rand AL. Quantification of regional myocardial blood flow in vivo with H215O. *Circulation*. 1984;70(4):724-733. doi:10.1161/01.CIR.70.4.724
43. Horton RW, Pedley TA, Meldrum BS. Regional cerebral blood flow in the rat as determined by particle distribution and by diffusible tracer. *Stroke*. 1980;11(1):39-44. doi:10.1161/01.STR.11.1.39
44. Heymann MA, Payne BD, Hoffman JIE, Rudolph AM. Blood flow measurements with radionuclide-labeled particles. *Prog Cardiovasc Dis*. 1977;20(1):55-79. doi:10.1016/S0033-0620(77)80005-4
45. Herrero P, Markham J, Bergmann S. Quantification of myocardial blood flow with H2150

and positron emission tomography: assessment and error analysis of a mathematical approach. *J Comput Assist Tomogr*. 1989;13(5):862-873.

46. Frackowiak RSJ, Lenzi GL, Jones T, Heather JD. Quantitative measurement of regional cerebral blood flow and oxygen metabolism in man using15O and positron emission tomography: Theory, procedure, and normal values. *J Comput Assist Tomogr*. 1980;4(6):727-736. doi:10.1097/00004728-198012000-00001
47. Berridge MS, Adler LP, Nelson AD, et al. Measurement of human cerebral blood flow with [15O]butanol and positron emission tomography. *J Cereb Blood Flow Metab*. 1991;11(5):707-715. doi:10.1038/jcbfm.1991.127
48. Schelbert HR, Schelbert HR, Phelps ME, et al. Nitrogen-13-Ammonia as an Indicator of Myocardial Blood Flow. *Circulation*. 1981;63(6):1259–1272. http://pt.wkhealth.com/pt/re/aha/pdfhandler.00003017-198106000-00007.pdf
49. Huang SC, Williams BA, Krivokapich J, Araujo L, Schelbert HR, Angeles L. Rabbit myocardial 82Rb kinetics and a compartmental model for blood flow estimation. *Am J Physiol*. 1989;256:H1156-H1164.
50. Bennewith KL, Durand RE. Drug-induced alterations in tumour perfusion yield increases in tumour cell radiosensitivity. *Br J Cancer*. 2001;85(10):1577-1584. doi:10.1054/bjoc.2001.2123
51. Arman R, Habib Z. PET versus SPECT: strength, limitations, and challenges. *Nucl Med Commun*. 2008;29:193-207.
52. Wadsworth BJ, Pan J, Dude I, et al. 2-18 F-Fluoroethanol Is a PET Reporter of Solid Tumor Perfusion. *J Nucl Med*. 2017;58:815-820. doi:10.2967/jnumed.116.183624
53. Maddahi J. Properties of an ideal PET perfusion tracer: New PET tracer cases and data. *J Nucl Cardiol*. 2012;19:30-37. doi:10.1007/s12350-011-9491-8
54. Angelidis G, Giamouzis G, Karagiannis G, et al. SPECT and PET in ischemic heart failure. *Heart Fail Rev*. 2017;22(2):243-261. doi:10.1007/s10741-017-9594-7
55. Lanz B, Poitry-Yamate C, Gruetter R. Image-derived input function from the vena cava for 18F-FDG PET studies in rats and mice. *J Nucl Med*. 2014;55(8):1380-1388. doi:10.2967/jnumed.113.127381
56. Zierler K. Equations for measuring blood flow by external monitoring of radioisotopes. *Circ Res*. 1965;16(4):309-321. doi:10.1161/CIRCRESAHA.119.315412

57. Bruehlmeier M, Roelcke U, Schubiger PA, Ametamey SM. Assessment of hypoxia and perfusion in human brain tumors using PET with 18F-fluoromisonidazole and 15O-H2O. *J Nucl Med*. 2004;45:1851-1859.
58. Lehtiö K, Oikonen V, Grönroos T, et al. Imaging of blood flow and hypoxia in head and neck cancer: Initial evaluation with [15O]H2O and [18F]Fluoroerythronitroimidazole PET. *J Nucl Med*. 2001;42(11):1643-1652.
59. Dunnwald LK, Gralow JR, Ellis GK, et al. Tumor metabolism and blood flow changes by positron emission tomography: Relation to survival in patients treated with neoadjuvant chemotherapy for locally advanced breast cancer. *J Clin Oncol*. 2008;26(27):4449-4457. doi:10.1200/JCO.2007.15.4385
60. Cal-González J, Herraiz JL, España S, Desco M, Vaquero JJ, Udías JM. Positron range effects in high resolution 3D pet imaging. *IEEE Nucl Sci Symp Conf Rec*. Published online 2009:2788-2791. doi:10.1109/NSSMIC.2009.5401950
61. Sinclair A., Morrison A., Young C., L P. *Canadian Medical Imaging Inventory*. CADTH; 2018. https://www.cadth.ca/imaginginventory
62. Moses W. Fundamental limits of spatial resolution in PET. *Nucl Instrum Methods Phys Res A*. 2011;648:S236-S240.
63. Trotter MJ, Chaplin DJ, Durand RE, Olive PL. The use of fluorescent probes to identify regions of transient perfusion in murine tumors. *Int J Radiat Oncol Biol Phys*. 1989;16(4):931-934. doi:10.1016/0360-3016(89)90889-4
64. Chaplin DJ, Olive PL, Durand RE. Intermittent Blood Flow in a Murine Tumor: Radiobiological Effects. *Cancer Res*. 1987;47(2):597-601.
65. Chaplin DJ, Horsman MR, Trotter MJ. Effect of nicotinamide on the microregional heterogeneity of oxygen delivery within a murine tumor. *J Natl Cancer Inst*. 1990;82(8):672-676. doi:10.1093/jnci/82.8.672
66. Trotter MJ, Chaplin DJ, Olive PL. Use of a carbocyanine dye as a marker of functional vasculature in murine tumours. *Br J Cancer*. 1989;59(5):706-709. doi:10.1038/bjc.1989.148
67. Durand RE, Aquino-Parsons C. Clinical relevance of intermittent tumour blood flow. *Acta Oncol (Madr)*. 2001;40(8):929-936. doi:10.1080/02841860152708206
68. Durand RE, Aquino-Parsons C. Non-constant tumour blood flow: Implications for

therapy. *Acta Oncol (Madr)*. 2001;40(7):862-869. doi:10.1080/02841860152703508

69. Minchinton AI, Durand RE, Chaplin DJ. Intermittent blood flow in the KHT sarcoma-flow cytometry studies using hoechst 33342. *Br J Cancer*. 1990;62(2):195-200. doi:10.1038/bjc.1990.259
70. Grazul-Bilska AT, Borowicz PP, Reynolds LP, Redmer DA. Vascular perfusion with fluorescent labeled lectin to study ovarian functions. *Acta Histochem*. 2013;115(8):893-898. doi:10.1016/j.acthis.2013.03.006
71. Durand RE, Lepard NE. Contribution of transient blood flow to tumour hypoxia in mice. *Acta Oncol (Madr)*. 1995;34(3):317-323. doi:10.3109/02841869509093982
72. Kalluri R. The biology and function of fibroblasts in cancer. *Nat Rev Cancer*. 2016;16(9):582-598. doi:10.1038/nrc.2016.73
73. Sahai E, Astsaturov I, Cukierman E, et al. A framework for advancing our understanding of cancer-associated fibroblasts. *Nat Rev Cancer*. 2020;20(March). doi:10.1038/s41568-019-0238-1
74. Denu R, Nemcek S, Bloom D, et al. Fibroblasts and mesenchymal stromal/stem cells are phenotypcially indistinguishable. *Acta Haematol*. 2016;136(2):85-97.
75. Peng Y, Lei Z, Yang P, et al. Direct contacts with colon cancer cells regulate the differentiation of bone marrow mesenchymal stem cells into tumor associated fibroblasts. *Biochem Biophys Res Commun*. 2014;451(1):68-73. doi:10.1016/j.bbrc.2014.07.074
76. Shangguan L, Ti X, Krause U, et al. Inhibition of TGF-β/Smad signaling by BAMBI blocks differentiation of human mesenchymal stem cells to carcinoma-associated fibroblasts and abolishes their protumor effects. *Stem Cells*. 2012;30(12):2810-2819. doi:10.1002/stem.1251
77. Sha M, Jeong S, Qiu B jun, et al. Isolation of cancer-associated fibroblasts and its promotion to the progression of intrahepatic cholangiocarcinoma. *Cancer Med*. 2018;7(9):4665-4677. doi:10.1002/cam4.1704
78. Schmidt-Hansen B, Klingelhöfer J, Grum-Schwensen B, et al. Functional significance of metastasis-inducing S100A4(Mts1) in tumor-stroma interplay. *J Biol Chem*. 2004;279(23):24498-24504. doi:10.1074/jbc.M400441200
79. O'Connell JT, Sugimoto H, Cooke VG, et al. VEGF-A and Tenascin-C produced by S100A4 + stromal cells are important for metastatic colonization. *Proc Natl Acad Sci U S*

A. 2011;108(38):16002-16007. doi:10.1073/pnas.1109493108

80. Grum-Schwensen B, Klingelhofer J, Berg CH, et al. Suppression of tumor development and metastasis formation in mice lacking the S100A4(mts1) gene. *Cancer Res*. 2005;65(9):3772-3780. doi:10.1158/0008-5472.CAN-04-4510
81. Öhlund D, Handly-Santana A, Biffi G, et al. Distinct populations of inflammatory fibroblasts and myofibroblasts in pancreatic cancer. *J Exp Med*. 2017;214(3):579-596. doi:10.1084/jem.20162024
82. Costa A, Kieffer Y, Scholer-Dahirel A, et al. Fibroblast Heterogeneity and Immunosuppressive Environment in Human Breast Cancer. *Cancer Cell*. 2018;33(3):463-479.e10. doi:10.1016/j.ccell.2018.01.011
83. Pelon F, Bourachot B, Kieffer Y, et al. Cancer-associated fibroblast heterogeneity in axillary lymph nodes drives metastases in breast cancer through complementary mechanisms. *Nat Commun*. 2020;11(1). doi:10.1038/s41467-019-14134-w
84. Paunescu V, Bojin FM, Tatu CA, et al. Tumour-associated fibroblasts and mesenchymal stem cells: More similarities than differences. *J Cell Mol Med*. 2011;15(3):635-646. doi:10.1111/j.1582-4934.2010.01044.x
85. Chauhan VP, Martin JD, Liu H, et al. Angiotensin inhibition enhances drug delivery and potentiates chemotherapy by decompressing tumour blood vessels. *Nat Commun*. 2013;4:2516. doi:10.1038/ncomms3516
86. Diop-Frimpong B, Chauhan VP, Krane S, Boucher Y, Jain RK. Losartan inhibits collagen I synthesis and improves the distribution and efficacy of nanotherapeutics in tumors. *Proc Natl Acad Sci U S A*. 2011;108(7):2909-2914. doi:10.1073/pnas.1018892108
87. Chauhan VP, Chen IX, Tong R, et al. Reprogramming the microenvironment with tumorselective angiotensin blockers enhances cancer immunotherapy. *Proc Natl Acad Sci U S A*. 2019;166(22):10674-10680. doi:10.1073/pnas.1819889116
88. Zhao Y, Cao J, Melamed A, et al. Losartan treatment enhances chemotherapy efficacy and reduces ascites in ovarian cancer models by normalizing the tumor stroma. *Proc Natl Acad Sci U S A*. 2019;116(6):2210-2219. doi:10.1073/pnas.1818357116
89. Kumar V, Boucher Y, Liu H, et al. Noninvasive assessment of losartan-induced increase in functional microvasculature and drug delivery in pancreatic ductal adenocarcinoma. *Transl Oncol*. 2016;9(5):431-437. doi:10.1016/j.tranon.2016.07.004

90. Godugu C, Patel A, Doddapaneni R, Marepally S, Jackson T, Singh M. Inhalation delivery of telmisartan enhances intratumoural distribution of nanoparticles in lung cancer models. *J Control Release*. 2013;28(1):86-95. doi:10.1038/jid.2014.371
91. Ozdemir B, Pentcheva-Hoang T, Carstens J, et al. Depletion of carcinoma-associated fibroblasts and fibrosis induces immunosuppression and accelerates pancreas cancer with diminished survival. *Cancer Cell*. 2014;25(6):719-734.
92. Santos A, Jung J, Aziz N, Kissil J, Puré E. Targeting fibroblast activation protein inhibits tumor stromagenesis and growth in mice. *J Clin Invest*. 2009;119(12):3613-3625. doi:10.1172/JCI38988DS1
93. Brennen WN, Rosen DM, Wang H, Isaacs JT, Denmeade SR. Targeting carcinoma-associated fibroblasts within the tumor stroma with a fibroblast activation protein-activated prodrug. *J Natl Cancer Inst*. 2012;104(17):1320-1334. doi:10.1093/jnci/djs336
94. Sava P, Ramanathan A, Dobronyi A, et al. Human pericytes adopt myofibroblast properties in the microenvironment of the IPF lung. *JCI Insight*. 2017;2(24):1-13. doi:10.1172/jci.insight.96352
95. Gabasa M, Ikemori R, Hilberg F, Reguart N, Alcaraz J. Nintedanib selectively inhibits the activation and tumour-promoting effects of fibroblasts from lung adenocarcinoma patients. *Br J Cancer*. 2017;117(8):1128-1138. doi:10.1038/bjc.2017.270
96. Chen IX, Chauhan VP, Posada J, et al. Blocking CXCR4 alleviates desmoplasia, increases T-lymphocyte infiltration, and improves immunotherapy in metastatic breast cancer. *Proc Natl Acad Sci U S A*. 2019;116(10):4558-4566. doi:10.1073/pnas.1815515116
97. Netti PA, Berk DA, Swartz MA, Grodzinsky AJ, Jain RK. Role of extracellular matrix assembly in interstitial transport in solid tumors. *Cancer Res*. 2000;60(9):2497-2503.
98. Nieskoski MD, Marra K, Gunn JR, et al. Collagen Complexity Spatially Defines Microregions of Total Tissue Pressure in Pancreatic Cancer. *Sci Rep*. 2017;7(1):1-12. doi:10.1038/s41598-017-10671-w
99. Liu L, Liu L, Yao HH, Zhu ZQ, Ning ZL, Huang Q. Stromal myofibroblasts are associated with poor prognosis in solid cancers: A meta-analysis of published studies. *PLoS One*. 2016;11(7):1-16. doi:10.1371/journal.pone.0159947
100. Marsh D, Suchak K, Moutasim KA, et al. Stromal features are predictive of disease mortality in oral cancer patients. *J Pathol*. 2011;223(4):470-481. doi:10.1002/path.2830

101. Paulsson J, Micke P. Prognostic relevance of cancer-associated fibroblasts in human cancer. *Semin Cancer Biol*. 2014;25:61-68. doi:10.1016/j.semcancer.2014.02.006
102. Haave H, Gulati S, Brekke J, Lybak S, Vintermyr OK, Aarstad HJ. Tumor stromal desmoplasia and inflammatory response uniquely predict survival with and without stratification for HPV tumor infection in OPSCC patients. *Acta Otolaryngol*. 2018;138(11):1035-1042. doi:10.1080/00016489.2018.1497809
103. Gray LH, Conger AD, Ebert M, Hornsey S, Scott OC. The concentration of oxygen dissolved in tissues at the time of irradiation as a factor in radiotherapy. *Br J Radiol*. Published online 1953. doi:10.1259/0007-1285-26-312-638
104. Michael BD, Adams GE, Hewitt HB, Jones WBG, Watts ME. A Posteffect of Oxygen in Irradiated Bacteria: A Submillisecond Fast Mixing Study. *Radiat Res*. 1973;54(2):239. doi:10.2307/3573702
105. Michael B, Davies S, Held K. Ultrafast chemical repair of DNA single and double stran break precursors in irradiated V79 cells. In: *Mechanisms of DNA Damage and Repair*. ; 1986:89-100. doi:10.1007/BF00352220
106. Vordermark D, Horsman M. *Hypoxia as a Biomarker and for Personalized Radiation Oncology*. Vol 198.; 2016. doi:10.1007/978-3-662-49651-0
107. Walsh JC, Lebedev A, Aten E, Madsen K, Marciano L, Kolb HC. The clinical importance of assessing tumor hypoxia: Relationship of tumor hypoxia to prognosis and therapeutic opportunities. *Antioxidants Redox Signal*. 2014;21(10):1516-1554. doi:10.1089/ars.2013.5378
108. Janssens GO, Rademakers SE, Terhaard CH, et al. Accelerated radiotherapy with carbogen and nicotinamide for laryngeal cancer: Results of a phase III randomized trial. *J Clin Oncol*. 2012;30(15):1777-1783. doi:10.1200/JCO.2011.35.9315
109. Thomlinson RH, Gray LH. The histological structure of some human lung cancers and the possible implications for radiotherapy. *Br J Cancer*. 1955;9(4):539-549. doi:10.1038/bjc.1955.55
110. Tannock IF. Oxgen diffusion and the distribution of cellular radiosensitivity in tumours. *Br J Radiol*. 1972;45:515-524.
111. Tannock IF. The relation between cell proliferation and the vascular system in a transplanted mouse mammary tumour. *Br J Cancer*. 1968;22(2):258-273.

doi:10.1038/bjc.1968.34

112. Hirst DG, Hirst VK, Joiner B, Prise V, Shaffi KM. Changes in tumour morphology with alterations in oxygen availability: Further evidence for oxygen as a limiting substrate. *Br J Cancer*. 1991;64(1):54-58. doi:10.1038/bjc.1991.238
113. Hirst DG, Denekamp J, Hobson B. Proliferation kinetics of endothelial and tumour cells in three mouse mammary carcinomas. *Cell Prolif*. 1982;15(3):251-261. doi:10.1111/j.1365-2184.1982.tb01044.x
114. Olive PL, Vikse CAA, Trotter MJ. Tissue Oxygenation Manipulation and Tumor Blood Flow. *Int J Radiat Oncol Biol Phys*. 1992;22:397-402.
115. Vukovic V, Haugland HK, Morrison AJ, et al. Hypoxia-inducible factor-1α is an intrinsic marker for hypoxia in cervical cancer xenografts. *Cancer Res*. 2001;61(20):7394-7398.
116. Chaplin DJ, Hill SA. Temporal heterogeneity in microregional erythrocyte flux in experimental solid tumours. *Br J Cancer*. 1995;71(6):1210-1213. doi:10.1038/bjc.1995.235
117. Pigott KH, Hill SA, Chaplin DJ, Saunders MI. Microregional fluctuations in perfusion within human tumours detected using laser Doppler flowmetry. *Radiother Oncol*. 1996;40:45-50. doi:10.1016/0167-8140(96)01730-6
118. Braun RD, Lanzen JL, Dewhirst MW. Fourier analysis of fluctuations of oxygen tension and blood flow in R3230Ac tumors and muscle in rats. *Am J Physiol Circ Physiol*. 1999;277(46):H551-H568. doi:10.1152/ajpheart.1999.277.2.h551
119. Kimura H, Braun RD, Ong ET, et al. Fluctuations in red cell flux in tumor microvessels can lead to transient hypoxia and reoxygenation in tumor parenchyma. *Cancer Res*. 1996;56(23):5522-5528.
120. Lanzen J, Braun RD, Klitzman B, Brizel D, Secomb TW, Dewhirst MW. Direct demonstration of instabilities in oxygen concentrations within the extravascular compartment of an experimental tumor. *Cancer Res*. 2006;66(4):2219-2223. doi:10.1158/0008-5472.CAN-03-2958
121. Brurberg KG, Skogmo HK, Graff BA, Olsen DR, Rofstad EK. Fluctuations in pO2 in poorly and well-oxygenated spontaneous canine tumors before and during fractionated radiation therapy. *Radiother Oncol*. 2005;77(2):220-226. doi:10.1016/j.radonc.2005.09.009

122. Ellingsen C, Øvrebø KM, Galappathi K, Mathiesen B, Rofstad EK. pO 2 fluctuation pattern and cycling hypoxia in human cervical carcinoma and melanoma xenografts. *Int J Radiat Oncol Biol Phys*. 2012;83(4):1317-1323. doi:10.1016/j.ijrobp.2011.09.037
123. Brurberg KG, Graff BA, Olsen DR, Rofstad EK. Tumor-line specific pO2 fluctuations in human melanoma xenografts. *Int J Radiat Oncol Biol Phys*. 2004;58(2):403-409. doi:10.1016/j.ijrobp.2003.09.049
124. Brurberg KG, Graff BA, Rofstad EK. Temporal heterogeneity in oxygen tension in human melanoma xenografts. *Br J Cancer*. 2003;89(2):350-356. doi:10.1038/sj.bjc.6601047
125. Cárdenas-Navia LI, Yu D, Braun RD, Brizel DM, Secomb TW, Dewhirst MW. Tumor-dependent kinetics of partial pressure of oxygen fluctuations during air and oxygen breathing. *Cancer Res*. 2004;64(17):6010-6017. doi:10.1158/0008-5472.CAN-03-0947
126. Sham E, Durand RE. Cell kinetics and repopulation parameters of irradiated xenograft tumours in SCID mice: Comparison of two dose-fractionation regimens. *Eur J Cancer*. 1999;35(5):850-858. doi:10.1016/S0959-8049(99)00019-2
127. Durand RE, Raleigh JA. Identification of nonproliferating but viable hypoxic tumor cells in vivo. *Cancer Res*. 1998;58(16):3547-3550.
128. Durand RE, Sham E. The lifetime of hypoxic human tumor cells. *Int J Radiat Oncol Biol Phys*. 1998;42(4):711-715. doi:10.1016/S0360-3016(98)00305-8
129. Ljungkvist ASE, Bussink J, Kaanders JHAM, et al. Hypoxic cell turnover in different solid tumor lines. *Int J Radiat Oncol Biol Phys*. 2005;62(4):1157-1168. doi:10.1016/j.ijrobp.2005.03.049
130. Hall E, Giaccia A. *Radiobiology for the Radiologist*. 7th ed. Wolters KluwerLippincott Williams & Wilkins; 2012.
131. Oh J, Magnuson A, Benoist C, Pittet MJ, Weissleder R. Age-related tumor growth in mice is related to integrin α 4 in CD8+ T cells. *JCI insight*. 2018;3(21):1-13. doi:10.1172/jci.insight.122961
132. Harada H, Inoue M, Itasaka S, et al. Cancer cells that survive radiation therapy acquire HIF-1 activity and translocate towards tumour blood vessels. *Nat Commun*. 2012;3:710-783. doi:10.1038/ncomms1786
133. Höckel M, Schlenger K, Aral B, Mitze M, Schäffer U, Vaupel P. Association between tumor hypoxia and malignant progression in advanced cancer of the uterine cervix.

Cancer Res. 1996;56(19):4509-4515. doi:10.1056/NEJM199604183341606

134. Palcic B, Skarsgard L. Reduced Oxygen Enhancement Ratio at Low Doses of Ionizing Radiation. 1984;100:328-339.
135. Commission CNS. Natural Background Radiation. doi:10.1136/bmj.2.5041.411
136. Donnelly EH, Nemhauser JB, Smith JM, et al. Acute radiation syndrome: Assessment and management. *South Med J*. 2010;103(6):541-546. doi:10.1097/SMJ.0b013e3181ddd571
137. Munro TR. The Relative Radiosensitivity of the Nucleus and Cytoplasm of Chinese Hamster Fibroblasts. *Radiat Res*. 1970;42(3):451. doi:10.2307/3572962
138. von Sonntag C. The chemistry of free radical-mediated DNA damage. In: *Physical and Chemical Mechanisms in Molecular Radiation Biology*. ; 1991:287-324.
139. Huels MA, Boudaïffa B, Cloutier P, Hunting D, Sanche L. Single, double, and multiple double strand breaks induced in DNA by 3-100 eV electrons. *J Am Chem Soc*. 2003;125(15):4467-4477. doi:10.1021/ja029527x
140. Pimblott SM, LaVerne JA. Production of low-energy electrons by ionizing radiation. *Radiat Phys Chem*. 2007;76(8-9):1244-1247. doi:10.1016/j.radphyschem.2007.02.012
141. Prütz WA. "chemical repair" in irradiated DNA solutions containing thiols and/or disulphides. Further evidence for disulphide radical anions acting as electron donors. *Int J Radiat Biol*. 1989;56(1):21-33. doi:10.1080/09553008914551151
142. Sunada S, Hirakawa H, Fujimori A, Uesaka M, Okayasu R. Oxygen Enhancement Ratio in Radiation-Induced Initial DSBs by an Optimized Flow Cytometry-based Gamma-H2AX Analysis in A549 Human Cancer Cells. *Radiat Res*. 2017;188(5):671-674. doi:10.1667/rr14824.1
143. Olive PL, Banáth JP. Phosphorylation of histone H2AX as a measure of radiosensitivity. *Int J Radiat Oncol Biol Phys*. 2004;58(2):331-335. doi:10.1016/j.ijrobp.2003.09.028
144. Bristow RG, Hill RP. Hypoxia and metabolism: Hypoxia, DNA repair and genetic instability. *Nat Rev Cancer*. 2008;8(3):180-192. doi:10.1038/nrc2344
145. Kumareswaran R, Ludkovski O, Meng A, Sykes J, Pintilie M, Bristow RG. Chronic hypoxia compromises repair of DNA double-strand breaks to drive genetic instability. *J Cell Sci*. 2012;125(1):189-199. doi:10.1242/jcs.092262
146. Frankenberg-Schwager M, Frankenberg D, Harbich R. Different Oxygen Enhancement Ratios for Induced and Unrejoined DNA Double-Strand Breaks in Eukaryotic Cells.

Radiat Res. 1991;128(3):243. doi:10.2307/3578046

147. Zhang H, Koch CJ, Wallen CA, Wheeler KT. Radiation-Induced DNA Damage in Tumors and Normal Tissues. III. Oxygen Dependence of the Formation of Strand Breaks and DNA-Protein Crosslinks. *Radiat Res*. 1995;142(2):163. doi:10.2307/3579024
148. Chapman JD, Dugle DL, Reuvers AP, Meeker BE, Borsa J. Studies on the radiosensitizing effect of oxygen in chinese hamster cells. *Int J Radiat Biol*. 1974;26(4):383-389. doi:10.1080/09553007414551361
149. Olive PL, Wlodek D, Banath JP. DNA Double-Strand Breaks Measured in Individual Cells Subjected to Gel Electrophoresis. *Cancer Res*. 1991;51(17):4671-4676.
150. Núñez MI, McMillan TJ, Valenzuela MT, Ruiz De Almodóvar JM, Pedraza V. Relationship between DNA damage, rejoining and cell killing by radiation in mammalian cells. *Radiother Oncol*. 1996;39(2):155-165. doi:10.1016/0167-8140(96)01732-X
151. Ng CE, Mazaheri K, Payant C, Raaphorst GP. Evaluation of cell survival, DNA double strand breaks, and DNA synthesis during concurrent camptothecin and X-radiation treatments. *Int J Cancer*. 2001;96(5):277-285. doi:10.1002/ijc.1031
152. Tsai JY, Chen FH, Hsieh TY, Hsiao YY. Effects of indirect actions and oxygen on relative biological effectiveness: Estimate of DSB induction and conversion induced by gamma rays and helium ions. *J Radiat Res*. 2015;56(4):691-699. doi:10.1093/jrr/rrv025
153. Mori R, Matsuya Y, Yoshii Y, Date H. Estimation of the radiation-induced DNA double-strand breaks number by considering cell cycle and absorbed dose per cell nucleus. *J Radiat Res*. 2018;59(3):253-260. doi:10.1093/jrr/rrx097
154. Neumaier T, Swenson J, Pham C, et al. Evidence for formation of DNA repair centers and dose-response nonlinearity in human cells. *Proc Natl Acad Sci U S A*. 2012;109(2):443-448. doi:10.1073/pnas.1117849108
155. Tommasino F, Friedrich T, Jakob B, Meyer B, Durante M, Scholz M. Induction and processing of the radiation-induced gamma-H2AX signal and its link to the underlying pattern of DSB: A combined experimental and modelling study. *PLoS One*. 2015;10(6):1-25. doi:10.1371/journal.pone.0129416
156. Stenerlöw B, Karlsson KH, Cooper B, Rydberg B. Measurement of Prompt DNA Double-Strand Breaks in Mammalian Cells without Including Heat-Labile Sites: Results for Cells Deficient in Nonhomologous End Joining. *Radiat Res*. 2003;159(4):502-510.

doi:10.1667/0033-7587(2003)159[0502:mopdds]2.0.co;2

157. Iliakis G, Metzger L, Muschel RJ, McKenna WG. Induction and Repair of DNA Double Strand Breaks in Radiation-resistant Cells Obtained by Transformation of Primary Rat Embryo Cells with the Oncogenes H-ras and v-myc. *Cancer Res*. 1990;50(20):6575-6579. doi:10.1016/0360-3016(90)90783-g

158. Cornforth M, Bedford J. A Quantitative Comparison of Potentially Lethal Damage Repair and the Rejoining of Interphase Chromosome Breaks in Low Passage Normal Human Fibroblasts. *Radiat Res*. 1987;111(3):385-405.

159. Koch CJ. *The Effect of Oxygen on the Repair of Radiation Damage by Cells and Tissues*. Vol 8.; 1979. doi:10.1016/b978-0-12-035408-5.50011-3

160. Elkind M, Swain R, Alescio T. Oxygen, nitrogen, recovery and radiation therapy. In: *Cellular Radiation Biology.* MD Williams & Wilkins; 1965:442-461.

161. Wenzl T, Wilkens JJ. Modelling of the oxygen enhancement ratio for ion beam radiation therapy. *Phys Med Biol*. 2011;56(11):3251-3268. doi:10.1088/0031-9155/56/11/006

162. Meesungnoen J, Jay-Gerin J-P. High-LET Ion Radiolysis of Water: Oxygen Production in Tracks. *Radiat Res*. 2009;171(3):379-386. doi:10.1667/rr1468.1

163. Braun RD, Lanzen JL, Snyder SA, Dewhirst MW. Comparison of tumor and normal tissue oxygen tension measurements using OxyLite or microelectrodes in rodents. *Am J Physiol - Hear Circ Physiol*. 2001;280(6 49-6):2533-2544. doi:10.1152/ajpheart.2001.280.6.h2533

164. Turaka A, Buyyounouski MK, Hanlon AL, Horwitz EM, Greenberg RE, Movsas B. Hypoxic prostate/muscle Po 2 ratio predicts for outcome in patients with localized prostate cancer: Long-term results. *Int J Radiat Oncol Biol Phys*. 2012;82(3):e433-e439. doi:10.1016/j.ijrobp.2011.05.037

165. Brizel DM, Sibley GS, Prosnitz LR, Scher RL, Dewhirst MW. Tumor hypoxia adversely affects the prognosis of carcinoma of the head and neck. *Int J Radiat Oncol Biol Phys*. 1997;38(2):285-289. doi:10.1016/S0360-3016(97)00101-6

166. Brizel DM, Scully SP, Harrelson JM, et al. Tumor oxygenation predicts for the likelihood of distant metastases in human soft tissue sarcoma. *Cancer Res*. 1996;56(5):941-943.

167. van Putten LM, Kallman RF. Oxygenation status of a transplantable tumor during fractionated radiation therapy. *J Natl Cancer Inst*. 1968;40(3):441-451.

doi:10.1093/jnci/40.3.441

168. Bentzen SM, Grau C. Direct estimation of the fraction of hypoxic cells from tumour-control data obtained under aerobic and clamped conditions. *Int J Radiat Biol*. 1991;59(6):1435-1440. doi:10.1080/09553009114551281

169. Song CW, Griffin RJ, Lee Y-J, et al. Reoxygenation and Repopulation of Tumor Cells after Ablative Hypofractionated Radiotherapy (SBRT and SRS) in Murine Tumors. *Radiat Res*. 2019;192(2):159-168. doi:10.1667/rr15346.1

170. Garcia-Barros M, Paris F, Cordon-Cardo C, et al. Tumor response to radiotherapy regulated by endothelial cell apoptosis. *Science (80-)*. 2003;300(5622):1155-1159.

171. Lee I, Levitt SH, Song CW. Improved tumour oxygenation and radiosensitization by combination with nicotinamide and pentoxifylline. *Int J Radiat Biol*. 1993;64(2):237-244. doi:10.1080/09553009314551351

172. Horsman MR, Khalil AA, Nordsmark M, Grau C, Overgaard J. Measurement of pO2 in a murine tumour and its correlation with hypoxic fraction. *Adv Exp Med Biol*. 1994;345:493-499. doi:10.1007/978-1-4615-2468-7_66

173. Horsman MR, Khalil AA, Nordsmark M, Grau C, Overgaard J. Relationship between radiobiological hypoxia and direct estimates of tumour oxygenation in a mouse tumour model. *Radiother Oncol*. Published online 1993. doi:10.1016/0167-8140(93)90188-E

174. Wouters B, Brown J. Cells at intermediate oxygen levels can be more important than the “hypoxic fraction” in determining tumor response to fractionated radiotherapy. *Radiat Res*. 1997;147(5):541-550.

175. Raleigh JA, Koch CJ. Importance of thiols in the reductive binding of 2-nitroimidazoles to macromolecules. *Biochem Pharmacol*. Published online 1990. doi:10.1016/0006-2952(90)90086-Z

176. Arteel GE, Thurman RG, Raleigh JA. Reductive metabolism of the hypoxia marker pimonidazole is regulated by oxygen tension independent of the pyridine nucleotide redox state. *Eur J Biochem*. 1998;253(3):743-750. doi:10.1046/j.1432-1327.1998.2530743.x

177. Koch CJ, Evans SM, Lord EM. Oxygen dependence of cellular uptake of EF5 [2-(2-nitro-1H-imidazol-1-yl)-N-(2, 2, 3, 3, 3-pentafluoropropyl)a cet amide]: Analysis of drug adducts by fluorescent antibodies vs bound radioactivity. *Br J Cancer*. 1995;72(4):869-874. doi:10.1038/bjc.1995.426

178. Koch CJ. Measurement of absolute oxygen levels in cells and tissues using oxygen sensors and 2-nitroimidazole EF5. *METHODS Enzymol*. 2002;352:3-31.
179. Mahy P, De Bast M, Gallez B, et al. In vivo colocalization of 2-nitroimidazole EF5 fluorescence intensity and electron paramagnetic resonance oximetry in mouse tumors. *Radiother Oncol*. 2003;67:53-61. doi:10.1016/S0167-8140(03)00028-8
180. Kavanagh MC, Tsang V, Chow S, et al. A comparison in individual murine tumors of techniques for measuring oxygen levels. *Int J Radiat Oncol Biol Phys*. 1999;44(5):1137-1146. doi:10.1016/S0360-3016(99)00104-2
181. Evans SM, Jenkins WT, Joiner B, Lord EM, Koch CJ. 2-Nitroimidazole (EF5) binding predicts radiation resistance in individual 9L s.c. tumors. *Cancer Res*. 1996;56(2):405-411.
182. Arteel GE, Thurman RG, Yates JM, Raleigh JA. Evidence that hypoxia markers detect oxygen gradients in liver: Pimonidazole and retrograde perfusion of rat liver. *Br J Cancer*. 1995;72(4):889-895. doi:10.1038/bjc.1995.429
183. Gross MW, Karbach U, Groebe K, Franko AJ, Mueller-Klieser W. Calibration of misonidazole labeling by simultaneous measurement of oxygen tension and labeling density in multicellular spheroids. *Int J Cancer*. Published online 1995. doi:10.1002/ijc.2910610422
184. Raleigh JA, Chou S-C, Arteel GE, Horsman MR. Comparisons among Pimonidazole Binding, Oxygen Electrode Measurements, and Radiation Response in C3H Mouse Tumors. *Radiat Res*. 2006;151(5):580. doi:10.2307/3580034
185. Kim IH, Lemmon MJ, Brown JM. The Influence of Irradiation of the Tumor Bed on Tumor Hypoxia: Measurements by Radiation Response, Oxygen Electrodes, and Nitroimidazole Binding. *Radiat Res*. 1993;135(3):411. doi:10.2307/3578883
186. Rasey JS, Koh WJ, Evans ML, Peterson LM, Lewellen TK. Quantifying regional hypoxia in human tumours with positron emission tomography of [18F]fluoromisonidazole: a Pretherapy Study of 37 Patients. *Int J Radiat Oncol Biol Phys*. 1996;36(2):417-428.
187. Komar G, Seppänen M, Eskola O, et al. 18F-EF5: A new PET tracer for imaging hypoxia in head and neck cancer. *J Nucl Med*. 2008;49(12):1944-1951. doi:10.2967/jnumed.108.053785
188. Silvoniemi A, Suilamo S, Laitinen T, et al. Repeatability of tumour hypoxia imaging

using [18F]EF5 PET/CT in head and neck cancer. *Eur J Nucl Med Mol Imaging*. 2018;45(2):161-169. doi:10.1007/s00259-017-3857-3

189. Komar G, Lehtiö K, Seppänen M, et al. Prognostic value of tumour blood flow, [18F]EF5 and [18F]FDG PET/CT imaging in patients with head and neck cancer treated with radiochemotherapy. *Eur J Nucl Med Mol Imaging*. 2014;41(11):2042-2050. doi:10.1007/s00259-014-2818-3
190. Chitneni SK, Bida GT, Yuan H, et al. 18F-EF5 PET imaging as an early response biomarker for the hypoxia-activated prodrug SN30000 combined with radiation treatment in a non-small cell lung cancer xenograft model. *J Nucl Med*. 2013;54(8):1339-1346. doi:10.2967/jnumed.112.116293
191. Ali R, Apte S, Vilalta M, et al. 18F-EF5 PET is predictive of response to fractionated radiotherapy in preclinical tumor models. *PLoS One*. 2015;10(10):1-14. doi:10.1371/journal.pone.0139425
192. Sanduleanu S, van der Wiel AMA, Lieverse RIY, et al. Hypoxia pet imaging with [18f]-hx4—a promising next-generation tracer. *Cancers (Basel)*. 2020;12(5). doi:10.3390/cancers12051322
193. Smith TG, Talbot NP. Prolyl Hydroxylases and Therapeutics. *Antioxidants Redox Signal*. 2010;12(4):431-433. doi:10.1089/ars.2009.2901
194. Sim J, Cowburn AS, Palazon A, et al. The Factor Inhibiting HIF Asparaginyl Hydroxylase Regulates Oxidative Metabolism and Accelerates Metabolic Adaptation to Hypoxia. *Cell Metab*. 2018;27(4):898-913.e7. doi:10.1016/j.cmet.2018.02.020
195. Semenza GL. Hypoxia-Inducible Factor 1 (HIF-1) Pathway. *Sci STKE*. 2007;(407):cm8.
196. Bracken CP, Fedele AO, Linke S, et al. Cell-specific regulation of hypoxia-inducible factor (HIF)-1α and HIF-2α stabilization and transactivation in a graded oxygen environment. *J Biol Chem*. 2006;281(32):22575-22585. doi:10.1074/jbc.M600288200
197. Prabhakar NR, Semenza GL. Oxygen sensing and homeostasis. *Physiology*. 2015;30(5):340-348. doi:10.1152/physiol.00022.2015
198. Sobhanifar S, Aquino-Parsons C, Stanbridge EJ, Olive P. Reduced expression of hypoxia-inducible factor-1α in perinecrotic regions of solid tumors. *Cancer Res*. 2005;65(16):7259-7266. doi:10.1158/0008-5472.CAN-04-4480
199. Nordsmark M, Bentzen SM, Rudat V, et al. Prognostic value of tumor oxygenation in 397

head and neck tumors after primary radiation therapy. An international multi-center study. *Radiother Oncol*. 2005;77(1):18-24. doi:10.1016/j.radonc.2005.06.038

200. Mortensen LS, Johansen J, Kallehauge J, et al. FAZA PET/CT hypoxia imaging in patients with squamous cell carcinoma of the head and neck treated with radiotherapy: Results from the DAHANCA 24 trial. *Radiother Oncol*. 2012;105(1):14-20. doi:10.1016/j.radonc.2012.09.015
201. Toustrup K, Sørensen BS, Nordsmark M, et al. Development of a hypoxia gene expression classifier with predictive impact for hypoxic modification of radiotherapy in head and neck cancer. *Cancer Res*. 2011;71(17):5923-5931. doi:10.1158/0008-5472.CAN-11-1182
202. Siemann DW, Horsman MR. Modulation of the tumor vasculature and oxygenation to improve therapy. *Pharmacol Ther*. 2015;153:107-124. doi:10.1016/j.pharmthera.2015.06.006
203. Koritzinsky M. Metformin: A novel biological modifier of tumor response to radiation therapy. *Int J Radiat Oncol Biol Phys*. 2015;93(2):454-464. doi:10.1016/j.ijrobp.2015.06.003
204. Zannella VE, Pra AD, Muaddi H, et al. Reprogramming metabolism with metformin improves tumor oxygenation and radiotherapy response. *Clin Cancer Res*. 2013;19(24):6741-6750. doi:10.1158/1078-0432.CCR-13-1787
205. Ljungkvist ASE, Bussink J, Rijken PFJW, Raleigh JA, Denekamp J, Van Der Kogel AJ. Changes in tumor hypoxia measured with a double hypoxic marker technique. *Int J Radiat Oncol Biol Phys*. 2000;48(5):1529-1538. doi:10.1016/S0360-3016(00)00787-2
206. Horsman MR, Nordsmark M, Hayer M, Overgaard J. Direct evidence that hydralazine can induce hypoxia in both transplanted and spontaneous murine tumours. *Br J Cancer*. 1995;72(6):1474-1478. doi:10.1038/bjc.1995.532
207. Guichard M, Lespinasse F, Trotter M, Durand R, Chaplin D. The effect of hydralazine on blood flow and misonidazole toxicity in human tumour xenografts. *Radiother Oncol*. 1991;20(2):117-123. doi:10.1016/0167-8140(91)90145-7
208. Trotter MJ, Acker BD, Chaplin DJ. Histological evidence for nonperfused vasculature in a murine tumor following hydralazine administration. *Int J Radiat Oncol Biol Phys*. 1989;17:785-789.

209. Bailey KM, Cornnell HH, Ibrahim-Hashim A, et al. Evaluation of the “steal” phenomenon on the efficacy of hypoxia activated prodrug th-302 in pancreatic cancer. *PLoS One*. 2014;9(12):1-18. doi:10.1371/journal.pone.0113586
210. Ugurel E, Connes P, Yavas G, et al. Differential effects of adenylyl cyclase-protein kinase A cascade on shear-induced changes of sickle cell deformability. *Clin Hemorheol Microcirc*. Published online 2020. doi:10.3233/CH-190563
211. Boivin P, Garbarz M, Dhermy D, Galand C. In vitro phosphorylation of the red blood cell cytoskeleton complex by cyclic AMP-dependent protein kinase from erythrocyte membrane. *BBA - Biomembr*. Published online 1981. doi:10.1016/0005-2736(81)90289-3
212. Deree J, Martins JO, Melbostad H, Loomis WH, Coimbra R. Insights into the regulation of TNF-α production in human mononuclear cells: The effects of non-specific phosphodiesterase inhibition. *Clinics*. 2008;63(3):321-328. doi:10.1590/S1807-59322008000300006
213. Song C, Makepeace C, Griffin R, et al. Increase in tumor blood flow by pentoxifylline. *Int J Radiat Oncol Biol Phys*. 1994;29(3):433-437.
214. Lee I, Kim JH, Levitt SH, Song CW. Increases in tumor response by pentoxifylline alone or in combination with nicotinamide. *Int J Radiat Oncol Biol Phys*. 1992;22(3):425-429. doi:10.1016/0360-3016(92)90846-A
215. Sensky PL, Prise VE, Ward AEM, Hirst DG. The effects of pentoxifylline on the relative perfusion of tumours growing in three sites in the mouse. *Br J Cancer*. 1993;68(6):1110-1114. doi:10.1038/bjc.1993.489
216. Kelleher D, Thews O, Vaupel P. Regional perfusion and oxygenation of tumors upon methylxanthine derivative administration. *Int J Radiat Oncol Biol Phys*. 1998;42(4):861-864.
217. Collingridge DR, Rockwell S. Pentoxifylline improves the oxygenation and radiation response of BA1112 rat rhabdomyosarcomas and EMT6 mouse mammary carcinomas. *Int J Cancer*. 2000;90:256-264. doi:10.1002/1097-0215(20001020)90:5<256::AID-IJC2>3.0.CO;2-R
218. Zywietz F, Böhm L, Sagowski C, Kehrl W. Pentoxifylline enhances tumor oxygenation and radiosensitivity in rat rhabdomyosarcomas during continuous hyperfractionated irradiation. *Strahlentherapie und Onkol*. 2004;180(5):306-314. doi:10.1007/s00066-004-

1198-1

219. Price MJ, Li LT, Tward JD, Bublik I, Mcbride WH, Lavey RS. Effect of nicotinamide and pentoxifylline on normal tissue and fsa tumor oxygenation. *Acta Oncol (Madr)*. 1995;34(3):391-395. doi:10.3109/02841869509093995

220. Sibtain A, Hill S, Goodchild K, Shah N, Saunders M, Hoskin PJ. The modification of human tumour blood flow using pentoxifylline, nicotinamide and carbogen. *Radiother Oncol*. 2002;62(1):69-76. doi:10.1016/S0167-8140(01)00493-5

221. Lee I, Boucher Y, Demhartner TJ, Jain RK. Changes in tumour blood flow, oxygenation and interstitial fluid pressure induced by pentoxifylline. *Br J Cancer*. 1994;69(3):492-496. doi:10.1038/bjc.1994.89

222. Honess DJ, Dennis IF, Bleehen NM. Pentoxifylline: its pharmacokinetics and ability to improve tumour perfusion and radiosensitivity in mice. *Radiother Oncol*. 1993;28(3):208-218. doi:10.1016/0167-8140(93)90060-L

223. Honess DJ, Andrews MS, Ward R, Bleehen NM. Pentoxifylline increases rif-1 tumour po2 in a manner compatible with its ability to increase relative tumour perfusion. *Acta Oncol (Madr)*. 1995;34(3):385-389. doi:10.3109/02841869509093994

224. Wyska E, Szymura-Oleksiak J, Pękala E, Obruśnik A. Pharmacokinetic modelling of pentoxifylline and lisofylline after oral and intravenous administration in mice. *J Pharm Pharmacol*. 2007;59(4):495-501. doi:10.1211/jpp.59.4.0003

225. Miller K, Louie A, Baltch AL, Smith RP, Davis PJ, Gordon MA. Pharmacokinetics of pentoxifylline and its metabolites in healthy mice and in mice infected with Candida albicans. *Antimicrob Agents Chemother*. 1998;42(9):2405-2409. doi:10.1128/aac.42.9.2405

226. Wyska E, Pekala E, Szymura-Oleksiak J. Interconversion and tissue distribution of pentoxifylline and lisofylline in mice. *Chirality*. 2006;18:644-651.

227. Sloczyńska K, Kózka M, Pękala E, Marchewka A, Marona H. In vitro effect of pentoxifylline and lisofylline on deformability and aggregation of red blood cells from healthy subjects and patients with chronic venous disease. *Acta Biochim Pol*. 2013;60(1):129-135. doi:10.18388/abp.2013_1962

228. Ambrus JL, Stadler S, Kulaylat M. Hemorrheologic effects of metabolites of pentoxifylline (Trental®). *J Med*. Published online 1995.

229. Bennewith KL, Durand RE. Quantifying transient hypoxia in human tumor xenografts by flow cytometry. *Cancer Res*. 2004;64(17):6183-6189. doi:10.1158/0008-5472.CAN-04-0289
230. Bennewith KL, Raleigh J a, Durand RE. Orally Administered Pimonidazole to Label Hypoxic Tumor Cells Advances in Brief Orally Administered Pimonidazole to Label Hypoxic Tumor Cells 1. *Cancer Res*. 2002;62:6827-6830.
231. Hussain M, Awan FR. Hypertension regulating angiotensin peptides in the pathobiology of cardiovascular disease. *Clin Exp Hypertens*. 2018;40(4):344-352. doi:10.1080/10641963.2017.1377218
232. Halici Z, Polat B, Cadirci E, et al. Inhibiting renin angiotensin system in rate limiting step by aliskiren as a new approach for preventing indomethacin induced gastric ulcers. *Chem Biol Interact*. 2016;258:266-275. doi:10.1016/j.cbi.2016.09.011
233. Zain M, Awan FR. Renin Angiotensin Aldosterone System (RAAS): Its biology and drug targets for treating diabetic nephropathy. *Pak J Pharm Sci*. 2014;27(5):1379-1391.
234. Michel MC, Foster C, Brunner HR, Liu L. A systematic comparison of the properties of clinically used angiotensin II type 1 receptor antagonists. *Pharmacol Rev*. 2013;65(2):809-848. doi:10.1124/pr.112.007278
235. Sun H, Li T, Zhuang R, Cai W, Zheng Y. Do renin-angiotensin system inhibitors influence the recurrence, metastasis, and survival in cancer patients? Evidence from a meta-analysis including 55 studies. *Med (United States)*. 2017;96(13). doi:10.1097/MD.0000000000006394
236. Murphy JE, Wo JY, Ryan DP, et al. Total Neoadjuvant Therapy with FOLFIRINOX in Combination with Losartan Followed by Chemoradiotherapy for Locally Advanced Pancreatic Cancer: A Phase 2 Clinical Trial. *JAMA Oncol*. 2019;5(7):1020-1027. doi:10.1001/jamaoncol.2019.0892
237. Durand RE, Aquino-Parsons C. The fate of hypoxic (pimonidazole-labelled) cells in human cervix tumours undergoing chemo-radiotherapy. *Radiother Oncol*. 2006;80(2):138-142. doi:10.1016/j.radonc.2006.07.022
238. Young AGH, Bennewith KL. Ionizing Radiation Enhances Breast Tumor Cell Migration In Vitro. *Radiat Res*. 2017;188(4):381. doi:10.1667/rr14738.1
239. Graham K, Unger E. Overcoming tumor hypoxia as a barrier to radiotherapy,

chemotherapy and immunotherapy in cancer treatment. *Int J Nanomedicine*. 2018;13:6049-6058. doi:10.2147/IJN.S140462

240. Teicher BA, Holden SA, Al-Achi A, Herman TS. Classification of Antineoplastic Treatments by Their Differential Toxicity toward Putative Oxygenated and Hypoxic Tumor Subpopulations in Vivo in the FSallC Murine Fibrosarcoma. *Cancer Res*. 1990;50(11):3339-3344.
241. Rankin EB, Giaccia AJ. Hypoxic control of metastasis. *Science (80-)*. 2016;352(6282):175-180. doi:10.1126/science.aaf2784
242. Cairns RA, Kalliomaki T, Hill RP. Acute (cyclic) hypoxia enhances spontaneous metastasis of KHT murine tumors. *Cancer Res*. 2001;61:8903-8908.
243. Spiegelberg L, Houben R, Niemans R, et al. Hypoxia-activated prodrugs and (lack of) clinical progress: The need for hypoxia-based biomarker patient selection in phase III clinical trials. *Clin Transl Radiat Oncol*. 2019;15:62-69. doi:10.1016/j.ctro.2019.01.005
244. Kaanders JHAM, Wijffels KIEM, Marres HAM, et al. Pimonidazole binding and tumor vascularity predict for treatment outcome in head and neck cancer. *Cancer Res*. 2002;62(23):7066-7074. http://ovidsp.ovid.com/ovidweb.cgi?T=JS&PAGE=reference&D=emed8&NEWS=N&AN=35424102
245. Dewhirst MW, Cao Y, Moeller B. Cycling hypoxia and free radicals regulate angiogenesis and radiotherapy response. *Nat Rev Cancer*. 2008;8(6):425-437. doi:10.1038/nrc2397
246. Chaudary N, Hill RP. Increased expression of metastasis-related genes in hypoxic cells sorted from cervical and lymph nodal xenograft tumors. *Lab Investig*. 2009;89(5):587-596. doi:10.1038/labinvest.2009.16
247. Cairns RA, Hill RP. Acute Hypoxia Enhances Spontaneous Lymph Node Metastasis in an Orthotopic Murine Model of Human Cervical Carcinoma. *Cancer Res*. 2004;64(6):2054-2061. doi:10.1158/0008-5472.CAN-03-3196
248. Chan N, Koritzinsky M, Zhao H, et al. Chronic hypoxia decreases synthesis of homologous recombination proteins to offset chemoresistance and radioresistance. *Cancer Res*. 2008;68(2):605-614. doi:10.1158/0008-5472.CAN-07-5472
249. Ljungkvist ASE, Bussink J, Kaanders JHAM, van der Kogel AJ. Dynamics of Tumor Hypoxia Measured with Bioreductive Hypoxic Cell Markers. *Radiat Res*.

2007;167(2):127-145. doi:10.1667/rr0719.1

250. Moore J V., Hasleton PS, Buckley CH. Tumour cords in 52 human bronchial and cervical squamous cell carcinomas: Inferences for their cellular kinetics and radiobiology. *Br J Cancer*. 1985;51(3):407-413. doi:10.1038/bjc.1985.55

251. Chapman JD, Baer K, Lee J. Characteristics of the metabolism-induced binding of misonidazole to hypoxic mammalian cells. *Cancer Res*. 1983;43(4):1523-1528.

252. Taylor YC, Rauth AM. Differences in the Toxicity and Metabolism of the 2-Nitroimidazole Misonidazole (Ro-07-0582) in HeLa and Chinese Hamster Ovary Cells. *Cancer Res*. 1978;38(9):2745-2752.

253. Walton MI, Bleehen NM, Workman P. Effects of localised tumour hyperthermia on pimonidazole (Ro 03-8799) pharmacokinetics in mice. *Br J Cancer*. 1989;59(5):667-673. doi:10.1038/bjc.1989.138

254. Laughlin KM, Tracy M, Chan CY, Lord EM. Biodistribution of the Nitroimidazole EF5 (2-[2-nitro-1H-imidazol-1-yl]-N-(2,2,3,3,3-pentafluoropropyl) acetamide) in Mice Bearing Subcutaneous. *J Pharmacol Exp Ther*. 1996;277(2):1049-1057.

255. Noguchi P, Wallace R, Johnson J, et al. Characterization of WiDr: A human colon carcinoma cell line. *In Vitro*. 1979;15(6):401-408. doi:10.1007/BF02618407

256. Friedl F, Kimura I, Osato T, Ito Y. Studies on a New Human Cell Line (SiHa) Derived from Carcinoma of Uterus. I. Its Establishment and Morphology. *Proc Soc Exp Biol Med*. 1970;135(2):543-545. doi:10.3181/00379727-135-35091a

257. Milross CG, Tucker SL, Mason KA, Hunter NR, Peters LJ, Milas L. The effect of tumor size on necrosis and polarographically measured pO2. *Acta Oncol (Madr)*. 1997;36(2):183-189. doi:10.3109/02841869709109228

258. Urano M, Chen Y, Humm J, Koutcher JA, Zanzonico P, Ling C. Measurements of Tumor Tissue Oxygen Tension Using a Time-Resolved Luminescence-Based Optical OxyLite Probe: Comparison with a Paired Survival Assay. *Radiat Res*. 2006;158(2):167-173. doi:10.1667/0033-7587(2002)158[0167:mottot]2.0.co;2

259. Lehmann S, Stiehl DP, Honer M, et al. Longitudinal and multimodal in vivo imaging of tumor hypoxia and its downstream molecular events. *Proc Natl Acad Sci*. 2009;106(33):14004-14009. doi:10.1073/pnas.0901194106

260. Kiraga Ł, Cheda Ł, Taciak B, et al. Changes in hypoxia level of CT26 tumors during

various stages of development and comparing different methods of hypoxia determination. *PLoS One*. 2018;13(11):1-12. doi:10.1371/journal.pone.0206706

261. Rafajová M, Zatovicová M, Kettmann R, Pastorek J, Pastoreková S. Induction by hypoxia combined with low glucose or low bicarbonate and high posttranslational stability upon reoxygenation contribute to carbonic anhydrase IX expression in cancer cells. *Int J Oncol*. Published online 2004. doi:10.3892/ijo.24.4.995
262. Dewhirst MW, Ong ET, Braun RD, et al. Quantification of longitudinal tissue pO2 gradients in window chamber tumours: Impact on tumour hypoxia. *Br J Cancer*. 1999;79(11-12):1717-1722. doi:10.1038/sj.bjc.6690273
263. Dewhirst MW, Ong ET, Klitzman B, et al. Perivascular Oxygen Tensions in a Transplantable Mammary Tumor Growing in a Dorsal Flap Window Chamber. *Radiat Res*. 1992;130(2):171. doi:10.2307/3578274
264. Freiberg RA, Hammond EM, Dorie MJ, Welford SM, Giaccia AJ. DNA Damage during Reoxygenation Elicits a Chk2-Dependent Checkpoint Response DNA Damage during Reoxygenation Elicits a Chk2-Dependent Checkpoint Response. *Mol Cell Biol*. 2006;26(5):1598-1609. doi:10.1128/MCB.26.5.1598
265. Wittenborn TR, Horsman MR. Targeting tumour hypoxia to improve outcome of stereotactic radiotherapy. *Acta Oncol (Madr)*. 2015;54(9):1385-1392. doi:10.3109/0284186X.2015.1064162
266. Bennewith KL, Dedhar S. Targeting hypoxic tumour cells to overcome metastasis. *BMC Cancer*. 2011;11(1):504. doi:10.1186/1471-2407-11-504
267. Hirata K, Terasaka S, Shiga T, et al. 18F-fluoromisonidazole positron emission tomography may differentiate glioblastoma multiforme from less malignant gliomas. *Eur J Nucl Med Mol Imaging*. 2012;39(5):760-770. doi:10.1007/s00259-011-2037-0
268. Cheng J, Lei L, Xu J, et al. 18F-fluoromisonidazole PET/CT: A potential tool for predicting primary endocrine therapy resistance in breast cancer. *J Nucl Med*. 2013;54(3):333-340. doi:10.2967/jnumed.112.111963
269. Humbert O, Riedinger JM, Vrigneaud JM, et al. 18F-FDG PET-Derived tumor blood flow changes after 1 cycle of neoadjuvant chemotherapy predicts outcome in triple-negative breast cancer. *J Nucl Med*. 2016;57(11):1707-1712. doi:10.2967/jnumed.116.172759
270. Bernstein JM, Kershaw LE, Withey SB, et al. Tumor plasma flow determined by dynamic

contrast-enhanced MRI predicts response to induction chemotherapy in head and neck cancer. *Oral Oncol*. 2015;51(5):508-513. doi:10.1016/j.oraloncology.2015.01.013

271. Huang Z, Yuh K, Lo S, et al. Validation of Optimal DCE-MRI Perfusion Threshold to Classify At-risk Tumor Imaging Voxels in Heterogeneous Cervical Cancer for Outcome Prediction. *Magn Reson Imaging*. 2014;32(10):1198-1205. doi:10.1097/CCM.0b013e31823da96d.Hydrogen
272. Sorensen A, Emblem K, Polaskova P, et al. Increased Survival of Glioblastoma Patients who Respond to Anti-angiogenic Therapy with Elevated Blood Perfusion. *Cancer Res*. 2012;72(2):402-407. doi:10.1038/jid.2014.371
273. Pan J, Pourghiasian M, Hundal N, et al. 2-[18F]Fluoroethanol and 3-[18F]fluoropropanol: Facile preparation, biodistribution in mice, and their application as nucleophiles in the synthesis of [18F]fluoroalkyl aryl ester and ether PET tracers. *Nucl Med Biol*. 2013;40(6):850-857. doi:10.1016/j.nucmedbio.2013.04.009
274. Tewsone T, Welch M. Preparation and preliminary biodistribution of "no carrier added" fluorine-18 fluoroethanol. *J Nucl Med*. 1980;21:559-564.
275. Aslakson CJ, Miller FR. Selective Events in the Metastatic Process Defined by Analysis of the Sequential Dissemination of Subpopulations of a Mouse Mammary Tumor. *Cancer Res*. 1992;52(6):1399-1405.
276. Patlak CS, Blasberg RG. Graphical evaluation of blood-to-brain transfer constants from multiple-time uptake data. Generalizations. *J Cereb Blood Flow Metab*. 1985;5(4):584-590. doi:10.1038/jcbfm.1985.87
277. Dexter DL, Kowalski HM, Blazar BA, et al. Heterogeneity of Tumor Cells from a Single Mouse Mammary Tumor. *Cancer Res*. 1978;38(10):3174-3181.
278. Lou Y, McDonald PC, Oloumi A, et al. Targeting tumor hypoxia: Suppression of breast tumor growth and metastasis by novel carbonic anhydrase IX inhibitors. *Cancer Res*. 2011;71(9):3364-3376. doi:10.1158/0008-5472.CAN-10-4261
279. Wang Z, Stefanko DP, Guo Y, et al. Evidence of functional brain reorganization on the basis of blood flow changes in the CAG140 knock-in mouse model of Huntington's disease. *Neuroreport*. 2016;27(9):632-639. doi:10.1097/WNR.0000000000000587
280. Tozer GM, Shaffi KM. Modification of tumour blood flow using the hypertensive agent, angiotensin II. *Br J Cancer*. 1993;67(5):981-988. doi:10.1038/bjc.1993.180

281. Tatsumi M, Yutani K, Kusuoka H, Nishimura T. Technetium-99m HL91 uptake as a tumour hypoxia marker: Relationship to tumour blood flow. *Eur J Nucl Med*. 1999;26(2):91-94. doi:10.1007/s002590050364
282. Yazdani S, Bansal R, Prakash J. Drug targeting to myofibroblasts: Implications for fibrosis and cancer. *Adv Drug Deliv Rev*. 2017;121:101-116. doi:10.1016/j.addr.2017.07.010
283. Ducharme J, Goertzen AL, Patterson J, Demeter S. Practical aspects of 18F-FDG PET when receiving 18F-FDG from a distant supplier. *J Nucl Med Technol*. 2009;37(3):164-169. doi:10.2967/jnmt.109.062950
284. Pinter M, Jain RK. Targeting the renin-angiotensin system to improve cancer treatment: Implications for immunotherapy. *Sci Transl Med*. 2017;9(410). doi:10.1126/scitranslmed.aan5616
285. Giuliani M, Gospodarowicz M. Radiation oncology in Canada. *Jpn J Clin Oncol*. 2018;48(1):22-25. doi:10.1093/jjco/hyx148
286. Kawashiri S, Tanaka A, Noguchi N, et al. Significance of stromal desmoplasia and myofibroblast appearance at the invasive front in squamous cell carcinoma of the oral cavity. *Head Neck*. 2009;31:1346-1353. doi:10.1002/HED
287. Jolly LA, Novitskiy S, Owens P, et al. Fibroblast-mediated collagen remodeling within the tumor microenvironment facilitates progression of thyroid cancers driven by brafv600e and pten loss. *Cancer Res*. 2016;76(7):1804-1813. doi:10.1158/0008-5472.CAN-15-2351
288. Brentnall TA, Lai LA, Coleman J, Bronner MP, Pan S, Chen R. Arousal of cancer-associated stroma: Overexpression of palladin activates fibroblasts to promote tumor invasion. *PLoS One*. 2012;7(1):1-14. doi:10.1371/journal.pone.0030219
289. Kawasaki H, Saotome T, Usui T, Ohama T, Sato K. Regulation of intestinal myofibroblasts by KRas-mutated colorectal cancer cells through heparin-binding epidermal growth factor-like growth factor. *Oncol Rep*. 2017;37(5):3128-3136. doi:10.3892/or.2017.5520
290. Ikemori R, Gabasa M, Duch P, et al. Epigenetic SmAd3 repression in tumor-associated fibroblasts impairs fibrosis and response to the antifibrotic drug nintedanib in lung squamous cell carcinoma. *Cancer Res*. 2020;80(2):276-290. doi:10.1158/0008-5472.CAN-19-0637

291. Roswall P, Bocci M, Bartoschek M, et al. Microenvironmental control of breast cancer subtype elicited through paracrine platelet-derived growth factor-CC signaling. *Nat Med*. 2018;24(4):463-473. doi:10.1038/nm.4494
292. Albrengues J, Bertero T, Grasset E, et al. Epigenetic switch drives the conversion of fibroblasts into proinvasive cancer-associated fibroblasts. *Nat Commun*. 2015;6:1-15. doi:10.1038/ncomms10204
293. Al-Kharashi LA, Al-Mohanna FH, Tulbah A, Aboussekhra A. The DNA methyl-transferase protein DNMT1 enhances tumorpromoting properties of breast stromal fibroblasts. *Oncotarget*. 2018;9(2):2329-2343. doi:10.18632/oncotarget.23411
294. Bhagat TD, Von Ahgrens D, Dawlaty M, et al. Lactate-mediated epigenetic reprogramming regulates formation of human pancreatic cancer-associated fibroblasts. *Elife*. 2019;8:1-23. doi:10.7554/eLife.50663
295. Hintz H, Gallant J, Vander Griend D, Coleman I, Nelson P, LeBeau A. Imaging Fibroblast Activation Protein Alpha in Prostate Cancer with Positron Emission 2 Tomography. *Clin Cancer Res*. 2020;(16):612-625. doi:10.1158/2326-6066.CIR-19-0855
296. Toms J, Kogler J, Maschauer S, et al. Targeting Fibroblast Activation Protein: Radiosynthesis and Preclinical Evaluation of an 18 F-labeled FAP Inhibitor . *J Nucl Med*. Published online 2020:jnumed.120.242958. doi:10.2967/jnumed.120.242958
297. Munson BR, Young DF, Okiishi TH, Huebsch WW. Steady, Laminar Flow in Circular Tubes. In: *Fundamental of Fluids Mechanics*. 6th ed. Don Fowley; 2009:313-317.

Appendices

Appendix A

A.1 Hagen-Poiseuille equation of laminar flow

Hagen-Poiseuille equation of laminar fluid flow in a cylindrical vessel relates the flow rate to the pressure gradient between two points in the vessel and resistance to fluid flow. Flow rate is proportional to the pressure gradient and inversely proportional to resistance[297]:

$$Q = \frac{\Delta p}{R} = \frac{\pi r^4 \Delta p}{8\mu L}$$

- Q is the volume of fluid flowing in the vessel
- Δp is the pressure gradient
- R is the resistance to flow
- r is the vessel radius
- μ is the viscosity of the fluid
- L is the length of the vessel, commonly substituted for 2r in cases of infinitely long or continuous vessels.

As can be inferred from the above equation, resistance to flow is proportional to the viscosity of the fluid and length of the vessel. Resistance is inversely proportional to the fourth power of the vessel radius. Resistance may be expressed as follows:

$$R = \frac{8\mu L}{\pi r^4}$$

A.2 Tumour kinetics equations and examples

Potential doubling time (T_{pot}) is the time that it would take for a tumour to double in size with no cell loss or turnover.

$$T_{pot} = \frac{T_C}{GF}$$

Where T_c is the cell cycle time and GF is the growth fraction. T_c and GF can be measured in model tumours by labelling proliferating tumour cells with uridine analogues to identify cells in S phase and harvesting at a known time later. Example, T_c = 24 hours, GF = 50% = 0.5.

$$T_{pot} = \frac{T_C}{GF} = \frac{24hr}{0.5} = 48hr$$

Therefore, the potential doubling time of the above hypothetical tumour is 48 hours. However, tumours do not typically grow at the rate predicted by T_{pot}. Instead, the cell loss factor (φ) is calculated by comparing the true doubling time (T_D), measured by imaging or calipers, to T_{pot}:

$$\varphi = 1 - (\frac{T_{pot}}{T_D})$$

Where φ indicates how many tumour cells are lost from the tumour for each cell division. For example, a φ of 1 indicates that 1 tumour cell is lost for each cell division. A φ of 1 indicates no net tissue growth. A φ of 0 indicates that T_{pot} and T_D are equal and therefore no cell loss occurs during tumour growth. Tumours exhibit a wide range of φ values, although typically greater than 0.5, indicating inefficient growth with cell loss.